maximum normal operating pressure). As shown in Table 2.6, the containment vessel design stresses are well below the allowable stresses (see Fig. 2.1 for stress locations). Therefore, this ES-3100 containment vessel is capable of shipping at a higher internal pressure. The external pressure requirement from 10 CFR 71.73(c)(6) is 150 kPa (21.7 psi) gauge. These design and operating pressures were used to calculate the stresses (Appendix 2.10.1) in all components of the containment boundary, which are well below the allowable limits at all operating conditions. The maximum normal operating pressure calculated for NCT in accordance with 10 CFR 71.4 and 10 CFR 71.71(c)(1) for the bounding load case is 200.20 kPa (29.036 psia). The maximum internal pressure differential calculated for NCT is 175.20 kPa (25.410 psi), which is the maximum normal operating pressure minus the reduced external pressure condition of 10 CFR 71.71(c)(3) [200.20 - 25.00 kPa (29.036 - 3.626 psia)] (Sect. 2.6.3). A summary of the package's design, NCT, and HAC pressures and temperatures is presented in Appendices 3.6.4 and 3.6.5. Allowable stress intensity limits and calculated stresses at the design evaluation conditions for the containment vessel are summarized in Tables 2.4 through 2.6. The stresses used in the design of all metal containment vessel components are in the elastic range of the material properties.

For conditions addressed by analysis, the margin of safety is calculated. The margin of safety (M.S.) is defined as:

Margin of Safety = Allowable Stress/ Actual Stress - 1.

In Regulatory Guide 7.11, below Table 1, the following quote is found: "Although NUREG/CR-1815 (Ref. 2) addresses the use of ferritic steels only, it does not preclude the use of austenitic stainless steels. Since austenitic stainless steels are not susceptible to brittle failure at temperatures encountered in transport, their use in containment vessels is acceptable to the staff and no tests are needed to demonstrate resistance to brittle failure." According to Regulatory Guide 7.11, because the containment vessel is manufactured from type 304L stainless steel (which is an austenitic stainless steel), "no tests are needed to demonstrate resistance to brittle failure." Therefore, brittle or fatigue failures are not anticipated under any design, transport, accident, or storage condition (Sects. 2.6 and 2.7). Material specifications for the ES-3100 packaging components are listed in Table 2.7.

Table 2.5. Allowable stress intensity (S_m) for the containment boundary materials of construction [a]

Description	Specification	S_m
Pipe body (Method 1)	ASME SA-312 welded or seamless pipe, type TP304L stainless steel	8.825×10^4 kPa (12,800 psi)[b]
Formed body, end cap and flange (Method 2)	ASME SA-182, F304L stainless steel	8.825×10^4 kPa (12,800 psi)[b]
Flange and end cap (Method 1)	ASME SA-182 Forging, F304L stainless steel	8.825×10^4 kPa (12,800 psi)[b]
Containment vessel sealing lid	ASME SA-479, stainless steel 304	8.825×10^4 kPa (12,800 psi)[b]
Containment vessel closure nut	ASME SA-479, UNS-S21800, Nitronic 60 SST	1.524×10^5 kPa (22,100 psi)

[a] *ASME Boiler and Pressure Vessel Code*, Sect. II, Part D, Table 2A at 148.89°C (300°F).
[b] Lower of two allowable values was chosen to limit deflection of the flange and lid attachment in accordance with note G7 in Table 2A of Part D.

Table 2.6. ES-3100 containment boundary design evaluation allowable stress comparisons [a]

Stress locations shown in Fig. 2.1	Internal pressure design evaluation containment boundary stress @ 699.82 kPa (101.5 psi) gauge		External pressure design evaluation containment boundary stress @ −149.62 kPa (−21.7 psi) gauge		Allowable stress or shear capacity (AS)
	kPa (psi) or kg (lb)	M.S.	kPa (psi) or kg (lb)	M.S.	kPa (psi) or kg (lb)
Top flat portion of sealing lid (center of lid)	6.895×10^3 (1000)	18.2	1.474×10^3 (213.8)	88.8	1.727×10^5 (19,200)[b]
Closure nut ring (Away from threaded portion)	8.621×10^4 (12,504)	4.3	4.246×10^4 [f] (6158)	9.8	4.571×10^5 (66,300)[c]
Top flat head (sealing surface region)	2.717×10^4 (3941)	8.74	1.665×10^4 [f] (2415)	14.9	1.324×10^5 (38,400)[c]
Cylindrical section (middle)	1.999×10^4 (2899)	3.41	4.273×10^3 (619.8)	19.7	8.825×10^4 (12,800)[d]
Cylindrical section (shell to flange interface)	3.016×10^4 (4374)	7.78	1.236×10^4 (1793)	20.4	1.324×10^5 (38,400)[c]
Cylindrical section (shell to bottom interface)	5.127×10^4 (7436)	4.16	1.096×10^4 (1589.8)	23.2	1.324×10^5 (38,400)[c]
Body flange threads load, kg (lb)	2.051×10^3 (4521)	9.01	9.072×10^2 [f] (2000)	21.6	2.053×10^4 (45266)[e]
Body flange thread region (under cut region)	5.926×10^4 (8595)	3.47	2.397×10^4 [f] (3476)	10	2.648×10^5 (38,400)[c]
Flat bottom head (center)	4.826×10^4 (7000)	1.74	1.032×104 (1496.6)	11.8	1.727×10^5 (19,200)[b]
Closure nut thread load, kg (lb)	2.051×10^3 (4521)	16.29	9.072×10^2 [f] (2000)	38.1	3.545×10^4 (78154)[e]

[a] Stresses are calculated using pressures, gasket and closure nut preload, and nominal dimensions for all containment boundary components in Appendix 2.10.1. Calculated stresses for external pressure were determined by multiplying the stress at the design conditions by a factor equal to the ratio of external pressure to design pressure and adding in contribution from preload. Allowable stress values are taken from Table 2.5.

[b] Stress interpreted as the sum of $P_l + P_b$; allowable stress intensity value is $1.5 \times S_m$.

[c] Stress interpreted as the sum of $P_l + P_b + Q$; allowable stress intensity value is $3.0 \times S_m$.

[d] Stress interpreted as the primary membrane stress (P_m); allowable stress intensity value is S_m.

[e] Allowable shear capacity is defined as $0.6 \times S_m \times$ thread shear area. Thread shear area = 38.026 cm^2 (5.894 $in.^2$).

[f] Stress and shear load in these areas are dominated by the 162.7 ± 6.8 N·m (120 ± 5 ft-lb) preload.

Table 2.7. ES-3100 packaging material specifications

Component	Specifications
	Drum assembly
Drum washers	1.375 OD × 0.812 ID × 0.25 in. thick, 300 Series stainless steel
Drum threaded weld studs	5/8–11 UNC × 7/8 Lg, ARC FT, type 304/304L stainless-steel studs
Drum hex nuts	5/8–11 UNC-2B, silicon bronze C65100
Drum lid weldment	Modified 30-gal, 16-gauge (MS27683-61) lid, type 304 or 304L stainless steel; and a 11-gauge thick sheet, type 304 or 304L stainless steel, ASME SA-240
Drum weldment	Modified 30-gal, 16-gauge (MS27683-7), type 304 or 304L stainless steel, ASME SA-240, manufactured per Drawing M2E801580A004 (Appendix 1.4.8)
Drum plugs	Nylon plastic plug, Micro Plastic, Inc.
	Impact limiter, insulation enclosure, neutron absorber, and drum packing material
Insulation and impact limiter (not removable)	Lightweight cast refractory insulation, Kaolite 1600, 358.8 ±48.1 kg/m^3 (22.4 ±3 lb/ft^3) density, cast in stainless-steel shells in the drum and top plug
Neutron absorber	Cat 277-4, 1681.9 +240.3/–80.1 kg/m^3 (105 +15/–5 lb/ft^3) density
Top plug (removable)	Type 304 or 304L stainless steel, ASME SA-240 (body), ASME SA-479 (lifting inserts)
Inner liners	Type 304 or 304L stainless steel, ASME SA-240 (body), ASME SA-479 (modified angle)
Silicone pads	Silicone rubber, 22 ±5 Shore A, color black/gray
Aluminum foil duct tape	McMaster Carr Part # 7616A21, temperature range –40 to 121°C (–40 to 250°F)
	Containment boundary
Containment vessel plug	Part # 04-2126, Modified VCO threaded plug, brass
Containment vessel hoist ring	3052T56, Swivel hoist ring, alloy steel (not used for shipment)
Containment vessel	Method 1: Type TP304L stainless steel ASME SA-312 (welded or seamless pipe body); type F304L, stainless steel, ASME SA-182 (flange, and end cap); type 304, stainless steel, ASME SA-479 (sealing lid), Nitronic 60 SST per ASME SA-479, UNS-S21800 (closure nut) Method 2: Type F304L stainless ASME SA-182 (body, flange, and end cap); type 304, stainless steel, ASME SA-479 (sealing lid), Nitronic 60 SST per ASME SA-479, UNS-S21800 (closure nut) All components per *ASME Boiler and Pressure Vessel Code*, Sect. II, Part D, Table 2A
Containment vessel O-rings	Elastomer, ethylene propylene, normal service temperature range of –40 to 150°C, Specification M 3BA712A14B13F17 in ASTM D-2000, per OO-PP-986
Containment vessel lid assembly retaining ring	Part # WSM-400-S02, type 302 stainless steel

Table 2.7. ES-3100 packaging material specifications (cont.)

Component	Specifications
Containment vessel O-ring lubricant	Clear dimethyl siloxane polymer
Containment vessel closure nut lubricant	Krytox #240AC
Containment vessel body dowel pins	0.2501/0.2503 OD × 0.50 long, 18-8 stainless steel
Containment vessel packing material	
Convenience cans	Stainless steel or tinned carbon steel with stainless-steel can handles and nylon-coated stainless-steel wire; nickel-alloy (200 series, passivated) in nylon mesh bag
Convenience bottles	Polyethylene or Teflon FEP
Silicone rubber pads	Silicone rubber, 22 ±5 Shore A, color black/gray
Can spacers	Stainless-steel can filled with Cat 277-4
Bagging	Polyethylene
Metal scouring scrubbers	Stainless steel, McMaster Carr Part # 7361T13

2.1.3 Weights and Centers of Gravity

The weights of the packaging components for the actual proposed contents ready for shipment and the test units are provided in Tables 2.8 and 2.9. The values listed for the test weights are the actual data recorded during compliance testing. The remaining weights listed for the shipping package are calculated weights. Nominal dimensions and densities were used in the calculations. Miscellaneous parts (nuts, and washers) are included.

The range of the centers of gravity for the ES-3100 shipping package with the various HEU arrangements and the test packages is shown in Fig. 2.2. A summary of the calculations are provided in Table 2.10.

2.1.4 Identification of Codes and Standards for Package Design

Based on the discussion in Sect. 2.1.2.2, the shipping package has been designed, analyzed, and will be fabricated, tested and maintained to the requirements of a Category I package. In accordance with the references from NUREG/CR-1815, Table 2.11 describes the appropriate codes and standards that are and will be used to comply with Category I packaging. These requirements have been extracted from NUREG/CR-3854 and NUREG/CR-3019.

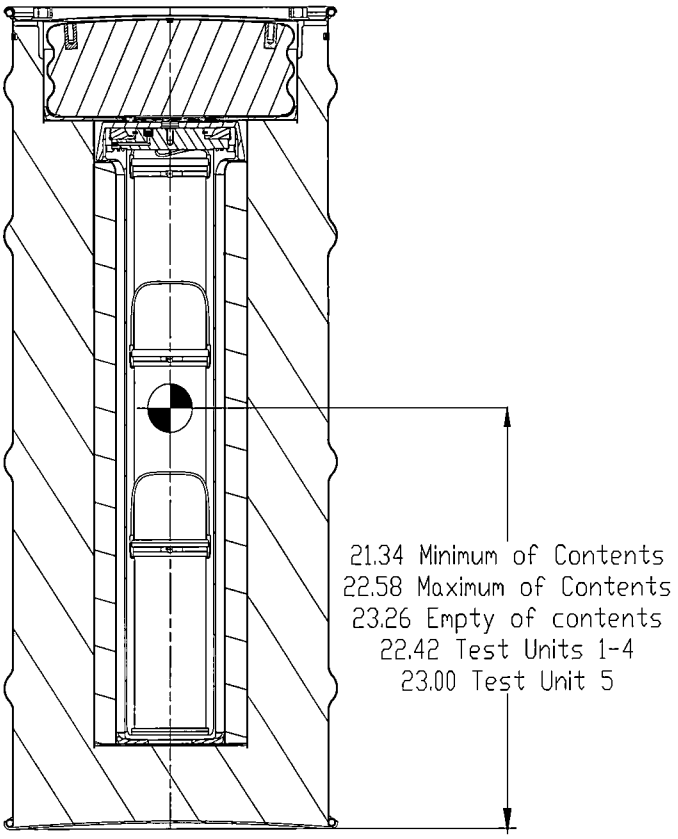

Note: Dimensions are in inches.

Fig. 2.2. ES-3100 shipping package center of gravity locations.

Table 2.8. Packaging weights for various ES-3100 shipping package arrangements [a]

Item	ES-3100 Three 10" tall can configuration kg (lb)	ES-3100 Six 4.875" tall can configuration kg (lb)	ES-3100 Five 4.875" tall can configuration kg (lb)	ES-3100 Six 4.75" tall can configuration kg (lb)	ES-3100 Three 8.75" tall can configuration kg (lb) [c]
			Drum assembly		
Drum assembly (drum body, lid, bottom, mid liner, inner liner, cast refractory insulation, cast neutron absorber, nuts, washers, and data plates) [b]	121.96 (268.87)	121.96 (268.87)	121.96 (268.87)	121.96 (268.87)	121.96 (268.87)
Top plug	8.9 (19.6)	8.9 (19.6)	8.9 (19.6)	8.9 (19.6)	8.9 (19.6)
Silicone support pads	1.04 (2.29)	1.04 (2.29)	1.04 (2.29)	1.04 (2.29)	1.04 (2.29)
Total drum assembly weight	**131.89 (290.76)**	**131.89 (290.76)**	**131.89 (290.76)**	**131.89 (290.76)**	**131.89 (290.76)**
			Containment Vessel		
Containment vessel (flange, dowel pins, cylindrical body, and end cap)	10.18 (22.44)	10.18 (22.44)	10.18 (22.44)	10.18 (22.44)	10.18 (22.44)
Lid assembly (sealing lid, VCO plug, retaining ring, closure nut and O-rings)	4.92 (10.85)	4.92 (10.85)	4.92 (10.85)	4.92 (10.85)	4.92 (10.85)
Total containment vessel weight	**15.10 (33.29)**	**15.10 (33.29)**	**15.10 (33.29)**	**15.10 (33.29)**	**15.10 (33.29)**
			Contents		
Convenience cans with handles	0.72 (1.59)	1.0 (2.22)	0.84 (1.85)	--	0.67 (1.47)
Silicone vibration pads	0.11 (0.23)	0.18 (0.41)	0.16 (0.353)	--	0.11 (0.23)
Nickel cans	--	--	--	1.84 (4.07)	--
Polyethylene bottles	--	--	--	--	--
Teflon FEP bottles	--	--	--	--	--
Spacers with handles	--	--	1.88 (4.14)	--	1.25 (2.76)
Polyethylene bagging or lifting sling	0.5 (1.10)	0.5 (1.10)	0.5 (1.10)	0.5 (1.10)	0.5 (1.10)
Metal scouring pads	--	--	--	--	0.14 (0.30)
HEU or HEU/Alloy content	35.2 (77.60)	35.2 (77.60)	35.2 (77.60)	24 (52.91)	35.2 (77.60)
Total proposed content weight	**36.52 (80.52)**	**36.89 (81.33)**	**38.57 (85.04)**	**26.34 (58.08)**	**37.86 (83.46)**
Total shipping package weight	**183.51 (404.57)**	**183.88 (405.38)**	**185.56 (409.09)**	**173.33 (382.13)**	**184.84 (407.51)**

Table 2.8. Packaging weights for various ES-3100 shipping package arrangements [a]

Item	ES-3100 Three 8.7" tall bottle configuration kg (lb)	ES-3100 Three Teflon bottle configuration kg (lb)	ES-3100 Empty CV configuration kg (lb)	ES-3100 with maximum weight contents kg (lb)
	Drum assembly			
Drum assembly (drum body, lid, bottom, mid liner, inner liner, cast refractory insulation, cast neutron absorber, nuts, washers, and data plates)	121.96 (268.87)	121.96 (268.87)	121.84 (268.61)[b]	121.96 (268.87)
Top plug	8.9 (19.6)	8.9 (19.6)	8.9 (19.6)	8.9 (19.6)
Silicone support pads	1.04 (2.29)	1.04 (2.29)	1.04 (2.29)	1.04 (2.29)
Total drum assembly weight	**131.89 (290.76)**	**131.89 (290.76)**	**131.78 (290.50)**	**131.89 (290.76)**
	Containment Vessel			
Containment vessel (flange, dowel pins, cylindrical body, and end cap)	10.18 (22.44)	10.18 (22.44)	10.18 (22.44)	10.18 (22.44)
Lid assembly (sealing lid, VCO plug, retaining ring, closure nut and O-rings)	4.92 (10.85)	4.92 (10.85)	4.92 (10.85)	4.92 (10.85)
Total containment vessel weight	**15.10 (33.29)**	**15.10 (33.29)**	**15.10 (33.29)**	**15.10 (33.29)**
	Contents			
Convenience cans with handles	--	--	--	--
Silicone vibration pads	--	--	--	--
Nickel can	--	--	--	--
Polyethylene bottles	0.345 (0.76)	--	--	--
Teflon FEP bottles	--	1.20 (2.65)	--	--
Spacers with handles	--	--	--	--
Polyethylene bagging or lifting sling	0.155 (0.34)	0.40 (0.88)	--	--
Metal scouring pads	--	--	--	--
HEU content	24.0 (52.91)	24.0 (52.91)	--	--
Total proposed content weight	**24.50 (54.01)**	**25.60 (56.44)**	**0**	**40.82 (90)**
Total shipping package weight	**171.49 (378.07)**	**172.59 (380.49)**	**146.88 (323.79)**	**187.81 (414.05)**

[a] Calculated weight using Pro/ENGINEER software with nominal dimensions and densities (Pro/ENGINEER Version 20).
[b] Weight excluding tamper indicating device.
[c] The weight of this configuration bounds the weight of the two 22.2 cm (8.75 in.) high cans that are brazed together containing the TRIGA fuel elements.

Table 2.9. Compliance test unit weights [a]

Item	Test Unit kg (lb)					
	1	2	3	4	5	6
Drum body assembly [b]	126.6 (279)	127.9 (282)	127.9 (282)	127.9 (282)	128.8 (284)	--
Top plug	9.5 (21)	9.5 (21)	9.53 (21)	8.6 (19)	9.5 (21)	--
Drum silicone support pads	0.9 (2)	0.9 (2)	0.9 (2)	0.5 (1)	0.9 (2)	--
Containment boundary [c]	15.4 (34)	15.0 (33)	15.0 (33)	14.5 (32)	15.0 (33)	15.0 (33)
Mock-up test contents [d]	49.9 (110)	49.9 (110)	50.3 (111)	49.9 (110)	3.6 (8)	
Contents [e]						6.3 (14)
Total test unit weight	202.3 (446)	202.8 (447)	203.7 (449)	201.8 (445)	157.4 (347)	21.3 (47)

[a] Total weight may be different from sum of individual component weights due to scale tolerance of ±0.45 kg (1 lb).
[b] This weight includes the drum, mid liner, inner liner, cast refractory, cast neutron absorber, bottom, lid, washers and nuts.
[c] This weight includes containment vessel cylindrical body, end cap, flanged top, and lid assembly.
[d] This weight includes convenience cans, silicone rubber pads, can handles, spacers (if required), and HEU mockup.
[e] This weight was added to reduce buoyancy of containment vessel during 15-m (50 ft) immersion test.

2.2 MATERIALS

2.2.1 Material Properties and Specifications

The mechanical properties and specifications of the packaging materials are presented in Tables 2.12–2.17. See the drawings in Appendix 1.4.8 for details of all components. Design temperature ranges are listed where they are required to establish the allowable stresses used in the design calculations for the containment boundary (Appendix 2.10.1). Service temperature ranges for the remaining shipping container components were obtained from the references shown in Tables 2.12–2.17.

Appendix 2.10.3 contains the Kaolite 1600 property values presented in Table 2.14, as well as additional Kaolite property and source information. Appendix 2.10.4 contains the Cat 277-4 property and source information. Appendix 2.10.5 contains *Compressive Strength and Coefficient of Thermal Expansion of BoroBond4*. (BoroBond4 was used in the prototype test units, but it is not used in the package to be certified.)

2.2.2 Chemical, Galvanic, or Other Reactions

Requirement. A package must be of materials and construction that assure that there will be no significant chemical, galvanic, or other reaction among the packaging components, among package contents, or between the packaging components and the package contents, including a possible reaction resulting from inleakage of water, to the maximum credible extent. Account must be taken for the behavior of materials under irradiation.

Table 2.10. Calculated center of gravity for the various ES-3100 shipping arrangements

Content description	Distance from drum's bottom (in.)
Cylinders, bars, slugs, broken metal - 35,200 g (77.60 lb) max - no can spacers	
3 full 4.88" cans + 3 empty 4.88" can	21.139
2 full 4.88" cans + 4 empty 4.88" cans	21.405
1 full 4.88" cans + 5 empty 4.88" cans	22.066
3 full 10" cans	22.071
2 full 10" cans + 1 empty 10" can	21.762
1 full 10"can + 2 empty 10" cans	22.075
3 full 8.75" cans	21.875
2 full 8.75" cans + 1 empty 8.75" can	21.662
1 full 8.75"can - 2 empty 8.75" cans	22.060
Cylinders, bars, slugs, broken metal - 35,200 g (77.60 lb) max - with can spacers	
3 full 8.75" cans + 2 spacers	22.245
2 full 8.75" cans + 1 empty 8.75" can + 2 spacers	21.802
1 full 8.75" can + 2 empty 8.75" cans + 2 spacers	22.072
3 full 4.88" cans + 2 empty 4.88" cans + 3 spacers	21.471
2 full 4.88" cans + 3 empty 4.88" cans + 3 spacers	21.500
1 full 4.88" cans + 4 empty 4.88" cans + 3 spacers	22.028
UNX crystals 24,000 g (52.910 lb) max - with no spacers	
3 full 8.94" high Teflon FEP bottles + bagging	22.674
2 full 8.94" high Teflon FEP bottles + 1 empty 8.94" high Teflon FEP bottle + bagging	22.383
1 full 8.94" high Teflon FEP bottle + 2 empty 8.94" high Teflon FEP bottles + bagging	22.543
Oxide - 24,000 g (52.910 lb) max - with no spacers	
6 full 4.75" high Nickel cans + bagging	22.631
5 full 4.75" high Nickel cans + 1 empty 4.75" high Nickel can + bagging	22.434
4 full 4.75" high Nickel cans + 2 empty 4.75" high Nickel can + bagging	22.343
3 full 4.75" high Nickel cans + 3 empty 4.75" high Nickel can + bagging	22.366
2 full 4.75" high Nickel cans + 4 empty 4.75" high Nickel can + bagging	22.511
1 full 4.75" high Nickel cans + 5 empty 4.75" high Nickel can + bagging	22.787
Oxide - 24,000 g (52.910 lb) max - with no spacers	
3 full 8.7" high polyethylene bottles + bagging	22.372
2 full 8.7" high polyethylene bottles + 1 empty 8.7" high polyethylene bottle + bagging	22.210
1 full 8.7" high polyethylene bottle + 2 empty 8.7" high polyethylene bottles + bagging	22.480

Table 2.11. Applicable codes and standards for Category I packaging

	Containment ASME Boiler and Pressure Vessel Code, Sect. III, Subsection NB	Criticality [a]
Materials		Cat 277-4[a]
Base materials	NB-2000 (except NB-2300) and NB-4100	
Welding materials	NB-2400	
Fabrication		
Forming, fitting, aligning, and joint preparation	NB-4200	
Welding	NB-4400	
Qualification of procedures and personnel	NB-4300	
Examination	NB-5000	[b]
Acceptance testing	NB-6000	[c]
Quality assurance	Subpart H in Title 10, CFR, Part 71	

[a] NUREG/CR-3854 states "The designer may specify a neutron absorber material by a commercial trade name or as a mixture of elements or common compounds. When appropriate, qualification data should be included to demonstrate that the material functions as specified. When special absorber materials are used to control criticality, an acceptance test should be performed for each container to ensure that the absorber material has been properly installed."

[b] NUREG/CR-3854 states "Packages designed to transport fissile material which contain neutron absorber material should be tested to demonstrate the presence of the neutron absorber material. The test description should include information similar to that requested for gamma shield testing 3.2.1. Fabrication records of the absorber material and its installation and testing should be maintained."

[c] NUREG/CR-3854 states "Gamma scanning or probing may be used to demonstrate the soundness of the neutron absorber. Alternatively, ultrasonic testing may be used. Whatever method is used, the following information should be provided in the test procedure:
(1) Description of the measuring technique including the electronics;
(2) The source type and strength used to measure the neutron absorber effectiveness;
(3) The standards and methods use to calibrate the source, sensors, and other pertinent equipment;
(4) The grid pattern used to check the neutron absorber;
(5) The type of gamma sensor used to measure the neutron absorber effectiveness;
(6) The specific test requirements and measurements;
(7) The acceptance criteria."

Table 2.12. Mechanical properties of the metallic components of the drum assembly[a]

Drum, bottom cover and lid	ASME SA-240 type 304 or 304L, stainless-steel plate	
Inner liners	ASME SA-240 type 304 or 304L, stainless-steel plate	
Top plug weldment	ASME SA-240 type 304 or 304L, stainless-steel plate	
Materials of construction	ASME SA-240 type 304	ASME SA-240 type 304L
Design stress intensity, MPa (ksi) at:		
-40°C (-40°F)	137.9 (20)	115.1 (16.7)
37.78°C (100°F)	137.9 (20)	115.1 (16.7)
93.33°C (200°F)	137.9 (20)	115.1 (16.7)
148.89°C (300°F)	137.9 (20)	115.1 (16.7)
Ultimate strength, MPa (ksi) at:		
-40°C (-40°F)	517.1 (75)	482.6 (70)
37.78°C (100°F)	517.1 (75)	482.6 (70)
93.33°C (200°F)	489.5 (71)	455.7 (66.1)
148.89°C (300°F)	456.4 (66.2)	422.0 (61.2)
Yield strength, MPa (ksi) at:		
-40°C (-40°F)	206.8 (30)	172.4 (25)
37.78°C (100°F)	206.8 (30)	172.4 (25)
93.33°C (200°F)	172.4 (25)	147.5 (21.4)
148.89°C (300°F)	154.4 (22.4)	132.4 (19.2)
Elongation in 5.08 cm (2 in.) (%)	40[b]	40[b]
Coefficient of thermal expansion, cm/cm/°C (in./in./°F) at:		
-40°C (-40°F)[c]	0.00001476 (0.0000082)[c]	0.00001476 (0.0000082)[c]
37.78°C (100°F)	0.00001548 (0.0000086)	0.00001548 (0.0000086)
93.33°C (200°F)	0.00001602 (0.0000089)	0.00001602 (0.0000089)
148.89°C (300°F)	0.00001656 (0.0000092)	0.00001656 (0.0000092)
Modulus of elasticity, GPa (Mpsi) at:		
-40°C (-40°F)	197.2 (28.6)	197.2 (28.6)
37.78°C (100°F)	194.0 (28.14)	194.0 (28.14)
93.33°C (200°F)	190.3 (27.6)	190.3 (27.6)
148.89°C (300°F)	186.2 (27.0)	186.2 (27.0)

[a] *ASME Boiler and Pressure Vessel Code*, Sect. II, Part D, Subpart 1, Tables 2A, U, and Y-1; and Subpart 2, Tables TE-1, B column, and TM-1.
[b] *ASME Boiler and Pressure Vessel Code*, Sect. II, Part A for ASME SA-240 material.
[c] MIL-HDBK-5H.

Table 2.13. Mechanical properties of the lid fastening components for the drum assembly

Drum weld studs	Specification
Material	ASTM A-493 Type 304/304L stainless steel
Fabrication standard	ASTM F593
Service temperature range, °C (°F)	−40 to 816 (−40 to 1500)[a]
Maximum allowable stress, S, MPa (ksi) at temperatures[a]	
−29°C to 38°C (−20 to 100°F)	129.6 (18.8)
93.3°C (200°F)	115.1 (16.7)
148.9°C (300°F)	103.4 (15.0)
Coefficient of thermal expansion, cm/cm/°C (in./in./°F)[a]	
21.1°C (70°F)	1.53×10^{-5} (8.5×10^{-6})
93.3°C (200°F)	1.60×10^{-5} (8.9×10^{-6})
148.9°C (300°F)	1.66×10^{-5} (9.2×10^{-6})
Drum hex-head nuts	**Specification**
Material	silicon bronze
Fabrication standard	ASTM F-467
UNS designation	C65100[b]
Minimum proof stress, MPa (ksi)	485 (70)[b]
Drum washer	**Specification**
Drum	1.375 OD × 0.812 ID × 0.25 in. thick, Series 300 stainless steel

[a] *ASME Boiler and Pressure Vessel Code*, Sect. II, Part D, Subpart 1, Table 3; and Subpart 2, Table TE-1, group 3, B value.
[b] ASTM F-467M.

Table 2.14. Mechanical properties of the cast refractory insulation

Material composition:	Cast Refractory, Kaolite 1600
Flexural tensile strength, kPa (psi)	133 (19.4)[a]
Standard deviation	32 (4.7)
Average coefficient of thermal expansion, cm/cm/°C (in./in./°F)	9.07×10^{-6} (5.04×10^{-6})[b]
Average modulus of rupture per ASTM C133-84, kPa (psi)	258.6 (37.5)[c]
Normal operating temperature, °C (°F)	−40 to 871 (−40 to 1600)[c]
Density after curing, kg/m^3 (lb/ft^3)	358.8 (22.4)[c]
Force/deflection curves	Smith, Appendix 2.10.3

[a] *Mechanical Properties of a Low-Density Concrete for the New ES-2 Shipping/Storage Container Insulation, Impact Mitigation Media and Neutron Absorber* (Appendix 2.10.3).
[b] Fax from J. Street, Thermal Ceramics, Inc. (Appendix 2.10.3).
[c] *Product Information, Refractory Castables and Monolithics* (Appendix 2.10.3).

Table 2.15. Mechanical properties of containment vessel O-rings

Material composition:	Ethylene propylene, Specification—M3BA712A14B13F17[a,b]
Normal service temperature range, °C (°F)	−40 to 150 (−40 to 302)[c]
Permissible exposure time at 150°C (302°F), h	1000[c]
Hardness durometer, Shore A	70 ± 5[a]
Minimum elongation, %	100[a]
Fabrication method	Molded[a]

[a] ASTM D-2000.
[b] Per Specification OO-PP-986.
[c] Parker O-ring Handbook, Sect. 2.13.2 and Fig. 2-24, p. 2-30.

Table 2.16. Mechanical properties of the metallic components of the containment boundary

Containment vessel: body; flange; and seal lid	Specifications
Material of construction: stainless steel, type 304L	ASME SA-312 (pipe); ASME SA-182 (flange, formed body, or end cap); ASME SA-479 (seal lid)
Design temperature range, °C (°F)	-40 to 176.67 (-40 to 350)
Minimum ultimate strength, MPa (ksi)	482.6 (70)[a]
Yield strength, 0.2% offset, MPa (ksi) at temperatures,	
37.8°C (100°F)	172 (25)[a]
149°C (300°F)	132 (19.2)[b]
176.67°C (350°F)	126.52 (18.35)[b]
Elongation in 5.08 cm (2 in.), %	57[c]
Modulus of elasticity, GPa (Mpsi) at temperature[b]	
-40°C (-40°F)	197.2 (28.60)
37.78°C (100°F)	194.0 (28.14)
93.33°C (200°F)	190.3 (27.60)
121.11°C (250°F)	188.2 (27.30)
148.89°C (300°F)	186.2 (27.00)
176.67°C (350°F)	184.4 (26.75)
Allowable stresses (S_m)[d] at 149°C (300°F)	
Welded pipe, MPa (ksi)	
149°C (300°F)	115.14 (16.7)
176.67°C (350°F)	112.03 (16.25)
Forged flanges, lids, end caps, MPa (ksi)	
at 149°C (300°F)	115.14 (16.7)
176.67°C (350°F)	112.03 (16.25)
Coefficient of thermal expansion, cm/cm/°C (in./in./°F) at temperatures[e]	
-40°C (-40°F)	0.00001476 (0.00000820)
37.78°C (100°F)	0.00001548 (0.00000860)
93.33°C (200°F)	0.00001602 (0.00000890)
121.11°C (250°F)	0.00001638 (0.00000910)
148.89°C (300°F)	0.00001656 (0.00000920)
176.67°C (350°F)	0.00001674 (0.00000930)
Containment vessel closure nut	**Specification**
Material of construction:	Nitronic 60, UNS-S21800
Elongation, %	10–12[f]
Design temperature range, °C (°F)	-40 to 176.67 (-40 to 350)
Ultimate strength, MPa (ksi), room temperature	1655–1813 (240–263)[f]
Yield strength, 0.2% offset, MPa (ksi), room temperature	1344–1496 (195 - 217)[f]
Coefficient of thermal expansion, cm/cm/°C (in./in./°F) at temperatures[e]	
93.33°C (200°F)	0.0000158 (0.0000088)
204.40°C (400°F)	0.00001660 (0.0000092)

[a] Listed in the appropriate material specification identified under materials of construction.
[b] *ASME Boiler and Pressure Vessel Code,* Sect. II, Part D, Tables Y-1 and TM-1.
[c] Value presented in THERM 1.2, thermal properties database by R. A. Bailey.
[d] *ASME Boiler and Pressure Vessel Code,* Sect. II, Part D, Table 2A.
[e] *ASME Boiler and Pressure Vessel Code,* Sect. II, Part D, Subpart 2, Table TE-1, Column B, except that -40°C is from MIL-HDBK-5H, Table 2.7.1.0.
[f] Value presented in ARMCO NITRONIC 60 Stainless Steel Product Data Bulletin, S-56b.

Table 2.17. Mechanical properties of the cast neutron absorber

Material	Cat 277-4
Service temperature range, °C (°F)	-40 to 150 (-40 to 302)
Modulus of elasticity in tension, GPa (Mpsi) at temperatures [a]	
-40°C (-40°F)	13.72 (1.991)
21.11°C (70°F)	4.72 (0.684)
37.78°C (100°F)	2.78 (0.403)
Coefficient of thermal expansion, cm/cm/°C (in./in./°F) at temperatures [b]	
-40°C (-40°F)	12.700×10^{-6} (7.056×10^{-6})
-20°C (-4°F)	13.000×10^{-6} (7.222×10^{-6})
0°C (32°F)	13.000×10^{-6} (7.222×10^{-6})
40°C (104°F)	12.600×10^{-6} (7.000×10^{-6})
60°C (140°F)	11.599×10^{-6} (6.444×10^{-6})
80°C (176°F)	10.400×10^{-6} (5.778×10^{-6})
100°C (212°F)	9.700×10^{-6} (5.389×10^{-6})
120°C (248°F)	9.101×10^{-6} (5.056×10^{-6})
Poisson Ratio	
-40°C (-40°F)	0.33 [a]
21.11°C (70°F)	0.28
37.78°C (100°F)	0.25
Density, g/cm^3 (lb/in.^{3})	1.682 (0.0608)

[a] *Mechanical Properties of 277-4* (Appendix 2.10.4).
[b] *Thermophysical Properties of Heat Resistant Shielding Material* (Appendix 2.10.4).

Analysis. Starting with the outer components, the packaging consists of the drum (austenitic type 304 stainless steel), weld studs (austenitic stainless steel), nuts (silicon bronze), insulation (cast refractory), neutron absorber (Cat 277-4), silicone support pads, containment vessel (austenitic type 304L stainless steel), closure nut (Nitronic 60), silicone support pads, can spacers (stainless steel and Cat 277-4), stainless-steel scrubbers, convenience cans (stainless steel, tin-plated carbon steel, or nickel-alloy [series 200, passivated]), polyethylene or Teflon FEP bottles, polyethylene bags, and the HEU contents.

The cast refractory insulation (Kaolite) is contained between the drum and mid liner and within the top plug assembly's stainless-steel sheet metal. Due to the alkaline nature of this material, greater permanence of the surrounding structure is assured. Also, this material has been used successfully for years as an insulation heat treatment liner adjacent to metal surfaces of furnaces.

The cast neutron absorber (Cat 277-4) is contained between the inner liner and mid liner. During the casting process, the chlorine content is limited to 100 parts per million. The small quantity of chlorine will not affect the stainless-steel liners.

The nuts used to attach the drum to the lid are silicon bronze. All other metal components of the packaging are either stainless steel, Nitronic 60, or tinned steel. All stainless-steel components are passivated per ASTM A380, Paragraph 6.4, and Table A2.1, Part II. Prior to assembly, the packaging will be kept inside a building or transported between buildings in an enclosed truck. The assembled components are protected from the weather and inspected at the time of packaging; therefore, the package will not contain any free water at the time it is loaded for transport. Under NCT, the only moisture present will be the relative humidity or moisture absorbed by the cast refractory or neutron absorber materials. When the package is subjected to a water-spray type environment, some water may leak into the cavity formed by the inner liner and occupied by the containment vessel. To minimize the possibility of any potentially corrosive situation, a visual examination of the interior surface of the inner liner and the exterior surface of the containment vessel shall be conducted prior to packing and following

transport of the shipping package (see Sect. 7). Any free water present and any corrosion discovered shall be promptly removed.

During immersion under HAC, water can enter the holes at the top of the drum, be absorbed into the cast refractory material, and fill all void spaces within the drum and inner liner. The insulating value of the insulation material may be decreased, and an overall weight increase would occur. The most important consideration is that the containment boundary remain intact and leaktight. This situation has been evaluated by completely immersing the containment vessel in a tank simulating 0.9-m and 15-m (3- and 50-ft) immersion depths. The containment vessel remained intact and water tight, as demonstrated by the analysis and testing discussed in Sect. 2.7.

All physical contact between the convenience cans and the containment vessel wall, bottom, or top is minimized through the use of the silicone support pads. The polyethylene or Teflon FEP bottles may be in contact with the stainless steel of the containment vessel, but will not react. All cans and bottles will provide the necessary separation of the HEU contents from the containment vessel walls. When space is available inside the containment vessel, stainless-steel metal scrubbers will be placed on the top and bottom of this partially canned assembly or an empty convenience can will be placed on top of this assembly inside the containment vessel. The passivated Nickel-alloy cans are galvanically similar to the stainless steel of the containment vessel and thus will not react. Additionally, polyethylene bagging may be used around the convenience container (in some cases the HEU is bagged inside the convenience container) as required by packaging personnel. Therefore, galvanic corrosion between the containment vessel wall and convenience containers is highly unlikely. In addition, the environment inside the containment vessel is free of electrolytic solutions, further assuring there will be no galvanic reactions occurring inside the containment vessel.

The material testing documented in Y/DZ-2720 (Appendix 2.10.9) does not identify the composition of the volatiles or gases generated during testing. Since Teflon fluorinated ethylene propylene (FEP), a fluorine-containing polymer, is used to transport uranyl nitrate crystals, the possible development of a corrosive environment inside the containment vessel is investigated. Based on the following literature, FEP is notable among addition polymers for its high thermal stability. It decomposes at temperatures above ~260°C (500°F). In air or in oxygen, FEP decomposes in one way at lower temperatures and in another at higher temperatures. In this discussion, "oxygen" implies oxygen at a pressure of 300 torr. In air, the partial pressure of oxygen is near 150 torr. Below about 525°C, the decomposition of FEP is first order, and the main decomposition product is hexafluoropropylene (C_3F_6), although tetrafluoroethylene (C_2F_4) is a near second in abundance. (Leidecker, Teflon thermal decomposition) The carbon-fluorine compound is one of the strongest compounds found in organic chemistry (its dissociation energy is 460 kJ/mol). The carbon chain is nearly completely covered by fluorine atoms, and is therefore protected against external influences. This results in the exceptionally high chemical resistance of FEP. (Daikin America) Based on the preceding statements, it is reasonable to conclude that most, if not all, of the gas coming from any decomposition of the Teflon FEP bottles would be hexafluoropropylene and tetrafluoroethylene rather than fluorine gas. The maximum temperature predicted (NCT or HAC) inside the ES-3100 containment vessel at the location near the Teflon FEP bottles is 123.85°C (254.93°F). This temperature is considerably below the lower limit of the FEP decomposition temperature [260°C (500°F)]. Due to the difference between the decomposition temperature of FEP [260°C (500°F)] and the maximum predicted temperature from testing [123.85°C (254.93°F)], essentially no C_3F_6 or C_2F_4 and no fluorine is expected to form during transport. Therefore, a corrosive environment with fluorine as the base is not anticipated. It should be noted that the offgassing rate and quantity used for Teflon FEP at lower temperatures in Appendices 3.6.4 and 3.6.5 are very conservative estimates. The actual values shown for the Teflon bottle sample in Y/DZ-2720 (Appendix 2.10.9) may have resulted from the cumulative tolerance in the testing setup and data recording, and not from actual offgassing.

For pyrophoric considerations, broken metal and alloy pieces shall be of a size that: a) the specific surface area does not exceed 1 cm^2/g or b) will not pass freely through a mesh size of 3/8 in. (0.95 cm) as discussed in Sect. 1.2.3, Appendix 1.4.10, and Sect. 7.1.2. Incidental small particles which do not pass the size restriction tests, and powders, foils, turnings, and wires may only be shipped if they are in a sealed, inerted container.

The containment boundary remains intact even when the drum and inner liner are filled with water; therefore, the package is acceptable to the maximum credible extent from the standpoint of chemical, galvanic, or other reactions.

2.2.3 Effects of Radiation on Materials

The HEU material is not irradiated. The neutron and photon dose rates (Sect. 5) are well below those required to damage any of the package materials by radiolytic interactions. However, NUREG-1609, Sect. 4.5.2.3, requires the applicant to demonstrate that any combustible gases generated in the package during a period of one year do not exceed 5% (by volume) of the free gas volume in any confined region of the package. No credit should be taken for getters, catalysts, or other recombination devices. Appendix 3.6.7 evaluates the various packaging arrangements for the generation of hydrogen gas due to the radiolysis of water vapor, free water, interstitial water, polyethylene bags, and polyethylene or Teflon bottles. When the content mass and the material composition are limited as shown in Appendix 3.6.7, the combustible gas concentration limit stated in NUREG-1609 is not exceeded. Getters, catalysts, or other recombination devices are not employed in any of the containment vessel packaging arrangements.

2.3 FABRICATION AND EXAMINATION

2.3.1 Fabrication

2.3.1.1 Drum assembly fabrication

The drum assembly is fabricated in accordance with equipment specifications JS-YMN3-801580-A002 (Appendix 1.4.2), JS-YMN3-801580-A003 (Appendix 1.4.4), and JS-YMN3-801580-A005 (Appendix 1.4.5). The later two specifications control the casting of the Kaolite 1600 and Cat 277-4 materials inside the liners, spacer cans and the top plug as appropriate.

The drum assembly and top plug are fabricated according to the design drawings (Appendix 1.4.8), and the portions of the codes, standards, and regulations to the extent described below:

1. *ASME, Boiler and Pressure Vessel Code*, Sect. VIII, Division 1, 2004 edition;
2. *ASME, Boiler and Pressure Vessel Code*, Sect. II, Parts A and C, 2004 edition;
3. *ASME, Boiler and Pressure Vessel Code*, Sect. IX, 2004 edition;
4. Military Standard, MS27683, *Drum, Metal-Shipping and Storage 16 to 80 Gallons*; and
5. ASTM A 380-99e1, *Standard Practice for Cleaning, Descaling, and Passivation of Stainless Steel Parts, Equipment and Systems*.

Detailed dimensional requirements, and the materials of construction are called out on the drawings in Appendix 1.4.8. Except for the weld studs, documented Certified Material Test Reports (CMTRs) are provided for all materials used in weldments for the fabrication of the drum, including weld

filler metal. The CMTRs are traceable to heat numbers and demonstrate compliance with the SA or SFA material specifications called out. For all other materials, documented Certificates of Compliance (CoC) are provided certifying that the materials provided comply with the requirements stated on the drawings and specifications. All welding is done in accordance with welding procedure specifications that are written and performance qualified in accordance with the ASME B&PV Code, Section IX. All welders are performance qualified to weld using these procedures, and their qualifications documented in accordance with the ASME Code, Section IX. The welding fabrication requirements stated in the ASME Code, Section VIII, Division 1, paragraphs UW-26 through UW-48 are met. All butt welds in rolled sheet, pipe and angle joints are full penetration butt welds. With the exception of the seam welds in the drum body, all welds shall be done by the GTAW, GMAW, PAW or a Capacitive Discharge (CD) stud welding process. The weld filler metal used in the fabrication of the drum assembly is procured to comply with the SFA specifications of Section II, Part C of the ASME Code that are stated in the welding procedure specifications. Weld filler metal is procured traceable to heat numbers, and CMTRs are furnished for each heat of weld wire filler. The control of weld filler permits a weld examiner to be able to determine the heat number of the weld filler used in any weld on the drum assembly. Weld symbols are provided on the drawings indicating for each weld the type of weld and dimensions of weld. These weld symbols are interpreted in accordance with the American Welding Society, Section A2.4.

2.3.1.2 Containment boundary fabrication

The containment boundary consists of the containment vessel, lid assembly and inner O-ring. The containment vessel is manufactured in accordance with the applicable requirements stated in the ASME Boiler and Pressure Vessel Code, Section III, Division 1, Subsection NB for Class 1 Components as described on the drawings in Appendix 1.4.8 and equipment specification JS-YMN3-801580-A001 (Appendix 1.4.3). The containment vessel is fabricated according to the design drawings and the following codes, standards, and regulations as described in JS-YMN3-801580-A001.

1. *ASME, Boiler and Pressure Vessel Code*, Sect. III, Division 1 Subsections NB and NCA, Class 1 Components, 2004 edition;

2. *ASME, Boiler and Pressure Vessel Code*, Sect. II, Parts A and C, 2004 edition;

3. *ASME, Boiler and Pressure Vessel Code*, Sect. IX, 2004 edition; and

4. ASTM A 380-99e1, *Standard Practice for Cleaning, Descaling, and Passivation of Stainless Steel Parts, Equipment and Systems.*

Detailed dimensional requirements, and the materials of construction are called out on the drawings in Appendix 1.4.8. CMTRs are provided for the materials used to fabricate these components in accordance with NCA-3860. The suppliers of these materials will meet the requirements of NCA-3800. Such parts are traceable to each containment vessel by means of a serial number. The fabricator maintains control of materials to ensure this traceability. Other metallic materials, and the O-ring seals are supplied with CoCs in accordance with NCA-3862(g) and (h). The weld filler metal used in the fabrication, and repair welding as permitted, of the containment vessels meets the applicable requirements of NB-2400. It is procured to comply with the SFA specifications of Section II, Part C of the ASME B&PV Code that is stated in the fabricator's welding procedure specifications. Weld metal is procured traceable to heat numbers, and CMTRs are furnished for each heat of weld wire filler used. The results of the delta ferrite determination is included in the CMTR for the weld filler metal (see NB-2433). There are two containment vessel assemblies shown on drawing M2E801580A012 (Appendix 1.4.8), part number M2E801580A012-1, and M2E801580A012-4. Part number M2E801580A012-4 is fabricated by welding a forged bottom and forged top flange to a cylindrical shell machined from seamless pipe as shown on the

drawing. All welds on the containment vessels are accomplished by either the GTAW or GMAW process, manual or automatic, at the discretion of the fabricator unless specifically called out on the drawings. Backing rings, even if removed after the weld has been made, are not be used. As previously stated, weld symbols are provided on the drawing indicating the type of weld and dimensions of the weld. These weld symbols are interpreted in accordance with the American Welding Society, section A2.4. The forming, fitting and alignment requirements stated in paragraph NB-4200 are met in the fabrication of the containment vessels unless more stringent requirements are called out on the design drawings.

The preferred fabrication method for the containment vessel body (part number M2E801580A012-1), is from a single forged billet or bar by any process that meets the requirements stated in JS-YMN3-801580-A001 (Appendix 1.4.3), and shown on the design drawings. Such processes may include forging, flow forming, or metal spinning. The formed, heat treated, and finished machined containment vessel body shall meet the applicable requirements of ASME SA 182 for Grade F304L for a forged component. After final forming, parts are solution annealed and quenched per the requirements of ASME SA 182 for Grade F304L. A certified heat treatment report is provided stating the following information for each furnace charge: the serial numbers of the containment vessel bodies heat treated in the furnace charge, the time and date of the heat treating, the person responsible for the heat treating, the time-temperature profile of the furnace and representative parts of the furnace charge, the quench medium, and all other pertinent details of the heat treating. Such a heat treating report is required for all heat treating, both in process annealing and final heat treatment.

2.3.2 Examination

2.3.2.1 Examination of the drum assembly fabrication

The drum and top plug assemblies are examined and tested according to the design drawings, and the portions of the codes, standards, and regulations to the extent described below:

1. *ASME, Boiler and Pressure Vessel Code*, Sect. VIII, Division 1, 2004 edition;
2. *ASME, Boiler and Pressure Vessel Code*, Sect. V, 2004 edition; and
3. SNT-TC-1A-1992, *Recommended Practice for Nondestructive Testing Personnel Qualification and Certification*, American Society For Nondestructive Testing, December 1992.

All welded or weld-repair surfaces shall be visually examined by a qualified weld examiner for indications of inclusions, cracks, or porosity using a written weld examination procedure. Weld examiners are qualified to perform visual weld inspections in accordance with SNT-TC-1A (2001 Edition), "Personnel Qualification and Certification in Nondestructive Testing;" or ANSI/ASNT CP-189 (2001 Edition), "ASNT Standard for Qualification and Certification of Nondestructive Testing Personnel;" published by the American Society for Nondestructive Testing. ASME Boiler and Pressure Vessel Code, Section IX is to be employed as the applicable requirement. Section VIII of the ASME B&PVC Code is invoked for acceptance criteria for Code specified examinations which are to be performed in accordance with the provisions of ASME B&PVC Section V. Any indication of inclusions, cracks, or porosity in the welds is cause for rejection. The item may be reworked to meet the specifications. The weld examination procedures, the weld examiners qualifications, and the weld examination reports are submitted to Y-12 for records. The acceptance criteria for joint fit-up and alignment, and for visual examination of welds are given in the ASME B&PV Code, Section VIII, Division 1, paragraphs UW-31 through UW-36. In addition, any visible defects such as lack of fusion, lack of penetration, linear or crack-like defects, and visible porosity, are cause for rejection. Straightening, flattening, and forming by mechanical or thermal means of some features and components after welding may be required to ensure proper assembly. The surfaces of areas of the weldment that have been worked are visually examined to ensure that no cracks are present or that the weldment has not

been degraded. Adjacent welds to these areas are also visually examined. The acceptance criteria is that no cracks are found. The areas worked and the visual inspections are noted on the dimensional inspection report. The external seam weld of the drum assembly is pressure tested by attaching removable lids on both the top and bottom false wire locations and injecting water and air inside the assembly up to the final pressure of 149.61 kPa (21.7 psia). After all testing, inspection and final machining, the drum assembly and top plug are dimensionally inspected. The dimensions, and features such as flatness, run-out, etc, to be inspected are indicated on the design drawings. A written inspection report is prepared, submitted and maintained for each ES-3100 drum assembly.

The above examination criteria address the stainless-steel components. However, the drum assembly also consists of the Kaolite 1600 material and the Cat 277-4 neutron poison. Acceptance criteria for the installation of the Kaolite 1600 material are addressed by specification JS-YMN3-801580-A003 (Appendix 1.4.4). This specification controls and documents the raw materials used for mixing, casting and vibration methodology, and the baking of the material inside the drum assembly. The final acceptance criterion is achieved by producing a cast Kaolite 1600 material density of 358.8 ± 48 kg/m^3 (22.4 ± 3 lb/ft^3). Acceptance criteria for the installation of Cat 277-4 neutron poison are addressed in specification JS-YMN3-801580-A005 (Appendix 1.4.5). This specification also controls and documents the raw materials used for mixing, casting and vibration methodology, and the final density of the casting [1682 +240/-80 kg/m^3 (105 +15/-5 lb/ft^3)]. Further examination criteria to verify the concentration and homogeneity of the Cat 277-4 in each drum assembly are also provided in specification JS-YMN3-801580-A005. The various parameters specified in NUREG/CR-3854 and in Table 2.11 for a neutron poison are addressed in detail in this specification.

2.3.2.2 Examination of the containment vessel fabrication

The containment vessel is examined and tested according to the design drawings and the following codes, standards, and regulations as described below:

1. *ASME, Boiler and Pressure Vessel Code*, Sect. III, Division 1 Subsections NB and NCA, Class 1 Components, 2004 edition;

2. ANSI N14.5-1997, *American National Standard for Radioactive Materials – Leakage Tests on Packages for Shipment*; *ASME, Boiler and Pressure Vessel Code*, Sect. V, 2001 edition and 2002 and 2003 addenda;

3. ASME, B & PVC, Section V, 2001 edition and 2003 addenda; and,

4. NT-TC-1A-1992, *Recommended Practice for Nondestructive Testing Personnel Qualification and Certification*, American Society For Nondestructive Testing, December 1992.

Procured materials are examined in accordance with the applicable paragraphs of NB-2500, and meet the stated acceptance criteria. The results of these examinations are be included with the CMTRs provided to Y-12. All welded or weld-repair surfaces shall be visually examined by a qualified weld examiner for indications of inclusions, cracks, or porosity. ASME Boiler and Pressure Vessel Code, Section IX is to be employed as the applicable requirements. Section III of the ASME B&PVC Code is invoked for acceptance criteria for Code specified examinations which are to be performed in accordance with the provisions of ASME B&PVC Section V. Prior written approval is obtained for any weld repair on materials, and the weld repair areas are both surface and volumetrically examined. The repair area is noted in a sketch supplied with the CMTR for the material that was weld repaired and the documented results of the weld examination are provided to Y-12. The markings on the weldment materials are not removed until after all weld examination is complete. The heat numbers of base metals and weld filler are

required on all weld examination reports. Control of weld filler by the fabricator permits a weld examiner to be able to determine the heat number of the weld filler used in any weld on the containment vessel.

As previously stated, the containment vessel body may be fabricated by two different methods shown on drawing M2E801580A012 (Appendix 1.4.8). Part number M2E801580A012-4 is fabricated by welding a forged bottom, and forged top flange to a cylindrical shell machined from seamless pipe as shown on the drawing. Prior to welding these components, all weld preparation areas and the surfaces within one inch of the weld are examined visually and with liquid penetrant. The acceptance criteria for these examination are those stated in NB-5130(a) through NB-5130(d). The applicable requirements in paragraphs NB-5110, NB-5120, NB-5210, NB-5220, NB-5260, and NB-5300 apply to the containment vessels. The plug weld shown on Drawing M2E801580A015 (Appendix 1.4.8) shall be examined visually and with penetrant. The applicable requirements in paragraphs NB-5110, and NB-5350 shall apply to the plug weld. Materials used in the penetrant examination of welds and in the final surface examination of finished components (see Section 3.7) shall be specifically recommended by their suppliers for use with austenitic stainless steels, and copies of the certification of contaminant content of materials used (see ASME, Section V, Article 6, T-641) shall be supplied with the examination reports. Repair welding shall meet the applicable requirements of NB-2500. Certified written weld examination reports together with the corresponding material surface examination reports, and weld map shall be submitted as stated in the procurement specification for the containment vessel. Weld examination reports for all weld and surface examination shall include: the containment vessel serial number, a weld map showing the location of the weld and examination area, the welder's name, the examiner's name, the time and date of the weld examination, the examination procedure(s) number used, the WPS number, the heat numbers of the materials joined, the heat number of the weld filler, and examiner's remarks. The examiner's remarks shall include the results of the examination and acceptance, or rejection of the weld based on the stated criteria. One set of radiographs shall be provided with radiographic examination reports. If the weld or surface is rejected, a description of the defect and sketch showing the location shall be provided.

The nonwelded containment vessel body, part number M2E801580A012-1, shall be formed from a single forged billet or bar by any process that meets the requirements stated in JS-YMN3-801580-A001 (Appendix 1.4.3), and shown on the design drawings (Appendix 1.4.8). Such processes may include forging, flow forming, or metal spinning. The formed, heat treated, and finished machined containment vessel body shall meet the applicable requirements of ASME SA 182 for Grade F304L for a forged component. Mechanical properties are verified by testing of coupons. The test coupons are to be machined from the same heats of materials used to form the containment vessel bodies, and shall have the same or greater amount of cold work (plastic strain) as the containment vessels will have as a result of the forming process. The mechanical tensile testing of coupons shall be done in accordance with ASME SA-370. A minimum of six test coupons shall be tested for each final heat treatment furnace charge. The first set of three test coupons, chosen at random, shall be tested without being heat treated. The second set of three or more test coupons shall be heat treated together with the containment vessel bodies, and then tested. The heating rates and maximum temperatures of the test coupons shall be representative of the entire furnace charge. Test coupons are not required to be heat treated with intermediate processing annealing steps, but are required in the final heat treatment furnace charge. The results of all the testing of the sample coupons shall be documented, certified and reported to Y-12. The mechanical properties test report shall contain the following information: a descriptor of the furnace charge in which the test coupons are to represent; the times and dates of the heat treating and the testing; the person responsible for the testing; a statement that these coupons are prior to or after heat treatment; a description of the testing including a sketch of the tensile test specimen; the make, model, serial number, and current calibration data of the testing machine(s) used in the testing; reference to the written testing procedure used; the resulting measure yield strength, ultimate strength, % elongation and % reduction in area; and any pertinent remarks.

2.4 LIFTING AND TIE-DOWN STANDARDS FOR ALL PACKAGES

This section addresses the requirements of 10 CFR 71.45, "Lifting and Tie-Down Standards for All Packages."

2.4.1 Lifting Devices

Requirement. Any lifting attachment that is a structural part of a package must be designed with a minimum safety factor of three against yielding when used to lift the package in the intended manner, and it must be designed so that failure of any lifting device under excessive load would not impair the ability of the package to meet other requirements of 10 CFR 71, Subpart E. Any other structural part of the package that could be used to lift the package must be capable of being rendered inoperable for lifting the package during transport, or must be designed with strength equivalent to that required for lifting attachments.

Analysis. The ES-3100 packages, as delivered for transport, have no lifting devices or structural parts that can be used for lifting. Therefore, the lifting devices requirements of 10 CFR 71.45 are not applicable.

2.4.2 Tie-Down Devices

Requirement. If there is a system of tie-down devices that is a structural part of the package, the system must be capable of withstanding, without generating stress in any material of the package in excess of its yield strength, a static force applied to the center of gravity of the package having a vertical component of two times the weight of the package with its contents, a horizontal component along the direction in which the vehicle travels of ten times the weight of the package with its contents, and a horizontal component in the transverse direction of five times the weight of the package with its contents. Any other structural part of the package that could be used to tie down the package must be capable of being rendered inoperable for tying down the package during transport, or must be designed with strength equivalent to that required for tie-down devices. Each tie-down device that is a structural part of a package must be designed so that failure of the device under excessive load would not impair the ability of the package to meet other requirements of this part.

Analysis. The ES-3100 package, as delivered for transport, has no tie-down devices that are structural parts of the package. Therefore, the tie-down requirements of 10 CFR 71.45 are not applicable. Safe tie down and transport of the package is accomplished by methods explained in the Sandia National Laboratories (SNL) Tie-Down Manual [*Tie-down Procedures for Type B Containers Shipped in Safe-Secure Trailer/Safeguards Transporter (SST/SGT)*]. For single-unit tie-down, a drum tie-down adapter is positioned on top of the drum and two chains, passing through the adapter, are attached to equipment positioned on the floor of the transport vehicle. The welded ring on the drum lid helps to initially position this drum tie-down adapter as well as prevent inadvertent assembly damage to the studs and nuts. Another method of securing the ES-3100 package is by the use of the Cargo-Restraint Transporter (CRT) or Cargo Pallet Assembly (CPA). In these methods, a frame is positioned around the base and top of either five or six packages. These frames are then chained or locked to the floor as depicted in SNL Tie-Down Manual. Tension is applied to the chains to eliminate any slack. The downward load resulting from the chain tensioning is insignificant when compared to the compression loading as specified in 10 CFR 71.71(c)(9).

2.5 GENERAL CONSIDERATIONS

Package structural evaluation is performed by the combination of full scale testing, similarity, and analysis as described in the following sections.

2.5.1 Evaluation by Test

The ES-3100 package was tested in accordance with a test plan developed by the National Transportation Research Center (NTRC) at the Oak Ridge National Laboratory (ORNL) (Appendix 2.10.8). Testing of ES-3100 prototype units was performed at the NTRC facility, except as noted below. Five full-scale test units were assembled with content weights ranging from 3.6 kg (8 lb) to 50.3 kg (111 lb). One of these test units (TU-4) was subjected to the tests specified in 10 CFR 71.71(c)(5) through (c)(10) excluding (c)(8) prior to the HAC sequential tests stipulated in 10 CFR 71.73 and shown in Table 2.18. Test Unit 2 was chilled prior to being subjected to any structural testing (i.e., 1.2-m NCT drop, 9-m HAC drop, HAC crush, and HAC puncture tests). This unit was chilled to a nominal temperature of −40°C (−40°F). This was accomplished by placing the unit in an environmental chamber in Bldg. 5800 at the Oak Ridge National Laboratory (ORNL) with initially setting of the chamber at ~ −57°C (−70°F) for 24 h. After this initial period, the control on the environmental chamber was set to ~ −43°C (−45°F) for another 48 h. Prior to the initiation of structural testing of this unit, it was removed from the environmental chamber and placed in an insulated box. Once transported to the NTRC, sequential structural testing, as shown in Table 2.19 was performed as quickly as possible. The other test units were first subjected to the free drop from 1.2 m (4 ft) test prior to the HAC testing of 10 CFR 71.73. These additional tests were conducted to show that the NCT testing would not reduce the effectiveness of the package to withstand HAC testing. Tables 2.18 and 2.19 summarize the testing procedure and the drop orientations for each ES-3100 test unit.

The essentially unyielding surface used for the 1.2-m (4 ft) drop test was the indoor drop test pad at the NTRC. All 9-m (30-ft) drop and crush tests were conducted at the outside drop pad at the NTRC. The indoor pad consists of a 5.08-cm (2-in.)-thick steel plate embedded inside a reinforced concrete pad ~127 cm (50 in.) thick. The outside drop pad consists of a 10.16-cm (4-in.)-thick steel plate embedded inside a reinforced concrete pad ~167.6 cm (66 in.) thick. An article has been prepared by the NTRC staff to describe the integrity of these test pads (Shappert 1991).

Table 2.18. Summary of NCT – 10CFR71.71 tests for ES-3100 package [a]

Test	TU-1 (heavy) 12° Slap-down	TU-2 (heavy) Side Drop	TU-3 (heavy) CG over Top Corner	TU-4 (heavy) Top Down	TU-5 (light) 12° Slap-down
Operational Leak Test (CALT5)	1	1	1	1	1
NCT – 10CFR71.71 (c)(5) Vibration				5	
NCT – 10CFR71.71 (c)(6) Water Spray				2	
NCT – 10CFR71.71 (c)(7) 1.2 m (4 ft) Free Drop	2	2	2	3	2
NCT – 10CFR71.71 (c)(9) Compression				6	
NCT – 10CFR71.71 (c)(10) Penetration				4	

[a] The numbers 1 through 6 indicate the sequence of the tests.

Table 2.19. Summary of HAC – 10CFR71.73 tests for ES-3100 package [a]

Test	TU-1 (heavy) 12° Slap-down	TU-2 (heavy) Side Drop	TU-3 (heavy) CG over Top Corner	TU-4 (heavy) Top Down	TU-5 (light) 12° Slap-down	TU-6 [b] 15m Immersion
10CFR71.73 (c) (1) Free Drop 9m (30 ft.)	1	1	1	1	1	
10CFR71.73 (c) (2) Crush 9m (30 ft.)	2	2	2	2	2	
10CFR71.73 (c) (3) Puncture 1m (40 in.)	3456	3	3	3	3	
Preheat to above 38 °C (100 °F) before Thermal test	7	4	4	4	4	
10CFR71.73 (c) (4) Thermal 800°C (1475°F)	8	5	5	5	5	
Operational Leak Test of CV (CALT5)	9	6	6	6	6	1
Full Containment Boundary Leak Test (He Leak Test)	10	7	7	7	7	
10CFR71.73 (c) (5) Immersion Test Fissile materials – 0.9 m (3 ft.)	11	8	8	8	8	
10CFR71.73 (c) (6) Immersion Test –All Packages 15 m (50 ft.)						2

[a] The numbers 1 through 11 indicate the sequence of the tests.
[b] TU-6 is only a containment vessel with ballast to ensure non-buoyancy.

Thermal testing of the five test units was conducted at the No. 3 furnace at Timken Steel Company in Latrobe, Pennsylvania. Prior to the testing, the furnace was characterized for temperature and heat recovery times. Oxygen content in stack gases of the furnace was not monitored because it was not anticipated that any of the package's materials of construction were combustible. There was some burning of the silicone pads which are placed between the inner liners and the top plugs of the packages. However, it should be noted that this furnace employs "pulsed" fire burners. This type of burner is unique in that the natural gas flow rate is varied based on furnace controller demands, but the flow of air through the burners is constant, even when no gas is flowing, thereby ensuring a very rich furnace atmosphere capable of supporting any combustion of package materials of construction. The support stand was welded to a large steel plate which had been placed on the floor of the furnace prior to heating. This steel plate acted as the radiating surface at the bottom of the furnace as well as providing the ability to hold the test stand rigidly in place. Before heating the furnace, workers practiced loading and unloading test packages from the cold furnace to assure that the furnace door would not remain open >90 s during each loading. In fact, the maximum time the door was open during any loading was 64 s.

Damage resulting from physical testing is quantitatively described including photographs in Sect. 2.7. The full-scale test units were fabricated in accordance with drawings created for production hardware. During the procurement process for the full-scale test units, several small changes were suggested by the manufacturer to improve the efficiency and to reduce the cost of fabrication. These changes were incorporated and tested. However, following compliance testing the following changes have been made to the proposed production hardware. First, a change in the neutron poison from BoroBond4 to Cat 277-4 has been adopted; second, the mid liner design has been changed to a continuous shell by reducing the diameter of the step in the inner liner for the CV flange from 22.35 cm (8.8 in.) to 21.84 cm (8.6 in.); and third, the silicone rubber pad thickness on the drum assembly bottom liner was increased by ~0.15 cm (0.06 in.). The second change increased the amount of Kaolite 1600 around the CV flange, increased the final volume of the neutron poison, and slightly decreased the volume of the Kaolite 1600 adjacent to the neutron poison. The third change was made to stiffen the rubber pad so it would remain in place during vibration normally incurred during transport. In order to evaluate the impact of these changes, analytical drop simulations were conducted and documented in Appendix 2.10.2. The drop simulations were conducted in the same attitude and temperature regime as those conducted during the compliance testing phase for certification. The results of the structural deformation from compliance testing, drop simulation using BoroBond4 and drop simulations using Cat 277-4 material are presented in Sect. 2.7.8. The analytical structural deformation results shown in Tables 2.52 through 2.61 are nearly identical between the two neutron poisons. The analytical results are also well representative of the results recorded during compliance testing. Analytical strain prediction in the structural components are also compared. Although there are minor differences between simulations, the overall magnitude of the strains are very similar. The thermal aspects of these changes are addressed in Sect. 3. NCT and HAC results predicted for an undamaged package show that the change in neutron poison actually reduces the final temperature of the containment vessel components. Therefore, the substitution of Cat 277-4 material and the minor changes in the inner and mid liners for production hardware should not reduce the effectiveness of the packaging when subjected to the regulatory requirements of 10 CFR 71 and the results of compliance testing would be analogous.

The contents used as surrogate payloads for the test units are shown on drawings M2E801580A029, and M2E801580A027. In the light-weight configuration, the contents consist of three 25.4 cm (10 in.) high convenience cans with handles, and 4 silicone rubber pads. These convenience cans, handles and silicone rubber pads are identical to those proposed for transport. The bottom convenience can was filled with tungsten grit until the convenience can and grit assembly weighed ~3 kg (6.6 lb). The actual weight of the tungsten grit was 2.77 kg (6.11 lb). The total content weight for the light- weight content configuration including the convenience cans, silicone rubber pads, can handles, and tungsten grit was ~3.6 kg (8 lb). In the heavy-weight configurations, the surrogate

payload consists of three steel cylindrical shaped components with handles, two can spacers filled with BoroBond4 and handles, and 6 silicone rubber pads. The can spacers, handles and silicone rubber pads are identical to those proposed for transport. These components weighed a total of approximately 50 kg (110.2 lb). These different weight assemblies bound the range of possible content configurations and structural deformation resulting from compliance testing. Since the decay heat of the proposed contents is ~0.4 W, little or no impact on the pressure or temperature of the package components will result during NCT. Differences in thermal capacitance of these surrogate payloads from the proposed HEU contents during HAC thermal testing are evaluated in Sect. 3.5.3.

2.5.2 Evaluation by Analysis

Although physical testing of the ES-3100 containers was performed generally at or near room temperature except for Test Unit-2, the effectiveness of the Kaolite insulating material at various temperature extremes was examined through the use of laboratory testing and structural analysis of a similar package, the ES-2LM (Handy 1997). For low-temperature service, Kaolite specimens were tested at -28.89 and -40°C (-20 and -40°F). These tests showed little change in the response of the material as compared to room temperature. Furthermore, structural analyses for bounding soft and stiff material cases were run. The Kaolite 1600 data used in these bounding analyses were from laboratory experiments that used a heavily cured sample (stiff) and a sample to which borax had been added (soft) [Oaks 1997]. Following the production run for the ES-2100 and DPP-2 shipping containers, new casting specimens were available for compression testing. In order to reduce the total cost of Kaolite testing, specimens were tested to approximately -40°C (-40°F) to cover both the cold conditions stipulated in 10 CFR 71.71(c)(2) and the -29°C (-20°F) temperature stipulated in 10 CFR 71.71(b)(1) and at 38°C (100°F). The results of Kaolite specimen testing are documented in Y/DW-1890 (Smith and Byington, Appendix 2.10.3) and Y/DW-1972 (Smith, Appendix 2.10.3). Upon further review of the data, the new test data was somewhat stiffer in the cold/high-density specimens than the data previously used in Y/DW-1972 (Smith, Appendix 2.10.3). Therefore, in order to encompass the extremes of all existing data, an additional drop simulation sequence using the new bounding curves has been conducted on the ES-3100 package as documented in Appendix 2.10.2. In addition to the analytical effort, the ES-3100 Test Unit-2 was pre-chilled to a nominal temperature of -40°C (-40°F). This was accomplished by placing the unit in an environmental chamber in Bldg. 5800 at ORNL and initially setting the chamber control to -56.7°C (-70°F) for 24 hours. After this initial period, the control on the environmental chamber was set to -42.8°C (-45° F) for at least 48 hours. Prior to the initiation of structural testing of this unit, it was removed from the environmental chamber and placed in an insulated box and transported to the NTRC. High-temperature [up to 38°C (100°F)] behavior was not addressed. However, in light of the fact that the insulation material is typically used as a cast refractory insulation in furnace applications, and that structural tests were performed in the range of 20.8 to 30.6°C (69.4 to 87°F) or just 7.4 to 17.2°C (13 to 30°F) below the high-temperature limit, it is not anticipated that any decline in impact absorption would be detrimental at 38°C (100°F).

2.6 NORMAL CONDITIONS OF TRANSPORT

This section demonstrates compliance with 10 CFR 71.43(f) and with 10 CFR 71.51(a)(1) and (b) following the tests and NCT conditions stipulated in 10 CFR 71.71. It is shown that the package will not experience any loss in shielding effectiveness or spacing and will not release any radioactive content or undergo leakage of water into the containment vessel during exposure to NCT. The four tests (water spray, free drop, compression, and penetration) made on Test Unit-4 were conducted in the 20.8 to 22.4°C (69.4 to 72.4°F) range, with the 1.2-m drop test conducted at 22.4°C (72.4°F). The maximum regulatory reference air leakage rate is $\leq 2.2840 \times 10^{-3}$ ref-cm^3/s. Compliance with this permitted activity

release limit is not dependent on filters or mechanical cooling systems. Following NCT compliance testing, the package was subjected to the sequential HAC test battery.

Title 10 CFR 71.71(b) specifies that the tests for NCT be conducted at the most unfavorable ambient temperature within the range of −28.89 to 38°C (−20 to 100°F). The drum is fabricated from type 304 stainless steel, and the containment boundary is fabricated from type 304L stainless steel, which is particularly suitable for low-temperature service. The Izod impact strength for the stainless steel used in the package components remains constant over a large range [specifically, from 21.11 to −195.5°C (70 to −320°F)] (*Stainless Steel Handbook*). Tensile strength increases from a minimum of 4.826×10^5 to 1.696×10^6 kPa (70,000 to 246,000 psi), and the yield strength increases about 10% over the same temperature range. The O-rings in the containment vessel have a normal service temperature range of −40 to 150°C [−40 to 302°F (Table 2.15)]. The normal service temperature range of the drum and containment vessel is −40 to 426.7°C (−40 to 800°F) [ASME, B&PV Code, Sect. II, Part D]. At −28.89°C (−20°F), the impact limiting material has been shown by tests to be stiffer than at 22.4°C (72.4°F). This condition has been evaluated by the compliance testing conducted on Test Unit-2. The reduction in tensile strength of the stainless steel from 22.4 to 38°C (73 to 100°F) is only approximately 2%, and the impact-limiting material test trends show that the impact-limiting material may become slightly softer. However, these slight reductions in tensile strength and absorption characteristics should not affect the results significantly compared to those conducted at 38°C (100°F).

Title 10 CFR 71.71(b) also states that the initial internal pressure within the containment system during NCT drop testing shall be considered as the maximum normal operating pressure. The maximum normal operating pressure is defined in 10 CFR 71.4 as the maximum gauge pressure that would develop in the containment system in a period of 1 year under the heat conditions specified in 10 CFR 71.71(c)(1). The internal pressure developed under these conditions in the ES-3100 containment vessel is calculated in Appendix 3.6.4 and discussed in Sects. 2.6.1.1 and 3.4.2. As noted in these sections, the internal pressure is calculated to be 200.20 kPa (29.036 psia). As shown in Appendix 2.10.1, the design absolute pressure of the containment vessel is 801.17 kPa (116.2 psia), and the hydrostatic test pressure stipulated in JS-YMN3-801580-A001 is 1135.57 kPa (164.7 psia). Thus, increasing the internal pressure of the containment vessel to a maximum of 200.20 kPa (29.036 psia) during NCT would have no detrimental effect. Table 2.20 provides a summary of the pressures and temperatures in the various shipping configurations. As discussed in Sect. 2.6.1.4, the containment vessel and the closure nut stresses for this pressure condition are well below the allowable stress values.

Title 10 CFR 71.71(c) specifies that the package service temperature must extend from −40 to 38°C (−40 to 100°F) with solar insolation. As shown in Sect. 3.4.1 and calculated in Appendix 3.6.2, the upper service temperature with solar insolation is calculated to be 87.81°C (190.06°F) for an empty ES-3100 containment vessel. Thermal cycling of the packages over the above temperature range from −40°C (−40°F) is considered an unlikely event, and the change would occur over a long period of time. In any event, the 127.81°C (230.06°F) thermal cycle would not result in brittle fracture or fatigue failure in the packaging. The acceptability of the packaging against brittle fracture is discussed in Sect. 2.6.2. The only concern for fatigue or endurance failure is related to the containment boundary cyclic pressure changes as the temperature varies from low to high. A 25°C (77°F) ambient temperature normally exists for the containment boundary during assembly. The containment boundary is sealed at an absolute pressure of ~101.35 kPa (14.70 psi). The internal absolute pressure at an average gas temperature of 87.81°C (190.06°F) is 200.20 kPa (29.036 psi) for the ES-3100 containment vessel (Table 2.20). The absolute internal pressure at −40°C or −40°F is 76.74 kPa (11.13 psi) for the containment vessel. Therefore, the maximum cyclic pressure differential for the containment vessel from low to high

temperatures is (200.20 – 76.74) kPa or 123.46 kPa (17.906 psi). This cyclic pressure is insignificant when considering the integrity of the containment boundary as shown by the stress levels discussed in Sect. 2.6.1.3.

The ES-3100 package has been tested to determine the effectiveness of the package following a sequential NCT 1.2-m (4-ft) drop test and an HAC test battery. Testing conducted on Test Unit-4 showed that there would be no loss or dispersal of radioactive contents and no significant increase in external surface radiation levels if the actual contents had been subjected to these tests, and no substantial reduction in the effectiveness of the packaging to survive the HAC testing. Thus, the requirements of 10 CFR 71.43(f) are satisfied.

Table 2.20. Summary of temperatures and pressures for NCT

Average gas evaluation temperature °C (°F)	Containment vessel absolute internal pressure kPa (psia)
-40 (-40) [a]	76.74 (11.13)
25.0 (77) [b]	101.35 (14.70)
87.81 (190.06) [c]	200.20 (29.036)

[a] Analysis conducted with no decay heat load in accordance with 10 CFR 71.71(c)(2).
[b] Assembly temperature and pressure.
[c] Due to the lack of measurable off-gassing, all ES-3100 containment vessel configurations with solar insolation, and 0.4 W decay heat produce the same internal pressure (Appendix 3.6.4).

2.6.1 Heat

Requirement. Exposure to an ambient temperature of 38°C (100°F) in still air and insolation as stated in 10 CFR 71.71(c)(1).

Analysis. An increase in ambient temperature to 38°C (100°F) with insolation will have no effect on the ability of the containment boundary to provide containment.

The maximum normal operating pressure is defined in 10 CFR 71.4 as the maximum gauge pressure that would develop in the containment system in a period of 1 year under the heat conditions specified in 10 CFR 71.71(c)(1). The internal pressure developed under these conditions in the ES-3100 containment vessel is calculated in Appendix 3.6.4 and discussed in Sects. 2.6.1.1 and 3.4.2. As noted in these sections, the internal pressure varies with temperature. Based on the isotopic determination of the proposed contents, a decay heat of 0.4W was calculated and used for the maximum internal heat load in evaluating the package for NCT (Sect. 3.1.2). The maximum calculated internal absolute pressure in the containment vessel with solar insolation and using the bounding case parameters is 200.20 kPa (29.036 psia). The design absolute pressure of the containment vessel is 801.17 kPa (116.20 psia), and the hydrostatic test pressure is 113.55 kPa (164.7 psia). Thus, increasing the internal pressure of the containment vessel to a maximum of 200.20 kPa (29.036 psia) during NCT would have no detrimental effect. Table 2.20 provides a summary of the pressures and temperatures for the various shipping configurations. As discussed in Sect. 2.6.1.4, the containment vessel and closure nut stresses for these pressure conditions are well below the allowable stress values. If the package is exposed to solar radiation at 38°C (100°F) in still air, the conservatively calculated temperatures at the top of the drum, on the surface of the containment vessel, and on the containment vessel near the O-ring sealing surfaces

are 117.72°C (243.89°F), 87.81°C (190.06°F), and 87.72°C (189.9°F), respectively (Sect. 3.4.1). Nevertheless, these temperatures are within the service limits of all packaging components, including the O-rings. The normal service temperature range of the O-rings used in the containment boundary is −40 to 150°C (−40 to 302°F) as shown in Table 2.15.

2.6.1.1 Summary of pressures and temperatures

An ambient temperature of 25°C (77°F) is assumed for the packaging at assembly. Since there are four ventilation holes near the top of the drum, and holes in the liner encapsulating the neutron poison material that are not hermetically sealed, the drum assembly will not become pressurized as the temperature increases. The containment boundary is sealed; thus, the internal pressure will change with temperature. Maximum calculated pressures at various temperatures (Sect. 3.4.1) are listed in Table 2.20.

2.6.1.2 Differential thermal expansion

The drum, inner liners, and containment vessel are all constructed of type 304 or 304L stainless steel. Radial and vertical expansion among these components will not cause any interferences or thermally induced stresses due to design clearances at assembly. Due to similarities of the coefficient of thermal expansion between type 304/304L and the containment vessel closure nut material (ASME SA-479), the compression of the O-rings does not change appreciably during the temperature excursion from 25°C (77°F) to the maximum temperature of 87.81°C (190.06°F).

The Kaolite 1600 insulation and Cat 277-4 material is poured and cast in place during the fabrication of the drum weldment (Drawing M2E801508A002, Appendix 1.4.8). Although some contraction of these materials may occur during curing, it is assumed for analysis purpose that a zero gap will exist between the Kaolite and the bounding drum and mid liner and a zero gap exists between the Cat 277-4 and the two liners. Due to differences in coefficients of thermal expansion, some radial and axial interferences are expected due to thermal growth of the inner liners. These radial and axial interferences and induced stresses are calculated in Appendix 3.6.3. A maximum von Mises stress of 6.693×10^4 kPa (9708 psi) was calculated for the inner liners. This stress value is well below the allowable yield strength of 1.324×10^5 kPa (19200 psi) at 148.9°C (300°F). A maximum von Mises stress of 1.379×10^3 kPa (200 psi) and 1.034×10^3 kPa (150 psi) occurs in the Cat 277-4 and Kaolite 1600 materials, respectively. Based on tabulated data and curves presented in Y/DW-1987 (Smith and Byington, Appendix 2.10.4) and the curves presented in Y/DW-1972 (Smith, Appendix 2.10.3) at 38°C (100°F), these compressive stresses are well below the failure limit of ~4.826×10^3 kPa (700 psi) and 5.171×10^3 kPa (750 psi) for the Cat 277-4 and Kaolite 1600 materials, respectively. Therefore, these thermally induced stresses will not reduce the effectiveness of the drum assembly.

The effects of differences in coefficient of thermal expansion between the HEU contents and their associated convenience cans, polyethylene or Teflon FEP bottles are not addressed. No credit is taken for the ability of the convenience can or bottle to maintain it structural integrity during transport. Section 4 of this document assumes the HEU content is in the form of an aerosol and all is available for release; therefore, no credit for the convenience can or bottle is taken. Based on assembly clearances and the flexibility of the polyethylene or Teflon FEP bottles, no radial or vertical interferences will develop during NCT. Based on assembly clearances and insignificant differences in the coefficient of thermal expansion between the stainless-steel, tin-plated carbon steel, or nickel-alloy convenience cans and the stainless-steel containment vessel, no radial or vertical interferences will develop during NCT testing.

2.6.1.3 Stress calculations

During normal conditions, stresses are only imposed by changes in internal pressure of the containment boundary as the temperature varies slowly over the operating range as shown in Table 2.20. Stress levels imposed on the package during NCT are insignificant, as shown in Tables 2.21, and 2.22. These tabulated stresses were determined by multiplying the stress at the design conditions (Appendix 2.10.1 and Table 2.6) by a factor equal to the ratio of operating pressures to design pressures and adding any contribution from the closure nut preload. This methodology is based on linear elastic material behavior. As shown in Sect. 2.6.1.4, all stresses in the containment boundary components are well below the *ASME Boiler and Pressure Vessel Code* allowable stress intensity limits.

2.6.1.4 Comparison with allowable stresses

NCT containment vessel stresses are calculated in accordance with the load combinations listed in Table 2.3 and their values are shown in Tables 2.21 and 2.22. The hot environment, cold environment, minimum external pressure, increased external pressure condition, and vibration normally incident to transport are addressed in Sects. 2.6.1, 2.6.2, 2.6.3 , 2.6.4, and 2.6.5, respectively. The fatigue or endurance limits for austenitic stainless steel are normally assumed to be about one-half the ultimate tensile strength (*Design Guidelines for Selection of Stainless Steel*, pp. 17–18). For type 304 stainless steel, one-half the ultimate tensile strength is 2.4×10^5 kPa (35,000 psi). Tensile and compressive hoop stresses of the magnitude shown in Tables 2.21 and 2.22 are insignificant compared to the endurance limit of 2.4×10^5 kPa (35,000 psi). As shown in Tables 2.21 and 2.22, the containment vessel stresses during NCT are insignificant. Even at the maximum test temperature and internal pressure (Sect. 3.5.3), the stresses in the containment boundaries were insignificant when compared with the allowable stress intensities shown in Tables 2.4 and 2.5. Corresponding calculated stress regions are shown in Fig. 2.1. Thermal expansion or contraction issues are addressed in Sects. 2.6.1.2 and 2.6.2.

2.6.2 Cold

Requirement. An ambient temperature of −40°C (−40°F) in still air and shade, as required by 10 CFR 71.71(c)(2).

Analysis. The drum is fabricated from type 304 stainless-steel sheet (Table 2.7). As discussed in Sect. 2.6, stainless steel is excellent for low-temperature service, particularly regarding tensile and impact strength. The thermal insulation (Kaolite) is a lightweight noncombustible cast refractory made from portland cement and vermiculite. The only moisture available for freezing at −40°C (−40°F) would be moisture that had not been removed during the curing and cool-down phase of fabrication. Because there will be no free water present for freezing and the insulation is a bonded mass of random fibers and cement, the properties of the insulation will not change appreciably. The matrix may become less flexible when subjected to the cold temperature, but the inner liner will remain in the position in which it was placed at the time of fabrication. The Kaolite 1600 insulation and Cat 277-4 materials are poured and cast in place during the fabrication of the drum weldment (Drawing M2E801508A002, Appendix 1.4.8). Although some contraction of these material may occur during curing, it is assumed for analysis purposes that a zero gap will exist between the Kaolite and the bounding drum and mid liner and a zero gap exists between the Cat 277-4 and the two liners. Due to differences in the coefficient of thermal expansion, some radial and axial interference is expected due to contraction of the outer drum and inner liners. These radial and axial interferences and induced stresses are calculated in Appendix 3.6.3. A maximum von Mises stress of 6.115×10^4 kPa (8869 psi) was calculated for the inner liners. This stress value is well below the allowable yield strength of 1.724×10^5 kPa (25000 psi) at −40°C (−40°F). A maximum von Mises stress of 979 kPa (142 psi) and 510 kPa (74 psi) occurs in the Cat 277-4 and Kaolite 1600 materials, respectively. Based on tabulated data and curves presented in Y/DW-1987 (Smith and

Byington, Appendix 2.10.4) and the curves presented Y/DW-1972 (Smith, Appendix 2.10.3) at −40°C (−40°F), these compressive stresses are well below the failure limit of ~ 6.895×10^3 kPa (1000 psi) and 5.308×10^3 kPa (770 psi) for the Cat 277-4 and Kaolite 1600 materials, respectively. Therefore, these thermally induced stresses will not reduce the effectiveness of the drum assembly.

The containment boundary is fabricated from type 304L stainless steel, which is suitable for low-temperature service, particularly regarding impact resistance. This material does not show a transition from ductile to brittle failure at this temperature. The *ASME Boiler and Pressure Vessel Code*, Sect. III, Subsection NB-2311, exempts impact testing of type 304L stainless steels. The Izod impact strength for type 304 stainless steel is 149.14 N·m (110 ft-lb) from 21.11 to −195.5°C (70 to −320°F). The tensile strength increases from ~4.826×10^5 to 1.696×10^6 kPa (70,000 to 246,000 psi) between 21.11 and −195.5°C (70 and −320°F), and the yield strength increases about 10% over the same range. NRC Regulatory Guide 7.6, Part B, states, "these designs were made of austenitic stainless steel which is ductile even at low temperatures. Thus, this guide does not consider brittle fracture." The drum, inner liner, top plug, and containment boundary are made from austenitic stainless steel. Similarly, the containment boundary closure nut material is a galling and wear resistant austenitic stainless steel. Therefore, brittle fracture of these structural materials at −40°C (−40°F) is not possible.

The specified O-rings used in the containment boundary have a continuous service temperature range of −40 to 150°C (−40 to 302°F) as shown in Table 2.15. The low temperature extreme has been verified by compliance testing of Test Unit-2 (Sect. 2.7.1.2). Test Unit-2 was pre-chilled to a nominal temperature of −40°C (−40°F). This was accomplished by placing the unit in an environmental chamber in Bldg. 5800 at ORNL and initially setting the chamber control to −56.7°C (−70°F) for 24 hours. After this initial period, the control on the environmental chamber was set to −42.8°C (−45°F) for at least 48 hours. Prior to the initiation of structural testing of this unit, it was removed from the environmental chamber and placed in an insulated box and transported to NTRC for testing.

As previously noted, the containment vessels will be assembled for shipment in a temperature environment of ~25°C (77°F). If the package should be exposed to −40°C (−40°F) for an extended period, all components will equalize near this low temperature. The absolute internal pressure inside the containment boundary would decrease to a pressure of 76.74 kPa (11.13 psi), assuming no decay heating (Table 2.20). Therefore, the pressure differential across the containment vessel at −40°C (−40°F) is −24.61 kPa (−3.57 psia) [76.739 − 101.35 kPa] (11.13 − 14.7 psia). Due to similarities of the coefficient of thermal expansion between type 304/304L and the containment vessel closure nut material (Nitronic 60, ASME SA-479), the compression of the O-rings does not change appreciably during the temperature excursion from 25°C (77°F) to −40°C (−40°F). The calculated stresses shown in Table 2.21 were determined by multiplying the stress at the design conditions (Appendix 2.10.1 and Table 2.6) by a factor equal to the ratio of operating pressure to design pressure and adding any contribution from the closure nut preload. This methodology is based on linear elastic material behavior. As shown in Sect. 2.6.1.4, all stresses in the containment boundary components are well below the *ASME Boiler and Pressure Vessel Code* allowable stress intensity limits. As demonstrated by the information presented above, the packaging is acceptable for NCT at −40°C (−40°F).

Table 2.21. ES-3100 containment boundary evaluation for both hot and cold conditions [a]

Stress locations shown in Fig. 2.1	Hot conditions [10 CFR 71.71(c)(1)] containment boundary stress @ 98.84 kPa 14.336 psi) gauge		Cold conditions [10 CFR 71(c)(2)] containment boundary stress @ −24.61 kPa (−3.57 psi) gauge		Allowable stress or shear capacity (AS)
	kPa (psi) or kg (lb)	M.S.	kPa (psi) or kg (lb)	M.S.	kPa (psi) or kg (lb)
Top flat portion of sealing lid (center of lid)	9.738×10^2 (141.2)	134.9	2.425×10^2 (35.17)	545	1.324×10^5 (19,200) [b]
Closure nut ring (away from threaded portion)	5.039×10^4 (7,308.8)	8.1	4.246×10^4 [f] (6,158)	9.8	4.571×10^5 (66,300) [c]
Top flat head (sealing surface region)	1.901×10^4 (2,757.2)	12.9	1.665×10^4 [f] (2,415)	14.9	2.648×10^5 (38,400) [c]
Cylindrical section (middle)	2.823×10^3 (409.5)	30.3	7.030×10^2 (102)	124.5	8.825×10^4 (12,800) [d]
Cylindrical section (shell to flange interface)	1.061×10^4 (1,538.2)	24.0	8.034×10^3 (1,165.2)	32	2.648×10^5 (38,400) [c]
Cylindrical section (shell to bottom interface)	7.241×10^3 (1,050.3)	35.6	1.803×10^3 (261.5)	145.8	2.648×10^5 (38,400) [c]
Body flange threads load, kg (lb)	1.069×10^3 (2,356.1)	18.2	9.072×10^2 [f] (2,000)	21.6	2.053×10^4 (45,266) [e]
Body flange thread region (under cut region)	2.961×10^4 (4,294.0)	7.9	2.256×10^4 [f] (3,272)	10	2.648×10^5 (38,400) [c]
Flat bottom head (center)	6.817×10^3 (988.7)	18.4	1.698×10^3 (246.2)	77	1.324×10^5 (19,200) [b]
Closure nut thread load, kg (lb)	2.356×10^3 (1,068.7)	32.2	9.072×10^2 [f] (2,000)	38.1	3.545×10^4 (78,154) [e]

[a] Calculated stresses were determined by multiplying the stress at the design conditions (Appendix 2.10.1) by a factor equal to the ratio of operating pressures to design pressures (independent of pressure direction) plus contribution from preload. Allowable stress values are taken from Table 2.5.

[b] Stress interpreted as the sum of $P_l + P_b$; allowable stress intensity value is $1.5 \times S_m$.

[c] Stress interpreted as the sum of $P_l + P_b + Q$; allowable stress intensity value is $3.0 \times S_m$.

[d] Stress interpreted as the primary membrane stress (P_m); allowable stress intensity value is S_m.

[e] Allowable shear capacity is defined as $0.6 \times S_m \times$ thread shear area. Thread shear area = 38.026 cm^2 (5.894 in.^{2}).

[f] Stress and shear load in these areas are dominated by the 162.7 ± 6.8 N·m (120 ± 5 ft-lb) preload.

2.6.3 Reduced External Pressure

Requirement. An absolute external pressure of 25 kPa (3.5 psi) is required by 10 CFR 71.71(c)(3).

Analysis. Reducing the absolute external pressure from ambient pressure to 25 kPa (3.626 psi) will have no effect on the drum assembly because the plastic plugs and aluminum tape covering the ventilation holes for the Cat 277-4 will allow the internal pressure of the drum assembly to equalize. This reduced pressure and a maximum internal pressure produces the maximum pressure differential across the containment boundary of 175.20 kPa (25.410 psi) [200.20 - 25 (29.036 - 3.626)]. The containment boundary is designed and fabricated in accordance with Sects. III and IX of the *ASME Boiler and Pressure Vessel Code* for an internal pressure differential of 699.82 kPa (101.5 psi) as shown in Appendix 2.10.1. A summary of the resulting stress intensities at various locations identified in Fig. 2.1 on the containment vessel in comparison with the ASME code allowable limits for this condition is shown in Table 2.22. These tabulated stresses were determined by multiplying the stress at the design conditions (Appendix 2.10.1 and Table 2.6) by a factor equal to the ratio of operating pressures to design pressures and adding any contribution from the closure nut preload. This methodology is based on linear elastic material behavior. As shown in Table 2.22, all stresses in the containment boundary components are well below the *ASME Boiler and Pressure Vessel Code* allowable stress intensity limits. Therefore, the ES-3100 packaging is acceptable for NCT at an absolute external pressure of 25 kPa (3.626 psi).

2.6.4 Increased External Pressure

Requirement. An absolute external pressure of 140 kPa (20 psi) is required by 10 CFR 71.71(c)(4).

Analysis. Increasing the absolute external pressure from ambient pressure to 140 kPa (20.31 psi) would have no effect on the drum assembly because the plastic plugs and aluminum tape covering the ventilation holes for the Cat 277-4 will allow the internal pressure of the drum assembly to equalize. At this increased external pressure, the maximum pressure differential across the containment boundary would be -63.26 kPa (-9.18 psi) [76.74 - 140 (11.13 - 20.31)], assuming the vessel's absolute pressure and temperature to be 76.74 kPa (11.13 psi) and -40°C (-40°F), respectively. Each containment boundary is designed and fabricated in accordance with Sects. III and IX of the *ASME Boiler and Pressure Vessel Code* for a minimum external pressure of 150 kPa (21.7 psi) gauge. A comparison of the resulting stress intensities at various locations on the containment vessel (Fig. 2.1) with the ASME code allowable limits for this condition is shown in Table 2.22. These tabulated stresses were determined by multiplying the stress at the design conditions (Appendix 2.10.1 and Table 2.6) by a factor equal to the ratio of operating pressures to design pressures and adding any contribution from the closure nut preload. This methodology is based on linear elastic material behavior. As shown in Table 2.22, all stresses in the containment boundary components are well below the *ASME Boiler and Pressure Vessel Code* allowable stress intensity limits. Therefore, the ES-3100 packaging is acceptable for NCT at an external absolute pressure of 140 kPa (20.31 psi).

Table 2.22. NCT ES-3100 containment boundary stress compared to the allowable stress at reduced and increased external pressures [a]

Stress locations shown in Fig. 2.1	Reduced external pressure [10 CFR 71.71(c)(3)] containment boundary stress @ 175.20 kPa (25.410 psi) gauge kPa (psi)		Increased external pressure [10 CFR 71.71(c)(4)] containment boundary stress @ −63.26 kPa (−9.18 psi) gauge kPa (psi)		Allowable stress or shear capacity (AS)
	kPa (psi) or kg (lb)	M.S.	kPa (psi) or kg (lb)	M.S.	kPa (psi) or kg (lb)
Top flat portion of sealing lid (center of lid)	1.726×10^3 (250.3)	75.7	6.236×10^2 (90.4)	211.3	1.324×10^5 (19,200) [b]
Closure nut ring (away from threaded region)	5.533×10^4 (8,025.6)	7.3	4.246×10^4 [f] (6,158)	9.8	4.571×10^5 (66,300) [c]
Top flat head (sealing surface region)	2.021×10^4 (2,931.7)	12.1	1.665×10^4 [f] (2415)	14.9	2.648×10^5 (38,400) [c]
Cylindrical section (middle)	5.004×10^3 (725.7)	16.6	1.808×10^3 (262.2)	47.8	8.825×10^4 (12,800) [d]
Cylindrical section (shell-to-flange interface)	1.325×10^4 (1,921.7)	19.0	9.374×10^3 (1,359.6)	27.2	2.648×10^5 (38,400) [c]
Cylindrical section (shell-to-bottom interface)	1.284×10^4 (1,861.6)	19.6	4.637×10^3 (672.5)	56.1	2.648×10^5 (38,400) [c]
Body flange threads load, kg (lb)	1.194×10^3 (2,631.1)	16.2	9.072×10^2 [f] (2,000)	21.6	2.053×10^4 (45,266)
Body flange thread region (under cut region)	3.354×10^4 (4,865.2)	6.9	2.397×10^4 [f] (3,476)	10	2.648×10^5 (38,400) [c]
Flat bottom head (center)	1.208×10^4 (1,752.4)	10.0	4.365×10^3 (633)	29.3	1.324×10^5 (19,200) [b]
Closure nut thread load, kg (lb)	1.194×10^3 (2,631.1)	28.7	9.072×10^2 [f] (2,000)	38.1	3.545×10^4 [e] (78,154)

[a] Calculated stresses were determined by multiplying the stress at the design conditions (Appendix 2.10.1) by a factor equal to the ratio of operating pressures to design pressures (independent of pressure direction) plus contribution from preload. Allowable stress values are taken from Table 2.5.

[b] Stress interpreted as the sum of $P_l + P_b$; allowable stress intensity value is $1.5 \times S_m$.

[c] Stress interpreted as the sum of $P_l + P_b + Q$; allowable stress intensity value is $3.0 \times S_m$.

[d] Stress interpreted as the primary membrane stress (P_m); allowable stress intensity value is S_m.

[e] Allowable shear capacity is defined as $0.6 \times S_m \times$ thread shear area. Thread shear area = 38.026 cm^2 (5.894 $in.^2$).

[f] Stress and shear load in these areas are dominated by the 162.7 ± 6.8 N·m (120 ± 5 ft-lb) preload.

2.6.5 Vibration

Requirement. Vibration normally incident to transportation is required by 10 CFR 71.71(c)(5).

Analysis. Vibration testing on a prototypical ES-3100 package (Test Unit-4) was conducted in accordance with the ES-3100 test plan (Appendix 2.10.8) and documented in the test report (Appendix 2.10.7). Testing was conducted with the package restrained as shown in Fig. 2.3. The containment vessel was assembled with the mock-up content weighing 49.90 kg (110 lb). The total weight of the test unit was 201.8 kg (445 lb). The unit was subjected to an endurance test with random vibrations modeled after the power spectral density plot for the Safe-Secure Trailer/Safeguards Transporter (SST/SGT) vibration envelope in the vertical axis (Cap, Appendix 2.10.6). At this level of vibration intensity, the test unit compares with MIL-STD-810F. MIL-STD-810F is a standard random vibration test for basic transportation vibrations generated by a large truck or tractor-trailer combination. MIL-STD-810F defines 60 min of testing as equal to 1609 km (1000 miles) of common carrier transportation. Assuming that the two random vibration tests are similar in intensity, Test Unit-4 had about 6436 km (4000 miles) of simulated random vibration testing. Based on a nominal shipping distance of 3218 km (2000 miles), Test Unit-4 was subjected to a test that was approximately two times more severe than that required by 10 CFR 71.71(c)(5). As shown by the following paragraphs, containment, shielding effectiveness, and subcriticality were maintained even when the package was subjected to such an arduous environment.

The test was run at ~22.8 °C (73 °F) rather than at the high or low temperatures specified for NCT. This was reasonable because the thermal coefficients of expansion of the flange and closure nut materials are very close. Therefore, the temperature extremes would not have a significant effect on the closure tightness.

Summarizing 10 CFR 71.43(f), the tests and conditions of NCT shall not substantially reduce the effectiveness of the packaging to withstand HAC sequential testing. The effectiveness of the ES-3100 to withstand HAC sequential testing is not diminished through application of the tests and conditions stipulated in 10 CFR 71.71. The justification for this statement is provided by physical testing of both the ES-2M (Byington 1997) and ES-3100 test packages. Due to the similarities in design, fabrication, and construction materials of the ES-2M and the ES-3100 packages, the physical characteristics of the Kaolite 1600 will hold true for both designs. The integrity of the Kaolite 1600 is not significantly affected by the NCT vibration and 1.2-m drop tests. Prior to testing the ES-2M design, each test unit was radiographed to determine the integrity of the Kaolite 1600 impact and insulation material. Following casting of the material inside the drum, some three-dimensional curving cracks were seen in some packages near the thinner top sections from the bottom of the liner to the bottom drum edge. After vibration testing, radiography of the ES-2M Test Unit-4 showed that the lower half of the impact limiter was broken into small pieces. In order to evaluate these findings, Test Unit-4 was reassembled and subjected to HAC sequential testing. After vibration and impact testing, many three-dimensional curving cracks were seen around the impact areas, and the inner liner was visibly deformed. Nevertheless, Test Unit-4 maintained the adequate spacing required for shielding effectiveness and subcriticality. Temperatures at the containment boundary were also similar to other packages not subjected to vibration testing prior to HAC testing. No inleakage of water was recorded following immersion. Additionally, Test Unit-4 of the ES-3100 test series was subjected to tests and conditions stipulated in 10 CFR 71.71(c)(5) through (c)(10), excluding (c)(8). Following completion of both the NCT and HAC tests, the containment vessel was removed, and a full-body helium leak test was conducted to the leaktight criterion ($\leq 2 \times 10^{-7}$ cm^3/s) in accordance with ANSI N14.5-1997.

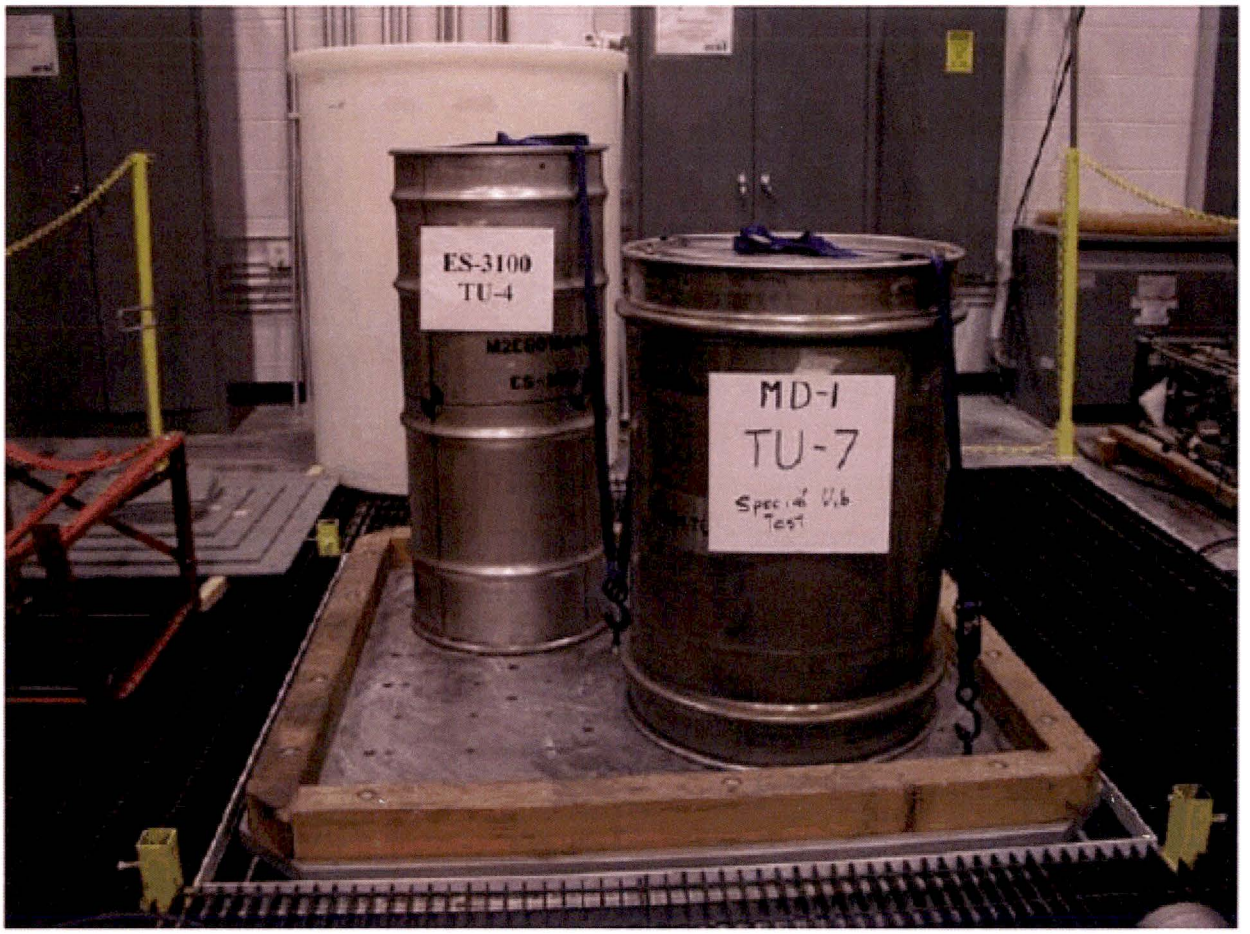

Fig. 2.3. ES-3100 vibration testing arrangement.
(MD-1 test unit removed during actual testing.)

Following compliance testing of the ES-3100 shipping package, minor changes were incorporated into the proposed design as described in Sect. 2.5.1. During the vibration test, the shipping package is restrained from movement in the vertical direction with a tie-down arrangement similar to that used on a SST/SGT for a single package. Based on the acceleration spectral density presented in Appendix 2.10.6, the largest contributor to shipping package motion is in the vertical direction. Since the containment vessel and contents are not restrained within the inner liner cavity, the containment vessel is free to bounce up and down. In the vertical direction, the top plug and the bottom of the inner liner restrict the movement of this vessel. Since the inner liner contour has not changed with respect to the containment vessel, and the fact that there are clearances between the containment vessel flange and the inner liner in the vertical direction, the cast neutron poison and inner liner are not directly impacted by the movement of the containment vessel. Therefore, changes in the neutron poison and minor radial dimension changes in the mid liner will not affect the outcome from vibration testing. Based on the success of the previously tested units and the fact that these proposed changes will have little or no effect on testing, vibration normally incident to transport does not reduce the effectiveness of the packaging during HAC testing. Thus, the requirements of 10 CFR 71.43(f) are satisfied.

Procedures will be followed to ensure that the packaging is assembled as specified (Sect. 7). The drum, lid, and fasteners are refurbished as required before each use. The ⅝-in.–diam flange nuts on the drum are torqued to 40.67 N·m (30 ft-lb) nominal. The closure nut on the containment boundary is

torqued to 162.7 N·m (120 ft-lb) nominal. The package is acceptable for vibration normally incident to transport in an SST/SGT.

2.6.6 Water Spray

Requirement. A water spray that simulates exposure to rainfall of ~5.08 cm (2 in.) per hour for at least 1 h is required by 10 CFR 71.71(c)(6).

Analysis. A water spray of 5.08 cm (2 in.) per hour was directed from above and around the periphery of the ES-3100 Test Unit-4 for a minimum of 1 h as shown in Fig. 2.4. The drum had four plastic plug-sealed ventilation holes near the top which prevents water from entering the insulation cavity. Aluminum duct tape, covering the installation holes in the mid liner, prevents water from entering the neutron poison cavity. There was evidence of water leakage into the volume between the containment boundary and the inner liner at the conclusion of the test. Water entered this cavity through the holes provided in the lid for the TID lugs, but none penetrated the containment boundary. The criticality analysis shown in Sect. 6 was conducted with moderation by water to the most reactive credible extent and close full reflection of the containment system by water on all sides. Because the package remained subcritical under these conditions, the ES-3100 package is acceptable for use under the water spray conditions of NCT.

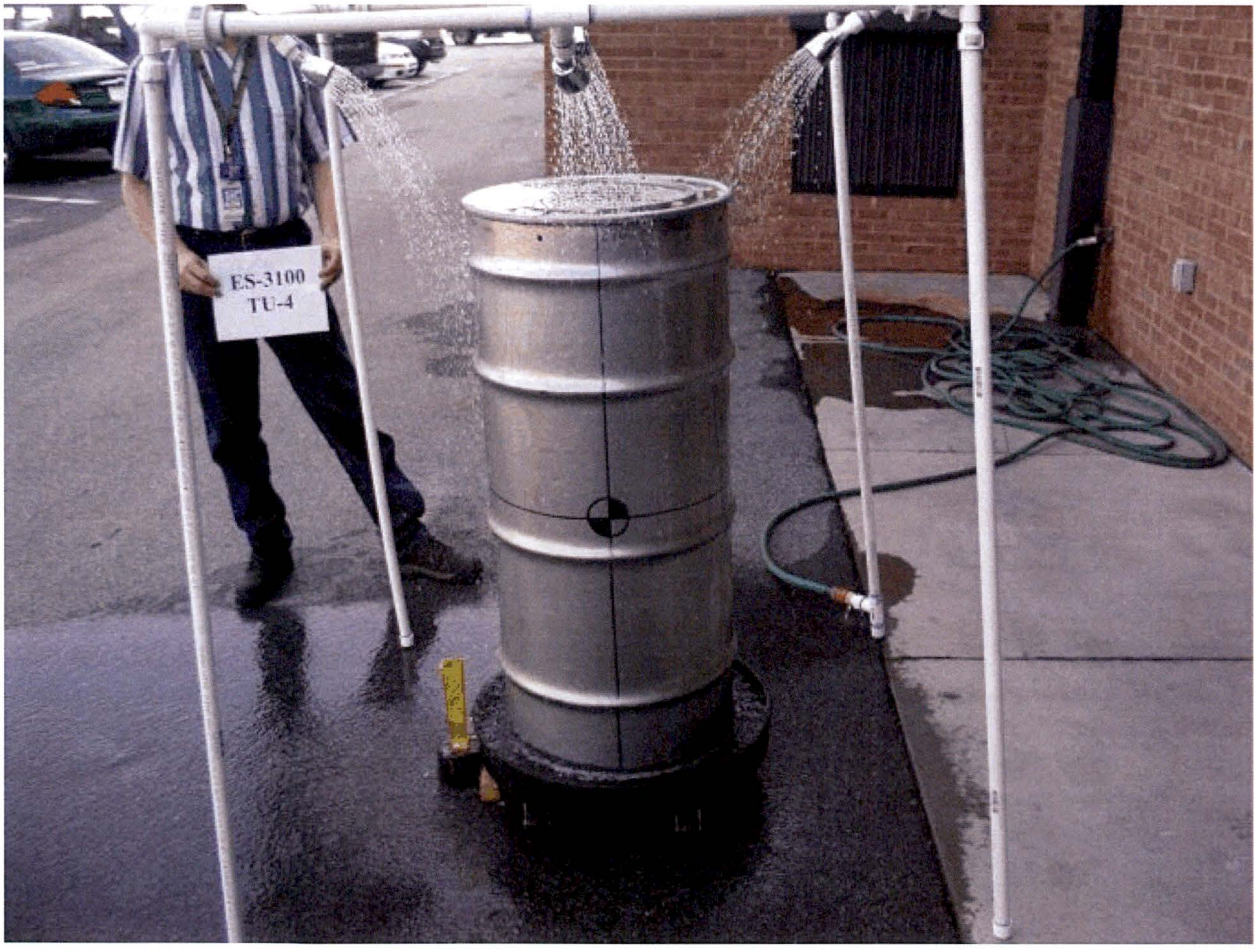

Fig. 2.4. Water spray test arrangement for Test Unit -4.

2.6.7 Free Drop

Requirement. A free drop of 1 m (4 ft) onto a flat, essentially unyielding, horizontal surface in a position for which maximum damage is expected is required by 10 CFR 71.71(c)(10). This test shall be made between 1½ and 2½ h after the conclusion of the water spray test (Sect. 2.6.6).

Analysis. The ES-3100 test package, Test Unit-4, previously sprayed with water (Sect. 2.6.6) with a measured gross weight of 201.85 kg (445 lb) and containing a content weight of 49.90 kg (110 lb) was tested in accordance with 10 CFR 71.71(c)(7). The temperature and pressure at the time of the drop test was 22.8°C (73°F) and ~101.35 kPa (14.70 psi), respectively. As discussed in Sect. 2.6, the response of the test package would not have been significantly different if it had been tested at the extremes of the temperature range dictated by 10 CFR 71.71(b) with the containment vessel at the maximum normal operating pressure.

The essentially unyielding surface used for this test was the indoor drop test pad at the NTRC. All 9-m (30-ft) drop and crush tests were conducted at the outside drop pad at the NTRC. The indoor pad consists of a 5.08-cm (2-in.) thick steel plate embedded inside a reinforced concrete pad ~127-cm (50-in.) thick. The outside drop pad consists of a 10.16-cm (4-in.) thick steel plate embedded inside a reinforced concrete pad ~167.6-cm (66-in.) thick. An article has been prepared by the NTRC staff to describe the integrity of these test pads (Shappert 1991).

Test Unit-4 was dropped from 1.2 m (4 ft) in a vertical position, with the drum's top initially striking the unyielding surface (Fig. 2.5). This attitude was assumed to be the most vulnerable orientation for producing damage to the sealing surfaces of the containment vessel and for introducing buckling into the cylindrical portion of the containment vessel body. The long axis of the drum was 0° from vertical. The test package made a free fall, with initial contact on the drum's lid. Damage consisted of shortening the drum height from 110.81 cm (43⅝ in.) to 110.49 cm (43½ in.) There were no breaks in the drum assembly. Additional details and sketches can be obtained from the test report (Appendix 2.10.7). Based on the HAC analytical structural deformation results shown in Sect. 2.7.8, the drop test damage would be nearly identical had this test been conducted on the proposed configuration using the Cat 277-4 neutron absorber. On this basis, the ES-3100 package meets the requirements of 10 CFR 71.71(c)(7).

In addition to the tests conducted on Test Unit-4, all test units (except Test Unit-6) were initially subjected to a free drop of 1.2-m (4 ft) onto a flat, essentially unyielding horizontal surface. As shown in Table 2.18, the orientations for these drops were two drops bottom to lid slapdown with the long axis of the drum ~ 12° from parallel to the drop pad; one drop with the long axis of the test unit parallel to the drop pad; one drop with the center of gravity drop over the drum/lid interface with the long axis of the drop rotated ~24.6° from perpendicular to the drop pad; and one with the long axis of the drum perpendicular to the drop pad. Package description, damage from testing, and drop orientation concerns are discussed in Sect. 2.7.1 for each test unit. Following the 1.2-m (4-ft) drop, each of these test units was subjected to the full HAC sequential test battery. The robustness of the ES-3100 containment vessel was demonstrated through whole boundary helium leak testing to $\leq 2.0 \times 10^{-7}$ cm^3/s (leaktight). This helium leak test eclipses the required criteria for both NCT and HAC based on the bounding case contents. Visual inspection of the containment boundaries showed no distortion or deformation from testing. Therefore, based on the various drop orientations, the severity of the HAC test sequence, and the testing conducted on Test Unit-4, the ES-3100 shipping package has been shown to meet the requirements of 10 CFR 71.43, 71.51(a)(1), and 71.71(c)(7).

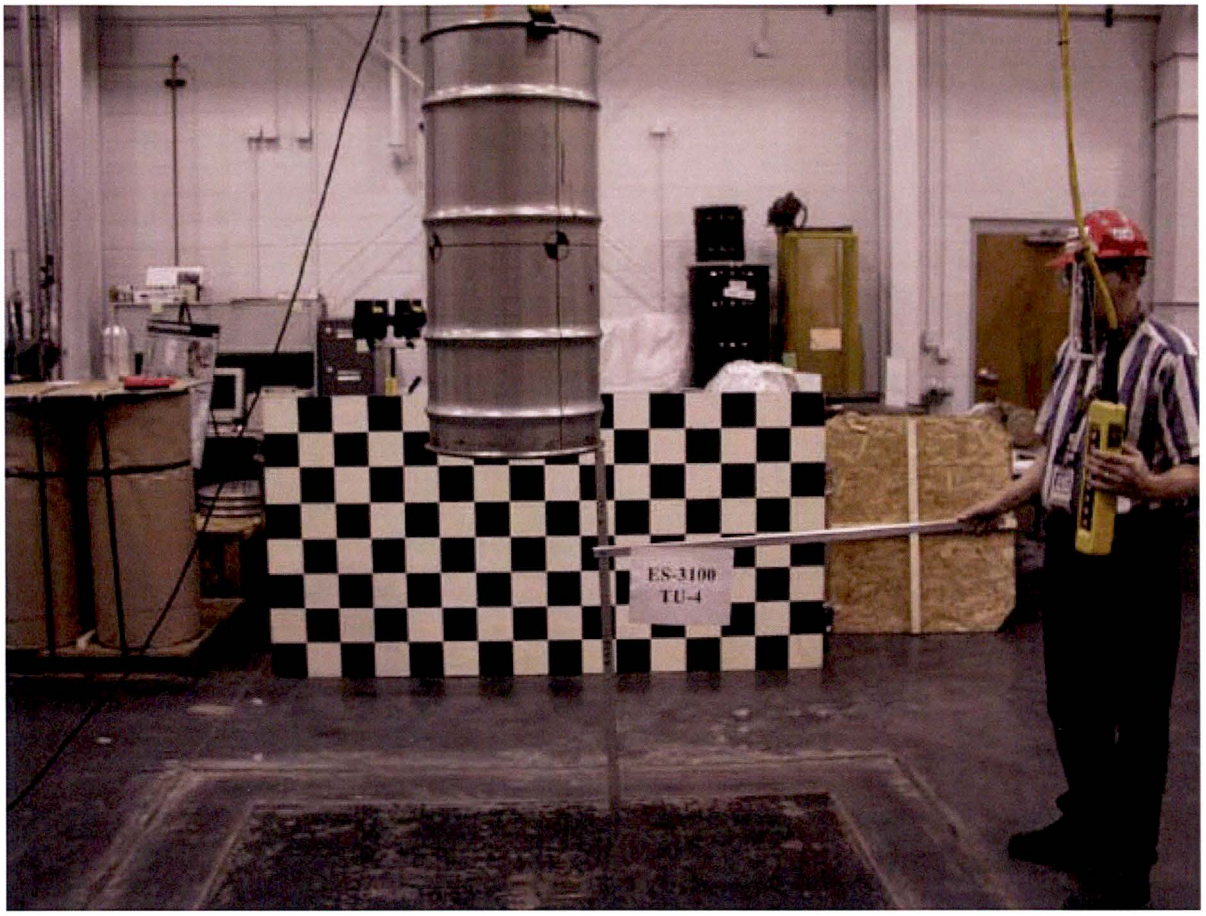

Fig. 2.5. NCT free drop test on Test Unit-4.

2.6.8 Corner Drop

Requirement. 10 CFR 71.71(c)(8) requires a free drop onto each corner of the package in succession, or in the case of a cylindrical package, onto each quarter of each rim, from a height of 0.3 m (1 ft) onto a flat, essentially unyielding, horizontal surface. This test applies only to fiberboard, wood, or fissile material rectangular packages not exceeding 50 kg (110 lb) and fiberboard, wood, or fissile material cylindrical packages not exceeding 100 kg (220 lb).

Analysis. This test is not applicable because the range of package weights for the ES-3100 [146.88 kg (323.79 lb) to 187.81 kg (414.05 lb)] exceed the above-weight restrictions for fissile material cylindrical packages.

2.6.9 Compression

Requirement. Title 10 CFR 71.71(c)(9) requires that packages weighing up to 5000 kg (11,000 lb) must be subjected for a period of 24 h to a compressive load applied uniformly to the top and bottom of the package in the position in which the package would normally be transported. The compressive load must be the greater of the following:

1. the equivalent of five times the weight of the package; or,
2. the equivalent of 13 kPa (2.0 psi) multiplied by the vertically projected area of the package.

Analysis. The proposed maximum weight of the ES-3100 shipping package is calculated to be 187.81 kg (414.05 lb) [Table 2.8]. As shown on Drawing M2E801580A010 (Appendix 1.4.8), the data plate states that the maximum gross weight of the ES-3100 shipping package is 190.51 kg (420 lb). In accordance with Item 1 above, the minimum compressive load would be 5 × 190.51 kg or 952.55 kg (2100 lb). The vertically projected area of the package is 1891 cm^2 (293.16 $in.^2$) or the area of the lid weldment. Based on Item 2 above, the minimum compressive load would be 13 kPa × 1891 cm^2 or 250.72 kg (552.75 lb). Therefore, the approach stipulated in Item 1 above represents the greatest compressive load for this configuration. A conservative 1043 kg (2300 lb) compressive load was uniformly applied to the top and bottom of Test Unit-4 for at least 24 h (Fig. 2.6). The test package had been sprayed with water as noted in Sect. 2.6.6. No change in height or diameter of the test unit resulted from the test.

Fig. 2.6. Compression test on Test Unit-4.

Due to the design of the ES-3100 drum lid, the applied compressive load was distributed equally around the lid and supported primarily through the outer drum contour and Kaolite 1600 substrate. Little or no load is transferred to the neutron poison (BoroBond4 in the test units) and internal liners. Therefore, the changes in the design of the liners and neutron poison proposed for this shipping package should not impact the outcome resulting from compression testing. Based on the results of compliance testing of Test Unit-4 and the insignificant changes in the design, the ES-3100 package meets the requirements of 10 CFR 71.71(c)(9).

2.6.10 Penetration

Requirement. Impact of the hemispherical end of a vertical steel cylinder of 3.2 cm (1.25 in.) diameter and 6 kg (13 lb) mass dropped from a height of 1 m (40 in.) onto the exposed package surface that is expected to be most vulnerable to puncture is required by 10 CFR 71.71(c)(10). The long axis of the cylinder must be perpendicular to the package surface.

Analysis. A 6-kg (13-lb) steel cylinder was dropped from 1 m (40 in.) onto the surface of Test Unit-4, which was previously subjected to water spray, free drop, vibration and compression tests. The penetration bar impacted the side of the drum at the welded seam near the package's center of gravity. The bar did not penetrate the drum, but an indentation 0.64-cm (0.25-in.) deep was recorded at the drum seam weld as shown in Fig. 2.7. The magnitude of this indentation is insignificant. Based on the HAC analytical structural deformation results shown in Sect. 2.7.8, the magnitude of indentation would be nearly identical had this test been conducted on the proposed configuration using the Cat 277-4 neutron absorber. On this basis, the ES-3100 package meets the requirements of 10 CFR 71(c)(10).

Fig. 2.7. Penetration test damage on Test Unit-4.

2.7 HYPOTHETICAL ACCIDENT CONDITIONS

This section demonstrates compliance with 10 CFR 71.73, "Hypothetical Accident Conditions." It shows that the package will experience no loss in shielding effectiveness or spacing and no release of radioactive content or leakage of water into the containment boundary during HAC. A summary of the tests and analyses conducted on the ES-3100 configuration is shown in Table 2.23.

Title 10 CFR 71.51 requires that the ES-3100 package satisfy the standards under HAC specified in 10 CFR 71.73. For the tests specified in 10 CFR 71.73, five test packages were subjected to the five sequential tests: free drop, crush, puncture, thermal, and immersion. The configuration for Test Units-1 through -4 used full-scale shipping packages with steel mock-ups similar to the maximum contents to be shipped in the ES-3100 configuration. Test Unit-5, also a full-scale shipping package, was dropped with a mock-up of the lightest component proposed for shipping. All test units were first subjected to the NCT free drop from 1.2 m (4 ft). In addition to the 1.2-m (4-ft) drop, Test Unit-4 was also subjected to the full battery of tests in accordance with applicable paragraphs of 10 CFR 71.71(c)(5) through (c)(10) except (c)(8). These preliminary tests were conducted to provide evidence that the ES-3100's ability to withstand HAC testing was not degraded through NCT testing. Demonstration of the ES-3100 package's ability to satisfy the requirements of HAC is provided in the following sections. A summary of the test results is provided in each area of Sect. 2.7; details are documented in the test report (Appendix 2.10.7).

Extensive computer impact simulation and analysis was conducted using LS-Dyna software. (LS-Dyna 2002) The results are documented in Appendix 2.10.2. Early in the design phase, the simulation was used to determine areas of large structural deformation and stress concentrations. Prior to the compliance testing in accordance with 10 CFR 71.71, the simulation was used to determine the drop orientation that would cause the most structural damage to the drum assembly and thereby propose a worst-case scenario for potential breeching of the containment boundary. Prior drop test programs have shown the slapdown orientation to cause the most structural degradation of a drum-style container. Computer software LS-DYNA-3D was used to simulate a 9-m (30-ft) drop orientation at a slapdown angle of 12° with a friction factor of $\mu = 0.0$ as calculated using the computer code Slapdown, Version 05.20.93. Slapdown calculated that no matter what friction factor was assumed, the tail-end velocity peaked at approximately 14° (Handy 1997, Appendix 6.10). The maximum tail-end velocity versus slapdown angle is presented in Fig. 6.10.4 in Handy 1997, and the logic for the development of this figure is explained in Appendix 6.10 in Handy 1997. Due to the mitigating effects of the length to diameter ratios and the relative closeness of the 12° increase in velocity to the maximums (shown in Fig. 6.10.4 in Handy 1997), the 12°slapdown is considered to be representative of the worst-case slapdown. Based on the correlation of data obtained from preliminary drop tests of the similar ES-2M configuration and computer-simulated drops, several orientations were eliminated from the drop test matrix (Table 2.23). Several other impact simulations have been conducted using a wide range of material properties for the impact limiter material (Kaolite 1600) to determine the variance in structural deformation. Results of these simulations are documented in Sect. 5.6 in Handy (1997). Although the analysis shows some variance, the magnitude of difference was not large enough to degrade the performance of the drum assembly and containment boundary. Due to the similarities in design, fabrication, and material used in construction of the shipping packages, these same results would hold true for the ES-3100 package.

Table 2.23. Test and analysis summary for the ES-3100 package [a]

Container	NCT water spray, compression, penetration, vibration	1.2-m (4 ft) drop	9-m (30 ft) drop and crush test				1.2-m (4-ft) puncture drop	Preheat over 38°C (100°F)	HAC thermal burn test	O-ring cavity leak check (operational)	Full-body helium leak test [b]	0.9-m (3-ft) immer. test	15-m (50-ft) immer. test
			Top drop	CG over lid corner	Bottom to lid slapdown	Side drop							
TU-1		1—YES			12° 2—YES		3—YES [c]	4—YES	5—YES	6–YES $\leq 1.0 \times 10^{-4}$ ref. cm^3/s	7—YES 1.6×10^{-7} cm^3/s	8—YES	
TU-2		1—YES				2—YES	3—YES	4—YES	5—YES	6–YES $\leq 1.0 \times 10^{-4}$ ref. cm^3/s	7—YES Pulsing between 1.0×10^{-9} to 1.4×10^{-6} cm^3/s	8—YES	
TU-3		1—YES		24.6° 2—YES			3—YES	4—YES	5—YES	6–YES $\leq 1.0 \times 10^{-4}$ ref. cm^3/s	7—YES 1.0×10^{-7} cm^3/s	8—YES	
TU-4	Yes	1—YES	2—YES				3—YES	4—YES	5—YES	6–YES $\leq 1.0 \times 10^{-4}$ ref. cm^3/s	7—YES 2.0×10^{-7} cm^3/s	8—YES	
TU-5		1—YES			12° 2—YES		3—YES	4—YES	5—YES	6–YES $\leq 1.0 \times 10^{-4}$ ref. cm^3/s	7—YES 3.1×10^{-8} cm^3/s	8—YES	
TU-6										1–YES $\leq 1.0 \times 10^{-4}$ ref. cm^3/s			2—YES
Impact Analysis		YES	YES	YES	YES	YES							
Thermal Analysis	YES [d]							YES	YES [d]				

[a] Numbering refers to sequence of activities.
[b] Full-body helium leak test conducted following HAC testing. Leakage value recorded after 20 minutes of the test period.
[c] Test Unit-1 was puncture tested in four different orientations.
[d] Thermal analysis was conducted to determine time for cooling to -40°C and to evaluate the application of decay heating and insolation during the cool-down phase.

Title 10 CFR 71.73(b) requires that the HAC tests, except for the water immersion tests, be conducted at the most unfavorable ambient temperature within the range of −29 to 38°C (−20 to 100°F). This requirement was previously discussed in Sect. 2.6 for NCT, in which it was concluded that the tests performed at 70 to 90°F ambient temperatures should provide essentially the same results, except for thermal, as those made at any ambient temperature between −29 to 38°C (−20 to 100°F). Buckling failures are not anticipated for this package design. This assumption is based on the fact that no evidence of buckling occurred when the package was subjected to the compression test in accordance with 10 CFR 71.71(c)(9); the water immersion tests in accordance with 10 CFR 71.73(c)(5) and 71.73(c)(6); and the 1.2-m and 9-m drop test conducted on Test Unit-4. Code calculations further substantiate that buckling failures of the containment vessel are not anticipated for this package design (Appendix 2.10.1).

Title 10 CFR 71.73(b) states that the HAC initial pressure within the containment boundary vessel during testing shall be considered as the maximum internal normal operating pressure. The internal pressures in the ES-3100 containment vessel at various temperatures for NCT are discussed in Sects. 3.4.1 and 3.4.2 and tabulated in Table 2.20. The maximum normal absolute operating pressure due to insolation and the bounding case parameters is 200.20 kPa (29.036 psia) for the containment vessel. This pressure is well below the design internal gauge pressure of 699.82 kPa (101.5 psi). Increasing the internal pressure in the containment boundary to the value noted above before a free drop (Sect. 2.7.1), crush (Sect. 2.7.2), puncture (Sect. 2.7.3), or water immersion (Sect. 2.7.5) testing would have no detrimental effect on the containment boundary's structural integrity due to the low stresses shown in Table 2.21. Temperature and pressure increases in the containment boundary due to the compliance thermal tests are discussed and evaluated in Sects. 2.7.4 and 3.5.3. A summary of these pressures is presented in Appendix 3.6.5.

Summarizing 10 CFR 71.43(f) and 71.55(d)(4), the tests and conditions of NCT will not substantially reduce the effectiveness of the packaging to withstand HAC sequential testing. The effectiveness of the ES-3100 to withstand HAC sequential testing is not diminished through application of the tests and conditions stipulated in 10 CFR 71.71. The justification for this statement is provided by physical testing of both the ES-2M and ES-3100 test packages, and the analytical structural deformation predicted in Appendix 2.10.2 (summarized in Sect. 2.7.8). Due to the similarities in design, fabrication, and material used in construction of both the ES-2M and the ES-3100 package, the physical characteristics of the Kaolite 1600 will hold true for both designs. The integrity of the Kaolite 1600 is not significantly affected by the NCT vibration and 1.2-m (4-ft) drop tests. Prior to testing the ES-2M design, each test unit was radiographed to determine the integrity of the Kaolite 1600 impact and insulation material. Following casting of the material inside the drum, some three-dimensional curving cracks were seen in some packages near the thinner top sections from the bottom of the liner to the bottom drum edge. After vibration testing, radiography of the ES-2M Test Unit-4 showed that the lower half of the impact limiter was broken into small pieces. In order to evaluate these findings, Test Unit-4 was reassembled and subjected to HAC sequential testing. After vibration and impact testing, many three-dimensional curving cracks were seen around the impact areas, and the inner liner was visibly deformed. Nevertheless, the ES-2M Test Unit-4 maintained the adequate spacing required for shielding effectiveness and subcriticality. Temperatures at the containment boundary were also similar to other packages not subjected to vibration testing prior to HAC testing. No inleakage of water was recorded following immersion. Additionally, Test Unit-4 of the ES-3100 test series was subjected to tests and conditions stipulated in 10 CFR 71.71(c)(5) through (c)(10), excluding (c)(8). Following completion of these NCT tests, the test unit was subjected to the full HAC test battery. Following these tests, the containment vessel was removed and subjected to a full-body helium leak test. Criteria for a leaktight condition was achieved. Based on the success of these units, vibration normally incident to transport does not reduce the effectiveness of the packaging during HAC testing. Thus, the requirements of 10 CFR 71.43(f) and 71.55(d)(4) are satisfied.

2.7.1 Free Drop

Requirement. A free drop of 9 m (30 ft) onto a flat, unyielding, horizontal surface, striking the surface in a position for which maximum damage is expected is required by 10 CFR 71.73(c)(1).

Analysis. Five test packages were drop tested from 9 m (30 ft) in accordance with 10 CFR 71.73(c)(1) with the set up as shown in Fig. 2.8. A description of the drop pad is presented in Sect. 2.6.7. Four different drop positions were used in the testing based on the analytical results from LS-Dyna drop simulations. The ES-3100 test units were designated as Test Units-1, through -5. Test Unit-4 was subjected to the full NCT testing (water spray, 1.2-m (4-ft) drop, compression, penetration, and vibration) prior to HAC testing. The gross weight of the ES-3100 test units varied between 157.4 kg (347 lb) and 203.7 kg (449 lb). Mock-up components weighing between 3.6 kg (8 lb) [Test Unit-5] to 50.3 kg (111 lb) [Test Unit-3] were used during testing. Discussion of the damage to each test package resulting from the 9-m (30 ft) drop is given in subsequent paragraphs. Rationale for the four drop positions is included in the discussion for each test unit. Minor changes to the mid liner and the substitution of the neutron poison from BoroBond4 to Cat 277-4 are further evaluated in Sect. 2.7.8.

Fig. 2.8. 9-m drop test arrangement for all test units.

2.7.1.1 End drop

Test Unit-4, weighing 201.8 kg (445 lb), was dropped from 9-m (30 ft) with the long axis of the drum perpendicular to the impact surface within 0.2°. The mock-up components are shown on Drawing M2E801580A027. The concern for this drop orientation was that the containment boundary assembly would crush, buckle or compress the insulation to a thickness that would result in excessive O-ring temperatures during the thermal testing cycle. Following initial impact, the package bounced very little before landing on its side. The damage to the drum consisted of reducing the overall height from 43.5 in. [following the 1.2 m (4 ft) drop] to a minimum 42.63 in. The diameter of the drum was measured at six locations along the long axis of the package and at two radial locations. The measurements and pictorials of the damage are recorded on Test Form 1 of procedure TTG-PRF-08 shown in the test report data sheets (Appendix 2.10.7) and are summarized in Tables 2.24 and 2.25 and Fig. 2.9.

Table 2.24. Recorded height damage to Test Unit-4 from 1.2-m and 9-m drop testing

	0°	90°	180°	270°
Pre-drop height (in.)	43.50	43.50	43.63	43.63
Post 1.2-m drop height (in.)	43.50	43.50	43.50	43.50
Post 9-m drop height (in.)	43.00	43.13	42.88	42.63

Table 2.25. Recorded diametrical damage to Test Unit-4 from 1.2-m and 9-m drop tests [Diameter (in.)]

Axial measurement location	0 to 180°			90 to 270°		
	Pre drop test	Post 1.2-m drop test	Post 9-m drop test	Pre drop test	Post 1.2-m drop test	Post 9-m drop test
Top false wire	19.25	19.25	19.25	19.38	19.38	19.38
Top rolling hoop	19.25	19.25	19.13	19.25	19.25	19.88
CG & top rolling hoop	19.25	19.25	19.81	19.25	19.25	19.38
CG rolling hoop	19.13	19.13	19.13	19.25	19.25	19.25
Bottom rolling hoop	19.13	19.13	19.25	19.25	19.25	19.25
Bottom false wire	19.38	19.38	19.25	19.25	19.25	19.25

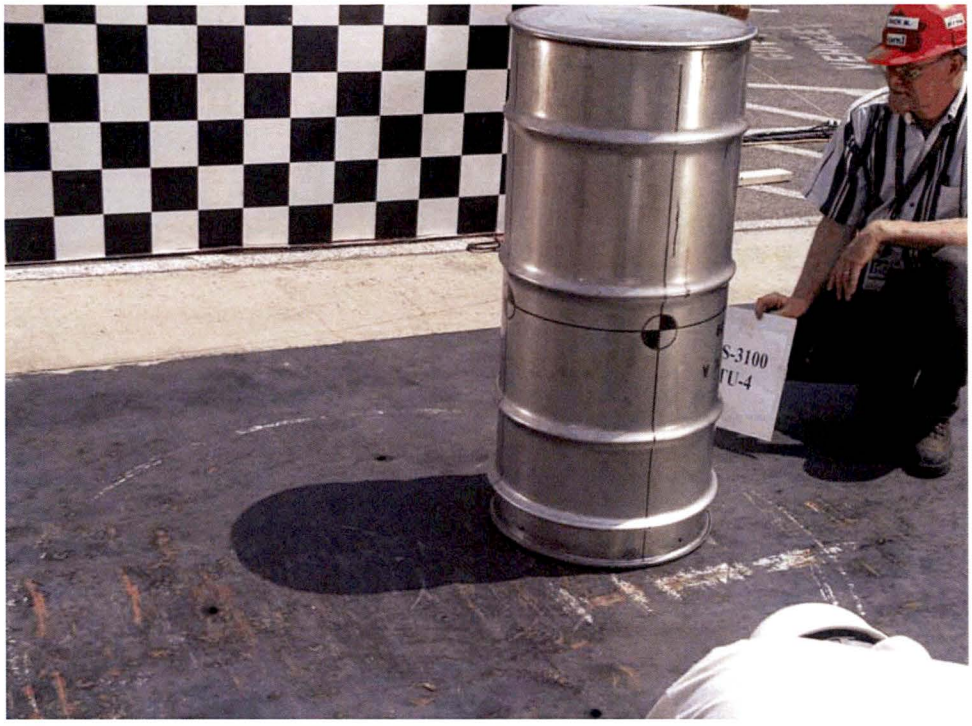

Fig. 2.9. 9-m drop test damage on Test Unit-4.

2.7.1.2 Side drop

Test Unit-2, weighing 202.8 kg (447 lb) was chilled to −40°C (−40°F) prior to conducting the drop tests. This unit was sequentially dropped from 1.2 m (4 ft), 9 m (30 ft), crushed from 9 m (30 ft), and puncture tested with the long axis of the drum parallel to the impact surface. The mock-up component used in Test Unit-2 is shown on Drawing M2E801580A027 and weighed 49.9 kg (110 lb). There were two concerns for this drop orientation. The primary concern was that the containment boundary assembly would crush or compress the insulation to a thickness that would result in excessive O-ring temperatures during the thermal testing cycle. Another concern was that the cold temperatures might cause excessive loads and deformation in the containment vessel body during impact. This, in turn, might cause leaking above the regulatory limit to occur. The test package made a free fall with initial contact occurring between the rolling hoops of the drum and the impact surface with the ambient temperature at 24.2°C (75°F). Since it was important to evaluate the package at the regulatory minimum temperature, individual results of each test were not recorded. Time required to measure the package between drops would have allowed the package to further increase in temperature. Cumulative results of damage to Test Unit-2 from drop testing is shown in Tables 2.26, 2.27, and 2.28 and Fig. 2.10.

Table 2.26. Recorded diametrical damage to Test Unit-2 from NCT and HAC drop testing [Diameter (in.)]

Axial measurement location	0 to 180°		90 to 270°	
	Pre drop test	Post drop test[a]	Pre drop test	Post drop test[a]
Top false wire	19.25	17.63	19.25	19.81
Top rolling hoop	19.25	17.38	19.25	19.75
CG & top rolling hoop	19.25	17.00	19.25	20.00
CG rolling hoop	19.25	16.00	19.25	20.25
Bottom rolling hoop	19.25	15.50	19.25	20.13
Bottom false wire	19.25	18.00	19.25	19.38

[a] Includes cumulative damage from 1.2-m drop, 9-m drop, and crush test.

Table 2.27. Recorded flat contour damage to Test Unit-2 from NCT and HAC drop testing

Axial measurement location	Flat width @ 0° (in.)	Flat width @ 180° (in.)
Top false wire	8	6.25
Top rolling hoop	9	8.88
CG & top rolling hoop	10.13	9.63
CG rolling hoop	9.88	12.00
Bottom rolling hoop	9.88	14.88
Bottom false wire	9.38	0
Crease (see Fig. 2.10 for location)		15.25

Table 2.28. Recorded height damage to Test Unit-2 from NCT and HAC drop testing

	0°	90°	180°	270°
Pre-drop height (in.)	43.50	43.50	43.50	43.50
Post-drop height (in.)[a]	44.75	43.75	42.75	43.63

[a] Includes cumulative damage from 1.2-m drop, 9-m drop, and crush test.

Fig. 2.10. Cumulative damage from 9-m drop and crush testing on Test Unit-2.

2.7.1.3 Corner drop

Test Unit-3, weighing 203.7 kg (449 lb), was dropped from 9 m (30 ft), with the long axis of the drum at an oblique angle of 24.8° (desired angle was 24.6°) from the impact surface. The mock-up component used in Test Unit-3 is shown on Drawing M2E801580A027 and weighed 50.3 kg (111 lb). The primary concern for this drop orientation was that the combination of plastic deformation at impact on the corner of the drum and the crushing or compacting of the adjacent insulation by the containment vessel flange would result in excessive O-ring temperatures during thermal testing. Another concern was that the mock-up contents would be forced against the containment boundary lid at impact. This, in turn, might yield the flange or closure nut, resulting in loss of containment. The test package made a free fall, with initial contact occurring between the top rim of the drum and the impact surface with the ambient temperature at 28°C (82.4°F). A secondary contact occurred between the bottom drum rim and the impact surface. No drum studs, nuts, or washers were lost due to the impact. The lid was still firmly attached to the drum assembly, with no visible separations or rips; thus, the position of the containment vessel inside the drum (and therefore the contents of the shipping container) was maintained. A general description of damage to Test Unit-3 is summarized in Tables 2.29 and 2.30. Pictorials of damage are shown on Fig. 2.11.

Table 2.29. Recorded height damage to Test Unit-3 from 1.2-m and 9-m drop testing

	0°	90°	180°	270°
Pre-drop height (in.)	43.50	43.50	43.50	43.50
Post 1.2-m drop height (in.)	43.00	43.50	43.63	43.50
Post 9-m drop height (in.)	40.63	43.25	43.75	43.38

Table 2.30. Recorded diametrical damage to Test Unit-3 from 1.2-m and 9-m drop testing [Diameter (in.)]

Axial measurement location	0 to 180°			90 to 270°		
	Pre drop test	Post 1.2-m drop test	Post 9-m drop test	Pre drop test	Post 1.2-m drop test	Post 9-m drop test
Top false wire	19.25	19.25	19.25	19.13	19.38	19.19
Top rolling hoop	19.13	19.13	18.63	19.13	19.25	19.88
CG & top rolling hoop	19.13	19.13	19.13	19.13	19.25	19.38
CG rolling hoop	19.13	19.13	19.13	19.13	19.25	19.38
Bottom rolling hoop	19.13	19.13	19.13	19.13	19.25	19.38
Bottom false wire	19.13	19.13	19.13	19.13	19.25	19.25

Fig. 2.11. Test Unit-3 damage from 1.2 and 9-m drop tests.

2.7.1.4 Oblique drops

Two oblique (slapdown) drops were conducted in the same attitude with maximum and minimum content weights to determine the structural response on the package in accordance with Regulatory Guide 7.8. Paraphrasing Regulatory Position 1.6, a local structural response might be greater during an impact test if the weight of the contents were less than the maximum. Therefore, Test Units-1 and -5 contained the maximum and minimum weight configurations, respectively.

2.7.1.4.1 Test Unit-1 slapdown

Test Unit-1, weighing 202.3 kg (446 lb) was dropped from 9-m (30 ft) with the long axis of the unit at an oblique angle of 12.2° (desired angle was 12°) to the essentially unyielding surface. The mock-up component used in Test Unit-1 is shown on Drawing M2E801580A027 and weighed 49.90 kg (110 lb). Based on Sect. 3.1 of Regulatory Guide 7.8, the structural performance of the package must be evaluated for the minimum and maximum weight of the contents. Therefore, this unit was tested above the maximum proposed content weight to see if the containment vessel would react differently from the much lighter mock-up used in Test Unit-5 in a similar drop orientation. The primary concern was that the orientation would cause greater angular acceleration of the contents near the package top. This in turn would cause the containment boundary to crush or compress the insulation to a thickness that would result in excessive O-ring temperatures during the thermal testing cycle. The test package made a free fall with initial contact occurring between the rolling hoops of the drum and the impact surface with the ambient temperature at 28°C (82.4°F). No drum studs, nuts, or washers were lost due to the impact. The lid was still firmly attached to the drum assembly, with no visible separations or rips; thus, the position of the containment vessel inside the drum (and therefore the contents of the shipping container) was maintained. A general description of damage is provided in Tables 2.31, 2.32, and 2.33 and Fig. 2.12.

Table 2.31. Recorded height damage to Test Unit-1 from 1.2-m and 9-m drop testing

	0°	90°	180°	270°
Pre-drop height (in.)	43.50	43.50	43.50	43.50
Post 1.2-m drop height (in.)	43.50	43.50	43.50	43.50
Post 9-m drop height (in.)	42.63	43.38	43.25	43.38
Buckle (in.)	44.50			

Table 2.32. Recorded diametrical damage to Test Unit-1 from 1.2-m and 9-m HAC drop testing [Diameter (in.)]

Axial measurement location	0 to 180°			90 to 270°		
	Pre drop test	Post 1.2-m drop test	Post 9-m drop test	Pre drop test	Post 1.2-m drop test	Post 9-m drop test
Top false wire	19.25	19.13	18.50	19.25	19.25	19.38
Top rolling hoop	19.25	19.00	18.50	19.25	19.25	19.38
CG & top rolling hoop	19.25	19.13	18.50	19.25	19.25	19.38
CG rolling hoop	19.25	19.13	18.63	19.25	19.25	19.38
Bottom rolling hoop	19.25	19.00	18.63	19.25	19.25	19.25
Bottom false wire	19.25	19.00	17.81	19.25	19.25	19.38

Table 2.33. Recorded flat contour damage to Test Unit-1 from 1.2-m and 9-m drop testing

Axial measurement location	Flats width maximum post 1.2-m drop (in.)	Flats width maximum post 9-m drop (in.)
Top false wire	5.25	8.00
Top rolling hoop	4.38	7.38
CG & top rolling hoop	4.50	7.13
CG rolling hoop	3.00	6.38
Bottom rolling hoop	4.00	6.75
Bottom false wire	4.63	10

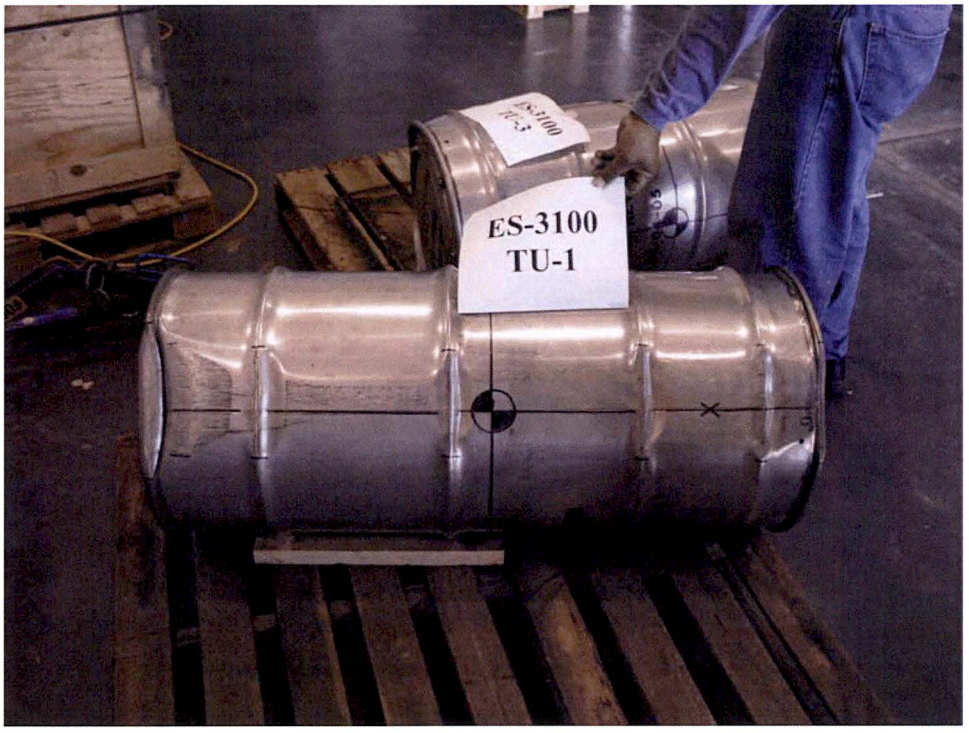

Fig. 2.12. 1.2 and 9-m drop test damage on Test Unit-1.

2.7.1.4.2 Test Unit-5 slapdown

Test Unit-5, weighing 157.4 kg (347 lb), was dropped from 9-m (30 ft), with the long axis of the drum at an oblique angle of 12.5° (desired angle was 12°) from the impact surface. The mock-up component (Drawing M2E801580A029), weighing 3.6 kg (8 lb), was the hardware with the majority of the mass located near the bottom of the containment vessel (Sect. 2.5.1). Based on Sect. 3.1 of Regulatory Guide 7.8, the structural performance of the package must be evaluated for the minimum and maximum weight of the contents. Therefore, this unit was tested at the minimum proposed weight to see if the containment vessel would react differently from the much heavier mock-up used in Test Unit-1 in a similar drop orientation. The test package made a free fall with initial contact occurring between the bottom rim of the drum and the impact surface with the ambient temperature at 30.6°C (87°F). A secondary contact occurred between the top drum lid and the impact surface. No drum studs, nuts, or washers were lost during this impact test. The lid was still firmly attached to the drum assembly, with no visible separations or rips; thus, the position of the containment vessel inside the drum (and therefore the contents of the shipping container) was maintained. A general description of damage is provided in Tables 2.34, 2.35, and 2.36 and Fig. 2.13.

Table 2.34. Recorded height damage to Test Unit-5 from 1.2-m and 9-m drop testing

	0°	90°	180°	270°
Pre-drop height (in.)	43.50	43.50	43.50	43.50
Post 1.2-m drop height (in.)	43.88	43.50	43.50	43.50
Post 9-m drop height (in.)	44.50	43.50	43.38	43.50

Table 2.35. Recorded diametrical damage to Test Unit-5 from 1.2-m and 9-m HAC drop testing [Diameter (in.)]

Axial measurement location	0 to 180°			90 to 270°		
	Pre drop test	Post 1.2-m drop test	Post 9-m drop test	Pre drop test	Post 1.2-m drop test	Post 9-m drop test
Top false wire	19.25	18.88	18.75	19.38	19.38	19.38
Top rolling hoop	19.25	19.00	18.75	19.25	19.25	19.38
CG & top rolling hoop	19.25	19.13	18.75	19.25	19.25	19.38
CG rolling hoop	19.25	19.13	18.75	19.25	19.25	19.25
Bottom rolling hoop	19.25	19.13	18.75	19.25	19.25	19.25
Bottom false wire	19.25	19.13	18.44	19.25	19.25	19.31

Table 2.36. Recorded flat contour damage to Test Unit-5 from 1.2-m and 9-m drop testing

Axial measurement location	Flats width maximum post 1.2-m drop (in.)	Flats width maximum post 9-m drop (in.)
Top false wire	5.38	8.38
Top rolling hoop	4.25	8.38
CG & top rolling hoop	3.88	7.63
CG rolling hoop	2.50	7.50
Bottom rolling hoop	3.25	8.25
Bottom false wire	5.00	9.25

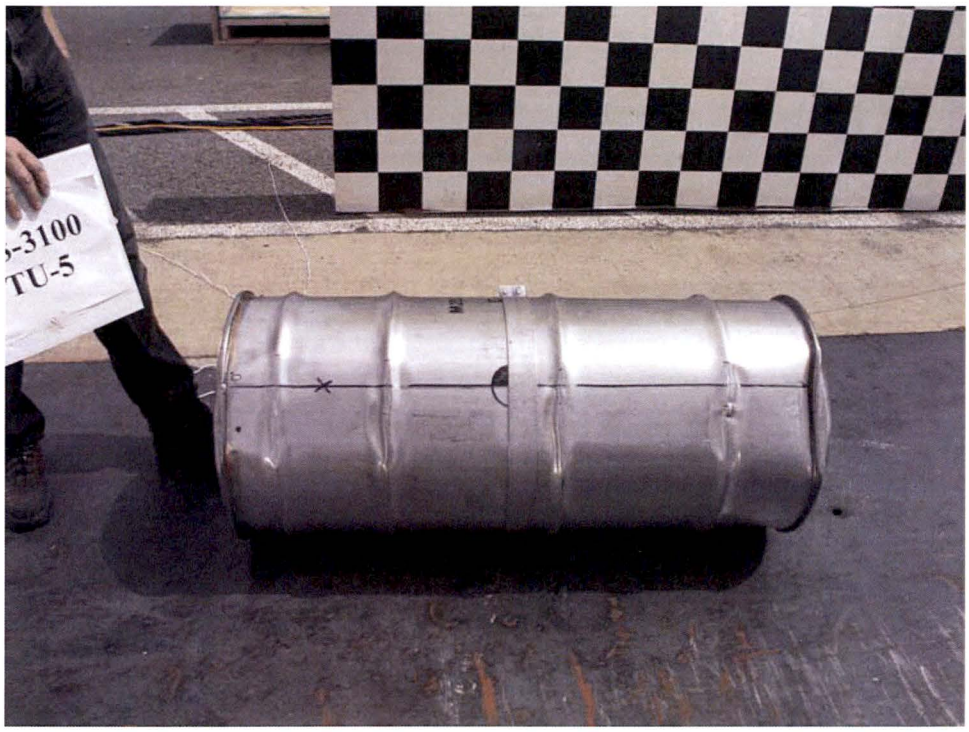

Fig. 2.13. 1.2 and 9-m drop test damage to Test Unit-5.

2.7.2 Crush

Requirement. Title 10 CFR 71.73(c)(2) requires that the specimen be subjected to a dynamic crush test in which the specimen is placed on a flat, essentially unyielding, horizontal surface so as to suffer maximum damage by the drop of a 500-kg (1100-lb) mass from 9 m (30 ft) onto the specimen. The mass must consist of a solid mild steel plate 1 m (40 in.) by 1 m (40 in.) and must fall in a horizontal attitude. The crush test is required only when the specimen has a mass ≤500 kg (1100 lb), an overall density ≤1000 kg/m^3 (62.4 lb/ft^3) based on external dimensions, and radioactive contents >1000 A_2 not as special form radioactive material. For packages containing fissile material, the radioactive contents greater than 1000 A_2 criterion does not apply.

Analysis. Five test packages were subjected to the dynamic crush test from 9 m (30 ft) in accordance with 10 CFR 71.73(c)(2). The previously drop-tested packages (described in Sect. 2.7.1) were restrained in the orientation used for drop testing. Discussion of the damage to each test package that resulted from the crush test is given in subsequent paragraphs, with details given in the test report. (Appendix 2.10.7) Rationale for the three drop positions is included in Sect. 2.7.1 for each test unit. The impact of the steel plate only increased the overall concern for each orientation.

Test Unit-1, weighing 202.3 kg (446 lb), was positioned in a horizontal attitude with the damaged portion of the test unit, resulting from prior drop tests, placed on the drop pad (0° mark facing down on test pad). The 500-kg (1100-lb) crush plate was centered over the sealing lid location on the containment vessel and dropped from 9 m (30 ft) and squarely contacted the top false wire of the drum at an ambient temperature of 29°C (84.2°F). Following initial impact, the package bounced very little before landing on its side. No drum studs, nuts, or washers were lost due to the impact. The lid was still firmly attached to the drum, with no visible separation or rips; thus, the position of the thermal barrier and neutron poison was maintained. A summary of the resulting damage is shown in Tables 2.37, 2.38, and 2.39. Since the length of the crush plate did not encompass the entire length of the test package, a crush edge indentation is recorded in Table 2.39. Additional pictorials of damage are shown on Fig. 2.14.

Table 2.37. Recorded height damage to Test Unit-1 from the 9-m crush test

	0°	90°	180°	270°
Pre-crush height (in.)	44.50	43.38	43.25	43.38
Post 9-m crust test height (in.)	44.88	43.38	44.00	43.63

Table 2.38. Recorded diametrical damage to Test Unit-1 from the 9-m crush test [Diameter (in.)]

Axial measurement location	0 to 180°		90 to 270°	
	Pre crush test	Post 9-m crush test	Pre crush test	Post 9-m crush test
Top false wire	18.50	15.63	19.38	20.63
Top rolling hoop	18.50	16.00	19.38	20.43
CG & top rolling hoop	18.50	16.25	19.38	20.25
CG rolling hoop	18.63	16.50	19.38	19.88
Bottom rolling hoop	18.63	18.25	19.25	19.50
Bottom false wire	17.81	17.81	19.38	19.25

Table 2.39. Recorded flat contour damage to Test Unit-1 from the 9-m crush test

Axial measurement location	Flats width maximum @ 0° (in.)	Flats width maximum@ 180° (in.)
Top false wire	9.00	8.50
Top rolling hoop	10.00	10.00
CG & top rolling hoop	10.00	10.13
CG rolling hoop	9.00	10.63
Bottom rolling hoop	8.25	--
Bottom false wire	9.75	--
Dent where edge of plate struck test unit	--	9.13

Fig. 2.14. Cumulative damage following 9-m crush on Test Unit-1.

Test Unit-2 (chilled package), weighing 202.8 kg (447 lb), was positioned in an horizontal attitude with the long axis of the drum parallel with respect to the drop pad. The damaged portion of the test unit, resulting from prior drop tests, was placed nearest the drop pad (0° mark facing down on pad). The 500-kg (1100-lb) crush plate was centered over the test unit's center of gravity and dropped from 9 m (30 ft) squarely onto the top false wire of the drum at an ambient temperature of 26.8°C (80.4°F). Following initial impact, the package bounced very little before landing on its side. No drum studs, nuts, or washers were lost due to the impact. The lid was still firmly attached to the drum, with no visible separation or rips; thus, the position of the thermal barrier and neutron poison was maintained. A summary of the cumulative damage is shown in Tables 2.26, 2.27, and 2.28 in Sect. 2.7.1.2. Additional pictorials of damage are shown on Fig. 2.10.

Test Unit-3, weighing 203.7 kg (449 lb), was positioned in the same oblique attitude as previously drop tested from 9 m (30 ft). The long axis of the drum was at an oblique angle of 24.7° (desired angle was 24.6°) from the impact surface with the damaged portion of the lid in contact with the drop pad (0° mark in contact with pad). The 500-kg (1100-lb) crush plate was dropped from 9 m (30 ft) with the center of gravity of both the plate and test unit in line at an ambient temperature of 30.5°C (86.9°F). The initial impact of the plate was with the edge of the drum bottom. A secondary contact occurred between the bottom drum rim and the impact surface. One drum stud was sheared from the test unit; however, the lid was still firmly attached to the drum, with no visible separation or rips. Therefore, the thermal barrier and neutron poison was maintained in position. Tables 2.40, 2.41, and 2.42 describe the measured damage which is recorded on Test Form 3 (Appendix 2.10.8). A photograph of the damage to Test Unit-3 is shown in Fig. 2.15.

Table 2.40. Recorded height damage to Test Unit-3 from the 9-m crush test

	0°	90°	180°	270°
Pre-crush height (in.)	40.63	43.25	43.75	43.38
Post 9-m crust test height (in.)	39.38	42.43	39.13	42.50

Table 2.41. Recorded flat contour damage to Test Unit-3 from the 9-m crush test

Axial measurement location	Flats width maximum pre crush (in.)	Flats width maximum post crush (in.)
Top of test unit	14.00	18.38
Bottom of test unit	0.00	17.88

Table 2.42. Recorded diametrical damage to Test Unit-3 from the 9-m crush test [Diameter (in.)]

Axial measurement location	0 to 180°		90 to 270°	
	Pre crush test	Post 9-m crush test	Pre crush test	Post 9-m crush test
Top false wire	19.25	19.25	19.19	19.06
Top rolling hoop	18.63	18.75	19.88	20.25
CG & top rolling hoop	19.13	19.25	19.38	19.75
CG rolling hoop	19.13	19.13	19.38	19.25
Bottom rolling hoop	19.13	19.13	19.38	19.75
Bottom false wire	19.13	18.00	19.25	19.38

Fig. 2.15. Cumulative damage following 9-m crush test on Test Unit-3.

Test Unit-4, weighing 201.8 kg (445 lb), was positioned vertically with the previously damaged drum top in contact with the drop pad. The 500-kg (1100-lb) crush plate was dropped from 9 m (30 ft) and squarely contacted the bottom of the test unit. The center of the 500-kg (1100-lb) crush plate was positioned over the radial test unit's center of gravity, in this case over the center of the drum's bottom at an ambient temperature of 29.8°C (85.6°F). Following initial impact, the package bounced very little before landing on its side. No drum studs, nuts, or washers were lost due to the impact. The lid was still firmly attached to the drum, with no visible separation or rips; thus, the position of the thermal barrier and neutron poison was maintained. A summary of the resulting damage is shown in Tables 2.43 and 2.44 and a photograph is shown in Fig. 2.16.

Table 2.43. Recorded height damage to Test Unit-4 from the 9-m crush test

	0°	90°	180°	270°
Pre-crush height (in.)	43.00	43.13	42.88	42.63
Post 9-m crust test height (in.)	39.38	40.38	40.63	39.75

Table 2.44. Recorded diametrical damage to Test Unit-4 from the 9-m crush test [Diameter (in.)]

Axial measurement location	0 to 180°		90 to 270°	
	Pre crush test	Post 9-m crush test	Pre crush test	Post 9-m crush test
Top false wire	19.25	19.25	19.38	19.38
Top rolling hoop	19.13	20.00	19.88	20.13
CG & top rolling hoop	19.81	20.00	19.38	20.06
CG rolling hoop	19.13	19.43	19.25	19.50
Bottom rolling hoop	19.25	19.94	19.25	20.00
Bottom false wire	19.25	19.25	19.25	19.25

Fig. 2.16. Cumulative damage from 9-m drop and crush testing on Test Unit-4.

Test Unit-5, weighing 157.4 kg (347 lb), was positioned in a horizontal attitude with the damaged portion of the test unit, resulting from prior drop tests, placed on the drop pad (0° mark facing down on test pad). The 500-kg (1100-lb) crush plate was centered over the test unit's center of gravity and dropped from 9 m (30 ft) squarely onto the top false wire of the drum at an ambient temperature of 29.6°C (85.3°F). Following initial impact, the package bounced very little before landing on its side. No drum studs, nuts, or washers were lost due to the impact. The lid was still firmly attached to the drum, with no visible separation or rips; thus, the position of the thermal barrier and neutron poison was maintained. A summary of the resulting damage is shown in Tables 2.45, 2.46, and 2.47. Additional pictorials of damage are shown on Fig. 2.17. Since the length of the crush plate did not encompass the entire length of the test package, additional indentations are recorded on Test Form 3.

Table 2.45. Recorded height damage to Test Unit-5 from the 9-m crush test

	0°	90°	180°	270°
Pre-crush height (in.)	44.50	43.50	43.38	43.50
Post 9-m crust test height (in.)	45.00	43.50	43.75	43.88

Table 2.46. Recorded diametrical damage to Test Unit-5 from the 9-m crush tests [Diameter (in.)]

Axial measurement location	0 to 180°		90 to 270°	
	Pre crush test	Post 9-m crush test	Pre crush test	Post 9-m crush test
Top false wire	18.75	18.69	19.38	19.38
Top rolling hoop	18.75	17.13	19.38	19.63
CG & top rolling hoop	18.75	17	19.38	20
CG rolling hoop	18.75	16.75	19.25	20
Bottom rolling hoop	18.75	16.50	19.25	19.75
Bottom false wire	18.44	17.00	19.31	19.38

Table 2.47. Recorded flat contour damage to Test Unit-5 from the 9-m crush test

Axial measurement location	Flats width maximum @ 0° (in.)	Flats width maximum @ 180° (in.)
Top false wire	8.88	0.00
Top rolling hoop	8.50	12.50
CG & top rolling hoop	8.00	12.00
CG rolling hoop	8.75	11.38
Bottom rolling hoop	10.25	11.38
Bottom false wire	11.38	10.50

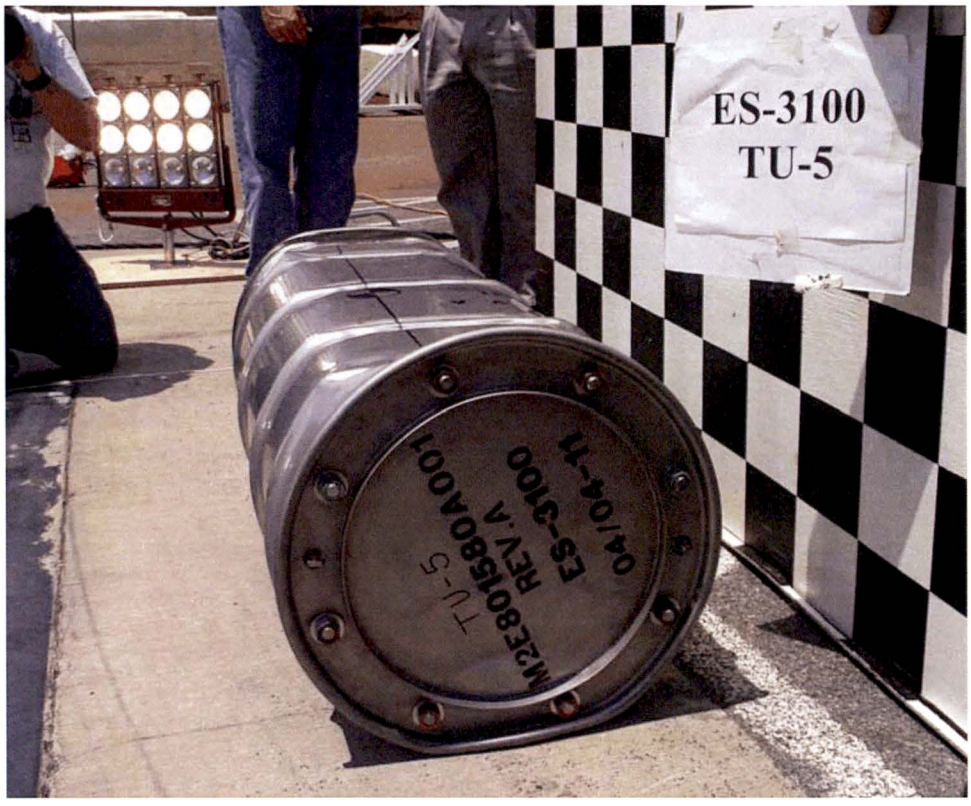

Fig. 2.17. Cumulative damage from 9-m drop and crush testing on Test Unit-5.

Conclusion. As noted in the discussion above, plastic deformation of the drum occurred in all test packages at the impacted areas. However, the position of the impact limiting material (Kaolite) and neutron poison material (BoroBond in the test packages) was maintained in all test packages. The maximum areal deformation along the side of the test packages was a flat measuring 31.75 cm (12.50 in.) wide at the drum's top rolling hoop and ending with a width of 26.67 cm (10.50 in.) at the drum bottom in Test Unit-5.

2.7.3 Puncture

Requirement. A free drop of 1 m (40 in.) from a position to obtain maximum damage onto the upper end of a solid, vertical, cylindrical, 15-cm (6-in.)–diameter mild steel bar mounted on an unyielding horizontal surface, is required by 10 CFR 71.73(c)(3). The bar must be ≥20 cm (8 in.) long with the top end rounded to 6-mm (0.25-in.) maximum radius. The long axis of the bar must be vertical.

Analysis. The five units previously dropped and crushed from 9-m (30 ft) [Sects. 2.7.1 and 2.7.2] were dropped from 1 m (40 in.) in accordance with 10 CFR 71.73(c)(3). The puncture bar was bolted to the steel plate of the inside drop pad surface at NTRC (see Sect. 2.6.7 regarding the indoor drop test pad). A description of the drop orientations and results are shown in Table 2.48. Figures 2.18 through 2.24 show the results of puncture testing.

Table 2.48. 1-m (40-in.) puncture drop test description and results

Test Unit	Test unit's long axis drop orientation	Axial and radial location from drum lid [a]	Recorded damage (indentation depth - in.)[b]	Photograph
1	Horizontal	Test Unit's CG (0° mark)	0.63	Fig. 2.18
1	Horizontal	8 in. down (180° mark)	0.38	Fig. 2.20
1	28° oblique from vertical	Drum lid's edge (90° mark)	three impact locations 1. 0.63 2. 0.38 3. 0.13	Fig. 2.18
1	40° oblique from vertical	In line with test unit's CG (270° mark)	two impact locations 1. 0.75 2. 0.13	Fig. 2.19
2	Horizontal	Test Unit's CG (0° mark)	0.13	Fig. 2.21
3	24.6° oblique from vertical	In line with test unit's CG (270° mark)	two impact locations 1. Additional flattening of lid 2. 0.88	Fig. 2.22
4	Vertical	Center of drum's lid & CG	0.13	Fig. 2.23
5	Horizontal	8 in. down (0° mark)	0.13	Fig. 2.24

[a] See detailed description of test units in Sect. 5.4.3 of ORNL/NTRC-013.
[b] For detailed description of damaged locations, see Test Form 4 for Test Units 1, 3, 4, and 5 and Test Form 3 for Test Unit-2.

Conclusion. Although all test units were deformed by this puncture test, no drum surfaces were breached, thereby maintaining the integrity of the thermal barrier and neutron poison.

2.7.4 Thermal

Requirement. Exposure of the specimen fully engulfed, except for a simple support system, in a hydrocarbon fuel/air fire of sufficient extent and in sufficiently quiescent ambient conditions to provide an average emissivity coefficient of at least 0.9, with an average flame temperature of at least 800°C (1475°F) for a period of 30 min, or any other thermal test that provides the equivalent total heat input to the package and that provides a time-averaged environmental temperature of 800°C (1475°F). The fuel source must extend horizontally at least 1 m (40 in.) but may not extend more than 3 m (10 ft) beyond any external surface of the specimen, and the specimen must be positioned 1 m (40 in.) above the surface of the fuel source. For purposes of calculation, the surface absorptivity must be either that value which the package may be expected to possess if exposed to the fire specified or 0.8, whichever is greater; and the convective coefficient must be that value which may be demonstrated to exist if the package were exposed to the fire specified. Artificial cooling may not be applied after cessation of external heat input, and any combustion of materials of construction must be allowed to proceed until it terminates naturally.

Analysis. The five test units previously subjected to both NCT and HAC drop testing were thermal tested in accordance with 10 CFR 71.73(c)(4). To determine the maximum temperatures reached during thermal testing, temperature indicating patches were placed at various locations throughout the test packages at assembly. The temperature range for each patch used is identified in Table 2.49. When the temperature of an indicator was reached, the color would change to black (i.e., blackout temperature). The range of possible blackout temperatures of the patches was from 51.67 to 260°C (125 to 500°F). For Test Units-1 through -5, Table 2.49 defines the number and location of the temperature indicating patches.

Fig. 2.18. 28° oblique and horizontal puncture tests on Test Unit-1.

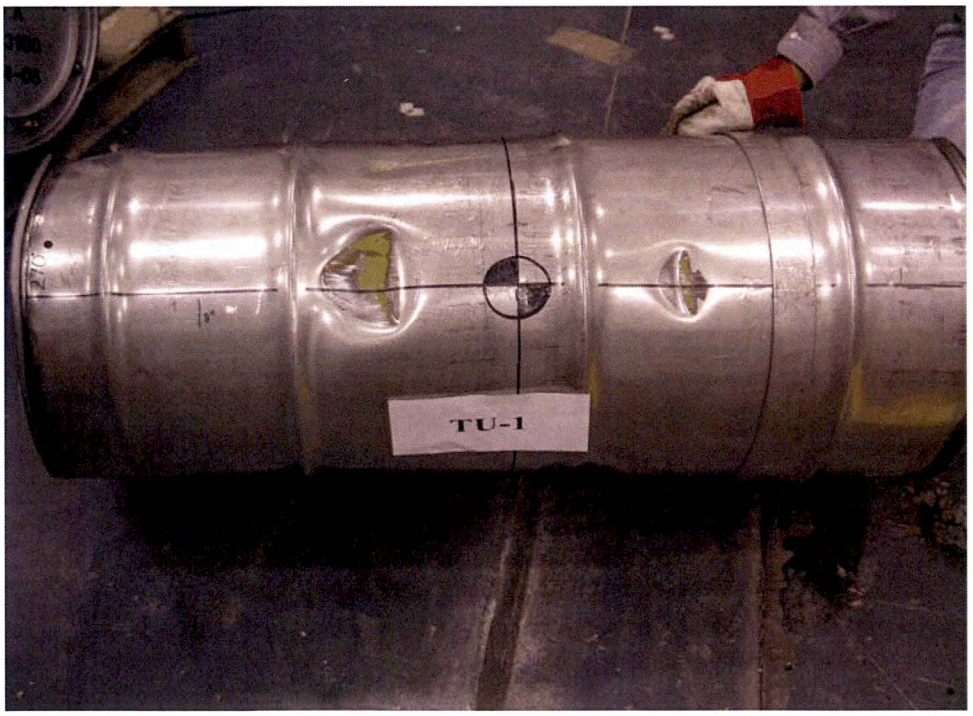

Fig. 2.19. 40° oblique puncture test on Test Unit-1.

Fig. 2.20. Horizontal puncture test over Test Unit-1's containment vessel flange.

Fig. 2.21. Horizontal CG puncture test on Test Unit-2.

Fig. 2.22. 24.6° oblique puncture test on Test Unit-3.

Fig. 2.23. Vertical puncture test on Test Unit-4.

Fig. 2.24. Horizontal puncture test over Test Unit-5's containment vessel flange.

Table 2.49. Thermax temperature indicating patches for test units

Patch Location	Internal surface	External surface	Temperature range °C (°F)	Test report figure (ORNL/NTRC-013)
Inner liner of drum assembly		8 (Full Range) 10 (5B & 5C)	52 to 260 (125 to 500) "B" 77 - 127 (171-261) "C" 132 - 182 (270-360)	5.3
Top plug weldment		4 (Full Range)	52 to 260 (125 to 500)	5.31
Containment vessel body flange	8 (4B & 4C)	8 (4B & 4C)	"B" 77 - 127 (171-261) "C" 132 - 182 (270-360)	5.28
Containment vessel body (end cap and cylinder)		5 (B)	"B" 77 - 127 (171-261)	5.28
Containment vessel sealing lid	4 (B)	4 (B)	"B" 77 - 127 (171-261)	5.29
Test mock-up components		6 (B)	"B" 77 - 127 (171-261)	5.26 & 5.27

Prior to the beginning of the thermal test, the No. 3 furnace at Timken Steel Company in Latrobe, Pennsylvania, was characterized for temperature and heat recovery times. Oxygen content in stack gases of the furnace was not monitored because it was not anticipated that any of the package's materials of construction were combustible. There was some burning of the silicone pads which are placed between the inner liners and the top plugs of the packages. However, it should be noted that this furnace employs "pulsed" fire burners. This type of burner is unique in that the natural gas flow rate is varied based on

furnace controller demands, but the flow of air through the burners is constant, even when no gas is flowing, thereby ensuring a very rich furnace atmosphere capable of supporting any combustion of package materials of construction. The support stand was welded to a large steel plate which had been placed on the floor of the furnace prior to heating. This steel plate acted as the radiating surface at the bottom of the furnace as well as providing the ability to hold the test stand rigidly in place. Before heating the furnace, workers practiced loading and unloading test packages from the cold furnace to assure that the furnace door would not remain open >90 s during each loading. In fact, the maximum time the door was open during any loading was 64 s.

A total of 18 thermocouples was installed on the furnace surfaces and on the test package support stand. (Appendix 2.10.7) All units were tested in a horizontal attitude with the end of the package facing the right and left side walls of the furnace. The test units were thermally tested with the 0° mark on the drum facing the floor of the furnace.

Each test unit was preheated to over 37.78°C (100°F) by placing the packages in an environmental chamber. The environmental chamber was heated by a torpedo-type kerosene space heater controlled by a mechanical bulb thermostat with a control range of 100°F to 200°F. The environmental chamber is a welded steel frame with fiberglass insulation panels. It was heated from the bottom with four floor register vents located around the perimeter and an 8 in. manual dampened center venting stove pipe. The setpoint temperature of the environmental chamber was monitored and adjusted for the duration of the preheat cycle. Initially, the thermostat was set to 66°C (150°F) for ~23 h. The thermostat set point was then reduced to ≥43°C (110°F) for the remainder of the preheat cycle. All packages were preheated for at least 47 h.

Six thermocouples were attached to the exterior surface of each test package after preheating. Metal retainer clips were welded to the drum to hold the thermocouples in place. The thermocouple tips were inserted underneath the metal clips and the wire was wrapped around the metal clip. To eliminate any radiant heat exchange between the thermocouples and the furnace walls, the tips and metal clips were covered with a ceramic coating.

No test package was loaded into the furnace until all functioning thermocouples on the furnace walls and support stand had a reading of 800°C (1475°F) or higher. All packages were placed in the preheated furnace on the support stand positioned with the long axis horizontal, the package lid facing toward a furnace side wall and oriented as described above. These packages were exposed to the radiation environment for a minimum of 30 min after all functioning furnace thermocouples, and at least five of the six test package exterior surface thermocouples reached a temperature of 800°C (1475°F). During the testing, the thermocouple temperature data were recorded every 15 s.

A minimum of 24 h prior to the beginning of all testing, the furnace was turned on with a set-point temperature of 871°C (1600°F). After each test, the furnace was allowed to reheat for a minimum of 45 min after obtaining the setpoint temperature before testing the next unit. The furnace control temperature data recorder ran continuously for the duration of the preheat. No test package was loaded into the furnace until all functioning thermocouples on the furnace walls and support stand had a reading of 800°C (1475°F) or higher.

Each test package was removed from the furnace and placed in an area where it was not exposed to artificial cooling. As the furnace door was opened for each test unit, smoking or flaming was visible from the TID lug hole at 0°. Flaming continued on some packages for 22 minutes and smoking continued up to one hour on others. All of the packages were allowed to cool naturally to room temperature. The post-thermal test weights of each unit were recorded on Test Form 1 of the test report.

(Appendix 2.10.8) The drums were disassembled, and the damage was photographed. The post-thermal test weight of each loaded containment vessel was also recorded. Each package was visually inspected, and the condition of the package and any observations were recorded.

After the containment vessels were removed from Test Units 1 through 5, two different leak tests were performed on each containment vessel. An operational leak test was conducted between the O-rings using a CALT5 leak tester. Following this operational leak test, a full body helium leak test was conducted. Details of these leak tests are provided in the test report (Appendix 2.10.7) and the results are summarized in Table 2.23. All five containment vessels were then removed from the drum assembly and immersed under a head of water of at least 0.9 m (3 ft) in a horizontal position for a period of ≥8 h. Following the immersion test of 10 CFR 71.73(c)(6), the containment boundary of Test Units-1 through -5 were opened to remove the contents, gather available data and look for signs of water in-leakage. No water in-leakage was detected in any of the units.

The blackout temperatures on the surface of all five containment boundaries, inner liners, and mock-up components used in the test packages are given in the test report (Test Form 5 for each test unit). Maximum blackout temperatures recorded on the surface of all test units are tabulated in Table 2.50. These values and temperature adjustments are discussed in Sect. 3.5.3.

Conclusion. All five test packages were intact following the 30-min exposure to the high-temperature thermal environment as required in 10 CFR 71.73(c)(4). Examination during disassembly showed that the containment boundary surfaces, flanges, fasteners, sealing surfaces, and O-rings were not damaged by the thermal testing. All five containment boundary assemblies met the subsequent 0.9-m (3-ft) water immersion test and maintained a full-body helium leak rate $\leq 2.0 \times 10^{-7}$ cm^3/s. Following compliance testing, minor changes were made to the mid liner, and the neutron poison was changed from BoroBond4 to Cat 277-4. In order to evaluate the impact of these changes, extensive analytical drop simulations were utilized. A detailed description of the models, material properties, and drop orientations evaluated is shown in Appendix 2.10.2. Results comparing structural deformation and maximum strains in the various material of construction are shown in Sect. 2.7.8. Based on the HAC analytical structural deformation results shown in Sect. 2.7.8, similar compliance test results would be expected had testing been conducted on packages employing the new proposed Cat 277-4 neutron poison. Therefore, the requirements of 10 CFR 71.73(c)(4) were satisfied, and containment was maintained.

2.7.4.1 Summary of pressures and temperatures

The ES-3100 shipping packages will typically be loaded at an ambient temperature and absolute pressure of ~25°C (77°F) and 101.35 kPa (14.70 psi), respectively. If the temperature of the package increases during shipment due to external temperature or solar insolation, the drum will not pressurize because four ventilation holes are drilled near the top of the drum, and the drum is not sealed at the drum lid–flange interface. The containment boundary is sealed at assembly. The internal pressure will increase due to transport temperatures, solar insolation (Sect. 3.4.1), decay heating, and the temperatures during HAC (Sect. 3.5.3). Temperature and pressures are summarized in Tables 3.21 and 3.11.

Table 2.50. Maximum HAC temperatures recorded on the test packages' interior surfaces

Temperature patch location [a]	ES-3100 Test Unit				
	1	2	3	4	5
	°C (°F)	°C (°F)	°C (°F)	°C (°F)	°C (°F)
Top plug bottom	149 (300)	163 (325)	177 (350)	177 (350)	177 (350)
Inner liner					
Flange step wall	135 (275)	163 (325)	135 (275)	135 (275)	135 (275)
BoroBond4 step	107 (225)	135 (275)	107 (225)	177 (350)[b]	121 (250)
CV body wall high	99 (210)	99 (210)	99 (210)	99 (210)	104 (219)
CV body wall middle	99 (210)	93 (199)	116 (241)[b]	93 (199)	99 (210)
Bottom flat portion	104 (219)	99 (210)	99 (210)	127 (261)	110 (230)
Containment boundary					
Lid (external top)	116 (241)	110 (230)	116 (241)	127 (261)	127 (261)
Lid (internal)	104 (219)	104 (219)	110 (230)	110 (230)	116 (241)
Flange (external)	116 (241)	110 (230)	110 (230)	116 (241)	121 (250)
Flange (internal)	104 (219)	99 (210)	116 (241)[b]	104 (219)	116 (241)
Body wall mid height	99 (210)	88 (190)	99 (210)	82 (180)	93 (199)
Bottom end cap (center)	99 (210)	99 (210)	88 (190)	110 (230)	99 (210)
Mock-up					
Side top	82 (180)	77 (171)	77 (171)	77 (171)	99 (210)
Side middle	77 (171)	77 (171)	77 (171)	77 (171)	93 (199)
Side bottom	77 (171)	77 (171)	77 (171)	77 (171)	88 (190)

[a] Refer to figures for exact locations and to Test Form 5 in the test report for recorded values. (ORNL/NTRC-013)
[b] Temperature indicating patch may have been damaged due to impact with surrounding structure. See Test Form 5 in ORNL/NTRC-013 for additional information.

The maximum HAC internal absolute pressure in the containment boundary of the ES-3100 has been calculated to be 595.99 kPa (86.441 psia). This predicted pressure is based on a conservative maximum adjusted average gas temperature of 123.85°C (254.93°F) as shown in Sect. 3.5.3 and Appendix 3.6.5.

2.7.4.2 Differential thermal expansion

The drum, inner liner, and containment vessel are all constructed of type 304 or 304L stainless steel. Because of design clearances used during assembly, radial and vertical expansion among these components will not cause any interferences or thermally induced stresses. Due to similarities of the coefficient of thermal expansion between type 304/304L and the containment vessel closure nut (ASTM A-479 and ARMCO Nitronic 60), the compression of the O-rings and the closure nut and containment vessel thread load do not change appreciably during the temperature excursion from 25°C (77°F) to the maximum adjusted containment vessel temperature of 152.22°C (306.0°F) [Sect. 3.5.3].

The Kaolite 1600 insulation and Cat 277-4 neutron poison are poured and cast in place during the fabrication of the drum assembly weldment (Drawing M2E801580A002, Appendix 1.4.8). This process produces a zero gap between the insulation and the bounding drum and inner liner and zero gap between the neutron poison and the mid and inner liners. Because of differences in coefficients of thermal expansion, some radial and axial interferences are expected from thermal growth of the liners. These radial and axial interferences have been addressed by the HAC thermal test. The results show that the stresses induced are minimal and do not reduce the effectiveness of the drum assembly.

Since there are ample clearances between the various size convenience containers and HEU contents, no induced thermal stresses from differences in coefficient of thermal will exist.

2.7.4.3 Stress calculations

The temperature gradient on the containment boundary was essentially uniform from top to bottom during the thermal tests (Table 2.50). The gradient around the periphery of the six test units was also essentially uniform and similar to the vertical gradient. As noted in the ES-3100 test report, the temperatures recorded on the containment vessels of all the test units were fairly uniform, both vertically and circumferentially. The maximum temperature variation on the containment vessels was ~50°F (from the test temperatures reported in Table 2.50). No damage would be expected on the containment vessel from thermal stresses resulting from a temperature differential of this magnitude. This conclusion is based on the guidelines given in the *ASME Boiler and Pressure Vessel Code*, Sect. III, Div. 1. Thermal stress is defined as a self-balancing stress produced by a nonuniform distribution of temperature (ASME B&PVC, Sect. III, Paragraph NB-3213.13). This paragraph further states that there are two types of thermal stresses: general thermal stress and local thermal stress. An example of a general stress is that produced by an axial temperature distribution in a cylindrical shell (ASME B&PVC, Paragraph NB-3213.9). This general stress is further classified (Paragraph NB-3213.9) as a secondary stress (that is, a normal stress or a shear stress developed by the constraint of adjacent materials or by self-constraint of the structure) [ASME B&PVC, Paragraph NB-3213.9]. Paragraph NB-3213.9 further states that the basic characteristic of a secondary stress is that it is self-limiting. Local yielding and minor distortions can satisfy the conditions that cause the stress to occur, and failure from a single application would not be expected. An example of a local thermal stress is a small hot spot in the wall of a pressure vessel (ASME B&PVC, Paragraph NB-3213.13). Local thermal stress is associated with almost complete suppression of the differential expansion and thus produces no significant distortion. Such stresses are considered only from a fatigue standpoint. Fatigue will not result from a one-time cyclic event such as an accidental fire.

The principal effect of the elevated temperature on stress levels is caused by the increase in the internal pressure. The calculated stresses as shown in Table 2.51 were determined by multiplying the stress at the design conditions (Appendix 2.10.1) by a factor equal to the ratio of operating pressures to design pressures and adding any contribution from the closure nut preload. This methodology is based on the application of linear elastic material behavior. As shown in Sect. 2.7.4.4, all stresses in the containment boundary components (based on nominal dimensions for the components) are well below the *ASME Boiler and Pressure Vessel Code* allowable stress intensity limits.

2.7.4.4 Comparison with allowable stresses

As noted in Sect. 2.7.4.3, the differential stresses resulting from temperatures recorded during HAC are negligible. Also, as shown in Table 2.51, stresses of this low magnitude do not affect the adequacy of the packaging. Corresponding calculated stress regions are shown in Fig. 2.1.

Table 2.51. HAC ES-3100 containment boundary stress compared to the allowable stress [a]

Stress locations shown in Fig. 2.1	Thermal condition 10 CFR 71.73 (c)(4) containment boundary stress @479.56 kPa (69.555 psi) gauge & 123.85°C (254.93°F) kPa (psi)		Immersion condition 10 CFR 71.73 (c)(6) containment boundary stress @−150 kPa (−21.76 psi) gauge & −2.22°C (28°F) kPa (psi)		Allowable stress (AS)
	kPa (psi) or kg (lb)	M.S.	kPa (psi) or kg (lb)	M.S.	kPa (psi) or kg (lb)
Top flat portion of sealing lid (center of head)	4.724×10^3 (685.3)	27.0	1.478×10^3 (214.4)	88.6	1.324×10^5 (19,200) [b]
Closure nut ring (away from threaded portion)	7.505×10^4 (10,885)	5.1	4.246×10^4 [f] (6,158)	9.8	4.571×10^5 (66,300) [c]
Top flat head (sealing surface region)	2.501×10^4 (3,627.4)	9.6	1.665×10^4 [f] (2,415)	14.9	2.648×10^5 (38,400) [c]
Cylindrical section (middle)	1.370×10^4 (1,986.6)	5.4	4.285×10^3 (621.5)	19.6	8.825×10^4 (12,800) [d]
Cylindrical section (shell-to-flange interface)	2.379×10^4 (3,450.8)	10.1	1.238×10^4 (1,795.3)	20.4	2.648×10^5 (38,400) [c]
Cylindrical section (shell-to-bottom interface)	3.513×10^4 (5,095.7)	6.5	1.099×10^4 (1,594.2)	23.1	2.648×10^5 (38,400) [c]
Body flange threads load, kg (lb)	1.691×10^3 (3,727.6)	11.1	9.072×10^2 [f] (2,000)	21.6	2.053×10^4 (45,266) [e]
Body flange thread region (under cut region)	4.924×10^4 (7,141.9)	4.4	2.397×10^4 [f] (3,476)	10	2.648×10^5 (38,400) [c]
Flat bottom head (center)	3.307×10^4 (4,796.9)	3.0	1.035×10^4 (1,500.7)	11.8	1.324×10^5 (19,200) [b]
Closure nut thread load, kg (lb)	1.691×10^3 (3,727.6)	20.0	9.072×10^2 [f] (2,000)	38.1	3.545×10^4 (78,154) [e]

[a] Calculated stresses were determined by multiplying the stress at the design conditions (Appendix 2.10.1) by a factor equal to the ratio of operating pressures to design pressures (independent of pressure direction) plus contribution from preload. Allowable stress values are taken from Table 2.5.

[b] Stress interpreted as the sum of $P_l + P_b$; allowable stress intensity value is $1.5 \times S_m$.

[c] Stress interpreted as the sum of $P_l + P_b + Q$; allowable stress intensity value is $3.0 \times S_m$.

[d] Stress interpreted as the primary membrane stress (P_m); allowable stress intensity value is S_m.

[e] Allowable shear capacity is defined as $0.6 \times S_m \times$ thread shear area. Thread shear area = 38.026 cm^2 (5.894 in.^{2}).

[f] Stress and shear load in these areas are dominated by the 162.7 ± 6.8 N·m (120 ± 5 ft-lb) preload.

2.7.5 Immersion—Fissile Material

Requirement. In those cases for which water leakage into the containment boundary has not been assumed for criticality analysis, the specimen must be immersed under a 0.9-m (3-ft) head of water in an attitude for which maximum leakage is expected, as required by 10 CFR 71.73(c)(5).

Analysis. The containment vessels for the ES-3100 test packages (Units-1 through -5) were removed from their respective drum assemblies following the thermal tests described in Sect. 2.7.4.

After examination for damage (distortion, warpage, heating), the volume between the O-rings was pressurized, and the O-ring seals were leak checked in accordance with the CALT5 manufacturer's instructions manual using the CALT5 leak tester. Following the O-ring cavity check, the containment vessel lids were drilled and tapped for a full-body helium leak check. The seals remained functional on all vessels, and the integrity of the containment vessel structure was maintained (indicated by a helium leak rate $\leq 2.0 \times 10^{-7}$ cm^3/s). Following these leak tests, each unit was then submerged under a 0.9-m (3-ft) head of water for at least 8 h. No water leakage into the vessel was seen in any of the test units. The results of this test for each unit are recorded on the data sheet of Procedure TTG-PRF-14 shown in the test report. (Appendix 2.10.8) It should be noted that the criticality analysis does assume water leakage into the ES-3100 containment vessel; however, the 0.9-m (3-ft) immersion tests were performed anyway.

2.7.6 Immersion—All Packages

Requirement. A separate, undamaged specimen must be immersed under water at a pressure equivalent to a 15-m (50-ft) head of water, as required by 10 CFR 71.73(c)(6). This requirement may be satisfied by an external pressure of 150 kPa (21.7 psi) gauge.

Analysis. Immersion under a 15-m (50-ft) head of water would result in water entering the drum because the plastic plugs covering the four ventilation holes could fail, and the drum/lid flange is not gasketed. The ES-3100 containment boundary has been designed and tested for an external pressure of 150 kPa (21.7 psi) gauge and an internal gauge pressure of 699.82 kPa (101.5 psi), using nominal dimensions for all boundary components. Each containment vessel design incorporates an O-ring seal of verified integrity to provide assurance that no water will penetrate the containment boundary. The containment boundary of Test Unit-6 was subjected to this 15-m (50-ft) water immersion test. No visual signs of water leakage into the containment boundary were recorded.

2.7.7 Deep Water Immersion Test (for Type B Packages Containing More than 10^5 A_2)

The amount of A_2s proposed for transport is ~293.99. Therefore, the deep water immersion test is not applicable.

2.7.8 Summary of Damage

After testing five full scale ES-3100 test packages under HAC, the drum, drum lid, and top plug were damaged as expected. The containment boundary flange, O-ring grooves, and closure nut were not damaged. Plastic deformation occurred in the five drum assemblies in the impact areas from the 1.2-m and 9-m (30-ft) drop, crush and subsequent puncture tests. No breaks were noted in the drum assembly, and no insulation was exposed. The resultant damage did not reduce the effective center-to-center package spacing to a point of criticality concern (Sect. 6).

The full scale test units were fabricated in accordance with drawings created for production hardware. During the procurement process for the full scale test units, several small changes were suggested by the manufacturer to improve the efficiency and to reduce the cost of fabrication. These changes were incorporated and tested. However, following compliance testing, the following changes have been made to the proposed production hardware. First, a change in the neutron poison from BoroBond4 to Cat 277-4 has been adopted; second, the mid liner design has been changed to a continuous shell by reducing the diameter of the step in the inner liner for the containment vessel flange

from 22.35 cm (8.8 in.) to 21.84 cm (8.6 in.); and third, the silicone rubber pad thickness on the drum assembly bottom liner was increased by ~0.15 cm (0.06 in.). The second change increased the amount of Kaolite 1600 around the containment vessel flange, increased the final volume of the neutron poison, and slightly decreased the volume of the Kaolite 1600 adjacent to the neutron poison. The third change was made to stiffen the rubber pad so it would remain in place during vibration normally incurred during transport. In order to evaluate the impact of these changes, analytical drop simulations were conducted and documented in Appendix 2.10.2. The drop simulations were conducted in the same attitude and temperature regime as those conducted during the compliance testing phase for certification. Temperature dependent material properties were used in the analysis. The results of the structural deformation from compliance testing, drop simulation using BoroBond4 and drop simulations using Cat 277-4 material are presented in the following tables and figures. The analytical structural deformation results shown in Tables 2.52 through 2.61 are nearly identical for the two neutron poisons. The analytical results are also well representative of the results recorded during compliance testing as depicted in Figs. 2.25 through 2.30. Analytical strain prediction in the structural components are also compared for the two neutron poisons. Although there are minor differences between the compliance testing and drop simulations, the overall magnitude of the strains is very similar. The thermal aspects of these changes are addressed in Sect. 3. NCT and HAC results predicted for an undamaged package show that the change in neutron poison actually reduces the final temperature of the containment vessel components. Therefore, the substitution of Cat 277-4 material and the minor changes in the inner and mid liners for production hardware should not reduce the effectiveness of the packaging when subjected to the regulatory requirements of 10 CFR 71.71 and 71.73, and the results of compliance testing would be analogous. Some of the test units lost approximately 0.45 kg (1 lb) of their gross weight due to boiling off of the water trapped in the refractory and BoroBond4 materials (Table 2.62).

Assuming all water loss is from the neutron poison, the BoroBond4 material lost ~ 9.4% of its water content. Using the temperature data recorded during HAC testing shown in Table 2.50 and applying the temperature adjustments discussed in Sect. 3.5.3, the average temperature of the neutron poison would be ~150°C (302°F). Since the ES-3100 test units were not fabricated packages with Cat 277-4, thermogravimetric analysis (TGA) was used to compare the neutron poison's propensity to lose water. The results of this analysis are shown in Appendix 2.10.4 (Thompson, *Summary of TGA Testing*). Samples of both BoroBond4 and Cat 277-4 were TGA tested, and the results were compared at 150°C (302°F). The BoroBond4 samples lost ~ 61.6% of their original water content. The dry Cat 277-4 lost a maximum of only 6.61%. The BoroBond4 TGA samples lost ~6.5 times the amount of water lost by the ES-3100 test units during HAC compliance testing. Assuming comparable results would be expected for the Cat 277-4 material due to similarity in the structural configuration, installation methodology, and LS-Dyna drop simulation structural deformation results, the Cat 277-4 water loss would be only 1.02%. Criticality safety analysis assumes a greater percent loss; therefore, additional conservatism is being applied in this SAR.

The maximum blackout temperature recorded adjacent to the O-rings during testing was 127.22°C (241°F) [Table 2.50]. Using the adjustments discussed in Sect. 3.5.3, the maximum adjusted temperature at the containment boundary O-rings during shipment under HAC was calculated to be 141.22°C (286.2°F). The normal operating temperature for these O-rings is −40 to 150°C (−40 to 302°F) as shown in Table 2.15. Therefore, containment will be maintained during HAC.

Table 2.52. Diametrical damage comparison of Test Unit-1 with analytical predictions [Diameter (in.)]

	0 to 180°			90 to 270°		
Axial measurement location	**Test results**	**Analytical results with BoroBond**	**Analytical results with Cat 277-4**	**Test results**	**Analytical results with BoroBond**	**Analytical results with Cat 277-4**
Top false wire	15.63	15	14.9	20.63	20.7	20.7
Top rolling hoop	16	15.3	15.1	20.44	20.8	20.8
CG & top rolling hoop	16.25	15.9	15.7	20.25	20.6	20.7
CG rolling hoop	16.5	16.4	16.2	19.88	20.1	20.4
Bottom rolling hoop	18.25	18.3	18.1	19.5	19.6	19.8
Bottom false wire	17.81	18.1	18	19.25	19.4	19.4

Table 2.53. Flat contour damage comparison of Test Unit-1 with analytical results

Axial measurement location	**Flats width @ 0° (in.)**			**Flats width @ 180° (in.)**		
	Test results	**Analytical results with BoroBond**	**Analytical results with Cat 277-4**	**Test results**	**Analytical results with BoroBond**	**Analytical results with Cat 277-4**
Top false wire	9	10.5	10.5	8.5	10.5	10.9
Top rolling hoop	10	11	11	10	11	11
CG & top rolling hoop	10	10.1	10.1	10.13	10.1	10.1
CG rolling hoop	9	8.4	8.4	10.63	10.1	10.1
Bottom rolling hoop	8.25	7.6	7.6	---	0	0
Bottom false wire	9.88	10.1	10.1	---	0	0

Fig. 2.25. Visual comparison of the cumulative damage on the crush side surface after the three drop tests (from top to bottom: Test Unit-1, analytical results with BoroBond, analytical results with Cat 277-4).

Table 2.54. Cumulative analytical 12° slapdown drop tests maximum effective plastic strain results

Component	Component material	Effective plastic strain (in./in.)			
		Offset crush		Centered crush	
		Model with BoroBond	Model with Cat 277-4	Model with BoroBond	Model with Cat 277-4
CV body	Type 304L stainless steel	0.0457	0.0564	0.0741	0.0643
CV lid	Type 304L stainless steel	0.0005	0.0013	0.0006	0.0018
CV closure nut	A-479 nitronic 60	0.0000	0.0001	0.0003	0.0000
Angle	Type 304 stainless steel	0.1045	0.1070	0.0917	0.0944
Drum	Type 304 stainless steel	0.3972	0.3920	0.3537	0.3443
Drum bottom	Type 304 stainless steel	0.2877	0.2879	0.2919	0.3000
Liner	Type 304 stainless steel	0.2702	0.2060	0.2363	0.2846
Lid	Type 304 stainless steel	1.0797	0.9689	1.0795	0.5828
Lid stiffener	Type 304 stainless steel	0.0838	0.0894	0.0303	0.0288
Drum lid studs	Type 304 stainless steel	>0.57	0.4018	0.3174	0.2390
Lid hex nut	Silicon bronze - C65100	0.0086	0.0028	0.0000	0.0000
Drum washer	300 series stainless steel	0.1003	0.0790	0.0597	0.0775
Top plug weldment	Type 304 stainless steel	0.2715	0.2665	0.1636	0.1644

Table 2.55. Diametrical damage comparison of Test Unit-2 with analytical predictions [Diameter (in.)]

Axial measurement location	0 to 180°			90 to 270°		
	Test results	Analytical results with BoroBond	Analytical results with Cat 277-4	Test results	Analytical results with BoroBond	Analytical results with Cat 277-4
Top false wire	17.63	18.1	18	19.81	19.6	19.6
Top rolling hoop	17.38	16.6	16.6	19.75	19.75	20.1
CG & top rolling hoop	17	16.5	16.5	20	20	20.4
CG rolling hoop	16	16.3	16.3	20.25	20.25	20.5
Bottom rolling hoop	15.5	16.1	16.1	20.13	20.13	20
Bottom false wire	18	17.6	17.6	19.25	19.38	19.4

Table 2.56. Flat contour damage comparison of Test Unit-2 with analytical predictions

Axial measurement location	Flats width @ 0° (in.)			Flats width @ 180° (in.)		
	Test results	Analytical results with BoroBond	Analytical results with Cat 277-4	Test results	Analytical results with BoroBond	Analytical results with Cat 277-4
Top false wire	8	9.2	9.2	6.25	0	0
Top rolling hoop	9	8.4	9.3	8.88	10.1	10.1
CG & top rolling hoop	10.13	8.4	8.4	9.63	8.4	9.3
CG rolling hoop	9.88	9.3	9.3	12	9.3	9.3
Bottom rolling hoop	9.88	9.3	9.3	14.88	10.1	10.1
Bottom false wire	9.38	10.1	10.1	0	0	0

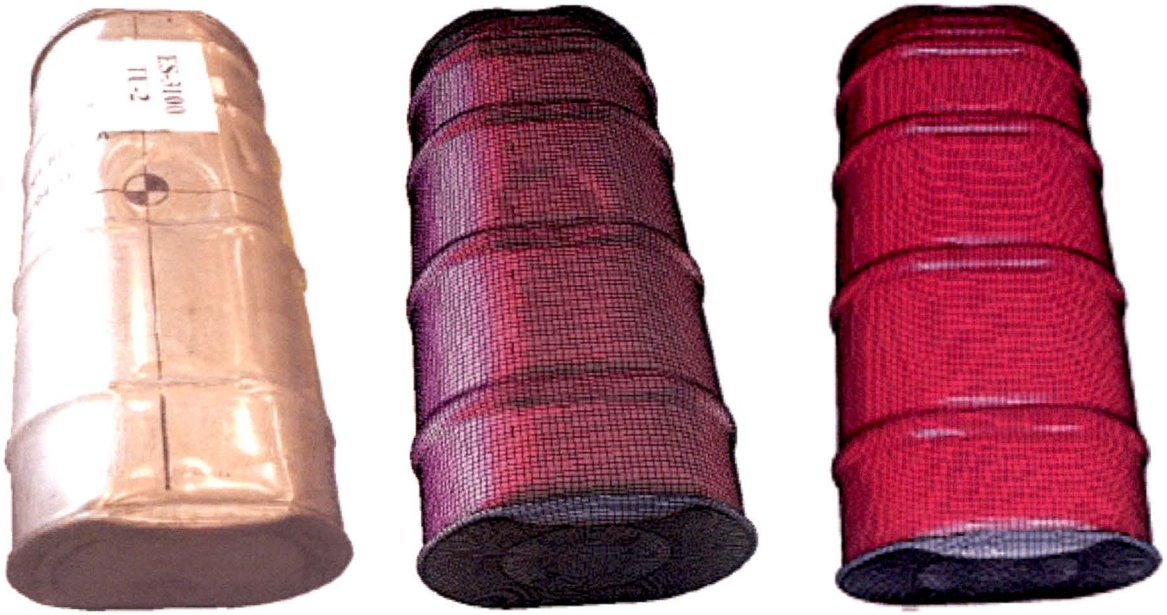

Fig. 2.26. Visual comparison of the cumulative damage on the rigid surface side after the four drop tests (from left to right: Test Unit-2, analytical results with BoroBond, analytical results with Cat 277-4).

Fig. 2.27. Visual comparison of the cumulative damage on the crush plate side after the three drop tests (from left to right: Test Unit-2, analytical results with BoroBond, analytical results with Cat 277-4).

Table 2.57. Cumulative analytical side drop test maximum effective plastic strain results

Component	Component material	Effective plastic strain (in./in.)	
		Model with BoroBond	Model with Cat 277-4
CV body	Type 304L stainless steel	0.0462	0.0525
CV lid	Type 304L stainless steel	0.0004	0.0004
CV closure nut	A-479 nitronic 60	0.0000	0.0005
Angle	Type 304 stainless steel	0.0816	0.0845
Drum	Type 304 stainless steel	0.2623	0.2814
Drum bottom	Type 304 stainless steel	0.2807	0.2827
Liner	Type 304 stainless steel	0.2005	0.2022
Lid	Type 304 stainless steel	0.6411	0.6413
Lid stiffener	Type 304 stainless steel	0.0217	0.0171
Drum studs	Type 304 stainless steel	0.1753	0.2364
Drum hex nut	Silicon bronze - C65100	0.0000	0.0018
Drum washer	300 series stainless steel	0.1034	0.0439
Top plug weldment	Type 304 stainless steel	0.1258	0.1286

Table 2.58. Diametrical damage comparison of Test Unit-3 with analytical predictions [Diameter (in.)]

Axial measurement location	0 to 180°			90 to 270°		
	Test results	Analytical results with BoroBond	Analytical results with Cat 277-4	Test results	Analytical results with BoroBond	Analytical results with Cat 277-4
Top false wire	19.25	19	19	19.06	19	19
Top rolling hoop	18.75	18.9	18.9	20.25	20.6	20.6
CG & top rolling hoop	19.25	19.4	19.4	19.75	19.9	19.8
CG rolling hoop	19.13	19.3	19.3	19.25	19.4	19.4
Bottom rolling hoop	19.13	19.3	19.3	19.75	20.4	20.4
Bottom false wire	18	18.6	18.6	19.38	19.4	19.4

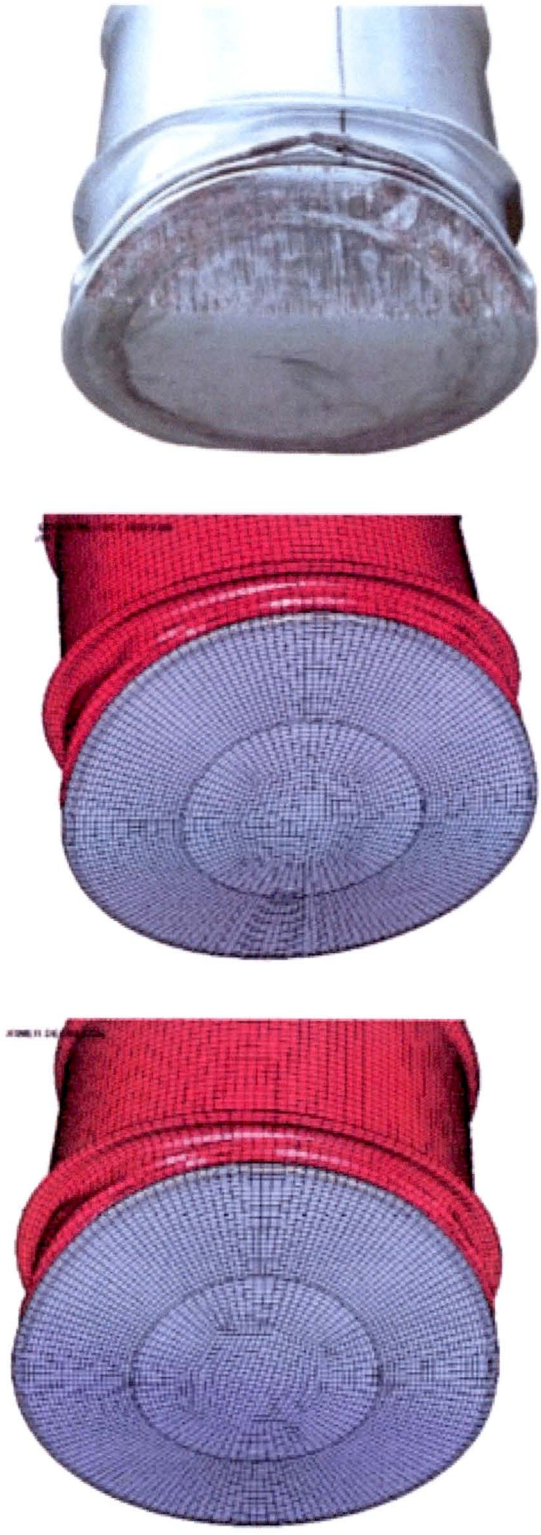

Fig. 2.28. Visual comparison of the cumulative bottom damage after the three drop tests (from top to bottom: Test Unit-3, analytical results with BoroBond, analytical results with Cat 277-4).

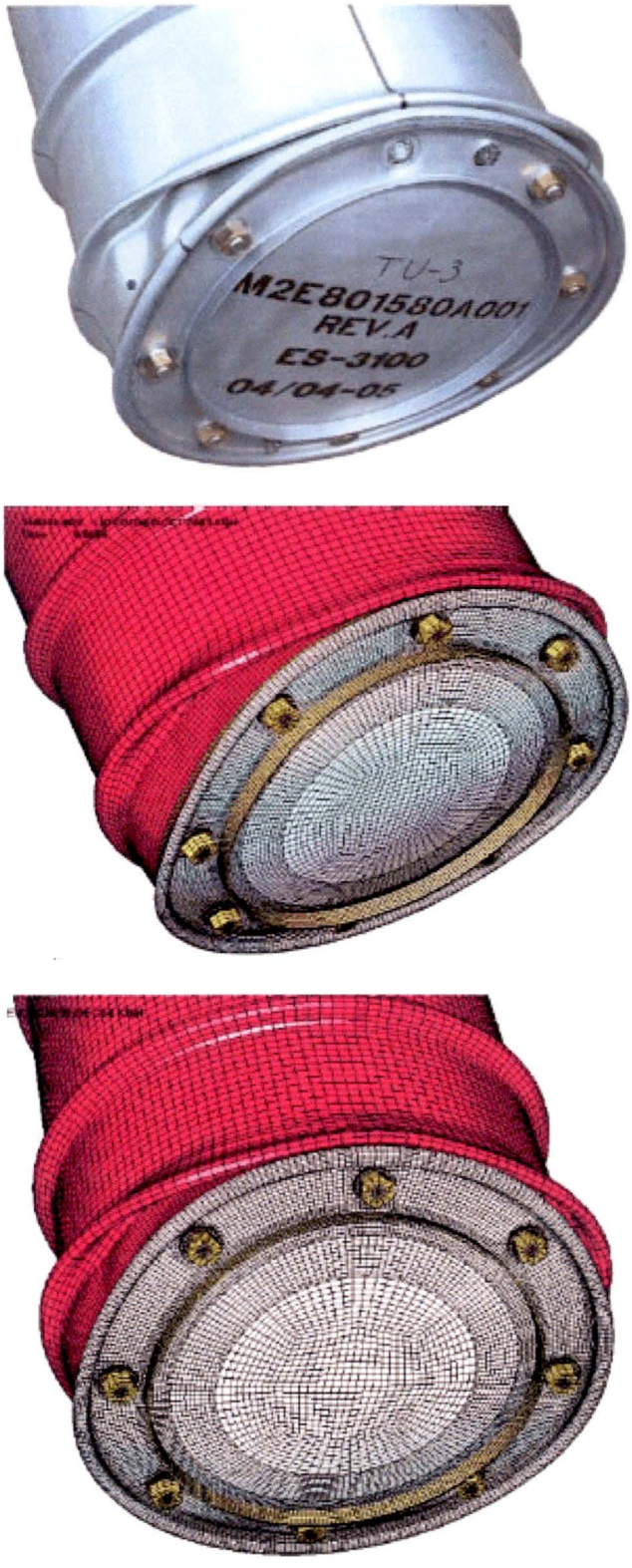

Fig. 2.29. Visual comparison of the cumulative lid damage after the three drop tests (from top to bottom: Test Unit-3, analytical results with BoroBond, analytical results with Cat 277-4).

Table 2.59. Cumulative analytical corner drop test maximum effective plastic strain results

Component	Component material	Effective plastic strain (in./in.)	
		Model with BoroBond	Model with Cat 277-4
CV body	Type 304L stainless steel	0.0364	0.0371
CV lid	Type 304L stainless steel	0.0024	0.0051
CV closure nut	A-479 nitronic 60	0.0000	0.0002
Angle	Type 304 stainless steel	0.0464	0.0462
Drum	Type 304 stainless steel	0.3787	0.3830
Drum bottom	Type 304 stainless steel	0.0731	0.0761
Liner	Type 304 stainless steel	0.5507	0.5254
Lid	Type 304 stainless steel	0.3579	0.3622
Lid stiffener	Type 304 stainless steel	0.0272	0.0272
Drum studs	Type 304 stainless steel	0.5578	0.5598
Drum hex nut	Silicon bronze - C65100	0.2258	0.2266
Drum washer	300 series stainless steel	0.1111	0.1528
Top plug weldment	Type 304 stainless steel	0.1170	0.1166

Table 2.60. Diametrical damage comparison of Test Unit-4 with analytical predictions [Diameter (in.)]

Axial measurement location	0 to 180°			90 to 270°		
	Test results	Analytical results with BoroBond	Analytical results with Cat 277-4	Test results	Analytical results with BoroBond	Analytical results with Cat 277-4
Top false wire	19.25	19.3	19.3	19.38	19.3	19.3
Top rolling hoop	20.00	20.2	20.1	20.13	20.2	20.1
CG & top rolling hoop	20.00	20.2	20.2	20.06	20.2	20.2
CG rolling hoop	19.44	20.1	20.1	19.5	20.1	20.1
Bottom rolling hoop	19.94	20.5	20.5	20	20.5	20.5
Bottom false wire	19.25	19.4	19.4	19.25	19.4	19.4

Fig. 2.30. Visual comparison of the cumulative damage after the three drop tests (from left to right: Test Unit-4, analytical results with BoroBond, analytical results with Cat 277-4).

Table 2.61. Cumulative analytical top drop test maximum effective plastic strain results

Component	Component material	Effective plastic strain (in./in.)	
		Model with BoroBond	Model with Cat 277-4
CV body	Type 304L stainless steel	0.0053	0.0083
CV lid	Type 304L stainless steel	0.0034	0.0072
CV closure nut	A-479 nitronic 60	0.0000	0.0011
Angle	Type 304 stainless steel	0.0304	0.0308
Drum	Type 304 stainless steel	0.1258	0.1237
Drum bottom	Type 304 stainless steel	0.0312	0.0267
Liner	Type 304 stainless steel	0.3585	0.3812
Lid	Type 304 stainless steel	0.1415	0.1389
Lid stiffener	Type 304 stainless steel	0.0098	0.0100
Drum studs	Type 304 stainless steel	0.1541	0.1535
Drum hex nuts	Silicon bronze - C65100	0.0170	0.0173
Drum washer	300 series stainless steel	0.0510	0.0506
Top plug weldment	Type 304 stainless steel	0.0944	0.0960

Table 2.62. ES-3100 test package weights before and after 10 CFR 71.73(c)(4) HAC thermal testing

Test Unit	Pre-test [a] weight kg (lb)	Post-test [a] weight kg (lb)	Thermal test weight loss kg (lb)	BoroBond4 original weight [b] kg (lb)	Water weight in BoroBond4[c] kg (lb)	Water loss percent [d] (%)
1	202.3 (446)	202.3 (446)	0.0 (0)	20.7 (45.64)	4.91 (10.82)	0.00
2	202.8 (447)	202.8 (447)	0.0 (0)	20.5 (45.19)	4.86 (10.72)	0
3	203.7 (449)	203.2 (448)	0.45 (1)	20.5 (45.19)	4.87 (10.74)	9.31
4	201.8 (445)	201.4 (444)	0.45 (1)	20.4 (44.97)	4.84 (10.66)	9.38
5	157.4 (347)	156.9 (346)	0.45 (1)	20.6 (45.42)	4.89 (10.77)	9.29

[a] Data from the test report. (Appendix 2.10.7)
[b] Weight of BoroBond4 and water obtained from casting data. (ES-3100 Weldments)
[c] This weight is based on TGA measurements and calculation showing that the minimum water percent is 23.71%.
[d] All weight loss attributed to loss of water in BoroBond4.

Following the thermal test, all five containment boundaries were subjected to leak testing of the O-ring cavity as well as the full-body helium leak check. To verify the entire containment boundary, all test units were drilled and tapped for a helium leak check using the procedure documented in the test report. (Appendix 2.10.7) The procedure consisted of creating a near vacuum inside the containment vessel and supplying a helium environment around the exterior of the assembly. The maximum recorded helium leak rate for any of these containment vessels was 2.0×10^{-7} cm^3/s as documented after 20 min of leak checking. This procedure measures leakage in the opposite direction to leakage from the vessel. It could be postulated that the additional pressure differential (ambient on the exterior and a near vacuum inside) would help to further compress the O-rings during this test. However, since the containment vessel closure nut is screwed down, the additional pressure does not compress the O-ring more than a few ten thousands of an inch based on mismatch between the internal and external threaded joint. Only rotation of the closure nut will alter O-ring compression significantly. Pictures taken of all containment vessel tops following testing showed that the closure nut had rotated a maximum of 0.15 cm (0.060 in.) [Fig. 2.31] from its original radial position obtained during assembly (Fig. 2.32) except for Test Unit-4, which showed no rotation. Based on the pitch of the closure nut, this rotation translates into only 0.0009 cm (0.00035 in.) decompression of the O-rings. This compares to the original nominal compression of 0.064 cm (0.025 in.). According to the *Parker O-Ring Handbook*, the minimum squeeze for all seals, regardless of cross section should be about 0.018 cm (0.007 in.). Using the nominal compression of 0.064 cm (0.025 in.) and subtracting the decompression from rotation and the minimal pressure differential compression, there is ample O-ring compression. Therefore, the leak test in either direction for this containment vessel arrangement is valid. As required in 10 CFR 71.73(c)(5), the containment vessels were submerged under a 0.9-m (3-ft) head of water following the leakage tests, with no water in-leakage permitted. Following this immersion test, the containment vessels were opened. The lid assembly, with the O-rings in place on the body, are joined together by torquing the closure nut and sealing lid assembly to 162.7 ± 6.8 N·m (120 ± 5 ft-lb). The lowest break-loose torque value of 40.7 N·m (30 ft-lb) was recorded for Test Unit-4. Visual inspection following the testing indicated that neither the vessel bodies, the O-rings, the seal areas, nor the vessel lid assemblies were damaged during the tests. In Test Unit-5, the convenience cans had buckled from the pressure differential caused during the leak testing operation. However, the containment vessel wall showed little or no signs of impact. Therefore, based on the success of these six test units (including the containment vessel of Test Unit-6) and the analytical drop simulation effort, the structural integrity of the ES-3100 package, with the previously mentioned modifications, meets all the applicable requirements of 10 CFR 71.73 for transport of the proposed contents.

Fig. 2.31. Containment vessel markings at assembly (swivel hoist ring removed prior to testing).

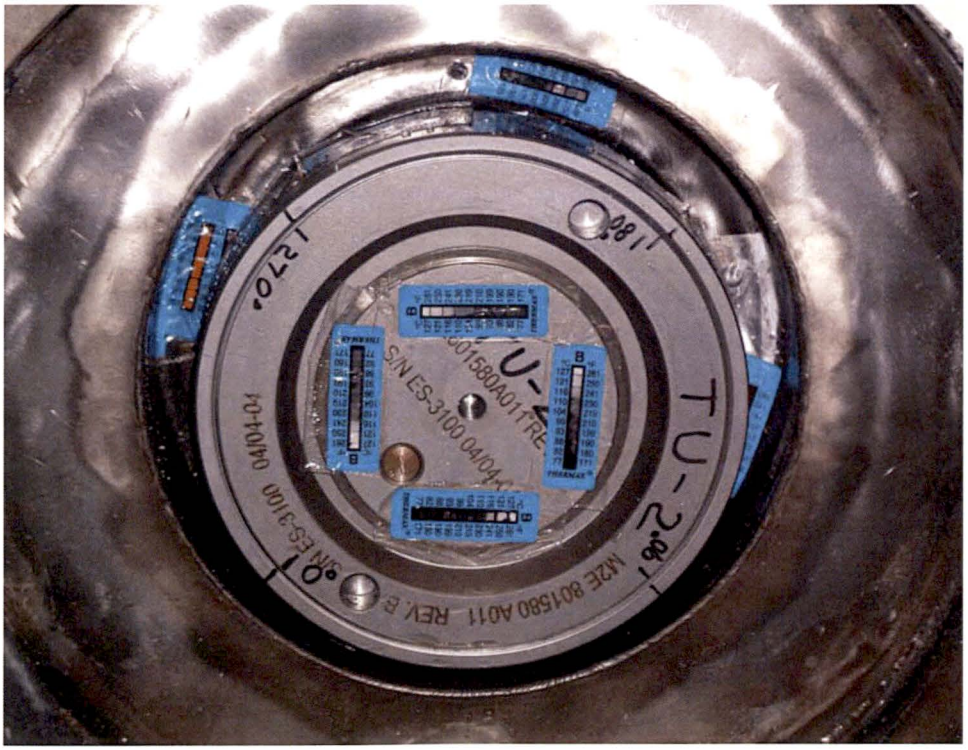

Fig. 2.32. Containment vessel marking after compliance testing.

2.8 ACCIDENT CONDITIONS FOR AIR TRANSPORT OF PLUTONIUM

The proposed contents are not shipped by air; therefore, this section is not applicable.

2.9 ACCIDENT CONDITIONS FOR FISSILE MATERIAL PACKAGES FOR AIR TRANSPORT

The expanded tests specified in 10 CFR 71.55(f)(1), (2), or (3) for fissile material package designs for air transportation were not conducted. The issue of subcriticality is addressed in Section 6 with content mass limits as addressed in Section 1.2.3 for air transport.

2.9a SPECIAL FORM

The package does not include any special form of radioactive material. Hence, the requirements of 10 CFR 71.75 and 71.77 are not applicable.

2.9b FUEL RODS

The contents do not utilize cladding for the containment of radioactive materials. Therefore, this requirement is not applicable.

2.10 APPENDICES

Appendix	Description
2.10.1	ES-3100 CONTAINMENT VESSEL ASME CODE EVALUATION (DAC-EA-900000-A006 and DAC-EA-900000-A007)
2.10.2	IMPACT ANALYSES OF ES-3100 DESIGN CONCEPTS USING BOROBOND AND CAT 277-4 NEUTRON ABSORBERS
2.10.3	KAOLITE PROPERTIES
2.10.4	CATALOG 277-4 PROPERTIES
2.10.5	BOROBOND4 PROPERTIES
2.10.6	RECOMMENDED RANDOM VIBRATION AND SHOCK TEST SPECIFICATIONS FOR CARGO TRANSPORTED ON SST AND SGT TRAILERS
2.10.7	TEST REPORT OF THE ES-3100 PACKAGE; VOL 1 - MAIN REPORT, ORNL/NTRC-013/V1; SEPT. 10, 2004
2.10.8	THE ES-3100 TEST REPORT; VOL. 3, APPENDIX K - TU-4 DATA SHEETS
2.10.9	PACKAGING MATERIALS OUTGASSING STUDY FINAL REPORT

THIS PAGE INTENTIONALLY LEFT BLANK.

Appendix 2.10.1

ES-3100 CONTAINMENT VESSEL ASME CODE EVALUATION (DAC-EA-900000-A006 and DAC-EA-900000-A007)

THIS PAGE INTENTIONALLY LEFT BLANK.

GENERAL DESIGN AND COMPUTATION SHEET

JOB ASME Code Subsection NB Stress Analysis of ES-3100 Containment Vessel		DATE 14 December 2006	SHEET 1 of 26
DAC NO. DAC-EA-900000-A006	REVISION NO. 2	COMPUTED C. R. Hammond	CHECKED BY R. M. Jessee

TABLE OF CONTENTS

GENERAL DESIGN AND COMPUTATION SHEET

JOB ASME Code Subsection NB Stress Analysis of ES-3100 Containment Vessel		DATE 14 December 2006	SHEET 2 of 26
DAC NO. DAC-EA-900000-A006	REVISION NO. 2	COMPUTED C. R. Hammond	CHECKED BY R. M. Jessee

OBJECTIVE

The design for the ES-3100 Containment Vessel is evaluated for compliance with ASME Code, Section III structural design rules using bounding loads taken from the U. S. Code of Federal Register and International Atomic Energy Agency Requirements.

EVALUATION INPUT (CRITERIA) AND SOURCE

REFERENCES USED

BWXT Y-12 drawings (Project: ES-3100 Shipping Package, all dated 10/29/03):

M2E801580A011, Rev. C, "Containment Vessel Assembly"

M2E801580A012, Rev. C, "Containment Vessel Body Assembly"

M2E801580A013, Rev. B, "Containment Vessel O-ring Details"

M2E801580A014, Rev. B, "Containment Vessel Lid Assembly"

M2E801580A015, Rev. C, "Containment Vessel Sealing Lid"

M2E801580A016, Rev. B, "Containment Vessel Closure Nut"

Texts

(B1.1) *Unified Inch Screw Threads*, ASME B1.1-1989, The American Society of Mechanical Engineers, 1989.

(B1.9) *Buttress Inch Screw Threads*, ANSI B1.9 – 1973, The American Society of Mechanical Engineers, 1973.

(CFR) *Packaging and Transportation of Radioactive Material*, 10CFR71, Code of Federal Regulations, the Nuclear Regulatory Commission, 2004.

(Code) *Class 1 Components, Section III, Rules for Construction of Nuclear Power Plant Components*, Division 1, 2001 Edition with 2003 Addenda, The American Society of Mechanical Engineers, 2003.

(IAEA) *Regulations for the Safe Transport of Radioactive Material, Requirements*, 1996 Edition (Revised), No. TS-R-1 (ST-1, Revised), International Atomic Energy Agency, 2000.

(Parker) *Parker O-Ring Handbook*, 2001 Edition, Catalog ORD 5700A/US, Parker Seals, 2001.

(Roark) R. J. Roark and W. C. Young, *Formulas for Stress and Strain*, 5th Ed., McGraw-Hill Book Company, 1975, p. 363.

(Section II) *Section II, Materials*, Part D – Properties, 2001 Edition with 2003 Addenda, The American Society of Mechanical Engineers, 2003.

GENERAL DESIGN AND COMPUTATION SHEET

JOB ASME Code Subsection NB Stress Analysis of ES-3100 Containment Vessel		DATE 14 December 2006	SHEET 3 of 26
DAC NO. DAC-EA-900000-A006	REVISION NO. 2	COMPUTED C. R. Hammond	CHECKED BY R. M. Jessee

ASSUMPTIONS MADE

Calculations are based on geometry and specifications from referenced drawings.

Results are rounded to significant figures although more digits may be retained in intermediate calculations.

IDENTIFICATION OF COMPUTER CALCULATION

Computer Type: Dell PC x86 Family processor Family 6 Model 8 Stepping 1 using the Microsoft Windows 2000 operating system level 5.00.2195 with Service Pack 4.

Computer Program Name, Revision, Verification, Applicability: Programs used were Algor (R) Linear Static Stress Version 12.26-WIN 28-OCT-2002, ALG.DLL VERSION:13180000 and FEMPRO Version 13.26-WIN 22-NOV-2002. Verification was by running example programs with known solutions on the same computer used for final calculations. The expected results were produced exactly. Hand calculations are used here to confirm results. The program is applicable to linear elastic solutions for bodies of revolution as needed here.

METHODS TO BE USED

The Finite Element Method is used to determine the response of the CV components to internal pressure and gasket seating loads. External pressure resistance of the cylindrical shell is evaluated following Code rules. The finite element results also serve to demonstrate the external pressure resistance of the lid and bottom of the CV. Buttress threads used to restrain the lid are evaluated by a method derived from an accepted way of determining the strength of standard threads.

ANALYSES AND/OR CALCULATIONS

DESIGN CONDITIONS

Internal Pressure: 101.5 psig at 300 F. per IAEA.

External Pressure: 21.7 psig at 300 F. per 10CFR71.73.

GENERAL DESIGN AND COMPUTATION SHEET

JOB ASME Code Subsection NB Stress Analysis of ES-3100 Containment Vessel		DATE 14 December 2006	SHEET 4 of 26
DAC NO. DAC-EA-900000-A006	REVISION NO. 2	COMPUTED C. R. Hammond	CHECKED BY R. M. Jessee

ALLOWABLE STRESS INTENSITIES

From Section II.

PART	SPECIFICATION	ALLOWABLESTRESS INTENSITY, PSI
Containment vessel	ASME SA-182, Type F304L forging or bar (<5 in. thick)	12,800 @ 300 F.*
Containment lid	ASME SA-479, 304 bar	12,800 @ 300 F.*
Closure nut	ASME SA-479, UNS-S21800 bar	22,100 @ 300 F.

* The lower of two allowable values was chosen to limit deflection of the flange.

NB-3133 COMPONENTS UNDER EXTERNAL PRESSURE

The design internal pressure is higher than the external pressure across the bottom of the vessel and the lid. Since stability or buckling was not an issue, these flat heads were evaluated for resistance to internal pressure only. They can resist the external pressure by linearity.

NB-3133.3 Cylindrical Shells and Tubular Products

Data: Outside diameter of cylindrical shell, $D_o = 5.04" + 2(0.100") = 5.24"$

Shell thickness, $T = 0.100"$

Total length, $L = 32.40" - (0.25")/2 - 1.10" = 31.18"$

$D_o/T = 52.4$

$L/D_o = 5.95$

From ASME Section II, Fig. G, $A = 0.00053$

From ASME Section II, Fig. HA-3, conservatively using the 400 F. curve, B(400 F.) = 4900.

The maximum acceptable external pressure in this case is $P_a = 4B/3(D_o/T) = 125$ psig.

This allowable value exceeds the design external pressure and the shell is acceptable.

NB-3133.6 Cylinders Under Axial Compression

Data: Inside radius, $R = 5.04"/2 = 2.52"$

$A = 0.125/(R/T) = 0.0050$

From ASME Section II, Fig. HA-3, conservatively using the 400 F. curve, B(400 F.) = 7100.

This is the maximum acceptable compressive stress limited by axial buckling. The maximum external pressure applied to the axial cross section of the cylinder at 400 F. can be derived using nominal values from:

$$7100\,psi = \frac{p_e \frac{\pi}{4}(5.24in.)^2}{\frac{\pi}{4}\left[(5.24in.)^2 - (5.04in.)^2\right]}$$

p_e = 532 psi. This is less than the design external pressure and the shell is still acceptable.

NB-3200 DESIGN BY ANALYSIS

Individual axisymmetric finite element models were constructed of the CV body, the lid, and the closure nut and identified es5100, es3100lid, and es3100nut, respectively. Two loading conditions were applied to each model per Section III requirements: internal pressure and gasket seating. Load Case 1 is internal pressure including gasket load and Load Case 2 is gasket load alone.

The material properties at 300 F. obtained from Section II are as follows:

MATERIAL	MODULUS OF ELASTICITY	POISSON'S RATIO*
304 or 304L stainless steel	27,000,000 psi	0.3
UNS-S21800 stainless steel	27,000,000 psi**	0.3

* Typical values. Stress distributions are not sensitive to Poisson's ratios near 0.3 .

** Not in Tables. Based on principal constituents same as 304 stainless (18% Cr, 8% Ni).

Gasket load

Two concentric O-rings are specified to provide a redundant and testable seal. Per normal ASME practice, the O-ring grooves were not included in the finite element model. Elements reasonably close to the actual O-ring locations were chosen and elements representing the O-rings were added to the model of the CV. The gasket force was applied by displacing the top surface by 0.139 in. – 0.114 in. = 0.025 in. This way a reduction in gasket load will be caused by deformation of the CV from application of pressure.

Each O-ring has a 0.139 inch cross section diameter and is specified to have a 70 +/- 5 Shore A durometer reading. The O-ring manufacturer's catalog (Parker, P. 2-15) gives ranges of distributed force required to compress O-rings. The O-ring grooves cut into the flange surface are specified to be 0.114 inch deep. The lid is expected to be pressed down so contact is metal-to-metal. Then the O-rings will be compressed

$$\frac{0.025in.}{0.139in.} \times 100\,{}^{\circ}/_{\circ} = 18.0\,{}^{\circ}/_{\circ}$$

This is equivalent to a strain of 0.18 in./in.

Attachment A shows the effective distributed compression force for different amounts of compression based on values of distributed force averaged between high and low values for the highest allowed durometer reading, 75. The distributed force for 18% compression was about 20 lb/in. The stress-strain relationship for a thin annular shell t thick of average radius r loaded axially by the force F=20 lb/in($2\pi r$) and an elastic modulus E is approximately

$$\frac{20lb/in(2\pi r)}{2\pi rt} = E\varepsilon = E(0.18in/in).\ \text{So}$$

$$E = \frac{20lb/in}{0.18t}.$$

For the outer O-ring, the thickness is 3.04584 in. – 2.96172 in. and E_o = 1321 psi. For the inner O-ring, the thickness is 2.817 in. – 2.718 in. and E_i = 1122 psi.

These moduli were applied to the respective O-ring elements in the CV model.

Pressure was applied over the inner surface of the CV model up to the outer edge of the inner O-ring groove per Code rules. Two nodal forces had to be applied at the inner corner of the flange area since the program could not apply pressure to two faces of one element. The pressure and gasket seating forces were resisted by stiff elastic boundary elements canted 7 degrees out from the axis of symmetry to simulate the effect of the 7 degree surface on the threads to meet Code rules to consider radial forces and resulting hoop stress at the threads.

Results from the O-ring elements and the boundary element restraint are collected in Attachment B. The local 2-axes of the O-ring elements are parallel to the CV axis of symmetry, the global Z-axis. The values from load case 2 are -237.1 psi for the first set of elements representing the outer O-ring and -201.3 psi for the inner O-ring. These stresses were achieved by applying a displacement of 0.025 inches. The equivalent distributed loads in the O-ring elements are -237.1 psi (3.04584 in. – 2.96172 in.) = -19.94 lb/in. and -201.3 psi (2.817 in. – 2.718 in.) = -19.93 lb/in. which are within 1% of the target, 20 lb/in.

The gasket reaction forces and internal pressure were applied to a model of the lid. The nodal forces are shown in Attachment C. The lid was restrained by a portion of the surface under the nut. The contact area was moved radially inward until there was no tension developed during Load Case 1. The dimensions of the contact area may not be exact but the Code requirement to maintain equilibrium of forces and moments is met. One of the contact nodes for Load Case 2 was in tension but equilibrium of force and moment were still maintained by the force distribution applied to the model of the nut. Also Load Case 2 produces such low stresses that optimizing the model for it is unnecessary.

The interface forces were applied to a model of the nut. The force magnitude and moment of the distributed forces was maintained using small added nodal forces as shown in Attachment D.

The distribution of stress intensity is shown on Figs. 1 – 10. Stress intensities are very low relative to the basic allowable stress for the material. Code compliance is trivial since the Code tests subdivide the computer results but the sum is less than the allowable for any of the subsets. By the numbers.

NB-3221.1 General Primary Membrane Stress Intensity

General primary membrane stress intensity is limited to the basic allowable stress intensity at temperature. That is 12,800 psi in the CV. The general primary membrane stress intensity is based on stresses averaged across the thickness of a section. The highest calculated stress intensities (called 2 times Tresca Stress by the program) were 7436 psi for Load Case 1 and 1203 psi for Load Case 2. Average stress is always less than peak stress so the CV is acceptable.

Fig. 4 is a close look at the cylindrical section. The stress intensity away from thickened sections appears to be less than 3000 psi. As a check the average elastic stresses in the middle of the cylindrical side of the vessel are easily calculated from equilibrium. Section III of the ASME Code provides values in Nonmandatory Appendix A. The tolerance on critical dimensions is ±0.01 in. and is taken into consideration to calculate maximum values of stress intensity.

A-2221 General Primary Membrane Stress Intensity

$$S = (pR/t) + (p/2) = 101.5\,psig\left(\frac{5.04\,in. + 0.01\,in.}{2(0.10\,in. - 0.01\,in.)}\right) + \frac{101.5\,psig}{2} = 2898\,psi.$$

A-2222 Maximum Value of Primary Plus Secondary Stress Intensity

$$S = 2pY^2/(Y^2 - 1) = \frac{2(101.5\,psig)\left(\frac{5.04\,in. + 0.01\,in.}{5.04\,in. + 0.01\,in. - 2(0.10\,in. - 0.01\,in.)}\right)^2}{\left(\frac{5.04\,in. + 0.01\,in.}{5.04\,in. + 0.01\,in. - 2(0.10\,in. - 0.01\,in.)}\right)^2 - 1} = 2899\,psi.$$

This confirms the computer solution for the cylindrical section.

There is a small radial membrane stress in the CV bottom but there is no need to calculate it since the sum of all order stresses is less than the allowable for the membrane stress.

The highest calculated stress intensity in the lid was 2398 psi for Load Case 1 and 872 psi for Load Case 2. The general primary membrane radial stress in the lid is zero from equilibrium so the highest average membrane stress is p/2 = 200 psi/2 = 100 psi. The allowable stress intensity is also 12,800 psi so the lid is acceptable.

NB-3221.2 Local Membrane Stress Intensity

Local membrane stress intensity is the average stress across the thickness of a cross section at the junction between the side and bottom of the CV. The allowable value of this stress component is 1.5 times the basic allowable stress. Figs. 4 and 5 show that the peak values of stress at this junction are below the basic allowable so the average must also be below the allowable and the CV is acceptable.

NB-3221.3 Primary Membrane plus Primary Bending Stress Intensity

Primary membrane plus primary bending stress intensity in the CV bottom and the lid.

Fig. 3 shows the stress intensity at the center of the CV bottom. The distribution is primarily due to bending and the peak value is less than 1.5 times the basic allowable stress intensity.

The stress in the bottom cover is complicated by attachment to the side but bending stress at the center can be checked by bounding stress by assuming both simple support and fixed support around the outside edge. From the Code Appendix:

A-5212 Radial bending stress at center (r = 0) and outside surface (x = t/2)

$$\sigma_r = p\frac{3(x)}{4t^3}\left[(3+\nu)(R^2-r^2)\right] = 101.5\,psig\,\frac{3(t/2)}{4t^3}\left[(3+0.3)\left(\frac{5.04\,in.}{2}\right)^2\right]$$

$$= 101.5\,psig\,\frac{3}{8(0.25\,in.)^2}\left[3.3(2.52\,in.)^2\right] = 12{,}762\,psi.$$

This equation is based on a simply supported outer edge. For a fixed edge, the stress at the same point using Roark (Table 24, Case 10b) is:

$$\sigma_r = p\frac{6}{16(0.25\,in.)^2}\left[(1+\nu)R^2\right] = 101.5\,psig\,\frac{3}{8(0.25\,in.)^2}\left[1.3(2.52\,in.)^2\right] = 5{,}028\,psi.$$

From Fig. 3 it is seen that the peak stress intensity at the center of the CV bottom is about 7,000 psi. This value is between the bending stresses for the simply supported and fixed edge cases as expected.

The pattern of stress intensity in the lid is also primarily bending of the relatively thin outboard edge with bearing under the restraining nut and some intensification at a fillet. The bending stress appears to be less than 300 psi which is far below the allowable.

NB-3222.3 Expansion Stress Intensity

Expansion stress intensity is undefined but can be bounded. The largest temperature range possible for the CV is between -40 F. which is the minimum temperature specified in 10CFR71 and 300 F. defined here. Suppose a tendril maintains a temperature of -14 F. while the surrounding material is heated to 300 F. The result is a 340 F. temperature difference across a sharp boundary – an infinite gradient. The stress in the tendril would be $\sigma = E\,\alpha_{(-40)-300}\,340^\circ$. E is the cold modulus of elasticity – 28,800,000 psi by interpolation from Table TM-1 in Section II. The temperature at the midpoint of the range is 170 F. and the instantaneous α at that temperature is 9.1 × 10^{-6} in/in/° F. from Table TE-1 in Section II. The bounding expansion stress is 89,000 psi. This is a fictitious elastic stress per the Code. Add to this the highest stress from the CV and lid models multiplied by an intensification factor of 2 since the finite element program may extrapolate to the surface too simplistically. That is 89,000 psi + 2 (7436 psi) = 100,000 psi. The alternating stress is half this value or 50,000 psi. The allowable number of cycles for this stress per Fig. I-9.2.1 in Code Mandatory Appendix I is 30,000. The vessel should acceptable for a few hundred years although a severe transportation accident should be counted as two cycles, one for impact and one for fire.

NB-3230 STRESS LIMITS FOR BOLTS

NB-3232.1 Average Stress

Average stress across a bolt cross section has a different allowable value. Since the CV is threaded to retain the lid special consideration is given to the neck above the lid. Allowable stress on bolts per Appendix III, Article III-2000, of Section III is one-third of the minimum specified yield strength of the material. This is half of the basic allowable but the service stress may be twice the allowable so we are back to an allowable service stress of 12,800 psi. Fig. 5 shows that the peak stress intensity in the neck region is under 6000 psi and the average service stress is much less so the CV is acceptable.

NB-3232.2 Maximum Stress

Maximum service stress in a bolt including bending stress may be three times the basic allowable bolt stress and since the bending component is included in the calculated stress the CV is clearly acceptable.

NB-3227.2 Pure Shear

Pure shear across threads on CV and Closure Nut. These threads are 7.0 inch 8 threads per inch push buttress threads Class 2A fit per ANSI B1.9-1973. The 7 degree slope of the mating surface was accounted for in the finite element models. The threads were not modeled in detail and they are evaluated using a traditional method (B1.1). Internal threads are limiting because the allowable stress for the CV material is about half the allowable stress for the nut material. The appropriate shear area on internal threads is the cylindrical area at the tip of the external thread with minimum height. That is the area at the minimum major diameter of the external thread called $MIN\ D_s$ in B1.9. $MIN\ D_s$ is the nominal D_s, $D - G$, where D is the nominal diameter and G is the allowance for easy assembly minus the tolerance on D. The minimum width of the internal thread at this radius, say t_e, is a function of the theoretical sharp thread form, H, defined as $0.89064p$ where p is the thread pitch, the crest truncation, f (=$0.14532p$), and the sum of radial allowance and tolerances (the *gap*). The *gap* based on thread tolerances is half the tolerance on the pitch diameter and half the tolerance on the major diameter of the thread. The gap should also include any outward radial deformation of the threads. Fig. 11 shows that due to rotation of the flange, the threads in the CV actually move inward and do not increase the gap. In any case the calculated displacements are smaller than the thread tolerances. So, limited to thread properties

$$gap = \frac{PD\,tol}{2} + \frac{G}{2} + \frac{D\,tol}{2} = \frac{0.0101\,in.}{2} + \frac{0.0067}{2} + \frac{0.0101\,in.}{2} = 0.0134\,in.$$

$$t_e = \left(0.89064\,p - 0.14532\,p - gap\right)\left(\tan(7^\circ) + \tan(45^\circ)\right)$$
$$= \left((0.89064 - 0.14532)(0.125\,in.) - 0.0134\,in.\right)(1.1228)$$
$$= 0.08956\,in.$$

$$MIN\,D_s = 7\,in. - 0.0067 - 0.0101\,in. = 6.9832\,\text{in.}$$

Three threads are fully engaged so the shear area is at least

$$A_{s,i} = 3(0.08956\,in.)\,\pi\,(6.9832\,in.) = 5.894\,in^2.$$

The shear capacity given the Code limit on shear stress of 0.6 S_m is 0.6 (12,800 psi)(5.894 in.^{2}) = 45,300 lb.

The load due to pressure to the outer edge of the inner O-ring groove is

$$W_{m1} = \pi \frac{101.5\,psi\,(5.624\,in.)^2}{4} = 2521\ lb.$$

The force due to gasket seating is

$$W_{m2} = 20\,lb./in.\,\pi\left[(5.359\,in. + 0.139\,in.) + (5.859\,in. + 0.139\,in.)\right] = 722.3\,lb.$$

The combined force is 3244 lb. This is much less than the shear capacity so the threads are acceptable for shear.

NB-3232.3 Fatigue Analysis of Bolts

Fatigue analysis of bolts is contained in Section 2 of the Safety Analysis Report for Packaging

CONCLUSIONS

The ES-3100 Containment Vessel meets ASME Code, Section III, requirements for structural design except for fatigue analysis of the threaded closure which was not evaluated. Fatigue analysis of the threaded closure is contained in Section 2 of the Safety Analysis Report for Packaging.

GENERAL DESIGN AND COMPUTATION SHEET

JOB ASME Code Subsection NB Stress Analysis of ES-3100 Containment Vessel		DATE 14 December 2006	SHEET 11 of 26
DAC NO. DAC-EA-900000-A006	REVISION NO. 2	COMPUTED C. R. Hammond	CHECKED BY R. M. Jessee

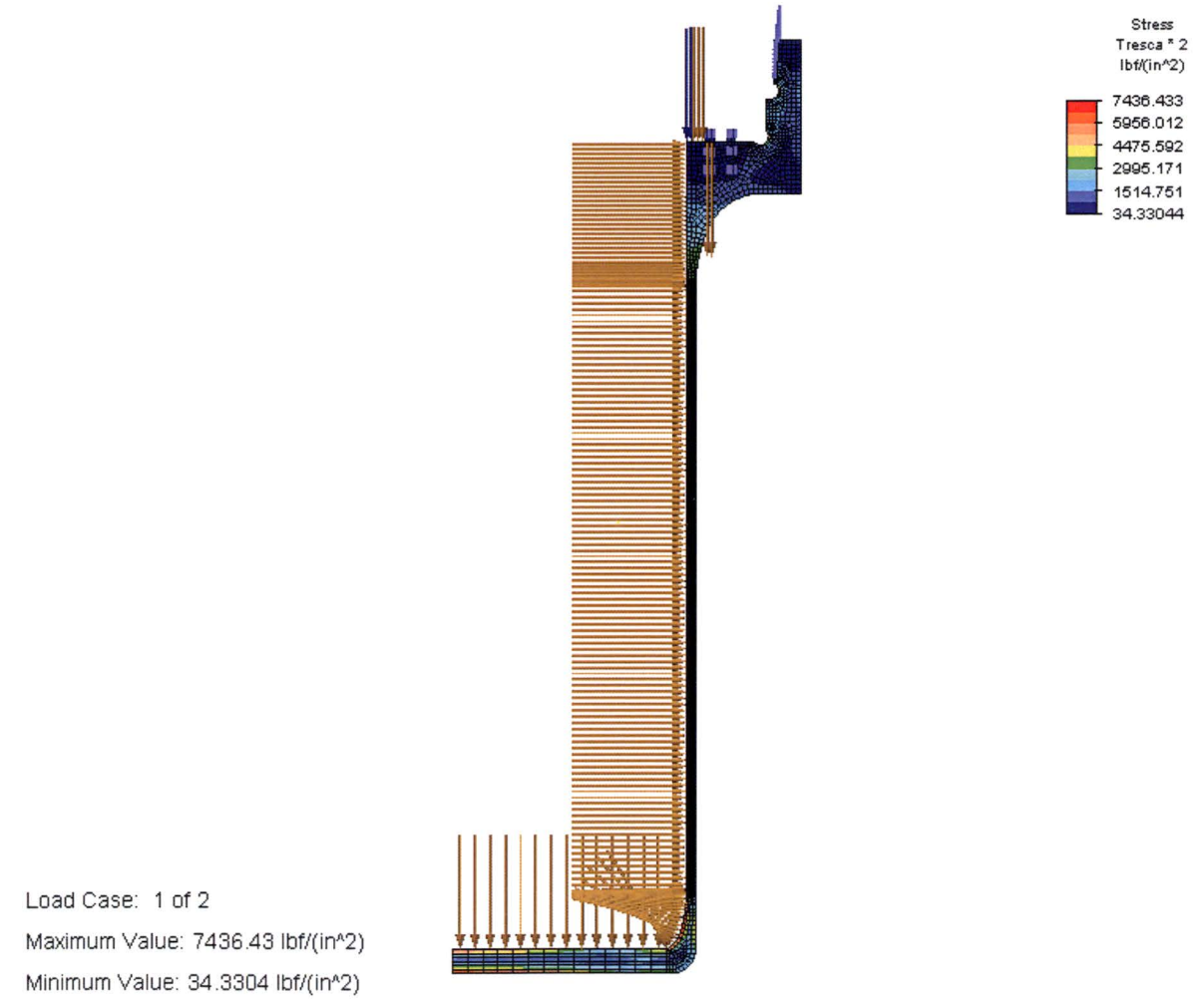

Fig. 1 – Stress Intensity in Containment Vessel due to Load Case 1

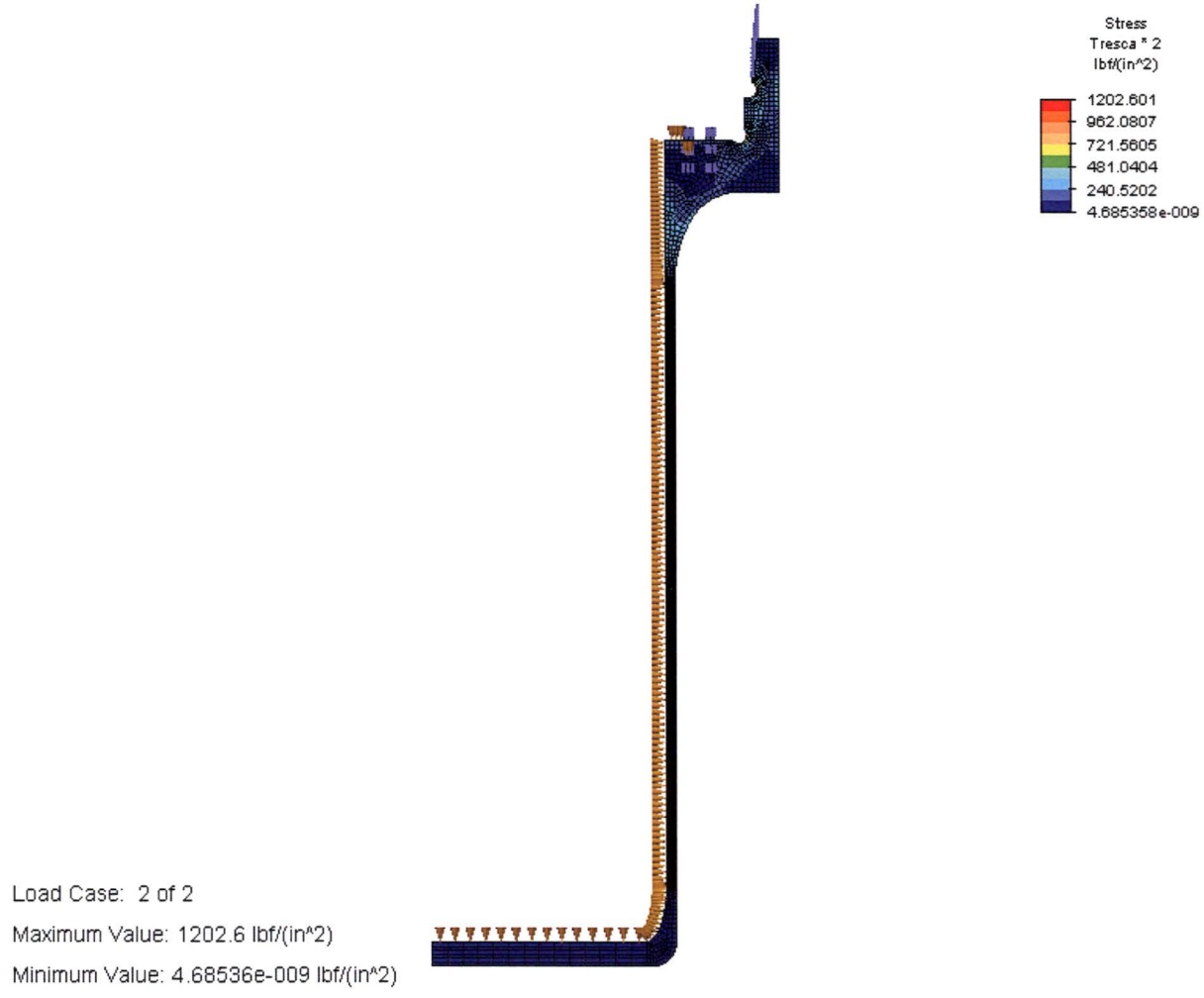

Fig. 2 – Stress Intensity in Containment Vessel due to Load Case 2

GENERAL DESIGN AND COMPUTATION SHEET

JOB ASME Code Subsection NB Stress Analysis of ES-3100 Containment Vessel		DATE 14 December 2006	SHEET 13 of 26
DAC NO. DAC-EA-900000-A006	REVISION NO. 2	COMPUTED C. R. Hammond	CHECKED BY R. M. Jessee

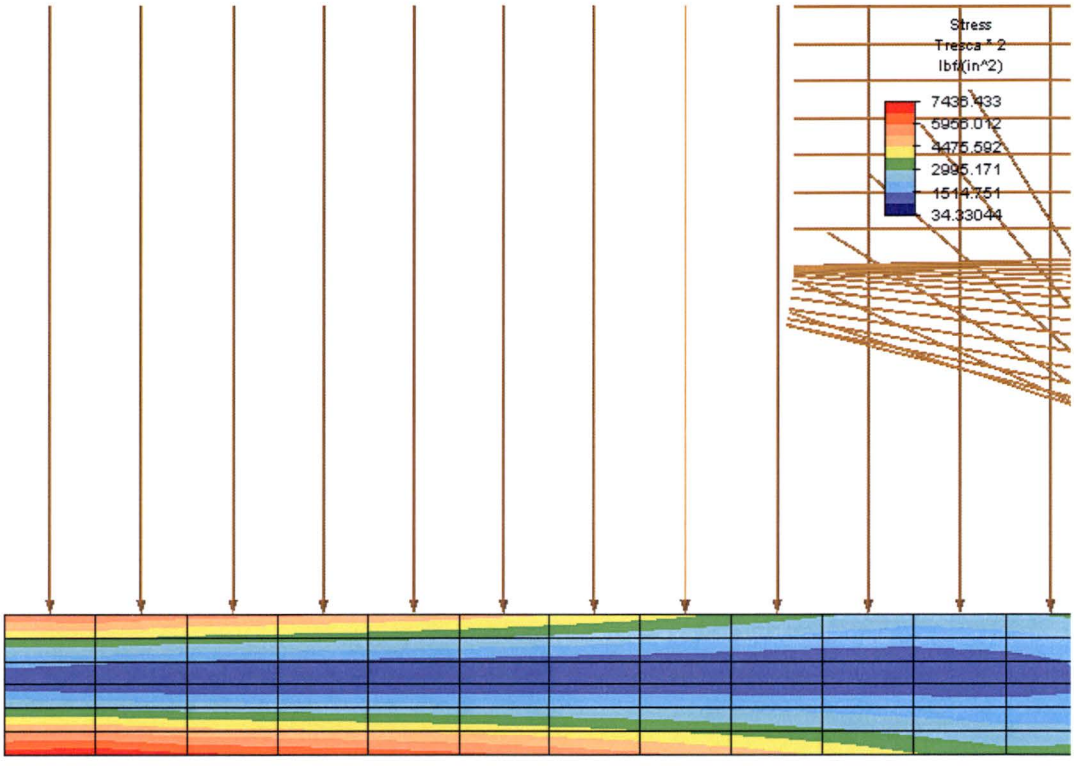

Load Case: 1 of 2

Maximum Value: 7436.43 lbf/(in^2)

Minimum Value: 34.3304 lbf/(in^2)

Fig. 3 – Stress Intensity in the Bottom of the Containment Vessel due to Load Case 1

.

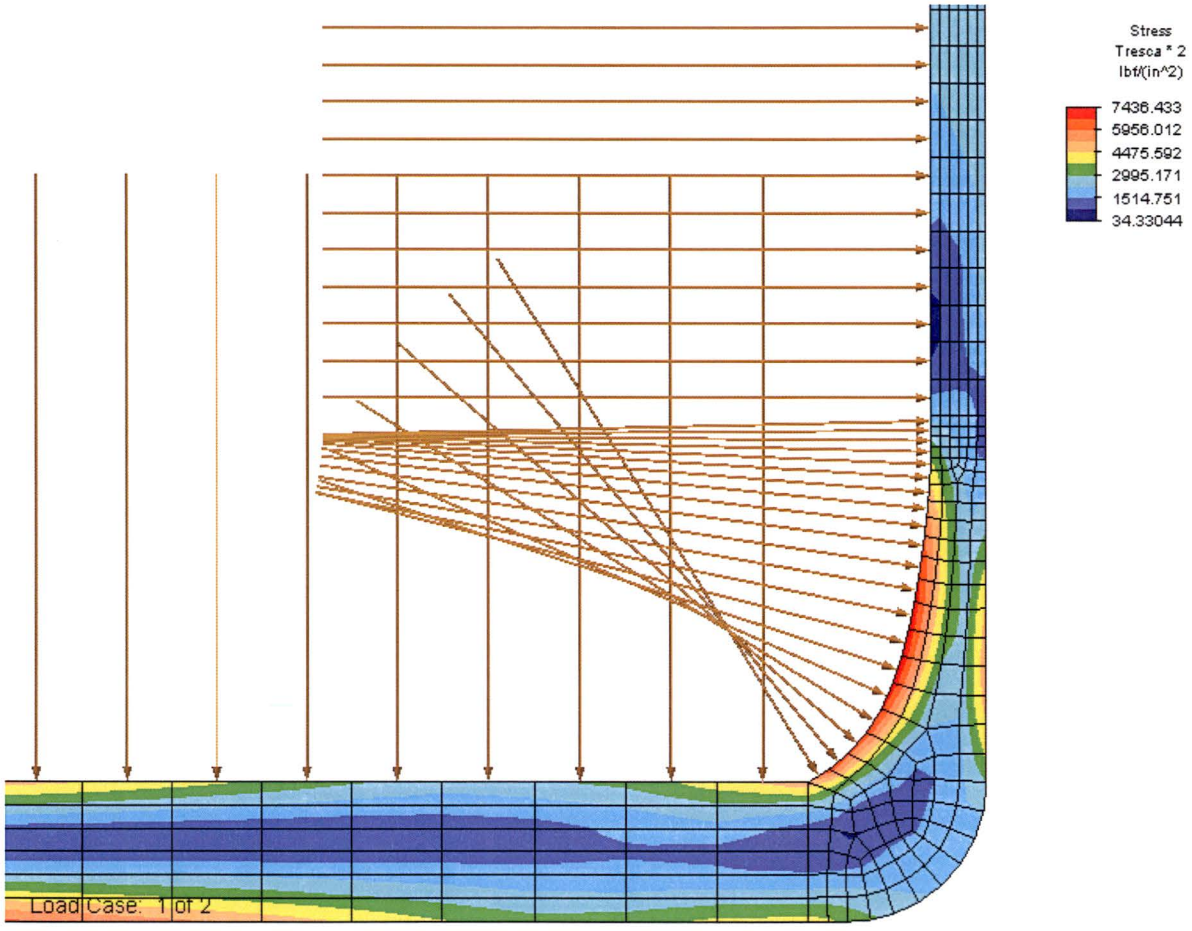

. Fig. 4 – Stress Intensity at Junction of Bottom and Side of Containment Vessel due to Load Case 1

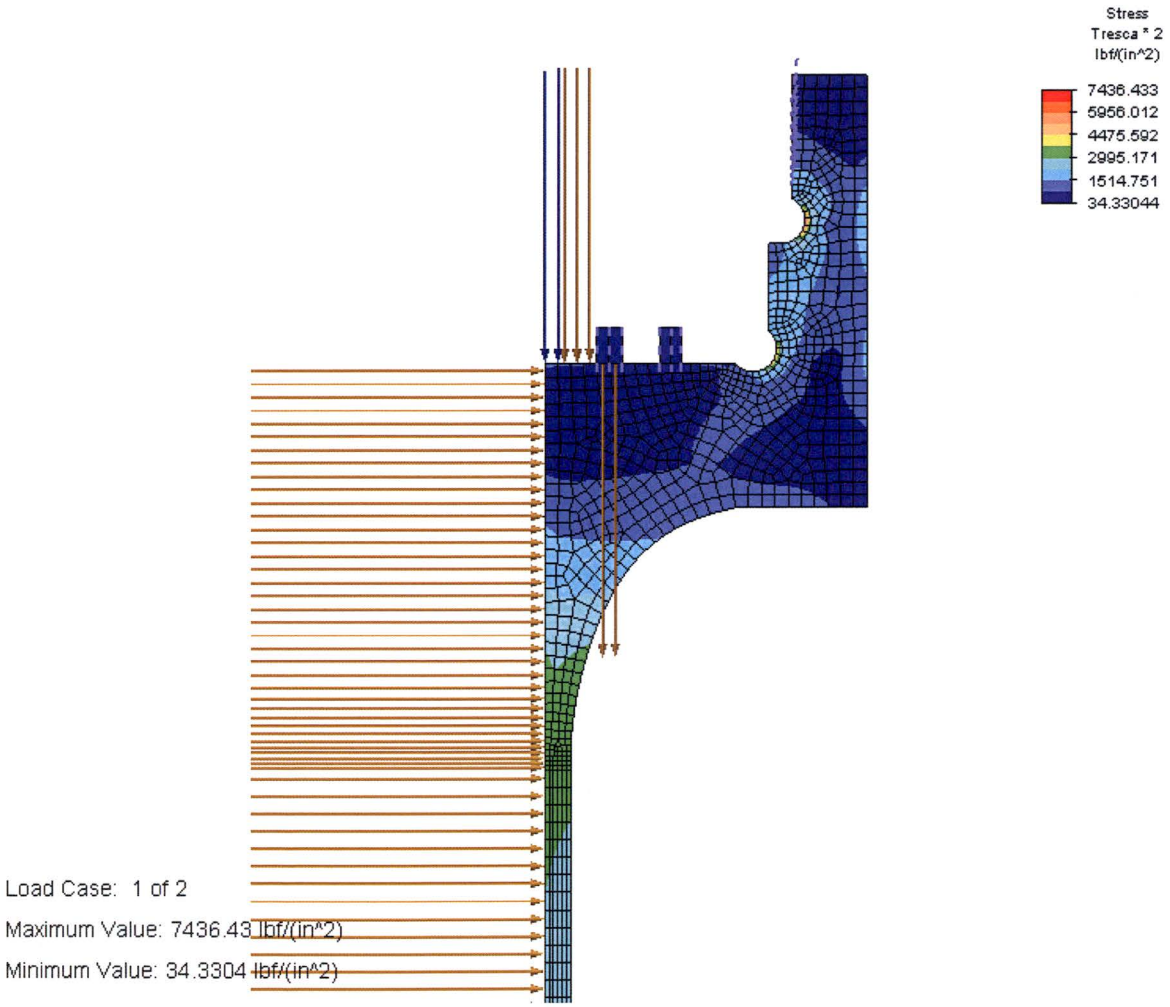

Fig. 5 – Stress Intensity in Flange Region of Containment Vessel due to Load Case 1

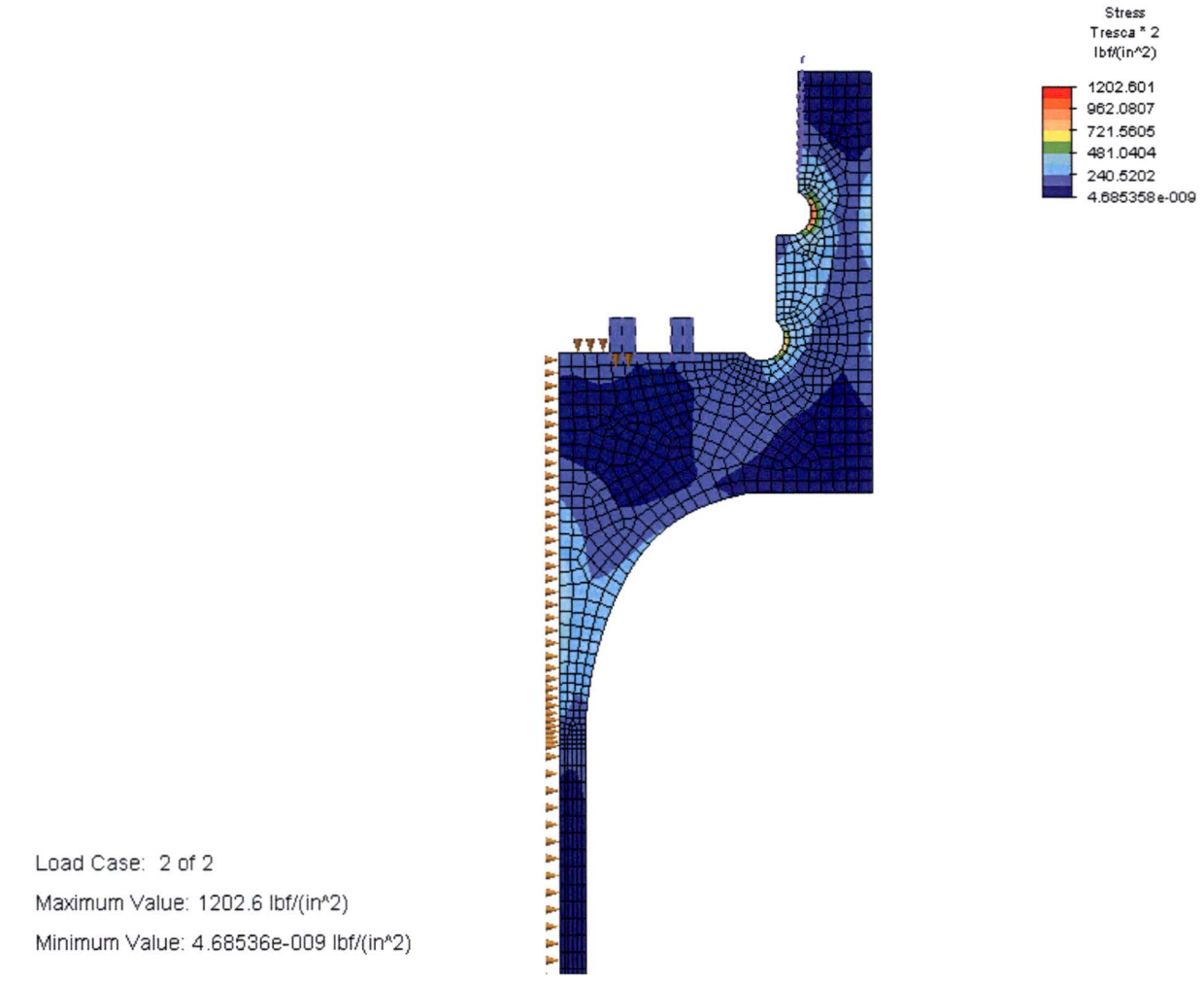

Fig. 6 – Stress Intensity in Flange Region of Containment Vessel due to Load Case 2

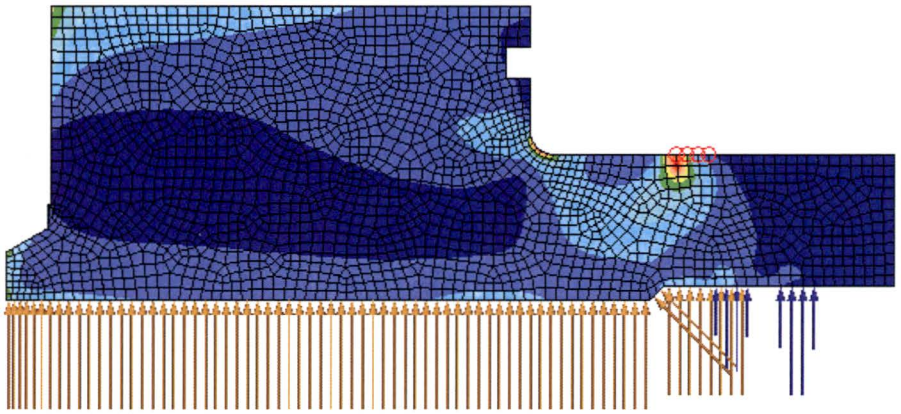

Load Case: 1 of 2

Maximum Value: 2398.09 lbf/(in^2)

Minimum Value: 3.73138 lbf/(in^2)

Fig. 7 – Stress Intensity in CV Lid due to Load Case 1

GENERAL DESIGN AND COMPUTATION SHEET

JOB ASME Code Subsection NB Stress Analysis of ES-3100 Containment Vessel		DATE 14 December 2006	SHEET 18 of 26
DAC NO. DAC-EA-900000-A006	REVISION NO. 2	COMPUTED C. R. Hammond	CHECKED BY R. M. Jessee

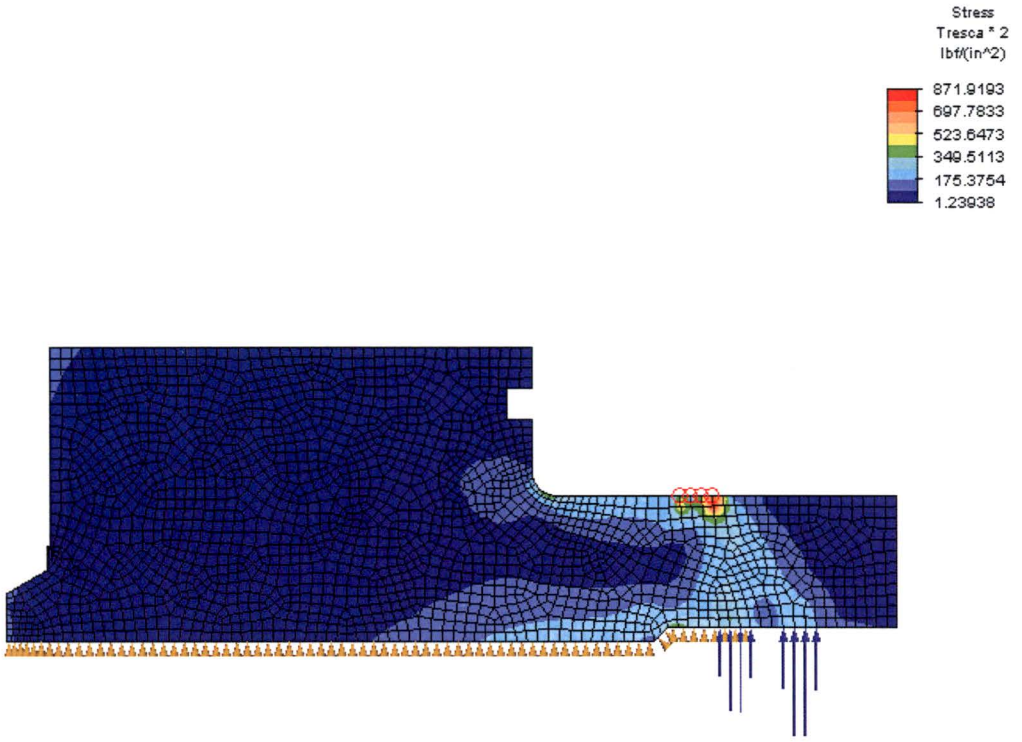

Load Case: 2 of 2

Maximum Value: 871.919 lbf/(in^2)

Minimum Value: 1.23938 lbf/(in^2)

Fig. 8 – Stress Intensity in CV Lid due to Load Case 2

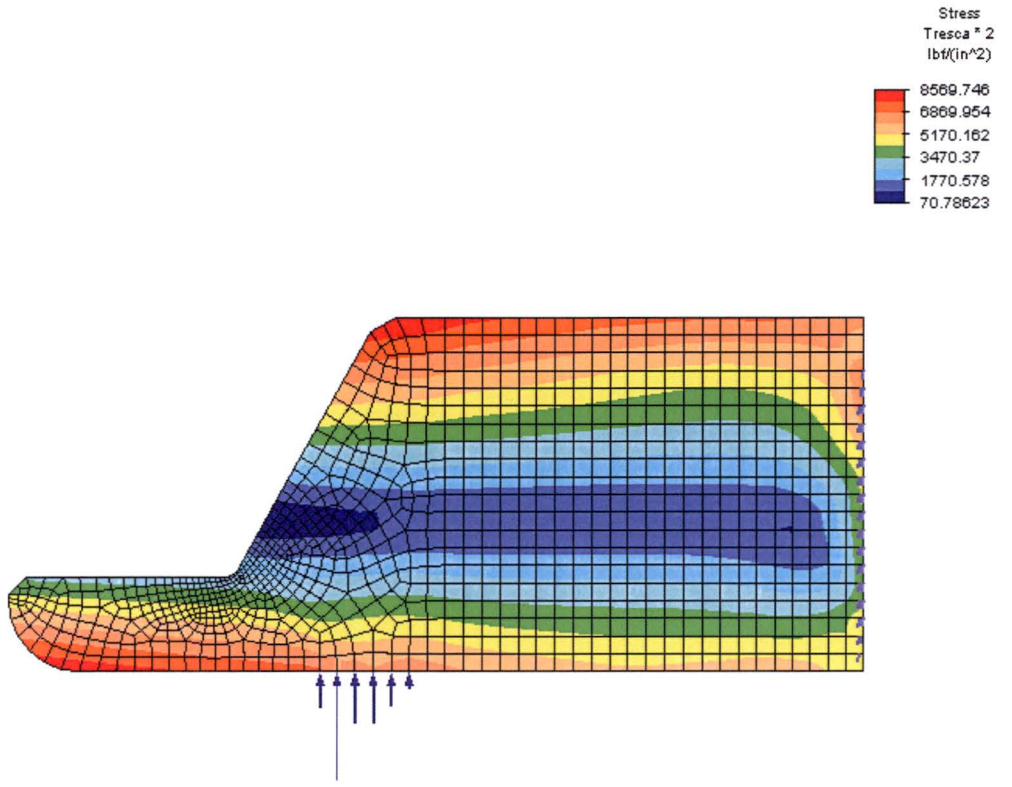

Load Case: 1 of 2

Maximum Value: 8569.75 lbf/(in^2)

Minimum Value: 70.7862 lbf/(in^2)

Fig. 9 – Stress Intensity in Nut due to Load Case 1

GENERAL DESIGN AND COMPUTATION SHEET

JOB ASME Code Subsection NB Stress Analysis of ES-3100 Containment Vessel		DATE 14 December 2006	SHEET 20 of 26
DAC NO. DAC-EA-900000-A006	REVISION NO. 2	COMPUTED C. R. Hammond	CHECKED BY R. M. Jessee

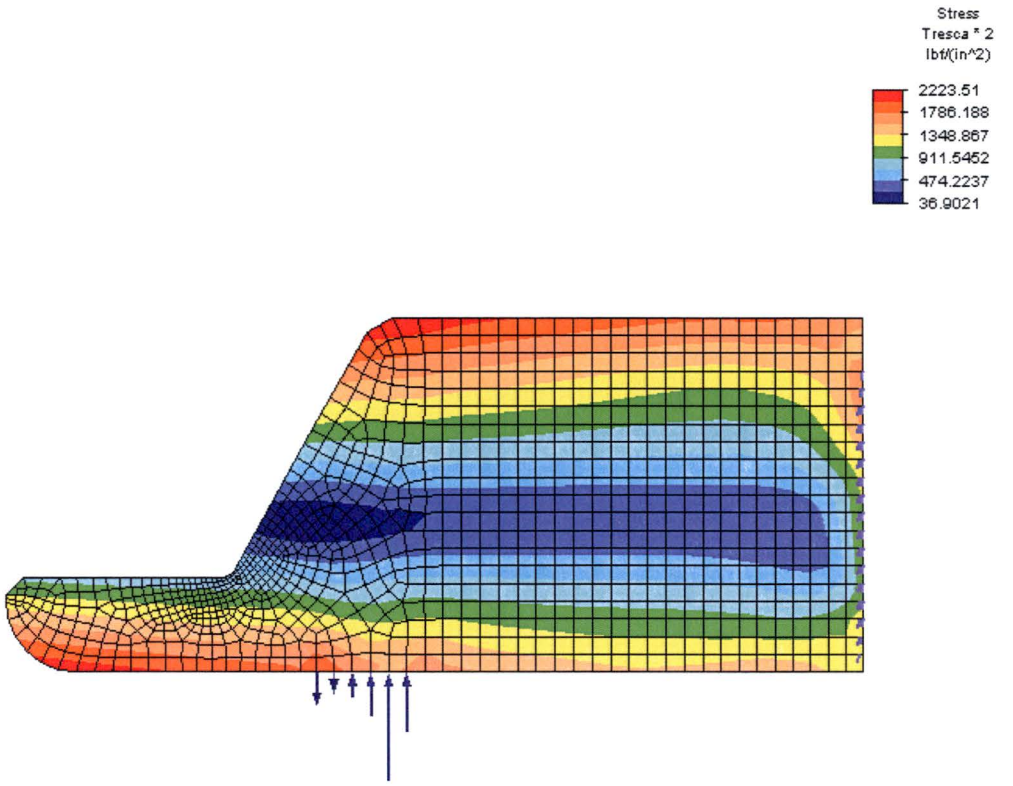

Load Case: 2 of 2

Maximum Value: 2223.51 lbf/(in^2)

Minimum Value: 36.9021 lbf/(in^2)

Fig. 10 – Stress Intensity in Nut due to Load Case 2

.

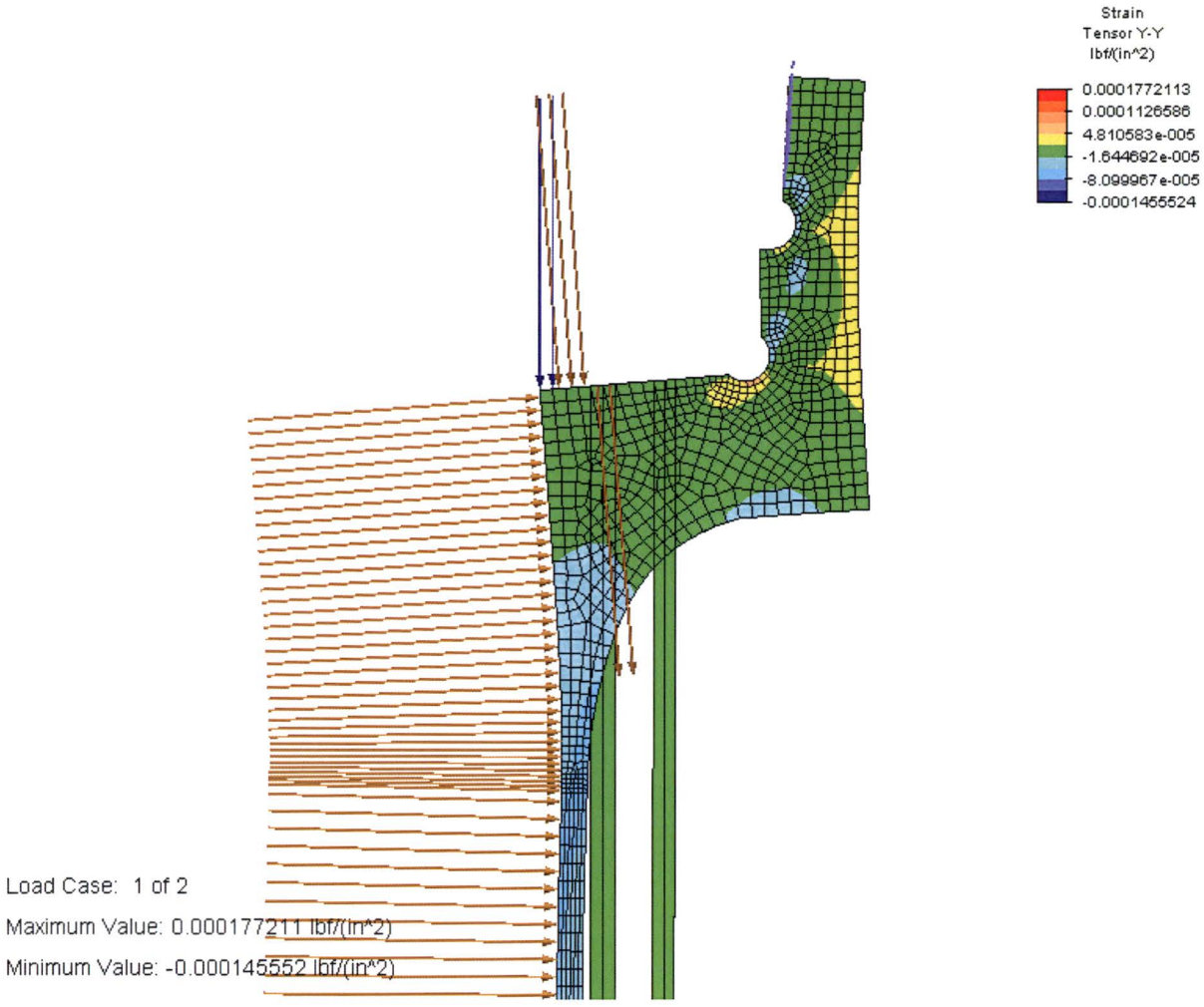

Fig. 11 – Radial Strain in the Flange Region of the Containment Vessel due to Load Case 1 (Distortion is Exaggerated)

GENERAL DESIGN AND COMPUTATION SHEET

JOB ASME Code Subsection NB Stress Analysis of ES-3100 Containment Vessel		DATE 14 December 2006	SHEET 22 of 26
DAC NO. DAC-EA-900000-A006	REVISION NO. 2	COMPUTED C. R. Hammond	CHECKED BY R. M. Jessee

ATTACHMENT A – O-RING SPRING CONSTANT

Compression of 0.139 in. dia. O-ring (Parker Seals, "O-Ring Handbook," ORD-5700A/US, 2001) [a]

Diameter =	0.139	D =	70	D =	80			
		Force						
% compression		Min	Max			Ave	Del	K
5	0.00695	0.93	6.1	2.5	10	4.8825	0.00695	702.518
10	0.0139	2	14	4.5	20	10.125	0.0139	728.4173
20	0.0278	4.5	30	9	45	22.125	0.0278	795.8633
30	0.0417	11	72	20	90	48.25	0.0417	1157.074
40	0.0556	19	160	40	180	99.75	0.0556	1794.065

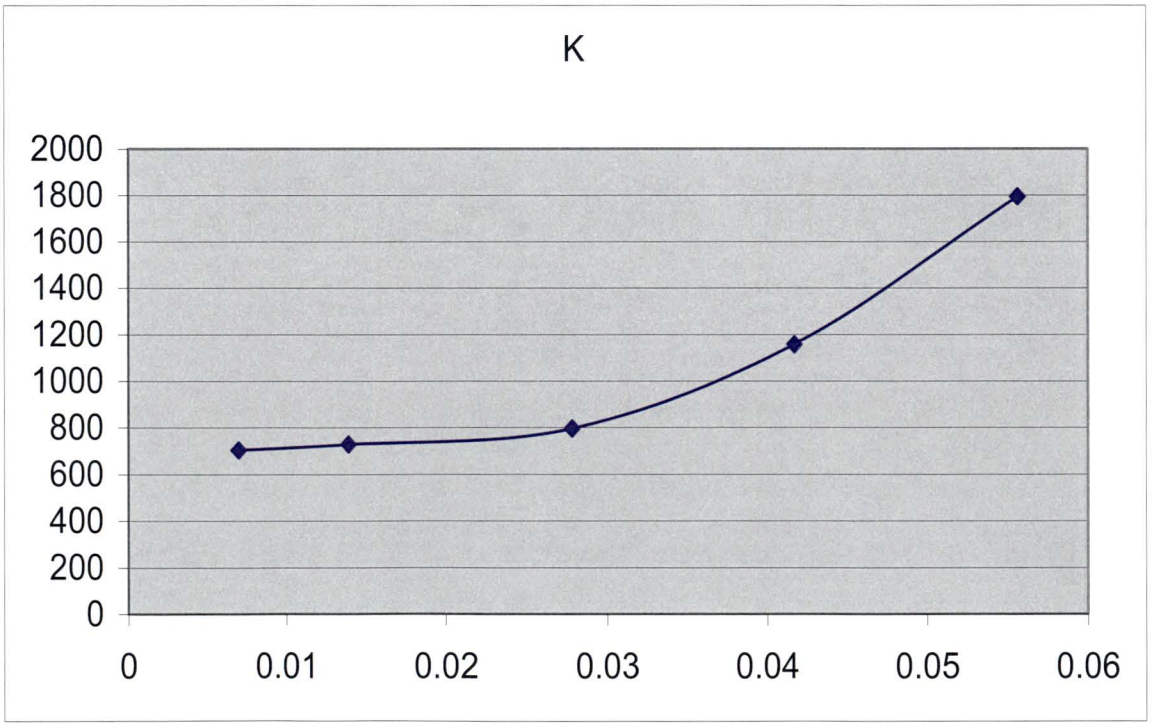

a. Page 2-15 in the O-ring Handbook.

ATTACHMENT B –RESULTS FOR O-RING ELEMENTS FROM FINITE ELEMENT ANALYSIS OF CONTAINMENT VESSEL

**** Nodal stresses for 2-D elasticity elements:

El. #	LC	ND	Sigma-11	Sigma-22	Sigma-33	Tau-12	Sigma-Max	Sigma-Min	Sigma-Int
1	1	I	7.151E-03	-2.347E+02	-3.629E-02	1.115E-02	7.152E-03	-2.347E+02	-3.629E-02
1	1	J	6.460E-03	-2.348E+02	-3.564E-02	1.099E-02	6.460E-03	-2.348E+02	-3.564E-02
1	1	K	7.565E-04	-2.348E+02	-4.589E-02	9.078E-03	7.568E-04	-2.348E+02	-4.589E-02
1	1	L	1.448E-03	-2.347E+02	-4.662E-02	9.233E-03	1.448E-03	-2.347E+02	-4.662E-02
1	2	I	-3.586E-03	-2.371E+02	-6.498E-03	8.397E-03	-3.586E-03	-2.371E+02	-6.498E-03
1	2	J	-3.713E-03	-2.371E+02	-6.454E-03	8.271E-03	-3.713E-03	-2.371E+02	-6.454E-03
1	2	K	5.712E-03	-2.371E+02	-7.804E-03	7.936E-03	5.712E-03	-2.371E+02	-7.804E-03
1	2	L	5.839E-03	-2.371E+02	-8.014E-03	8.062E-03	5.839E-03	-2.371E+02	-8.014E-03
2	1	I	8.755E-03	-2.348E+02	-3.608E-02	-8.886E-03	8.756E-03	-2.348E+02	-3.608E-02
2	1	J	8.182E-03	-2.350E+02	-3.552E-02	-8.763E-03	8.183E-03	-2.350E+02	-3.552E-02
2	1	K	-7.855E-05	-2.350E+02	-4.575E-02	-1.064E-02	-7.807E-05	-2.350E+02	-4.575E-02
2	1	L	4.944E-04	-2.348E+02	-4.633E-02	-1.077E-02	4.949E-04	-2.348E+02	-4.633E-02
2	2	I	-3.637E-03	-2.371E+02	-6.900E-03	-9.129E-03	-3.636E-03	-2.371E+02	-6.900E-03
2	2	J	-3.745E-03	-2.371E+02	-6.860E-03	-9.012E-03	-3.745E-03	-2.371E+02	-6.860E-03
2	2	K	5.687E-03	-2.371E+02	-8.074E-03	-9.358E-03	5.687E-03	-2.371E+02	-8.074E-03
2	2	L	5.795E-03	-2.371E+02	-8.250E-03	-9.475E-03	5.796E-03	-2.371E+02	-8.250E-03

**** 2-D Elasticity elements:

```
Number of elements       =     2
Number of materials      =     5
Maximum temperature pts  =     1
Analysis code            =     0
  0 : axisymmetric
  1 : plane strain
  2 : plane stress
Incompatible modes        =     0
  0 : included
  1 : not included
```

**** Nodal stresses for 2-D elasticity elements:

El. #	LC	ND	Sigma-11	Sigma-22	Sigma-33	Tau-12	Sigma-Max	Sigma-Min	Sigma-Int
1	1	I	1.838E-03	-1.987E+02	-3.397E-02	7.582E-03	1.838E-03	-1.987E+02	-3.397E-02
1	1	J	1.110E-03	-1.988E+02	-3.334E-02	7.464E-03	1.111E-03	-1.988E+02	-3.334E-02

```
1   1  K  1.855E-03 -1.988E+02 -4.282E-02  5.515E-03  1.856E-03 -1.988E+02
         -4.282E-02
1   1  L  2.583E-03 -1.987E+02 -4.364E-02  5.634E-03  2.583E-03 -1.987E+02
         -4.364E-02
1   2  I -1.419E-03 -2.013E+02 -5.945E-03  6.027E-03 -1.419E-03 -2.013E+02
         -5.945E-03
1   2  J -1.558E-03 -2.013E+02 -5.865E-03  5.923E-03 -1.558E-03 -2.013E+02
         -5.865E-03
1   2  K  3.687E-03 -2.013E+02 -7.071E-03  5.591E-03  3.687E-03 -2.013E+02
         -7.071E-03
1   2  L  3.825E-03 -2.013E+02 -7.268E-03  5.696E-03  3.825E-03 -2.013E+02
         -7.268E-03

2   1  I  1.931E-03 -1.988E+02 -3.367E-02 -3.542E-03  1.931E-03 -1.988E+02
         -3.367E-02
2   1  J  1.223E-03 -1.990E+02 -3.305E-02 -3.463E-03  1.223E-03 -1.990E+02
         -3.305E-02
2   1  K  1.761E-03 -1.990E+02 -4.236E-02 -5.358E-03  1.762E-03 -1.990E+02
         -4.236E-02
2   1  L  2.469E-03 -1.988E+02 -4.316E-02 -5.436E-03  2.469E-03 -1.988E+02
         -4.316E-02
2   2  I -1.833E-03 -2.013E+02 -6.185E-03 -5.247E-03 -1.833E-03 -2.013E+02
         -6.185E-03
2   2  J -1.970E-03 -2.013E+02 -6.110E-03 -5.152E-03 -1.969E-03 -2.013E+02
         -6.110E-03
2   2  K  3.840E-03 -2.013E+02 -7.192E-03 -5.486E-03  3.841E-03 -2.013E+02
         -7.192E-03
2   2  L  3.977E-03 -2.013E+02 -7.391E-03 -5.581E-03  3.978E-03 -2.013E+02
         -7.391E-03
```

GENERAL DESIGN AND COMPUTATION SHEET

JOB ASME Code Subsection NB Stress Analysis of ES-3100 Containment Vessel		DATE 14 December 2006	SHEET 25 of 26
DAC NO. DAC-EA-900000-A006	REVISION NO. 2	COMPUTED C. R. Hammond	CHECKED BY R. M. Jessee

ATTACHMENT C – O-RING INTERFACE LOADS

Axisymmetric nodal forces on lid from O-ring pressure

Inner O-ring

Node number	Node radius	Mean radius	Force/pressure factor	Load case 1 Pressure	Load case 1 Force	Load case 2 Pressure	Load case 2 Force
143	2.69812		0.053659565	198.825	10.66886299	201.3	10.80167042
		2.717935					
144	2.73775		0.108483245	198.825	21.56918112	201.3	21.83767716
		2.75756					
145	2.77737		0.110053385	198.825	21.88136433	201.3	22.15374646
		2.797185					
146	2.817		0.055622538	198.825	11.0591511	201.3	11.19681688

Outer O-ring

149	2.942		0.061513619	234.825	14.44493549	237.1	14.58487897
		2.962835					
150	2.98367		0.124314506	234.825	29.19215396	237.1	29.47496946
		3.0045					
151	3.02533		0.126050479	234.825	29.59980364	237.1	29.88656848
		3.046165					
152	3.067		0.063683896	234.825	14.95457097	237.1	15.09945183

GENERAL DESIGN AND COMPUTATION SHEET

JOB ASME Code Subsection NB Stress Analysis of ES-3100 Containment Vessel		DATE 14 December 2006	SHEET 26 of 26
DAC NO. DAC-EA-900000-A006	REVISION NO. 2	COMPUTED C. R. Hammond	CHECKED BY R. M. Jessee

ATTACHMENT D – INTERFACE LOADS ON NUT

Matching interface pressure loads
Load Case 1

	Side 1					Side 2			
Index	Radius	Szz	FORCEz	Force/Rad	Index	Radius	Szz	FORCEz	Force/Rad
0	2.50507	0				2.50964	0		
1	2.54629	-3300.16	-136.0161	-346.3364		2.53798	-800	-22.668	-57.53093
2	2.5875	-1230.75	-50.71921	-131.2359		2.56631	-3300.16	-97.27222	-249.6307
3	2.62871	-662.77	-27.31275	-71.7973		2.59693	-1230.75	-37.67941	-97.85079
4	2.66992	-65.6015	-2.703438	-7.217963		2.62754	-1230.75	-37.67941	-99.00416
5	2.71113	0				2.65816	-662.77	-20.2907	-53.93594
Sum			-216.7515	-556.5876		2.68877	-65.6015	-2.00839	-5.400099
						2.71939	0		
					Sum			-217.5981	-563.3526

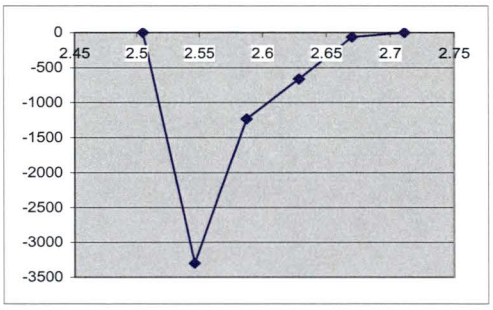

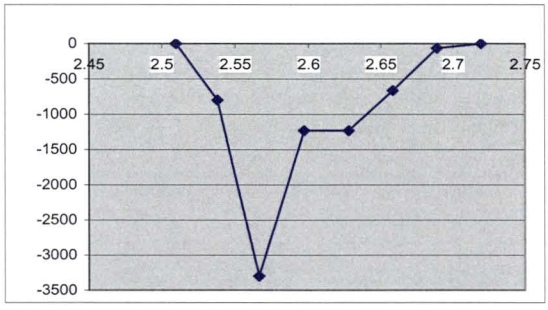

Load Case 2

	Side 1					Side 2			
Index	Radius	Szz	FORCEz	Force/Rad	Index	Radius	Szz	FORCEz	Force/Rad
0	2.50507	0				2.50964	0		
1	2.54629	301.824	12.43968	31.67502		2.53798	301.824	8.552183	21.70527
2	2.5875	-132.484	-5.459666	-14.12688		2.56631	100	2.9475	7.564199
3	2.62871	-398.673	-16.42931	-43.1879		2.59693	-132.484	-4.055998	-10.53314
4	2.66992	-1240.54	-51.12265	-136.4934		2.62754	-398.673	-12.20537	-32.07011
5	2.71113	0				2.65816	-1240.54	-37.97913	-100.9546
Sum			-60.57196	-162.1332		2.68877	-600	-18.369	-49.39002
						2.71939	0		
					Sum			-61.10982	-163.6784

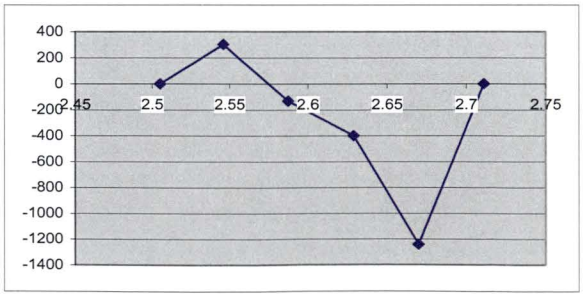

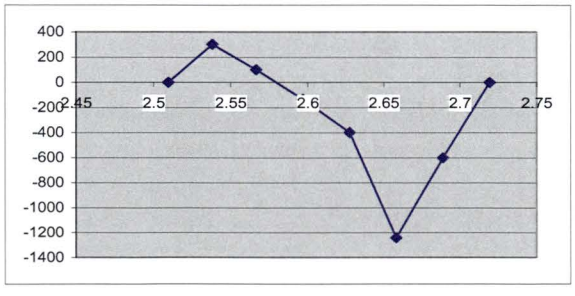

GENERAL DESIGN AND COMPUTATION SHEET

JOB Fatigue Analysis of ES-3100 CV Threads under Normal Conditions of Use		DATE 16 February 2005	SHEET 1 of 30
DAC NO. DAC-EA-900000-A007	REVISION NO. 0	COMPUTED C. R. Hammond	CHECKED BY M. L. Goins

1.0 TABLE OF CONTENTS

GENERAL DESIGN AND COMPUTATION SHEET

JOB Fatigue Analysis of ES-3100 CV Threads under Normal Conditions of Use		DATE 16 February 2005	SHEET 2 of 30
DAC NO. DAC-EA-900000-A007	REVISION NO. 0	COMPUTED C. R. Hammond	CHECKED BY M. L. Goins

2.0 OBJECTIVE

The 7°/45° Buttress threads, specified per ANSI B1.9-1973 7.0-8 Push, used to secure the lid of the ES-3100 Containment Vessel are evaluated for fatigue resistance under normal conditions of use. The evaluation is based on rules in NB-3232.3 from ASME B&PV Code, Section III.

3.0 EVALUATION INPUT (CRITERIA) AND SOURCE

3.1 REFERENCES USED

(B1.9) *Buttress Inch Screw Threads*, ANSI B1.9 – 1973, The American Society of Mechanical Engineers, 1973.

(Code) *Class 1 Components, Section III, Rules for Construction of Nuclear Power Plant Components*, Division 1, 2001 Edition with 2003 Addenda, The American Society of Mechanical Engineers, 2003.

(Drawing) "Containment Vessel Assembly," M2E801580A011, Rev. A, BWXT Y-12, 2003.

(Hammond) "ASME Code Subsection NB Stress Analysis of ES-3100 Containment Vessel," DAC-EA-900000-A006, Rev. 1, BWXT Y-12, 2004.

(Laughner & Hargan) *Handbook of Fastening and Joining of Metal Parts*, McGraw-Hill Book Company, 1956, pp. 167-168.

(Section II) *Section II, Materials*, Part D – Properties, 2001 Edition with 2003 Addenda, The American Society of Mechanical Engineers, 2003.

(SST/SGT) J. S. Cap, "Recommended Random Vibration and Shock Test Specifications for Cargo Transported on SST and SGT Trailers," letter to distribution, Sandia National Laboratory, Albuquerque, New Mexico, 2002.

3.2 DESIGN CONDITIONS

Hot NCT: Internal pressure of 17.786 psia at 190.06° F.

Cold NCT: Internal pressure of 11.13 psia at -40° F.

3.3 METHODS TO BE USED

A finite element model described in DAC-EA-900000-A006 by Hammond was used. The program was verified by running problems with known solutions. The file name for the model is ES3100CV1. Properties used in the model are shown in Appendix 2.

4.0 ANALYSES AND/OR CALCULATIONS

The previous analysis (Hammond) followed ASME Code rules to validate the vessel design under a bounding internal pressure of 101.5 psi. The design margin of the vessel, including the vessel body, the lid, and the retaining nut but not including threads on the nut or vessel body, was limited by stress intensity calculated at the side wall to bottom transition of the vessel. The actual maximum expected internal pressure is 17.786 psia or 17.786 psia – 14.7 psia = 3.1 psig. Away from the contact region between the lid and vessel body, stresses are proportional to pressure so the stress in the body and at the center of the lid will be reduced to 3.1 psi/101.5 psi = 0.0305 or 3.05% of values calculated previously. The design margin in the vessel becomes limited by stresses in the clamping region primarily due to gasket seating load or the load produced by tightening the nut. These calculations determine the load from torquing the nut and their effects on stress in the vessel components in the contact or clamping region.

4.1 TIGHTENING TORQUE

The specified nut torque is 120 +/- 5 ft.-lb. From Laughtner & Hargan, the ratio of axial force, P (lb.), to torque, T (in.-lb.) is

$$P/T = 2/(D\nu + d_p m), \text{ where}$$

D = mean bearing diameter of nut (in.),

dp = pitch diameter of screw thread (in.),

ν = coefficient of friction between nut and bearing surface,

$$m = \frac{\tan(\beta + \phi)}{\cos\alpha}, \text{ where}$$

α = one-half of thread profile angle (degrees),

β = helix angle (degrees), and

ϕ = friction angle the tangent of which is the friction coefficient.

The threads are 7 inch nominal diameter with 8 threads per inch or having a pitch of 0.125 in. From B1.9 the pitch diameter is

$$d_p = 7\,\text{in.} - 0.6(0.125\,\text{in.}) = 6.93\,\text{in.}$$

The helix angle on the pitch diameter is

$$\beta = \arctan\frac{0.125\,\text{in.}}{\pi(6.93\,\text{in.})} = 0.329^\circ.$$

The thread profile angle at the mating surfaces is 7° so $\alpha = 3.5^\circ$.

The mean effective bearing diameter of the nut is about 5.8 inches. That is D = 5.8 in.

The referenced drawing has the note: "During installation of container vessel lid assembly, apply a light coat of Krytox grease to the threads and under the nut." A typical value for coefficient of friction for lubricated threads is 0.11. In this case

$\phi = \arctan(0.11) = 6.3$.

$$m = \frac{\tan(0.329^\circ + 6.3^\circ)}{\cos(3.5^\circ)} = 0.12 .$$

$$P/T = 2/(5.8\,\text{in.}(0.11) + 6.93\,\text{in.}(0.12)) = 1.36 .$$

The maximum and the minimum force, assuming that the friction coefficient 0.11 is correct are

Pmax = 1.36 T = 1.36 (125 ft.-lb)(12 in./ft.) = 2,000 lb., rounding to 2 significant figures, and

Pmin = 1.36 (115 ft.-lb.)(12 in./ft.) = 1,900 lb.

According to Hammond the force required to seat the gaskets is
$W_{m2} = 20\,\text{lb./in.}\,\pi[(5.359\,\text{in.} + 0.139\,\text{in.}) + (5.859\,\text{in.} + 0.139\,\text{in.})] = 722.3\,\text{lb}$ and

the load due to the maximum allowable pressure, 101.5 psig, to the outer edge of the inner O-ring groove is

$$W_{m1} = \pi\frac{101.5\,\text{psig}\,(5.624\,\text{in.})^2}{4} = 2521\,\text{lb} .$$

The sum of gasket seating and pressure forces is 3,244 lb. so the specified torque is not adequate for the bounding pressure. However, the highest expected internal pressure is 17.786 psia which is (17.786 psia – 14.7 psia =) 3.1 psig so

$$W_{m1} = \pi\frac{3.1\,\text{psig}\,(5.624\,\text{in.})^2}{4} = 77\,\text{lb} .$$

The sum of gasket seating force and actual pressure force is 799 lb and there is a large margin on torque required to maintain a tight gasket and consequently the required torque is not sensitive to the coefficient of friction.

The minimum cross section area of the CV subject to the axial force from torquing the nut is at the undercut just below the threads. The inside diameter at the undercut is 6.85 in. +2(0.09 in.) = 7.03 in. The outside diameter in the same plane is 7.50 in. The minimum cross section area considering the tolerances listed on the drawing is $\pi((7.50\,\text{in.} - 0.01\,\text{in.})^2 - (7.03\,\text{in.} + 0.01\,\text{in.})^2))/4 = 5.14\,\text{in}^2$.

The average axial stress due to the force due to maximum torque at this section is

$\bar{\sigma}_{\text{torque}}$ = 2,000 lb. / 5.14 in^2 = 389 psi.

The maximum diameter at the root of a thread on the CV is 7.04 in. That is called the maximum major diameter of the internal thread which per B1.9 is D – h + PDtol. + 0.80803 p, where D is the major diameter (7 in.), h is the basic height of thread engagement (0.6 p), PDtol. is tolerance on pitch diameter (0.0101 in.), and p is pitch (0.125 in.). The cross section area at the root of the thread is thus the same as the minimum area at the undercut (i.e. 7.03 in. + 0.01 in. including tolerance) and the average stress is the same.

The finite element model used by Hammond to evaluate pressure resistance was modified to simulate the effect of the axial force due to torquing the nut. The section of the vessel between the flange surface and the threads was forced to shrink in the axial direction by applying an artificial temperature drop of 100° F. and manipulating the axial coefficient of thermal expansion to produce an axial force of 2,000 lb. Fig. 1 shows the effected region of the vessel with dots at the locations where axial stresses were recorded. The O-ring elements were removed and the entire flange surface was held in place by stiff axial spring elements. Nodal axial stresses were obtained across the two horizontal sections. There were two stresses calculated at each point, one above and one below the section boundary. The stress in the section without the temperature-dependent properties was recorded to avoid including thermal strain in the stress calculation. The results from the final run are shown on the spreadsheet along with the axial stress calculated at each point across the two sections in Appendix 1.

The net axial forces across each section were calculated by multiplying the axial stress over the tributary area. There was a slight but acceptable difference (4%) between the upper and lower sections attributed to model coarseness. The net force across the section with the highest axial stress was about 2% greater than 2000 lb.

The plot of axial stress shown in Appendix 1 clearly indicates that the peak stress at the left edge is higher than an extrapolated equivalent linear bending stress. The value of peak stress due to preload from torque, 3,476 psi, is so low that we can substitute this peak stress for the sum of membrane and bending stress in combination with axial stress from other loads.

The gasket seating force between the lid and CV body is the sum of gasket seating forces at both O-rings or 722.3 lb. total. The pressure force due to the 101.5 psig from the earlier calculation over the area to the back side of the inner O-ring groove is

$$F_P = 101.5\,\text{psi}\,\pi(2.817\,\text{in.})^2 = 2530\,\text{lb.}$$

In general, stress intensities are not linear functions of applied force but in our case of the axial force due to torque on the nut alone, stress intensities will increase by the ratio 2000 lb./722.3 lb. = 2.77 . The calculated peak stress intensity due to gasket seating load alone (Load Case 2) were highest near points of high compression that would be affected by the applied torque. The peak values were 872 psi in the lid and 2224 psi in the nut (Hammond, pp. 18, 20). The stresses in these components due to torque would be 2.77(872 psi) = 2415 psi in the lid and 2.77(2224 psi) = 6158 psi in the nut.

Bending or radial stress near the center of the lid and stresses in the vessel body away from the contact region will be reduced to about 3.05% of previously calculated values.

The effect of an internal 3.1 psig pressure plus the torque is shown in Fig. 3. Maximum stress intensity is 3501 psi. This is in the same location as for the pressure plus gasket seat case, in the transition between the side and bottom of the vessel. The axial stress in this region due to 3.1 psi pressure and torque is shown on Fig. 4. The peak axial stress is 3714 psi. The slight pressure causes just a slight increase in stress over the case with torque alone. The stress intensities in the clamping regions of the lid and nut will become about (3714 psi/3476 psi) 2415 psi = 2580 psi and (3714 psi/3476 psi) 6158 psi = 6580 psi, respectively.

4.2 DIFFERENTIAL THERMAL EXPANSION

The range of temperatures to which the CV may be exposed is -40° F. to 190.06° F. The average thermal expansion coefficient for the 304 material of the CV between 70 and 200 F. is 8.9 10^{-6} in./in./° F. and greater for higher upper temperatures per Section II. From the HP Alloys web site the average thermal expansion coefficient of the Nitronic 60 material of the nut between 75 and 200 F. is 8.8 10^{-6} in./in./° F. and greater for higher upper temperatures. Since the temperatures on opposite sides of the thread mating surface are expected to be the same an upper bound on the stress due to differential thermal expansion is $\sigma_t = E_c \Delta T(\alpha_{CV} - \alpha_N)$, where E_c is the cold elastic modulus of either part, T is temperature, and α is average thermal expansion coefficient.

In the CV the stress, using a modulus interpolated from Table TM-1 in Section II, is

$$\sigma_{tCV} = 28.8\times10^6 \text{ psi}(190.06^\circ - (-40^\circ))(8.9\times10^{-6} \text{ in./in./}^\circ - 8.8\times10^{-6} \text{ in./in/}^\circ)$$
$$= 663 \text{ psi}.$$

The nut material has a slightly lower modulus listed so the stress in the nut will be slightly less. The room temperature modulus of the nut material is 26.2×10^6 psi per the HP Alloy website. The cold temperature modulus is not available but an approximation is obtained by comparing the modulus of Nitronic 60 at room temperature with the modulus of 304 at room temperature. From Table TM-1, the modulus of 304 at 70F. is 28.3×106 psi. Stress in the nut at the threads is about

$$\sigma_{tN} = \frac{26.2\times10^6 \text{ psi}}{28.3\times10^6 \text{ psi}} 663 \text{ psi} = 613 \text{ psi}.$$

The CV material has the higher thermal expansion coefficient so the effect of temperature increase is to reduce preload on the lid. Consider the mid-height of the threads to be fixed. The fixed plane is 1.100 in. – 0.55 in. / 2 = 0.825 in. above the mating plane. The lid is 0.5 in. thick under the nut and the lid will grow the same amount as the CV. The nut has 0.325 in. of material below the fixed plane and the difference in growth between the CV and the nut is

$$0.325 \text{in.}(190.06^\circ - (-40^\circ))(8.9\times10^{-6} \text{ in./in./}^\circ - 8.8\times10^{-6} \text{ in./in./}^\circ)$$
$$= 0.0000075 \text{in}.$$

Even if the torque load in the metal is ignored, the O-rings are compressed at least

Comp. = (0.139 in.-0.004 in.) – (0.114 in.+0.001 in.) = 0.020 in.

and a reduction in compression of 0.004% due to temperature change is insufficient to unload the O-rings enough to allow leakage.

4.3 TRANSPORTATION LOADS

The highest shock acceleration expected during transport is 11g in the vertical direction compared to a maximum horizontal acceleration of 5g per SST/SGT. The contents of the CV are specified to not exceed 90 lbs. The lid can be viewed as three disks, the volumes of which are:

Disk	Volume Formula	Volume, in^3
Top	$\pi(3.98\text{in.})^2(0.56\text{in.})/4$	6.97
Middle	$\pi(6.741\text{in.})^2(0.500\text{in.})/4$	17.84
Bottom	$\pi(5.00\text{in.})^2(0.05\text{in.})/4$	0.98
Sum		25.8

The weight density of the lid material is about 0.29 lb./cu. in. so the weight of the lid is about 7.5 lb. Assume the threads must restrain 100 lbs. as the package is transported. Assuming the CV is upright, gravity provides 1g downward acceleration so the nut must restrain at most a net of 100 lbm. (11g – 1g) = 1,000 lbf. The average stress at the minimum cross section due to shock load is 1,000 lb. / 5.14 in^2 = 195 psi.

4.4 FATIGUE ANALYSIS

For each use of the vessel, the part of the CV equivalent to a bolt is loaded in tension by a torque producing a maximum axial load of 2,000 lb., an average stress of 389 psi and a peak stress (including bending) of 3,563 psi. When the vessel is pressurized to 3.1 psi the peak axial stress is 3,714 psi. This is the peak stress at the undercut which has a stress concentration factor of about 3. Per the Code, paragraph NB-3232.3 (c), the fatigue strength reduction factor for the threads shall not be less than 4 so the fatigue stress on the threads is 3,714 psi (4/3) = 4,952 psi.

Conservatively ignoring the interplay between the CV and the nut and lid, the stress due to impact during transportation is added to produce a maximum tensile stress of 4,952 psi + 195 psi = 5,147 psi. The thermal expansion reduces the preload so it will not extend the stress range. The range is zero to 5,147 psi and the alternating stress is half of the range or 5,147 psi / 2 = 2,574 psi.

The threads are evaluated for cyclic service by comparison with the design Curve A on Table I—9.2.2. For alternating stresses below 23,700 psi the allowable number of cycles exceeds 10^{11}. In every case the stress in the nut has been less than in the CV and since the nut material is also austenitic it does not limit fatigue design.

5.0 CONCLUSIONS

Force due to torquing the nut on the vessel was determined. The actual maximum expected internal pressure is low so the torque load produces much higher stresses in the vessel than pressure but the combined effect of torque and actual pressure was less than the conditions including bounding pressure used in the previous evaluation of the vessel design.

Thermal loads were evaluated relative to gasket compression it was shown that gaskets would remain seated through the maximum expected temperature change.

The threaded components of the ES-3100 Containment Vessel were evaluated per ASME Section III requirements and were found to have an allowable fatigue life in excess of 10^{11} cycles. Since the allowable life of the vessel is limited to a mere 30,000 cycles, the threads do not limit the life of the vessel.

GENERAL DESIGN AND COMPUTATION SHEET

JOB		DATE	SHEET
Fatigue Analysis of ES-3100 CV Threads under Normal Conditions of Use		16 February 2005	9 of 30
DAC NO. DAC-EA-900000-A007	REVISION NO. 0	COMPUTED C. R. Hammond	CHECKED BY M. L. Goins

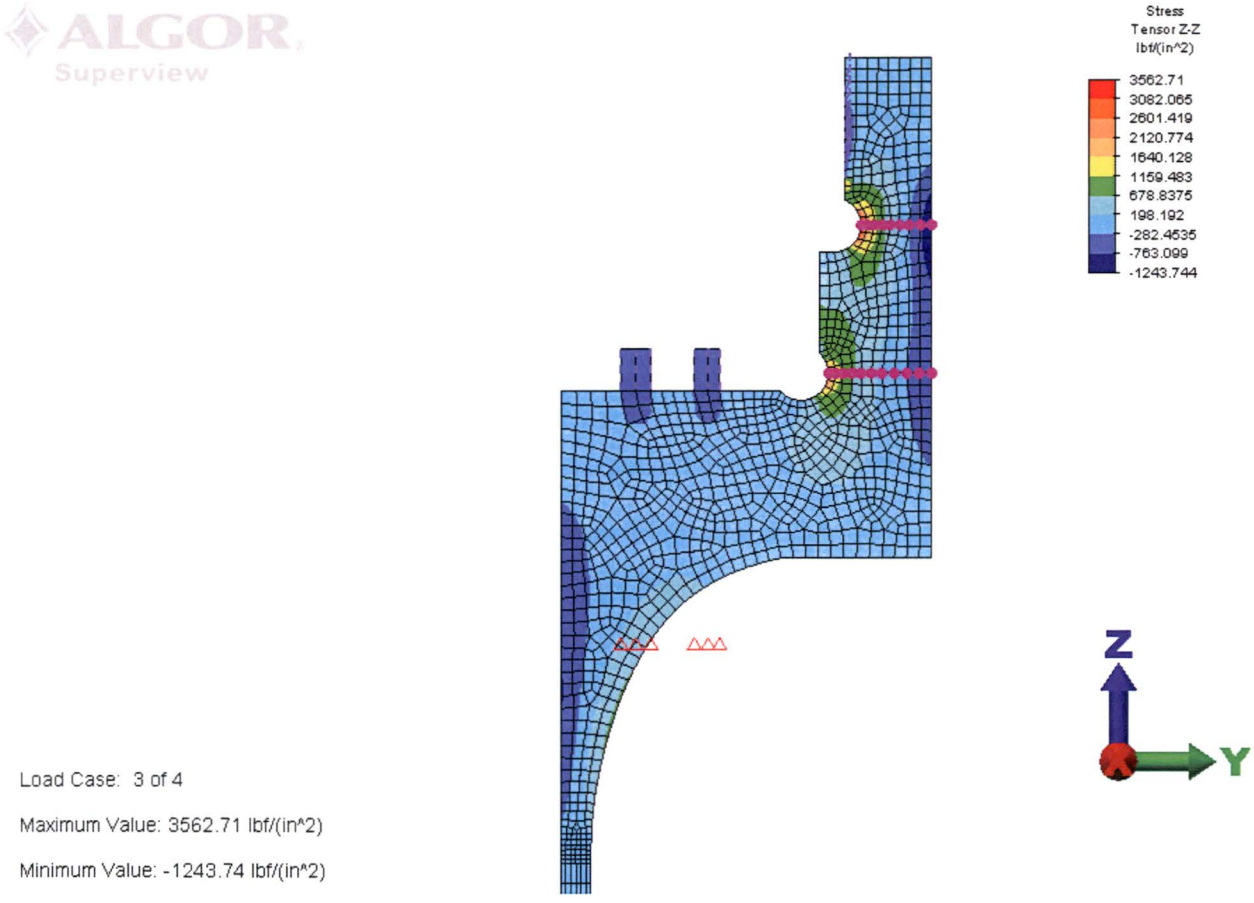

Fig. 1 – Axial Stress Due to Torque Load in Containment Vessel Neck

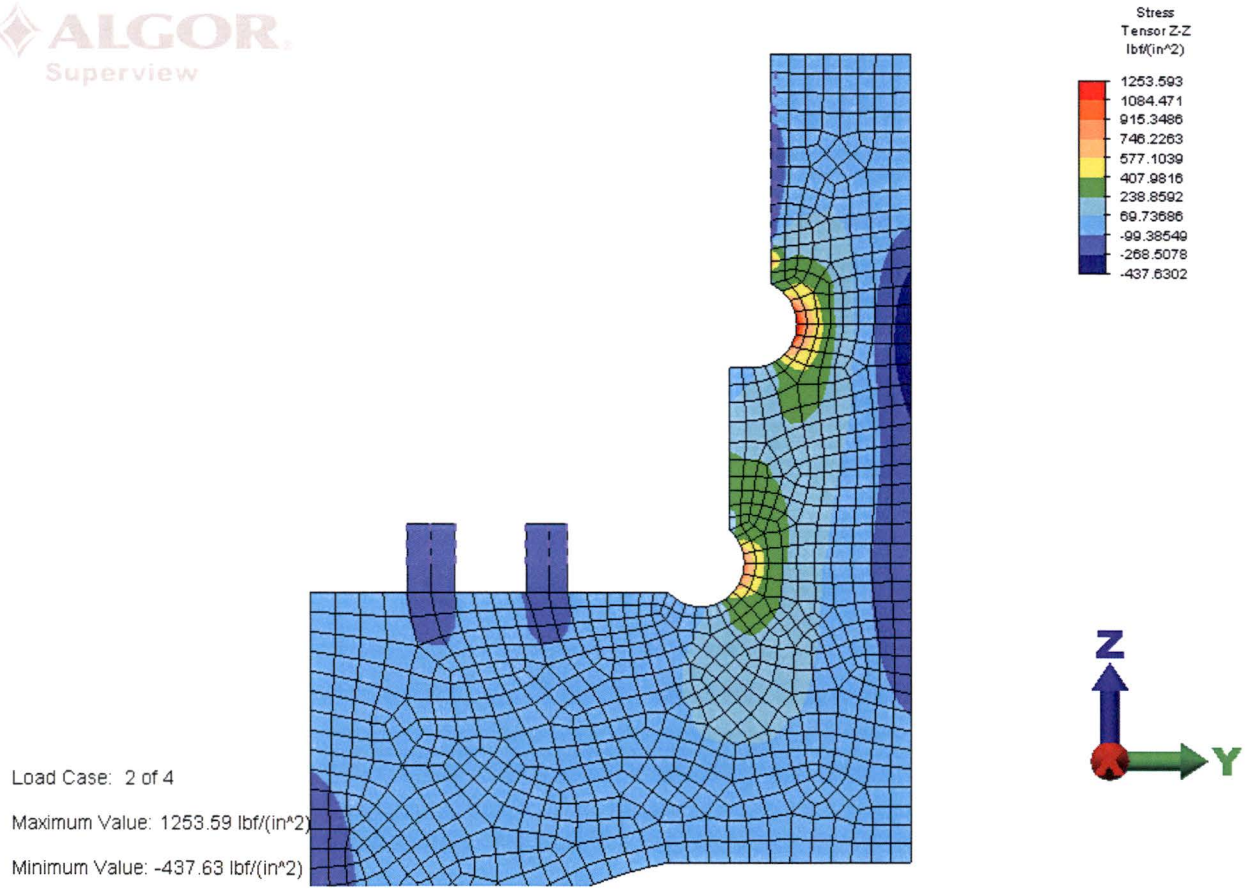

Fig. 2 – Axial Stress below the Threads in the Containment Vessel due to Gasket Seating Load

GENERAL DESIGN AND COMPUTATION SHEET

JOB		DATE	SHEET
Fatigue Analysis of ES-3100 CV Threads under Normal Conditions of Use		16 February 2005	11 of 30
DAC NO. DAC-EA-900000-A007	REVISION NO. 0	COMPUTED C. R. Hammond	CHECKED BY M. L. Goins

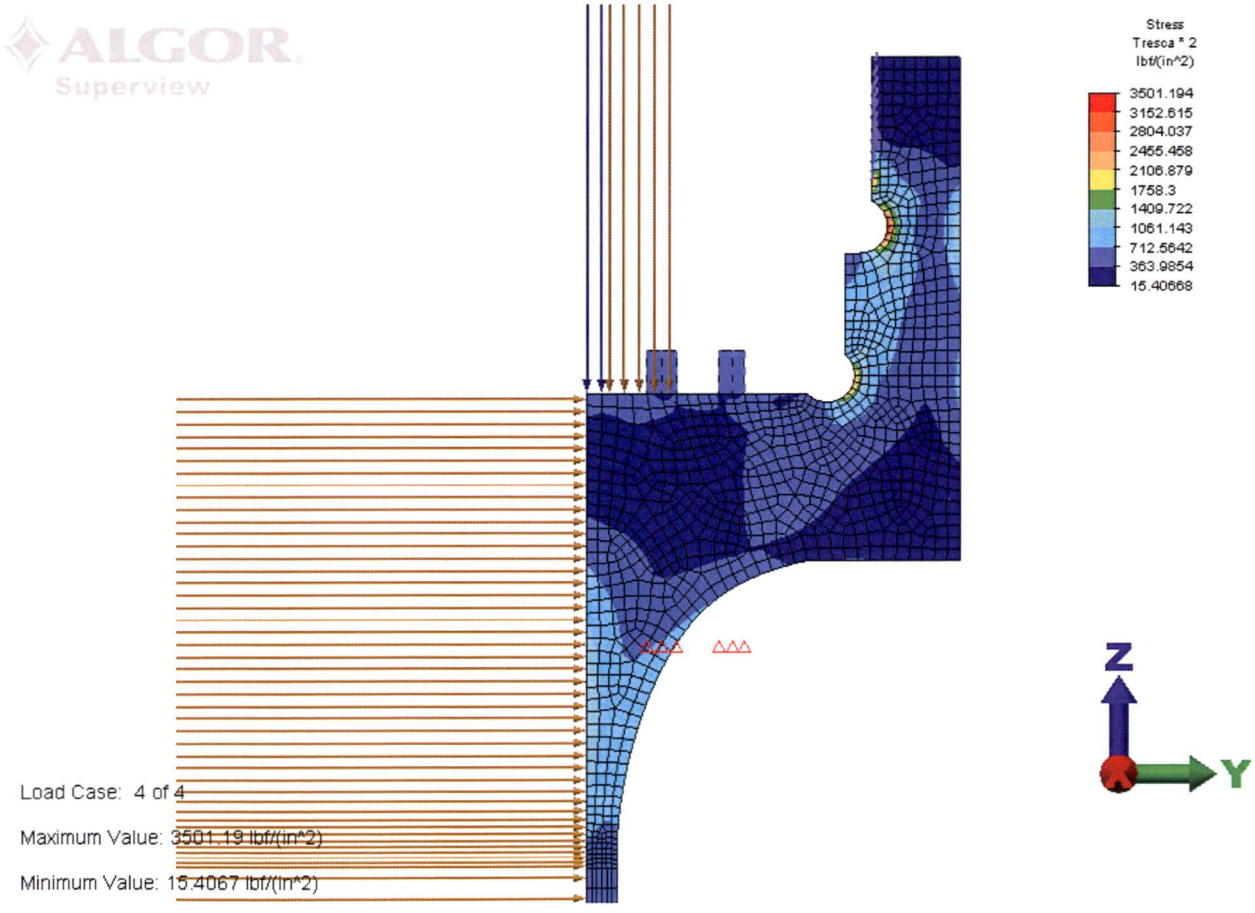

Fig. 3 –Stress Intensity below the Threads in the Containment Vessel due to 3.1 psi Pressure and Torque Loads

GENERAL DESIGN AND COMPUTATION SHEET

JOB	Fatigue Analysis of ES-3100 CV Threads under Normal Conditions of Use	DATE	16 February 2005	SHEET	12 of 30
DAC NO.	DAC-EA-900000-A007	REVISION NO.	0	COMPUTED	C. R. Hammond	CHECKED BY	M. L. Goins

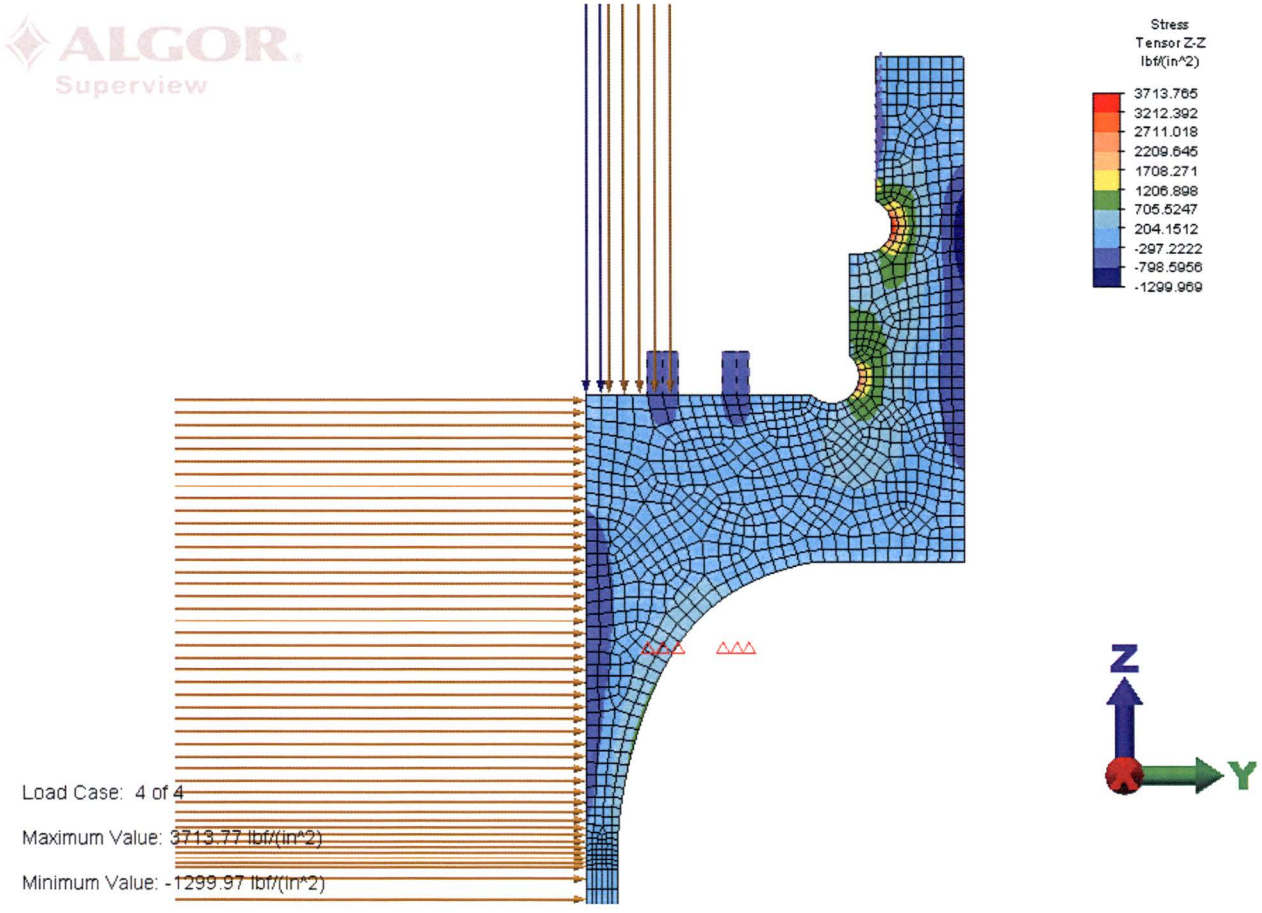

Fig. 4 – Axial Stress in Containment Vessel Due to 3.1 psi Pressure and Torque

Appendix 1 – Axial Stresses across Neck of ES-3100 due to Torque

Top Section

```
Current Load Case = 3

Node # 1894 ( X = 0, Y = 3.515, Z = 9.45 )

    Displaced Position : X = 0, Y = 3.51496, Z = 9.44997

    Displacement = DX: 0, DY: -4.55757e-005, DZ: -2.7064e-005, Magnitude: 5.30057e-005

    appears in 2 Elements

    Part: 8    Element: 1

    Current Result Value: 3476.397428 lbf/(in^2)

    Part: 6    Element: 152

    Current Result Value: 3562.710297 lbf/(in^2)

Node # 1895 ( X = 0, Y = 3.53702, Z = 9.45 )

    Displaced Position : X = 0, Y = 3.53697, Z = 9.44998

    Displacement = DX: 0, DY: -4.64674e-005, DZ: -1.54912e-005, Magnitude: 4.89816e-005

    appears in 4 Elements

    Part: 8    Element: 1

    Part: 8    Element: 2

    Current Result Value: 2076.571725 lbf/(in^2)

    Part: 6    Element: 151

    Part: 6    Element: 152

    Current Result Value: 2150.404851 lbf/(in^2)

Node # 1896 ( X = 0, Y = 3.55903, Z = 9.45 )

    Displaced Position : X = 0, Y = 3.55898, Z = 9.44998

    Displacement = DX: 0, DY: -4.70825e-005, DZ: -1.69066e-005, Magnitude: 5.0026e-005

    appears in 4 Elements

    Part: 8    Element: 2

    Part: 8    Element: 3

    Current Result Value: 1338.334401 lbf/(in^2)
```

```
    Part: 6    Element: 150

    Part: 6    Element: 151

    Current Result Value: 1388.726762 lbf/(in^2)

Node # 1897 ( X = 0, Y = 3.58545, Z = 9.45 )

    Displaced Position : X = 0, Y = 3.5854, Z = 9.44998

    Displacement = DX: 0, DY: -4.7175e-005, DZ: -1.82265e-005, Magnitude: 5.05735e-005

    appears in 4 Elements

    Part: 8    Element: 3

    Part: 8    Element: 4

    Current Result Value: 815.1134205 lbf/(in^2)

    Part: 6    Element: 149

    Part: 6    Element: 150

    Current Result Value: 856.9278605 lbf/(in^2)

Node # 1898 ( X = 0, Y = 3.61186, Z = 9.45 )

    Displaced Position : X = 0, Y = 3.61182, Z = 9.44998

    Displacement = DX: 0, DY: -4.7039e-005, DZ: -1.97662e-005, Magnitude: 5.10232e-005

    appears in 4 Elements

    Part: 8    Element: 4

    Part: 8    Element: 5

    Current Result Value: 422.3549006 lbf/(in^2)

    Part: 6    Element: 148

    Part: 6    Element: 149

    Current Result Value: 454.1958936 lbf/(in^2)

Node # 1899 ( X = 0, Y = 3.64356, Z = 9.45 )

    Displaced Position : X = 0, Y = 3.64352, Z = 9.44998

    Displacement = DX: 0, DY: -4.6803e-005, DZ: -2.12778e-005, Magnitude: 5.14127e-005

    appears in 4 Elements

    Part: 8    Element: 5
```

```
    Part: 8    Element: 6

    Current Result Value: 60.92361234 lbf/(in^2)

    Part: 6    Element: 147

    Part: 6    Element: 148

    Current Result Value: 92.87579812 lbf/(in^2)

Node # 1900 ( X = 0, Y = 3.67526, Z = 9.45 )

    Displaced Position : X = 0, Y = 3.67522, Z = 9.44998

    Displacement = DX: 0, DY: -4.64719e-005, DZ: -2.30637e-005, Magnitude: 5.18804e-005

    appears in 4 Elements

    Part: 6    Element: 145

    Part: 6    Element: 147

    Current Result Value: -276.2872177 lbf/(in^2)

    Part: 8    Element: 6

    Part: 8    Element: 7

    Current Result Value: -291.8618414 lbf/(in^2)

Node # 1901 ( X = 0, Y = 3.71263, Z = 9.45 )

    Displaced Position : X = 0, Y = 3.71258, Z = 9.44997

    Displacement = DX: 0, DY: -4.6099e-005, DZ: -2.48703e-005, Magnitude: 5.23798e-005

    appears in 4 Elements

    Part: 8    Element: 7

    Part: 8    Element: 8

    Current Result Value: -690.1878235 lbf/(in^2)

    Part: 6    Element: 145

    Part: 6    Element: 146

    Current Result Value: -699.5449043 lbf/(in^2)

Node # 1902 ( X = 0, Y = 3.75, Z = 9.45 )

    Displaced Position : X = 0, Y = 3.74996, Z = 9.44997

    Displacement = DX: 0, DY: -4.48856e-005, DZ: -2.93433e-005, Magnitude: 5.3626e-005
```

```
    appears in 2 Elements
    Part: 8     Element: 8
    Current Result Value: -1189.038154 lbf/(in^2)
    Part: 6     Element: 146
    Current Result Value: -1243.744425 lbf/(in^2)
```

Lower Section

```
Current Load Case = 3

Node # 1718 ( X = 0, Y = 3.4065, Z = 8.96 )
    Displaced Position : X = 0, Y = 3.40646, Z = 9.03102
    Displacement = DX: 0, DY: -3.86154e-005, DZ: 0.0710243, Magnitude: 0.0710243
    appears in 2 Elements
    Part: 6     Element: 1
    Current Result Value: 2381.970074 lbf/(in^2)
    Part: 3     Element: 713
    Current Result Value: 2573.760605 lbf/(in^2)
Node # 1719 ( X = 0, Y = 3.43091, Z = 8.96 )
    Displaced Position : X = 0, Y = 3.43087, Z = 9.03103
    Displacement = DX: 0, DY: -3.82805e-005, DZ: 0.071027, Magnitude: 0.071027
    appears in 4 Elements
    Part: 6     Element: 1
    Part: 6     Element: 2
    Current Result Value: 1429.725908 lbf/(in^2)
    Part: 3     Element: 712
    Part: 3     Element: 713
    Current Result Value: 1507.238598 lbf/(in^2)
```

```
Node # 1720 ( X = 0, Y = 3.45532, Z = 8.96 )

    Displaced Position : X = 0, Y = 3.45529, Z = 9.03102

    Displacement = DX: 0, DY: -3.93058e-005, DZ: 0.0710167, Magnitude: 0.0710167

    appears in 4 Elements

    Part: 3    Element: 711

    Part: 3    Element: 712

    Current Result Value: 1015.779644 lbf/(in^2)

    Part: 6    Element: 2

    Part: 6    Element: 3

    Current Result Value: 1035.108104 lbf/(in^2)

Node # 1721 ( X = 0, Y = 3.48462, Z = 8.96 )

    Displaced Position : X = 0, Y = 3.48458, Z = 9.03103

    Displacement = DX: 0, DY: -3.78762e-005, DZ: 0.0710297, Magnitude: 0.0710297

    appears in 4 Elements

    Part: 3    Element: 710

    Part: 3    Element: 711

    Current Result Value: 699.5787633 lbf/(in^2)

    Part: 6    Element: 3

    Part: 6    Element: 4

    Current Result Value: 752.6151572 lbf/(in^2)

Node # 1722 ( X = 0, Y = 3.51391, Z = 8.96 )

    Displaced Position : X = 0, Y = 3.51388, Z = 9.03103

    Displacement = DX: 0, DY: -3.73704e-005, DZ: 0.0710323, Magnitude: 0.0710323

    appears in 4 Elements

    Part: 3    Element: 707

    Part: 3    Element: 710

    Current Result Value: 479.8616501 lbf/(in^2)

    Part: 6    Element: 4
```

```
    Part: 6    Element: 5

    Current Result Value: 524.8054716 lbf/(in^2)

Node # 1723 ( X = 0, Y = 3.54907, Z = 8.96 )

    Displaced Position : X = 0, Y = 3.54903, Z = 9.03101

    Displacement = DX: 0, DY: -3.89625e-005, DZ: 0.0710096, Magnitude: 0.0710096

    appears in 4 Elements

    Part: 3    Element: 704

    Part: 3    Element: 707

    Current Result Value: 286.7099034 lbf/(in^2)

    Part: 6    Element: 5

    Part: 6    Element: 6

    Current Result Value: 319.4018001 lbf/(in^2)

Node # 1724 ( X = 0, Y = 3.58422, Z = 8.96 )

    Displaced Position : X = 0, Y = 3.58418, Z = 9.03101

    Displacement = DX: 0, DY: -3.94127e-005, DZ: 0.071011, Magnitude: 0.071011

    appears in 4 Elements

    Part: 3    Element: 704

    Part: 3    Element: 705

    Current Result Value: 104.2072763 lbf/(in^2)

    Part: 6    Element: 6

    Part: 6    Element: 7

    Current Result Value: 126.0936862 lbf/(in^2)

Node # 1725 ( X = 0, Y = 3.62567, Z = 8.96 )

    Displaced Position : X = 0, Y = 3.62563, Z = 9.03101

    Displacement = DX: 0, DY: -3.94951e-005, DZ: 0.0710126, Magnitude: 0.0710126

    appears in 4 Elements

    Part: 6    Element: 7

    Part: 6    Element: 8
```

```
    Current Result Value: -69.65167919 lbf/(in^2)

    Part: 3    Element: 705

    Part: 3    Element: 706

    Current Result Value: -87.34285327 lbf/(in^2)

Node # 1726 ( X = 0, Y = 3.66711, Z = 8.96 )

    Displaced Position : X = 0, Y = 3.66707, Z = 9.03101

    Displacement = DX: 0, DY: -3.94338e-005, DZ: 0.0710146, Magnitude: 0.0710146

    appears in 4 Elements

    Part: 6    Element: 8

    Part: 6    Element: 9

    Current Result Value: -274.1379622 lbf/(in^2)

    Part: 3    Element: 706

    Part: 3    Element: 708

    Current Result Value: -286.8211743 lbf/(in^2)

Node # 1727 ( X = 0, Y = 3.70856, Z = 8.96 )

    Displaced Position : X = 0, Y = 3.70852, Z = 9.03102

    Displacement = DX: 0, DY: -3.91153e-005, DZ: 0.0710191, Magnitude: 0.0710191

    appears in 4 Elements

    Part: 6    Element: 9

    Part: 6    Element: 10

    Current Result Value: -489.6421277 lbf/(in^2)

    Part: 3    Element: 708

    Part: 3    Element: 709

    Current Result Value: -498.9915546 lbf/(in^2)

Node # 1728 ( X = 0, Y = 3.75, Z = 8.96 )

    Displaced Position : X = 0, Y = 3.74996, Z = 9.03102

    Displacement = DX: 0, DY: -3.89012e-005, DZ: 0.0710215, Magnitude: 0.0710215

    appears in 2 Elements
```

GENERAL DESIGN AND COMPUTATION SHEET

JOB		DATE	SHEET
Fatigue Analysis of ES-3100 CV Threads under Normal Conditions of Use		16 February 2005	20 of 30
DAC NO. DAC-EA-900000-A007	REVISION NO. 0	COMPUTED C. R. Hammond	CHECKED BY M. L. Goins

```
Part: 6     Element: 10

Current Result Value: -726.5076374 lbf/(in^2)

Part: 3     Element: 709

Current Result Value: -737.209287 lbf/(in^2)
```

GENERAL DESIGN AND COMPUTATION SHEET

JOB	Fatigue Analysis of ES-3100 CV Threads under Normal Conditions of Use	DATE	16 February 2005	SHEET	21 of 30
DAC NO.	DAC-EA-900000-A007	REVISION NO.	0	COMPUTED	C. R. Hammond	CHECKED BY	M. L. Goins

Appendix 1 - Axial stress across neck of ES-3100 CV due to torque

Top section - Part 8

Y, in.	Sigma ZZ, psi	Delta R, in.	Force, lb.	Force (hard way), lb.
3.515	3476.397428	0.01101	845.3215421	846.6454383
3.53702	2076.571725	0.022015	1015.974973	1015.974255
3.55903	1338.334401	0.024215	724.7039558	724.9284512
3.58545	815.1134205	0.026415	485.0563535	485.0560153
3.61186	422.3549006	0.029055	278.4897363	278.5917067
3.64356	60.92361234	0.0317	44.21307309	44.21307309
3.67526	-291.8618414	0.034535	-232.7580525	-232.8478243
3.71263	-690.1878235	0.03737	-601.6610939	-601.6610939
3.75	-1189.038154	0.018685	-523.4799217	-522.1757588
		Sum	2035.860566	2038.724263

Lower section - Part 3

3.4065	2573.760605	0.012205	672.3481194	673.5525828
3.43091	1507.238598	0.02441	793.1201445	793.1201445
3.45532	1015.779644	0.026855	592.2332744	592.4428079
3.48462	699.5787633	0.029295	448.7096535	448.7093316
3.51391	479.8616501	0.032225	341.4125422	341.5551249
3.54907	286.7099034	0.035155	224.7626947	224.7625364
3.58422	104.2072763	0.0383	89.88171407	89.92121045
3.62567	-87.34285327	0.041445	-82.46461971	-82.46456285
3.66711	-286.8211743	0.041445	-273.8969268	-273.8971135
3.70856	-498.9915546	0.041445	-481.8928886	-481.8925638
3.75	-737.209287	0.02072	-359.9081529	-358.9138467
		Sum	1964.305555	1966.895652

Section difference = 0.036518771

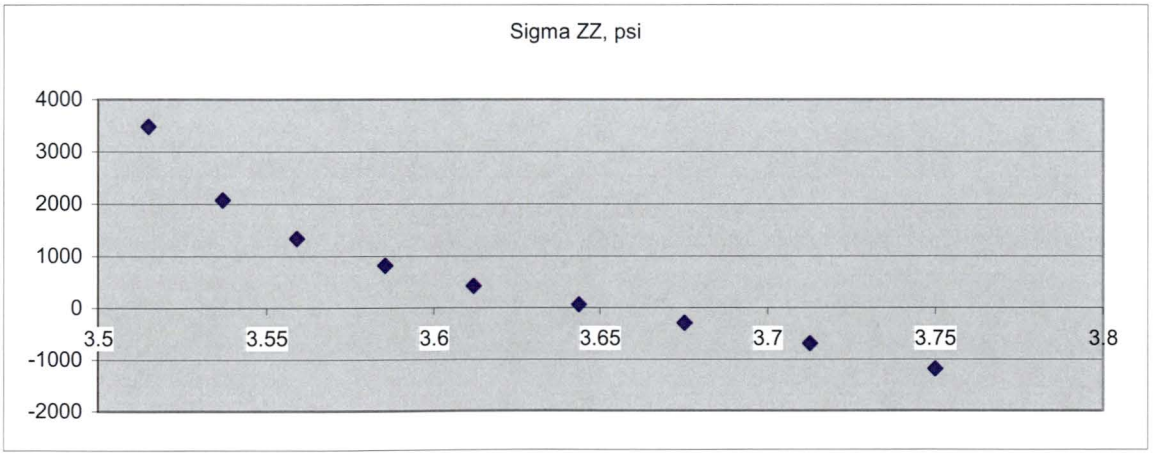

Appendix 2 – Finite Element Data

Summary

Description

Thread Analysis

Model Information

Analysis Type - Static Stress with Linear Material Models
Units - English (in) - (lbf, in, s, deg F, deg R, V, ohm, A, in*lbf)
Model location - C:\ALGOR12\es3100CV1

Analysis Parameters Information

Load Case Multipliers

Static Stress with Linear Material Models may have multiple load cases. This allows a model to be analyzed with multiple loads while solving the equations a single time. The following is a list of load case multipliers that were analyzed with this model.

Load Case	Pressure/ Surface Forces	Acceleration/ Gravity	Displaced Boundary	Thermal	Voltage
1	1	0	1	0	0
2	0	0	1	0	0
3	0	0	0	1	0
4	0.0305	0	0	1	0

Multiphysics Information

Default Nodal Temperature	70°F
Source of Nodal Temperature	None
Time step from Heat Transfer Analysis	Last

Processor Information

Type of Solver	Sparse
Disable Calculation and Output of Strains	No
Calculate Reaction Forces	Yes
Invoke Banded Solver	Yes
Avoid Bandwidth Minimization	No
Stop After Stiffness Calculations	No
Displacement Data in Output File	No
Stress Data in Output File	No
Equation Numbers Data in Output File	No
Element Input Data in Output File	No
Nodal Input Data in Output File	No
Centrifugal Load Data in Output File	No

Part Information

Part ID	Part Name	Element Type	Material Name
1	Plate & shell	2-D	[Customer Defined] (Part 1)
2	Bottom corner	2-D	[Customer Defined] (Part 2)
3	Top transition	2-D	[Customer Defined] (Part 3)
4	Outer O-ring	2-D	[Customer Defined] (Part 4)
5	Inner O-ring	2-D	[Customer Defined] (Part 5)
6	Top flange neck	2-D	[Customer Defined] (Part 6)
8	Thread region	2-D	[Customer Defined] (Part 8)

Element Properties used for:

- Plate & shell
- Bottom corner
- Top transition
- Thread region

Element Type	2-D
Geometry Type	Axisymmetric
Material Model	Isotropic
Thickness	1 in
Stress Free Reference Temperature	70°F
Principle Axes Transformational Angle	0°
Nodal Order Method	Default
Nodal Order Y Coordinate	0 in
Nodal Order Z Coordinate	0 in

Element Properties used for:

- Outer O-ring
- Inner O-ring

Element Type	2-D
Geometry Type	Axisymmetric
Material Model	Isotropic
Thickness	1 in
Stress Free Reference Temperature	0°F
Principle Axes Transformational Angle	0°
Nodal Order Method	Default
Nodal Order Y Coordinate	0 in
Nodal Order Z Coordinate	0 in

GENERAL DESIGN AND COMPUTATION SHEET

JOB Fatigue Analysis of ES-3100 CV Threads under Normal Conditions of Use		DATE 16 February 2005	SHEET 25 of 30
DAC NO. DAC-EA-900000-A007	REVISION NO. 0	COMPUTED C. R. Hammond	CHECKED BY M. L. Goins

Element Properties used for:

- Top flange neck

Element Type	2-D
Geometry Type	Axisymmetric
Material Model	Orthotropic
Thickness	1 in
Stress Free Reference Temperature	170°F
Principle Axes Transformational Angle	0°
Nodal Order Method	Default
Nodal Order Y Coordinate	0 in
Nodal Order Z Coordinate	0 in

Material Information

[Customer Defined] (Part 1) - 2-D

Material Model	Standard
Material Source	Not Applicable
Material Source File	
Date Last Updated	2004/09/28-14:35:06
Material Description	Customer defined material properties
Mass Density	7.50e-4 lbf*s^2/in/in^3
Modulus of Elasticity	27e6 lbf/in^2
Poisson's Ratio	0.3
Thermal Coefficient of Expansion	9.2e-6 1/°F
Shear Modulus of Elasticity	10384615 lbf/in^2

[Customer Defined] (Part 2) - 2-D

Material Model	Standard
Material Source	Not Applicable
Material Source File	
Date Last Updated	2004/09/28-14:36:43
Material Description	Customer defined material properties
Mass Density	7.50e-4 lbf*s^2/in/in^3
Modulus of Elasticity	27e6 lbf/in^2
Poisson's Ratio	0.3
Thermal Coefficient of Expansion	9.2e-6 1/°F
Shear Modulus of Elasticity	10384615 lbf/in^2

[Customer Defined] (Part 3) - 2-D

Material Model	Standard
Material Source	Not Applicable
Material Source File	
Date Last Updated	2004/09/28-14:38:39
Material Description	Customer defined material properties
Mass Density	7.50e-4 lbf*s^2/in/in^3
Modulus of Elasticity	27e6 lbf/in^2
Poisson's Ratio	0.30
Thermal Coefficient of Expansion	9.2e-6 1/°F
Shear Modulus of Elasticity	10384615 lbf/in^2

[Customer Defined] (Part 4) - 2-D

Material Model	Standard
Material Source	Not Applicable
Material Source File	
Date Last Updated	2004/09/28-14:39:52
Material Description	Customer defined material properties
Mass Density	0 lbf*s^2/in/in^3
Modulus of Elasticity	1321 lbf/in^2
Poisson's Ratio	0
Thermal Coefficient of Expansion	0 1/°F
Shear Modulus of Elasticity	660.5 /^{2}

[Customer Defined] (Part 5) - 2-D

Material Model	Standard
Material Source	Not Applicable
Material Source File	
Date Last Updated	2004/09/28-14:40:41
Material Description	Customer defined material properties
Mass Density	0 lbf*s^2/in/in^3
Modulus of Elasticity	1122 lbf/in^2
Poisson's Ratio	0
Thermal Coefficient of Expansion	0 1/°F
Shear Modulus of Elasticity	561. /^{2}

[Customer Defined] (Part 6) - 2-D

Material Model	OrthotropicTempDep
Material Source	Not Applicable
Material Source File	
Date Last Updated	2004/10/14-14:27:16
Material Description	Customer defined material properties
Mass Density	7.50e-4 lbf*s^2/in/in³
Index 1 - Temperature	170 °F
Index 1 - E1	27e6 lbf/in²
Index 1 - E2	27e6 lbf/in²
Index 1 - E3	27e6 lbf/in²
Index 1 - V12	.3
Index 1 - V13	.3
Index 1 - V23	.3
Index 1 - G12	10384615 lbf/in²
Index 1 - G13	10384615 lbf/in²
Index 1 - G23	10384615 lbf/in²
Index 1 - Alpha 1	0 1/°F
Index 1 - Alpha 2	1.45e-3 1/°F
Index 1 - Alpha 3	0 1/°F

[Customer Defined] (Part 8) - 2-D

Material Model	Standard
Material Source	Not Applicable
Material Source File	
Date Last Updated	2004/09/28-14:43:25
Material Description	Customer defined material properties
Mass Density	7.50e-4 lbf*s^2/in/in^3
Modulus of Elasticity	27e6 lbf/in^2
Poisson's Ratio	0.30
Thermal Coefficient of Expansion	9.2e-6 1/°F
Shear Modulus of Elasticity	10384615 lbf/in^2

Processor Output

Processor Summary

```
ALGOR (R) Static Stress with Linear Material Models
Version 16.00-WIN 29-SEP-2004
Copyright (c) 1984-2004 ALGOR, Inc. All rights reserved.

-------------------------------------------------
                     DATE: FEBRUARY 16, 2005
                     TIME: 07:55 AM
               INPUT MODEL: C:\ALGOR12\es3100CV1

            PROGRAM VERSION: 16000001
            ALG.DLL VERSION: 13240000
      AlgConfig.DLL VERSION: 15000000
       agsdb_ar.DLL VERSION: 14000004
       amgsolve.DLL VERSION: 03220000
-------------------------------------------------

      Linear Stress

1**** CONTROL INFORMATION

      number of node points          (NUMNP)   =          2061
      number of element types        (NELTYP)  =             8
      number of load cases           (LL)      =             4
```

```
      number of frequencies          (NF)      =            0
      analysis type code             (NDYN)    =            0
      equations per block            (KEQB)    =            0
      bandwidth minimization flag    (MINBND)  =            0
      gravitational constant         (GRAV)    =    3.8640E+02
      number of equations            (NEQ)     =         4092

 **** PRINT OF NODAL DATA SUPPRESSED
 **** PRINT OF EQUATION NUMBERS SUPPRESSED
 **** PRINT OF TYPE-4 ELEMENT DATA SUPPRESSED
 **** PRINT OF TYPE-4 ELEMENT DATA SUPPRESSED
 **** PRINT OF TYPE-4 ELEMENT DATA SUPPRESSED
 **** PRINT OF TYPE-4 ELEMENT DATA SUPPRESSED
 **** PRINT OF TYPE-4 ELEMENT DATA SUPPRESSED
 **** PRINT OF TYPE-4 ELEMENT DATA SUPPRESSED
 **** PRINT OF TYPE-4 ELEMENT DATA SUPPRESSED
 **** PRINT OF TYPE-7 ELEMENT DATA SUPPRESSED
 **** Hard disk file size information for processor:

      Available hard disk space on current drive =   3849.848 megabytes

1**** NODAL LOADS (STATIC) OR MASSES (DYNAMIC)

   NODE  LOAD      X-AXIS      Y-AXIS      Z-AXIS      X-AXIS      Y-AXIS      Z-AXIS
  NUMBER CASE      FORCE       FORCE       FORCE       MOMENT      MOMENT      MOMENT

    1685    1  0.000E+00  0.000E+00 -6.362E+00  0.000E+00  0.000E+00  0.000E+00
    1685    4  0.000E+00  0.000E+00 -1.943E-01  0.000E+00  0.000E+00  0.000E+00
    1686    1  0.000E+00  0.000E+00 -6.424E+00  0.000E+00  0.000E+00  0.000E+00
    1686    4  0.000E+00  0.000E+00 -1.962E-01  0.000E+00  0.000E+00  0.000E+00

1**** ELEMENT LOAD MULTIPLIERS

      load case      case A     case B     case C     case D     case E
      ---------    ---------- ---------- ---------- ---------- ----------

          1         1.000E+00  0.000E+00  1.000E+00  0.000E+00  0.000E+00
          2         0.000E+00  0.000E+00  1.000E+00  0.000E+00  0.000E+00
          3         0.000E+00  0.000E+00  0.000E+00  1.000E+00  0.000E+00
          4         3.050E-02  0.000E+00  0.000E+00  1.000E+00  0.000E+00
```

Appendix 2.10.2

IMPACT ANALYSES OF ES-3100 DESIGN CONCEPTS USING BOROBOND AND CAT 277-4 NEUTRON ABSORBERS

THIS PAGE INTENTIONALLY LEFT BLANK.

Index

Part B - Design with HABC Cylinder (continued)

1.0 Problem Statement

This calculation summarizes the impact simulation computer runs made in support of the ES-3100 shipping package design effort. From the summer of 2003 through the spring of 2004 the design impact simulations were run with borobond as the neutron absorber. During the summer of 2004, the ES-3100 with the borobond neutron absorber was tested to the 10CFR71 impact requirements. In August 2004 a decision was made to change the neutron absorber material to a high alumina borated cement (HABC). The HABC material is also known as "Catalog 277-4" or just "277-4", but the HABC notation is used in this report. The August 2004 absorber change also involved some minor design changes to the configuration of the package liners surrounding the HABC material. Material testing on the HABC material occurred during the Fall of 2004. The simulation impacts were run in the late Fall of 2004.

This calculation is presented in two parts, Part A and Part B. Part A summarizes the impact simulations made for the initial borobond design. Part B summarizes the impact analyses made with the HABC design. A beginning section, Section 1.0 and an ending section, Section 9.0, address both designs. The Part A borobond design simulations are documented in Sections 2 through 5. The Part B, HABC simulations are documented in Sections 6 through 8. A detailed explanation of changes to the Part A, borobond models to develop the Part B HABC models is given in Part B, Section 6.1.

A qualitative, cross sectional view of a ES-3100 package with the initial design borobond neutron absorber (presented in Part A) is shown in Figure 1.1. The ES-3100 shipping package is a stainless steel drum with kaolite insulation material. The overall dimensions of the overpack are a height of about 44 inches and a diameter of about 19.4 inches. At the top of the overpack is a bolted lid restrained by eight, 5/8 inch welded studs. The lid restrains a removable plug filled with the kaolite material. The plug covers a cavity in which the stainless steel containment vessel (CV) is placed. The CV is about 32.9 inches tall with a 5.4 inch inside diameter and a body wall thickness of 0.1 inches. The CV closure is a flat plate constrained by a threaded ring. In the shipping package, and immediately surrounding the CV cavity is a 0.90 inch thick layer of borobond, a neutron absorbing cast material. All the kaolite and borobond materials are wrapped by stainless steel liners. In this model, there is a slight indentation (about 0.32 in) of the liner near the CV flange region into the kaolite, as can be seen in Figure 1.1.

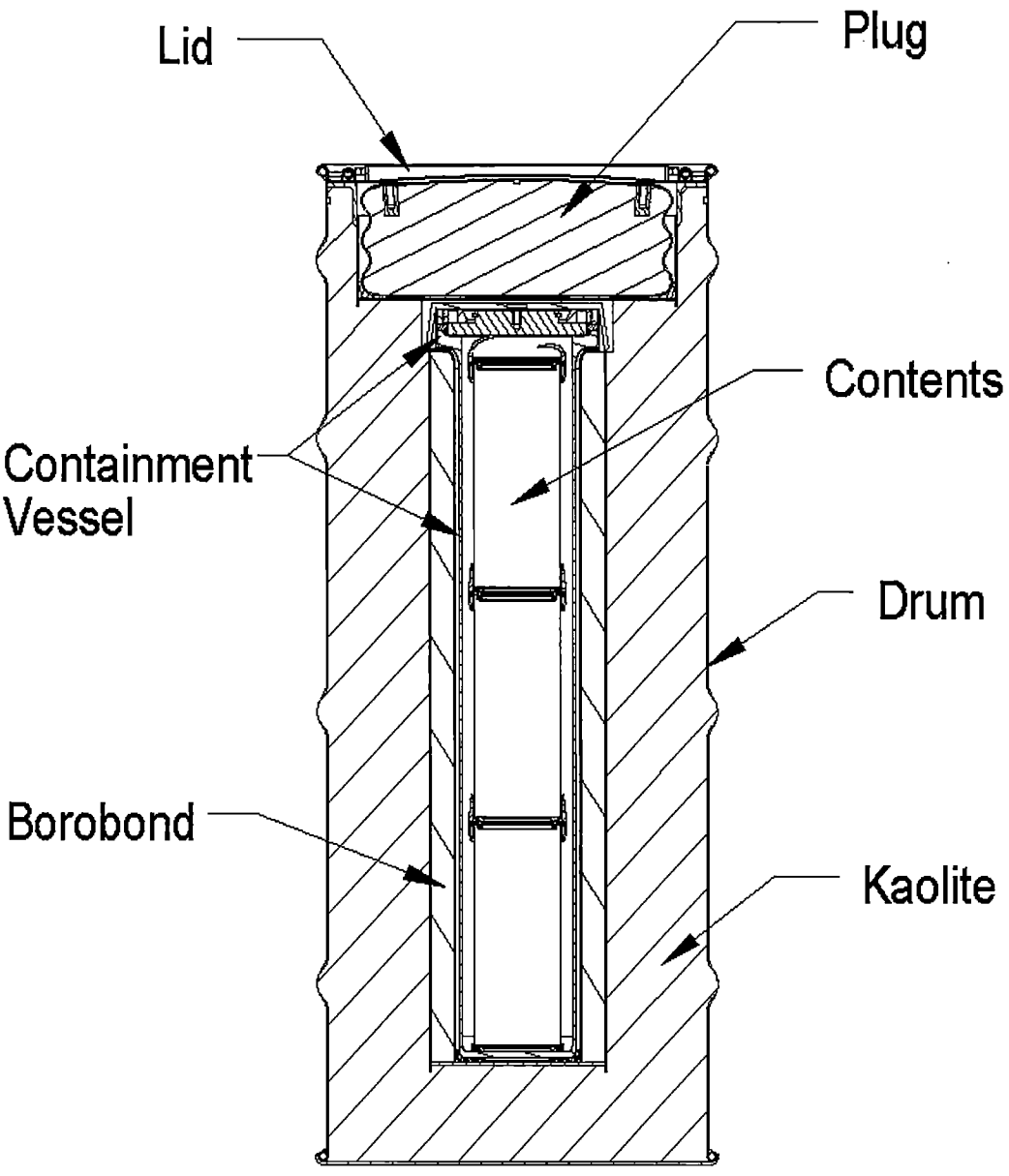

Figure 1.1 - Configuration of the Initial, Borobond Neutron Absorber ES-3100 Package, Presented in Part A

The redesigned package with the HABC (Part B) is shown in Figure 1.2. As can be qualitatively seen in the figure, the liner between the HABC and the kaolite is moved out slightly and there is no indentation into the kaolite near the CV flange. The HABC design changes are minor as shown by qualitatively comparing Figures 1.1 and 1.2. The detailed differences between the Part A borobond model and the Part B, HABC model are presented in Part B, Section 6.

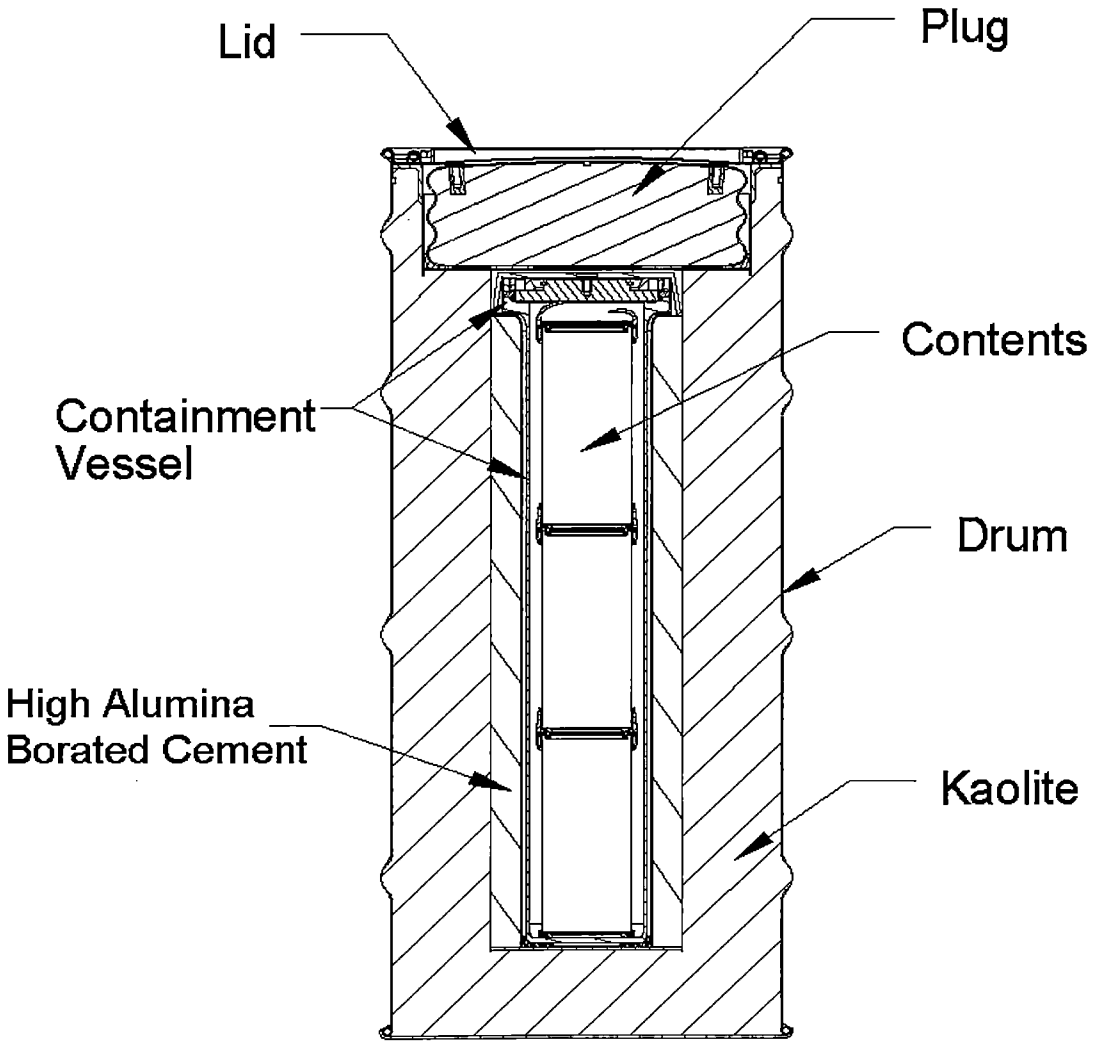

Figure 1.2 - Configuration of the Redesigned ES-3100 with the HABC as the Neutron Absorber, Presented in Part B

The Part A and Part B impact simulations were modeled with the pre-processor software TrueGrid (reference 5.1), solved with the software LS-Dyna (reference 5.2), and results obtained with the post-processor LS-Post (reference 5.3). The computers used for these simulations were Dell dual processor machines (Y12 machines ep0134, ep0141 and ep0142). TrueGrid was run on a Silicon Graphics Workstation (Y12 machine ew204). Typical solution times for one impact ranged from 1 to 4 days.

The impact simulations of the ES3100 package are driven by the 10CFR71, subpart F, sections 71.71 and 71.73 impact requirements. LS-Dyna allows successive restarts to be made which enables cumulative damage to be obtained in the shipping package model. Part A, Section 2.1, describes the specific impact simulations performed for the initial borobond design. Part B, Section 6.1, describes the simulations performed for the HABC design. Sections 3.12 and 7.7 compare the respective model results to physical test results.

2.0 Analytical Model

Two models were used in the dynamic impact runs for the borobond design of the ES-3100 shipping container; a detailed model and a simplified model. A detailed model included the drum closure details, CV details and generally a finer element mesh. The detailed model was used for all the runs, except the study which evaluated the response of the drum to various punch angles. A simplified model was used to investigate the variation in punch angles. The detailed model is discussed in Section 2.1 and the simplified model is discussed in Section 2.2.

Design drawings were used to develop the ES-3100 analytical models. The reference 5.5 AutoSketch software was used as an aid in the creation of the TrueGrid input file. The running of TrueGrid created the bulk of the LS-Dyna input file (e.g., the nodal data, element data, contact surfaces, etc). The LS-Dyna command lines and material properties were created in a separate file and edited into the TrueGrid created LS-Dyna input file. The resulting file was a complete LS-Dyna input file which was then submitted for execution.

2.1 Model Description - Detailed Model

Figure 2.1.1 shows the typical detailed model assembly for the ES-3100. All of the entities shown (rigid surface, crush plate, shipping package and punch) exist in the model, however, only the entities of concern in an impact were active in that impact. In the 4-foot impact and 30-foot impact only the shipping package and the rigid plate were in contact. The crush plate and the punch existed in the model, however, there was no contact between them and the shipping package. During the crush impact, the crush plate contacts the shipping package, which then contacts the rigid plate. During the crush impact, the punch exists, but is not contacted. During the punch impact, the crush plate and the rigid surface are deleted from the model, allowing contact to be made between the shipping package and the punch.

Figure 2.1.2 shows the components of the detailed model in an exploded view. The element mesh is not included in Figure 2.1.1, nor in Figure 2.1.2 for clarity. Representative element meshes for the detailed model are shown in Figures 2.1.3 and 2.1.4.

Various impact configurations of the ES-3100 detailed model are documented in this calculation. Figure 2.1.5 shows icons representing the impact configurations run for the design effort. The 4-foot impact and the punch impact are not as structurally demanding as is the 30-foot free fall impact, nor the 30-foot crush impact. Therefore, only the 30-foot impact and the crush impact were performed in the design effort runs. Figure 2.1.6

Part A - Initial Design with Borobond Cylinder

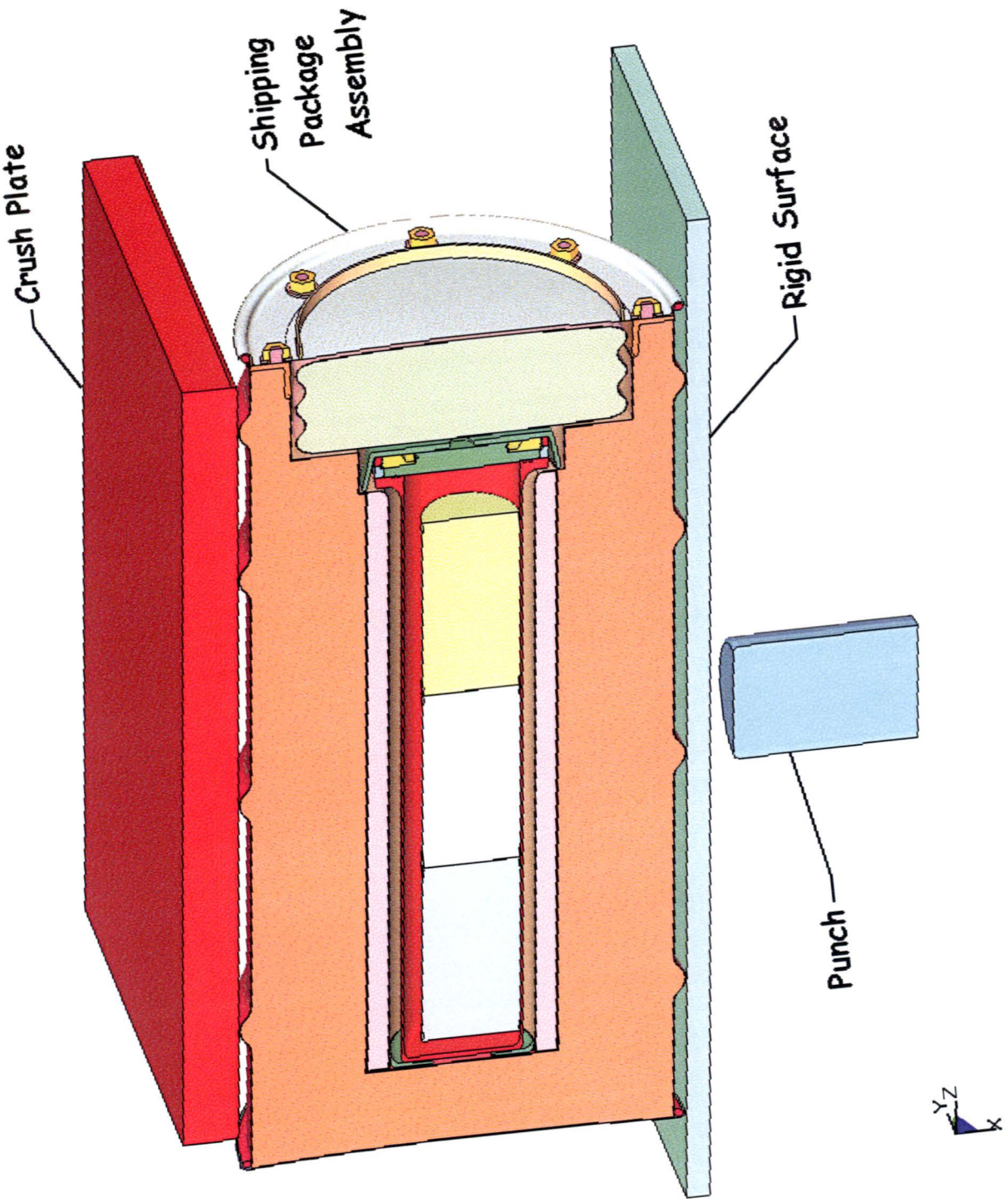

Figure 2.1.1 - Typical ES-3100 Detailed Model Assembly

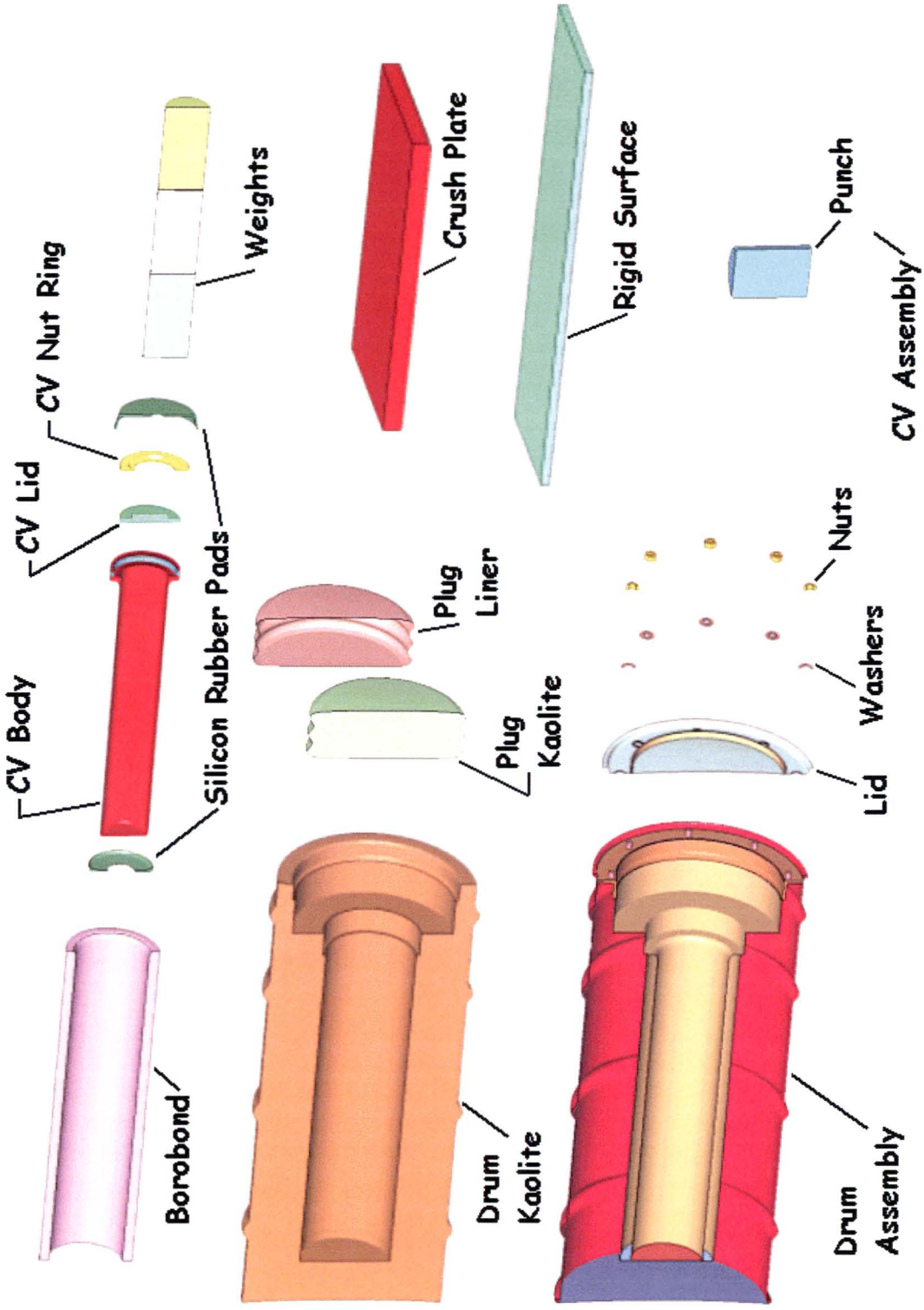

Figure 2.1.2 - ES-3100 Detailed Model Components

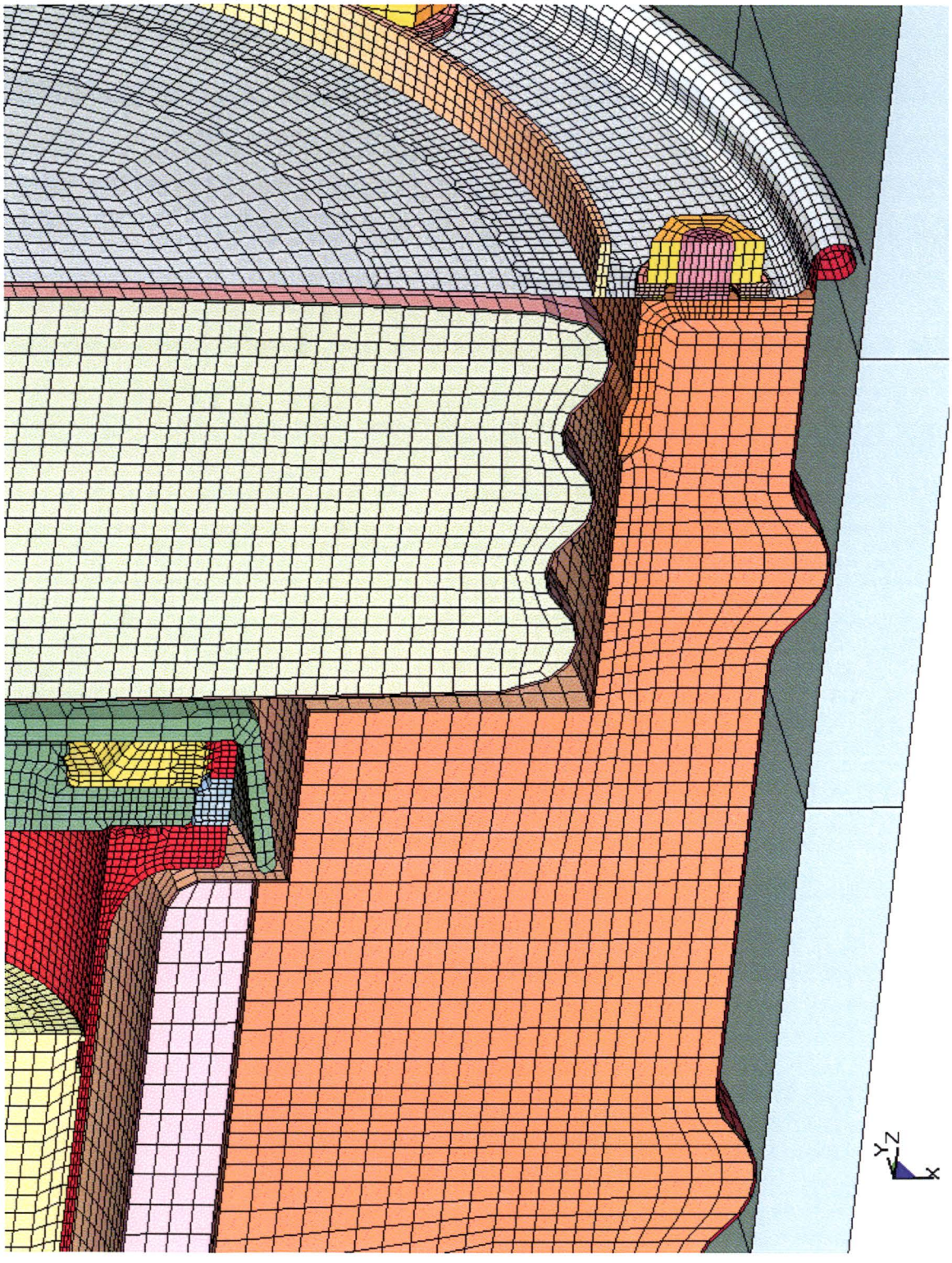

Figure 2.1.3 - Typical Element Mesh in the Upper Container Region of the Detailed Model

Part A - Initial Design with Borobond Cylinder

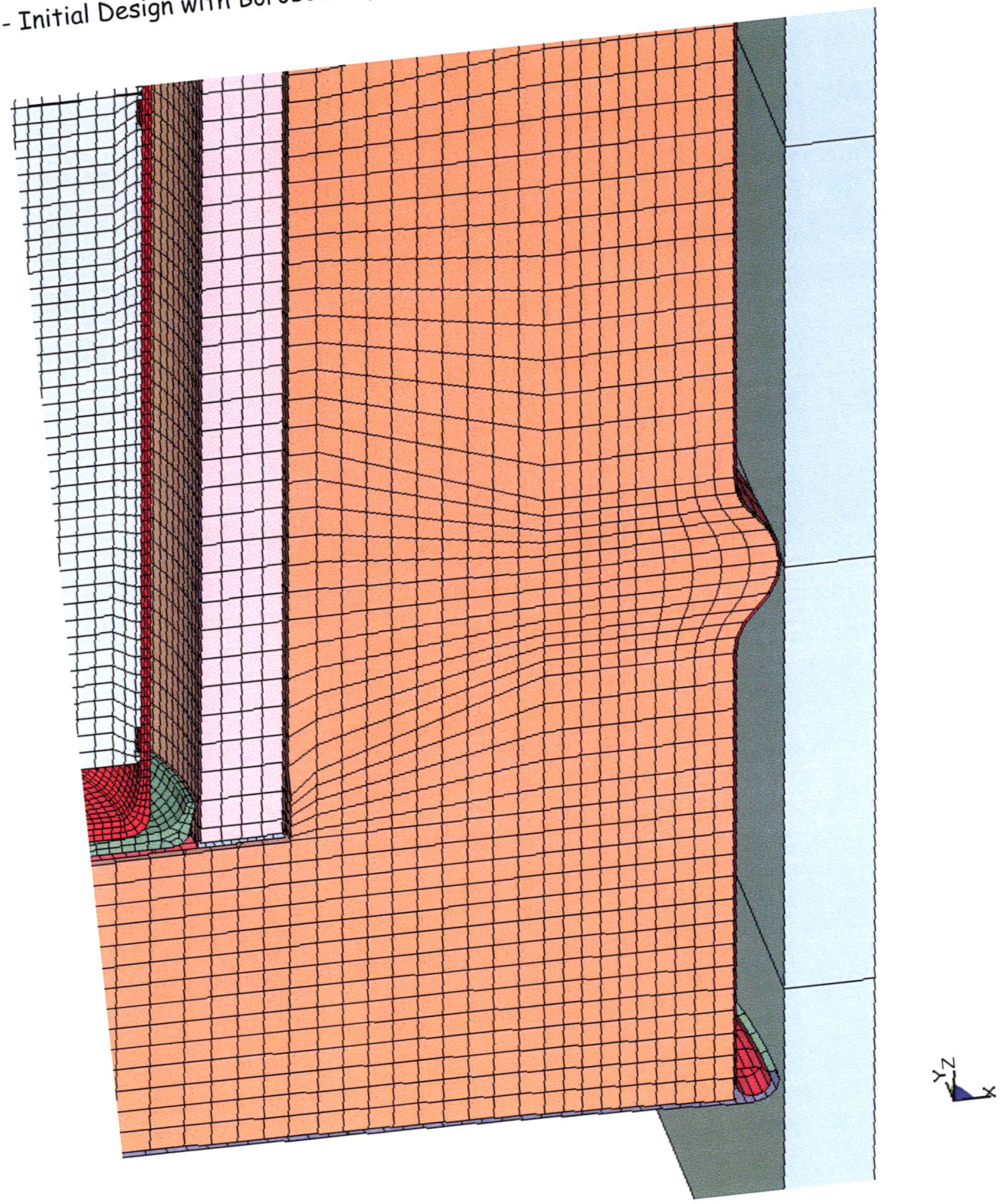

Figure 2.1.4 - Typical Element Mesh in the Lower Container Region of the Detailed Model

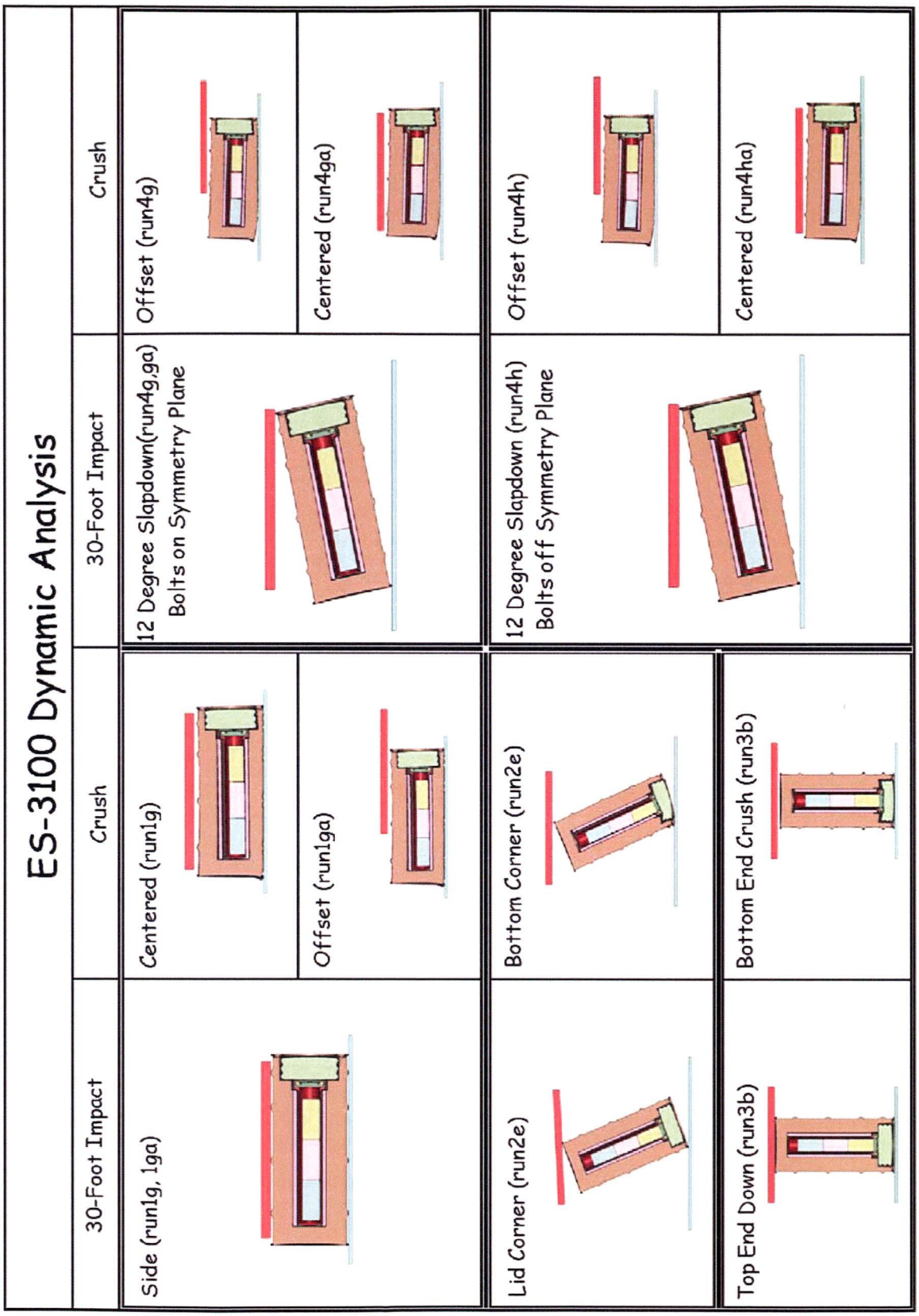

Figure 2.1.5 - LS-Dyna Design Runs for Successive 30-Foot and 30-Foot Crush Impacts

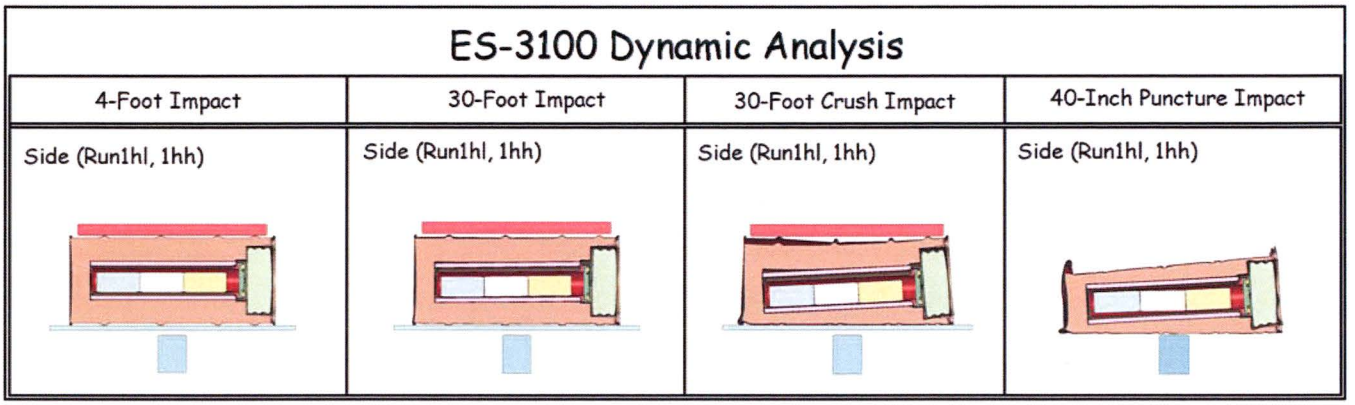

Figure 2.1.6 - Four Successive Impacts with the ES-3100 Bounding Kaolite Stiffness Models

shows icons representing the configurations run for the successive 4-foot + 30-foot + 30-foot crush + 40-inch punch impacts. The Figure 2.1.6 impacts were performed with the upper (-40°F, run1hh) and lower bound (100°F, run1hl) kaolite properties (see Section 2.3.5). The Figure 2.1.5 design runs were made with averaged kaolite properties (see Section 2.3.5). The run numbers (e.g., run1g, etc) are listed in Table 2.1.1 along with a verbal description of the impacts. Table 2.1.1 also identifies the Kaolite material model used for each run (see Section 2.3.5 for definition of the material properties).

Cumulative damage to the shipping package is obtained through successive impact restart solutions of LS-Dyna. At the beginning of the first impact, the initial velocity is assigned to the appropriate model nodes for the first impact. The solution is initiated and is considered over, when the kinetic energy reaches a constant value (after a minimum is reached) and when the rebound velocity reaches a constant value. Consideration was also given to the motion of the masses internal to the CV with regard to a primary impacts against the CV wall. When a run is considered over, the solution is halted and a restart file is written by LS-Dyna. The restart file captures the state of the container assembly at that point in the execution (including nodal velocities and element strains). A restart input file (text file) is then created which defines changes to be made to the model. The restart input file is used to redefine the velocity for the nodes of interest in a successive impact, or delete materials (components) if desired. The redefined velocity becomes the initial velocity, for the successive impact. The successive impact solution is then initiated with the restart file written by the halting of the previous impact and the restart input file. The velocities used in this analysis are: 193 in/sec for the 4-foot impact; 528 in/sec for the 30-foot impact; and 176 in/sec for the 40-inch punch impact.

Table 2.1.1 - Description of the ES-3100 Impacts Using the Detailed Model		
Run ID	Description	Kaolite Model†
Run1g	30-foot side impact + 30-foot crush with plate centered on drum	Average stiffness, 22.4 lb/0ft^3
Run1ga	30-foot side impact + 30-foot crush with plate centered on CV flange	Average stiffness, 22.4 lb/ft^3
Run1hl	4-foot side impact + 30-foot side impact + 30-foot crush impact + 40-inch punch impact	Lower bound stiffness, 27 lb/ft^3
Run1hh	4-foot side impact + 30-foot side impact + 30-foot crush impact + 40-inch punch impact	Upper bound stiffness, 27 lb/ft^3
Run2e	30-foot CG over lid corner impact + 30-foot crush on bottom corner	Average stiffness, 22.4 lb/ft^3
Run3b	30-foot top end impact + 30-foot bottom end crush	Average stiffness, 22.4 lb/ft^3
Run4g	30-foot, 12° slapdown with lid studs on plane of symmetry + 30-foot crush with plate centered on CV flange	Average stiffness, 22.4 lb/ft^3
Run4ga	30-foot, 12° slapdown with lid studs on plane of symmetry + 30-foot crush with plate centered on drum	Average stiffness, 22.4 lb/ft^3
Run4h	30-foot, 12° slapdown with lid studs off plane of symmetry + 30-foot crush with plate centered on the CV flange	Average stiffness, 22.4 lb/ft^3
Run4ha	30-foot, 12° slapdown with lid studs off plane of symmetry + 30-foot crush with plate centered on the drum	Average stiffness, 22.4 lb/ft^3
† - Defined in Section 2.3.5		

In the successive design impacts (Figure 2.15), a 30-foot impact was followed by a 30-foot crush impact. For these runs, the initial velocities of the shipping package assembly nodes were all defined as 528 in/sec in a direction normal and toward the rigid surface. When the initial impact was over, the run was halted and the velocities of the shipping package assembly nodes were all re-defined as 0.0 in/sec in the restart input file. This file also defined the velocity of the crush plate nodes as 528 in/sec in a direction towards the shipping package.

For the bounding kaolite stiffness runs (Figure 2.1.6), the impacts were successive 4-foot, 30-foot, 30-foot crush and 40-inch punch impacts. The 4-foot, 30-foot and 30-foot crush impacts were carried out as defined previously. The successive punch impact was initiated with the restart input file deleting the crush plate and the rigid plate from the model. The restart input file also redefined the velocity of the shipping package nodes to be towards the punch. This allowed the shipping package to pass through the original position of the rigid surface and impact the punch.

Table 2.1.2 gives the shipping package component masses and weights used in the detailed model analyses. Summations for assembly weights are also listed along with a total assembly weight. As discussed in the Section 2.3 on material models, an initial mass based on preliminary information supplied by the designer is adjusted to match expected hardware weights. This adjustment is required due to the faceted element faces on the inner and outer radius surfaces and the fact that small details are not explicitly modeled (holes, notches, etc). The total weight (full model) of the model is about 427.85 pounds, with 22.4 lb/ft^3 kaolite. The mass moment of inertia for the package is 90.84 $in*lb*sec^2$ about the global Y axis and the CG is located at Z = 22.4 inches.

Contact surfaces are used to allow adjacent components to separate, bear and/or slide along an adjacent surface. The contact used between the metal components of the model is a LS-Dyna single surface contact. Each node is reactive against every other element in the defined set. The contact between the borobond and its stainless steel liners; and the kaolite and its stainless steel liners is a surface to surface contact. All package nodes are defined as reactive to the rigid surface.

Table 2.1.2 - Analysis Weights for ES-3100

Material Number	Component Description	Run1g-Side		Run1hl-Side		Run1hh-Side		Run2e-Lid Corner		Run3b-Lid End		Run4g-Slapdown		Run4h-Slapdown	
		mass *	weight **	mass*	weight**	mass*	weight**	mass *	weight **	mass *	weight **	mass *	weight **	mass *	weight **
m 1	CV body	2.73E-02	21.10	2.73E-02	21.10	2.73E-02	21.10	2.73E-02	21.10	2.73E-02	21.10	2.73E-02	21.10	2.73E-02	21.10
m 2	CV body at flange	1.73E-03	1.34	1.73E-03	1.34	1.73E-03	1.34	1.73E-03	1.34	1.73E-03	1.34	1.73E-03	1.34	1.73E-03	1.34
m 3	CV lid	9.57E-03	7.39	9.57E-03	7.39	9.57E-03	7.39	9.57E-03	7.39	9.57E-03	7.39	9.57E-03	7.39	9.57E-03	7.39
m 4	CV screw ring	4.27E-03	3.30	4.27E-03	3.30	4.27E-03	3.30	4.27E-03	3.30	4.27E-03	3.30	4.27E-03	3.30	4.27E-03	3.30
m 5	angle	1.69E-02	13.02	1.69E-02	13.02	1.69E-02	13.02	1.69E-02	13.02	1.69E-02	13.02	1.69E-02	13.02	1.69E-02	13.02
m 6	drum	6.02E-02	46.50	6.02E-02	46.50	6.02E-02	46.50	6.02E-02	46.50	6.02E-02	46.50	6.02E-02	46.50	6.02E-02	46.50
m 7	drum bottom head	1.22E-02	9.42	1.22E-02	9.42	1.22E-02	9.42	1.22E-02	9.42	1.22E-02	9.42	1.22E-02	9.42	1.22E-02	9.42
m 8	weld drum to drum bottom head	1.18E-04	0.09	1.18E-04	0.09	1.18E-04	0.09	1.18E-04	0.09	1.18E-04	0.09	1.18E-04	0.09	1.18E-04	0.09
m 9	liner overlap to angle (0.03)	1.36E-04	0.11	1.36E-04	0.11	1.36E-04	0.11	1.36E-04	0.11	1.36E-04	0.11	1.36E-04	0.11	1.36E-04	0.11
m 10	liner (0.06)	3.95E-02	30.51	3.95E-02	30.51	3.95E-02	30.51	3.95E-02	30.51	3.95E-02	30.51	3.95E-02	30.51	3.95E-02	30.51
m 11	liner bottom (0.120) (see m 27 for	1.40E-03	1.08	1.40E-03	1.08	1.40E-03	1.08	1.40E-03	1.08	1.40E-03	1.08	1.40E-03	1.08	1.40E-03	1.08
m 12	lid shells (0.06)	7.25E-03	5.59	7.25E-03	5.59	7.25E-03	5.59	7.25E-03	5.59	7.25E-03	5.59	7.25E-03	5.59	7.25E-03	5.59
m 13	thin lid shell at bolts	1.37E-05	0.01	1.37E-05	0.01	1.37E-05	0.01	1.37E-05	0.01	1.37E-05	0.01	1.37E-05	0.01	1.37E-05	0.01
m 14	lid solids at the lid bolts	5.03E-05	0.04	5.03E-05	0.04	5.03E-05	0.04	5.03E-05	0.04	5.03E-05	0.04	5.03E-05	0.04	5.03E-05	0.04
m 15	lid stiffener	1.39E-03	1.07	1.39E-03	1.07	1.39E-03	1.07	1.39E-03	1.07	1.39E-03	1.07	1.39E-03	1.07	1.39E-03	1.07
m 16	drum bolts	5.06E-04	0.39	5.06E-04	0.39	5.06E-04	0.39	5.06E-04	0.39	5.06E-04	0.39	5.06E-04	0.39	5.06E-04	0.39
m 17	drum bolt nuts	1.20E-03	0.93	1.20E-03	0.93	1.20E-03	0.93	1.20E-03	0.93	1.20E-03	0.93	1.20E-03	0.93	1.20E-03	0.93
m 18	drum bolt washers	4.71E-04	0.36	4.71E-04	0.36	4.71E-04	0.36	4.71E-04	0.36	4.71E-04	0.36	4.71E-04	0.36	4.71E-04	0.36
m 19	plug liner	1.29E-02	10.00	1.29E-02	10.00	1.29E-02	10.00	1.29E-02	10.00	1.29E-02	10.00	1.29E-02	10.00	1.29E-02	10.00
m 20	plug kaolite	1.26E-02	9.70	1.52E-02	11.70	1.52E-02	11.70	1.26E-02	9.70	1.26E-02	9.70	1.26E-02	9.70	1.26E-02	9.70
m 21	drum kaolite	1.43E-01	110.08	1.72E-01	133.03	1.72E-01	133.03	1.43E-01	110.08	1.43E-01	110.08	1.43E-01	110.08	1.43E-01	110.08
m 22	drum borobond	5.66E-02	43.70	5.66E-02	43.70	5.66E-02	43.70	5.66E-02	43.70	5.66E-02	43.70	5.66E-02	43.70	5.66E-02	43.70
m 24	lower internal cv mass	4.75E-02	36.69	4.75E-02	36.69	4.75E-02	36.69	4.75E-02	36.69	4.75E-02	36.69	4.75E-02	36.69	4.75E-02	36.69
m 25	middle internal cv mass	4.75E-02	36.69	4.75E-02	36.69	4.75E-02	36.69	4.75E-02	36.69	4.75E-02	36.69	4.75E-02	36.69	4.75E-02	36.69
m 26	upper internal cv mass	4.75E-02	36.69	4.75E-02	36.69	4.75E-02	36.69	4.75E-02	36.69	4.75E-02	36.69	4.75E-02	36.69	4.75E-02	36.69
m 27	liner bottom solids	9.87E-04	0.76	9.87E-04	0.76	9.87E-04	0.76	9.87E-04	0.76	9.87E-04	0.76	9.87E-04	0.76	9.87E-04	0.76
m 29	visual rigid plane	7.80E-04	0.60	7.80E-04	0.60	7.80E-04	0.60	9.00E-04	0.69	8.00E-04	0.62	9.00E-04	0.69	9.00E-04	0.69
m 30	crush plate	1.42E+00	1099.99	1.42E+00	1099.99	1.42E+00	1099.99	1.42E+00	1099.99	1.42E+00	1099.99	1.42E+00	1099.99	1.42E+00	1099.99
m 31	punch	8.24E-02	63.62	8.24E-02	63.62	8.24E-02	63.62	8.24E-02	63.62	8.24E-02	63.62	8.24E-02	63.62	8.24E-02	63.62
m32	silicon rubber	1.65E-03	1.27	1.65E-03	1.27	1.65E-03	1.27	1.65E-03	1.27	1.65E-03	1.27	1.65E-03	1.27	1.65E-03	1.27
	dyna total model weight	2.06E+00	1592.05	2.09E+00	1617.00	2.09E+00	1617.00	2.06E+00	1592.15	2.06E+00	1592.07	2.06E+00	1592.15	2.06E+00	1592.15
	CV lid and nut ring		10.68		10.68		10.68		10.68		10.68		10.68		10.68
	CV body wt		22.44		22.44		22.44		22.44		22.44		22.44		22.44
	CV total wt		33.12		33.12		33.12		33.12		33.12		33.12		33.12
	plug liner and kaolite		19.70		21.69		21.69		19.70		19.70		19.70		19.70
	liner + angle		45.49		45.49		45.49		45.49		45.49		45.49		45.49
	drum body + kaolite + borobond4		256.94		279.90		279.90		256.94		256.94		256.94		256.94
	drum + lid + plug + kaolite + borobond4		284.65		309.60		309.60		284.65		284.65		284.65		284.65
	internal cv masses		110.08		110.08		110.08		110.08		110.08		110.08		110.08
	Total Package Weight		427.85		452.79		452.79		427.85		427.85		427.85		427.85
	Crush Plate Weight		1099.99		1099.99		1099.99		1099.99		1099.99		1099.99		1099.99
	Punch Weight		63.62		63.62		63.62		63.62		63.62		63.62		63.62
	Visual Rigid Plane		0.60		0.60		0.60		0.69		0.62		0.69		0.69
	Total Model Weight		1592.05		1617.00		1617.00		1592.15		1592.07		1592.15		1592.15

* - Mass is for the 1/2 model and is units of (pound * second^2) / inch

** - Weight is for the total package (2 x model weight) and is in units of pounds.

Friction factors are used in the contact surfaces of the models. Generally speaking, a static coefficient of 0.3 and a dynamic value of 0.2 is used. For the silicon rubber parts, a static coefficient of 0.6 and a dynamic value of 0.5 is assumed. The general factors of 0.3 (static) and 0.2 (dynamic) are also used for the shipping package contact with the rigid surface.

The design of the ES-3100 and the impact configurations are symmetrical. An analytical half model is used with conditions of symmetry defined for all nodes initially on the plane of symmetry. The drum bolting and the CV nut ring are modeled with surfaces initially in contact, but not pre-loaded. The CV is not pressurized. Gravity is included in the models.

The model typically used for a drum welded stud which secures the lid is shown in Figure 2.1.7. The mesh footprint in the stud is mirrored in the angle such that there is a one-to-one match of the stud nodes to angle nodes on the mating surface. The lower nodes on the studs are allowed to merge with the angle nodes. This is structurally conservative at the stud/angle intersection due to the fact that in the stud arc welding process a shoulder boss (area greater than the nominal stud area) is formed. The radius of the modeled studs is such that the faceted area of the stud model equates to the tensile stress area of the studs. Similarly to the stud/angle nodes, the nut/stud nodes are positioned and allowed to merge. The lid is modeled with shell elements, however, at the radius around each stud a transition to brick elements is made. This allows frictional bearing of the lid thickness onto the stud shank to be modeled. This modeling approach has been used and accepted for NNSA-licensed shipping packages that were subject to independent review and verification analysis (i.e., DPP-2 and ES-2100).

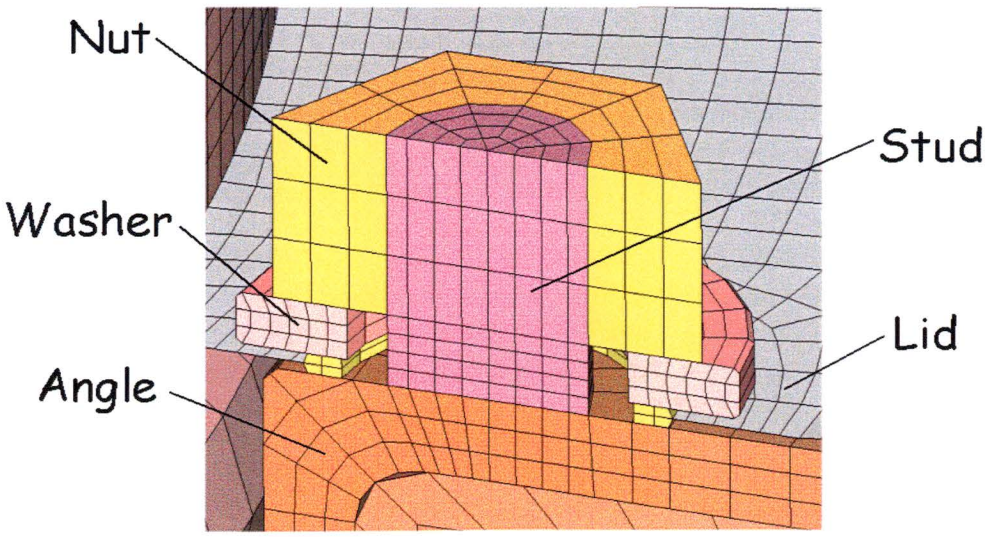

Figure 2.1.7 - Localized Model of a Stud

2.2 Model Description - Simplified Model

A series of punch impact runs were made on a simple model of the ES-3100 shipping container by varying the angle between the container liner and the punch, see Figure 2.2.1. In Figure 2.2.1, the position of the punch relative to the drum is shown with the angles in degrees. The purpose of the punch runs was to determine the response of the stainless steel drum liner due to the angled punch impacts. A series of eight, angled drops as shown in Figure 2.2.2 and described in Table 2.2.1 were made. In Figure 2.2.2, the punch is held stationary and the drum is positioned relative to the punch. The center of gravity of the shipping package was located directly above the side of the punch as shown in Figure 2.2.1. The initial velocity of the container is parallel to the axis of the punch as shown in Figure 2.2.2.

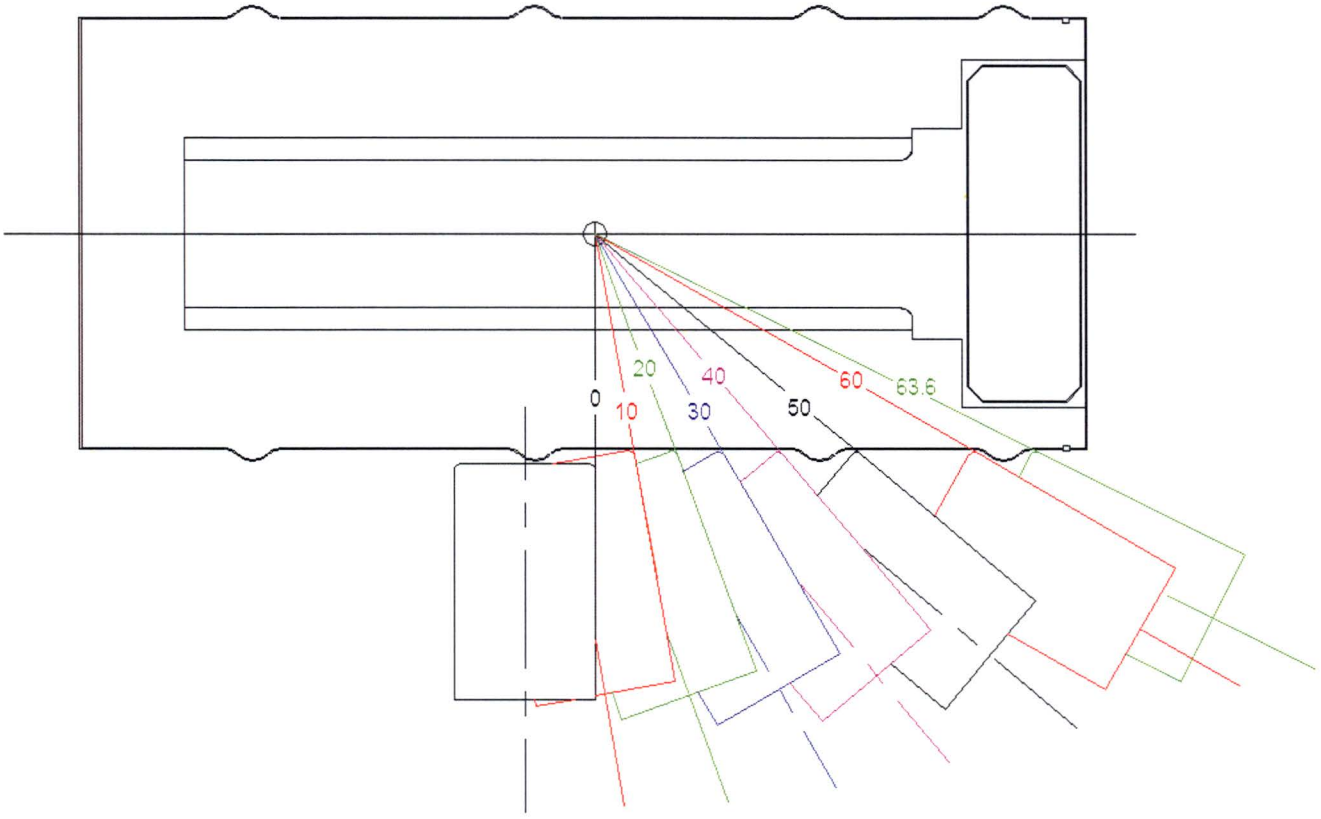

Figure 2.2.1 - Punch Angles on the Drum Liner

A simplified model of the ES-3100 was derived from the more detailed model (described in Section 2.1) for this series of runs. The model detail needed in the 4-foot, 30-foot, crush, and successive punch impact is not needed for the series of punch impacts. The purpose of the series of punch impacts is to evaluate the response of the drum skin to various punch angles.

The detailed model (section 2.1) was simplified (see below) to form the simple model. The detailed model was simplified except for the drum skin and the drum kaolite mesh nearest the punch impact. Figure 2.2.3 shows the simplified shipping package model used for the series of punch impacts. Figure 2.2.4 shows an exploded view of the simple model components.

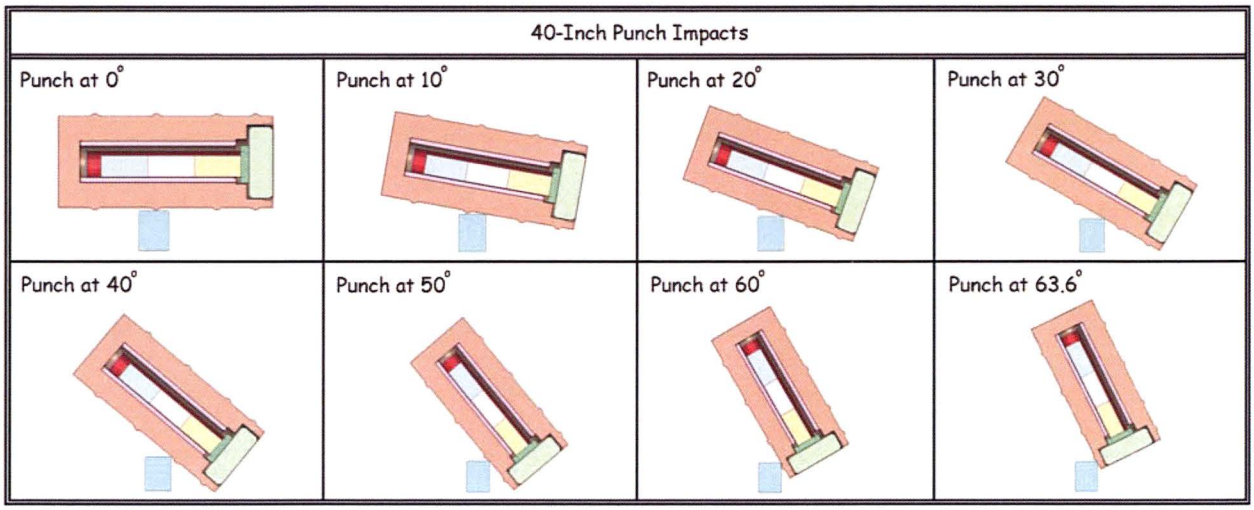

Figure 2.2.2 - ES-3100 Punch Configurations for the Series of Punch Impacts

Table 2.2.1 - Description of the ES-3100 Impacts with the Simplified Model Summarized in this DAC

Run ID †	Description †	Kaolite Model
Punch at 0°	40-inch punch impact at 0°	Average stiffness, 22.4 lb/ft^3 (note the density is altered slightly so that the punch model weights approximate the full model runs)
Punch at 10°	40-inch punch impact at 10°	
Punch at 20°	40-inch punch impact at 20°	
Punch at 30°	40-inch punch impact at 30°	
Punch at 40°	40-inch punch impact at 40°	
Punch at 50°	40-inch punch impact at 50°	
Punch at 60°	40-inch punch impact at 60°	
Punch at 63.6°	40-inch punch impact at 63.6°	
† - Angles in degrees, measured from a perpendicular to the drum axis as shown in Figure 2.2.1		

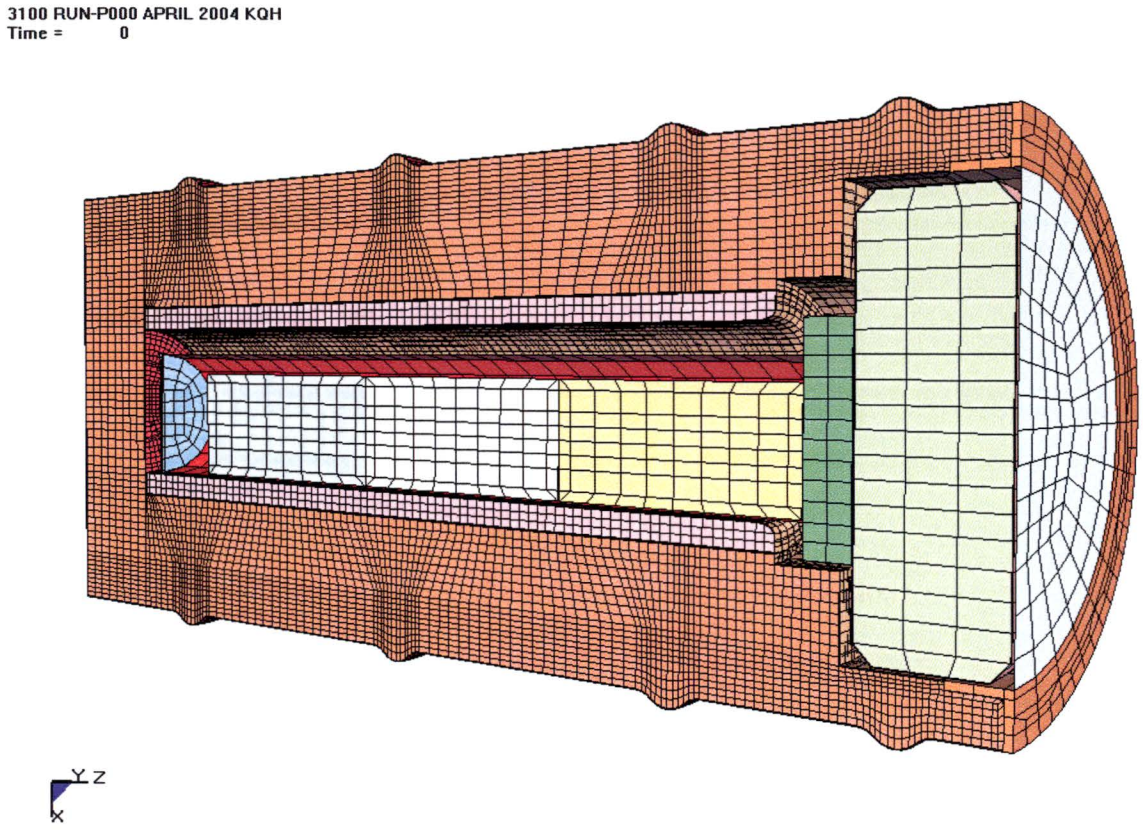

Figure 2.2.3 - Simplified ES-3100 Shipping Package Model for the Series of Punch Impacts

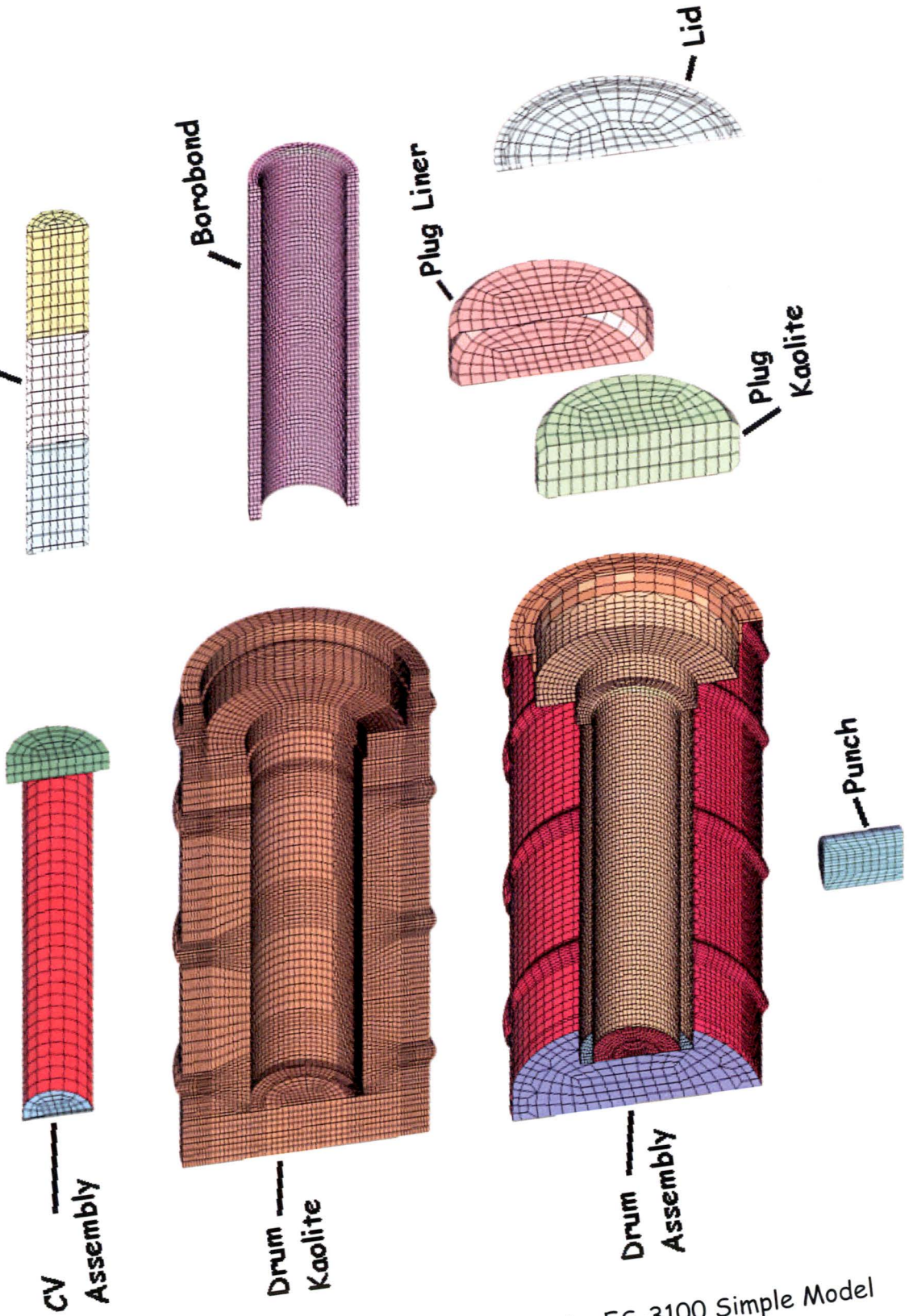

Figure 2.2.4 - Exploded View of the ES-3100 Simple Model

Since the concern is the response of the drum skin to the punch, detail in the shipping container components remote from this concern is not warranted and only the mass/stiffness effects on the region of concern become important. In general, there is a simplification of the element mesh (coarser element mesh) away from the punch impact location. Items such as the CV, the plug and the drum lid retention details were greatly simplified in modeling detail (compare Figures 2.2.3 and 2.2.4 verses Figures 2.1.1 through 2.1.4). The CV was simplified to a simple cylinder (shell elements) with a simple solid lid. The drum lid attachment details were replaced by a simple flat lid whose nodes were allowed to merge with the angle nodes. The container plug was also simplified to a simple disk with chamfered corners. This simple model allowed a savings on computer run time and storage allotment without sacrificing the item of concern, the response of the drum liner due to the angled punch.

An effort was made in the geometrical/mesh simplification to maintain the mass distribution of the container as close as is reasonable to the detailed model. Table 2.2.2 shows the weights for all the punch impacts. The total weight for the simple model package assembly was 427.91 pounds with the 22.4 lb/ft^3 kaolite. The mass inertia about the global Y axis for the simple model is 89.64 $in*lb*sec^2$ and the CG is located at Z= 23.0 inches.

Table 2.2.2 - Analysis Weights for Punch Runs

Material Number	Component Description	mass*	weight**
1	CV Body	2.6336E-02	20.33
2	CV Bottom Head	2.7398E-03	2.12
3	CV Flange/Lid	1.5492E-02	11.96
4	removed for punch runs	0.0000E+00	0.00
5	Angle	1.9249E-02	14.86
6	Drum	6.0236E-02	46.50
7	Drum Bottom	1.2318E-02	9.51
8	removed for punch runs	0.0000E+00	0.00
9	removed for punch runs	0.0000E+00	0.00
10	Liner	3.9641E-02	30.60
11	Liner Bottom	1.3361E-03	1.03
12	Lid	8.6358E-03	6.67
13	removed for punch runs	0.0000E+00	0.00
14	removed for punch runs	0.0000E+00	0.00
15	removed for punch runs	0.0000E+00	0.00
16	removed for punch runs	0.0000E+00	0.00
17	removed for punch runs	0.0000E+00	0.00
18	removed for punch runs	0.0000E+00	0.00
19	Plug Liner	1.2949E-02	10.00
20	Plug Kaolite	1.2573E-02	9.71
21	Drum Kaolite	1.4265E-01	110.13
22	Borobond	5.6607E-02	43.70
24	CV Lower Inner Weight	4.7530E-02	36.69
25	CV Middle Inner Weight	4.7530E-02	36.69
26	CV Upper Inner Weight	4.7530E-02	36.69
27	Liner Kaolite Cavity Bottom	9.3847E-04	0.72
28	removed for punch runs	0.0000E+00	0.00
29	removed for punch runs	0.0000E+00	0.00
30	removed for punch runs	0.0000E+00	0.00
31	Punch	8.2405E-02	63.62
32	removed for punch runs	0.0000E+00	0.00
pkg			427.91
punch			63.62
total		6.3670E-01	491.53
* - Mass is for the 1/2 model and is units of (pound * second^2) / inch			
** - Weight is for the total package (2 x model weight) and is in units of pounds.			

2.3 Material Models

The LS-Dyna material models used in the ES-3100 analytical model are shown in the Table 2.3.1 index. Note that the designation 304L (capital L) is used for clarity.

Table 2.3.1 - Material Model Index for the ES-3100 LS-Dyna Model

LS-Dyna Part #	Part Description	Material Description	Described in DAC Section
1	CV Body	304L	2.3.1
2	CV Body Neck	304L	2.3.1
3	CV Lid	304L	2.3.1
4	CV Nut Ring	A-479 Nitronic-60	2.3.2
5	Angle	304	2.3.3
6	Drum	304	2.3.3
7	Bottom Head	304	2.3.3
8	Attachment Shell Elements	304	2.3.3
9	Attachment Shell Elements	304	2.3.3
10	Liner	304	2.3.3
11	Liner Bottom	304	2.3.3
12	Lid Shell Elements	304	2.3.3
13	Attachment Shell Elements	304	2.3.3
14	Lid Solid Elements	304	2.3.3
15	Lid Stiffener	304	2.3.3
16	Studs	304	2.3.3†
17	Stud Nuts	Bronze	2.3.4
18	Stud Washers	304	2.3.3
19	Plug Liner	304	2.3.3
20	Plug Kaolite	Kaolite 1600	2.3.5
21	Drum Kaolite	Kaolite 1600	2.3.5
22	Borobond	Borobond 4	2.3.6
23	Not Used	Not Used	Not Used
24	Lower Internal CV Mass	Mild Steel	2.3.7
25	Middle Internal CV Mass	Mild Steel	2.3.7
26	Upper Internal CV Mass	Mild Steel	2.3.7
27	Liner Bottom	304	2.3.3
28	Not Used	Not Used	Not Used
29	Visual Rigid Plane	Rigid	2.3.8
30	Crush Plate	Mild Steel	2.3.7
31	Punch	Mild Steel	2.3.7
32	Silicon Rubber Pads	Silicon Rubber	2.3.9

† - An elastic/plastic model with material failure is used for the studs as explained in the noted section.

Density values listed in Section 2.3 were used as initial values for the material weights. Once the model was completed and initial runs made, the initial density was then ratioed such that the preliminary weights obtained from the designer were matched by the analysis results. Table 2.1.2 shows the resulting component and assembly weights for the detailed model.

The material presented in this section is for room temperature (about 70°) unless otherwise stated. Section 2.3.5 presents Kaolite data at room temperature in section 2.3.5.1, 100°F in section 2.3.5.2 and -40°F in section 2.3.5.3.

2.3.1 304L Stainless Steel

The material 304L is used for the CV components except the nut ring. A software database obtained from Lawrence Livermore National Lab personnel is used to obtain the 304L material data which is reproduced below.

```
Material density . . . . . .      0.28600   lb/in**3
Young's Modulus. . . . . .        2.800E+07 psi
Shear Modulus. . . . . .          1.085E+07 psi
Bulk Modulus . . . . . .          2.222E+07 psi
Poisson's ratio. . . . . .        0.2900
Yield stress at offset . . .  32000.0       psi
Engineering ultimate stress.  85000.0       psi
Elongation at failure. . . .     57.00      %
Yield offset . . . . . .          0.20000   %
---------- Calculated values ----------------------
Strain Hardening equation       s  = s0 e**m
Equation constants              s0 = 160455    m  = 0.27916
Yield point                     sy =  21735    ey = 0.00078
Ultimate (Engineering)          Su =  85000    Nu = 0.32202
Ultimate (True)                 sut= 112372    eut= 0.27916
Failure  (True)                 sft= 168989    eft= 1.20397
Energy to ultimate                    24605 in-lb/in**3
```

The LS-Dyna power law plasticity model (*MAT_POWER_LAW_PLASTICITY) is used for 304L. The material model is:

$$\sigma = K\varepsilon^m$$

were, K = strength coefficient = 160455 (psi)
m = hardening exponent = 0.27916

The density listed in the reference was an initial density (0.286 lb/in^3) and equates to an initial mass density of 7.4093e-4 lb*sec^2/in^4.

2.3.2 A-479 Nitronic-60

The CV nut ring is modeled with A-479 Nitronic-60 properties. The Reference 5.4 was used to obtain the following material data for the S21800 material.

Tensile Strength	95 ksi
Yield Strength	50 ksi
Elongation	35%

The modulus of elasticity is assumed to be 26.2e6 psi.

From this data the following tangent modulus was calculated for the LS-Dyna, *MAT_PLASTIC_KINEMATIC material model.

$$\varepsilon = \frac{\sigma}{E} = \frac{50000psi}{26.2e6psi} = 0.00192in/in$$

$$E_{\tan} = \frac{95000psi - 50000psi}{0.35 - 0.00192} \approx 129000psi$$

A poisson's ratio of 0.298 was used. A density of 0.2754 lb/in^3 was initially used. This equates to an initial mass density of 7.1347 lb*sec^2/in^4.

2.3.3 304 Stainless Steel

The general shipping container components were modeled as 304 stainless steel. The LS-Dyna material model *MAT_POWER_LAW_PLASTICITY was used for the general container components. The 304 material data was obtained from a software database obtained from Lawrence Livermore National Lab personnel and is reproduced below.

```
Material density . . . . . .      0.29000   lb/in**3
Young's Modulus. . . . . .        2.810E+07 psi
Shear Modulus. . . . . .          1.089E+07 psi
Bulk Modulus . . . . . .          2.230E+07 psi
Poisson's ratio. . . . . .        0.2900
Yield stress at offset . . .  34000.0       psi
Engineering ultimate stress.  87000.0       psi
Elongation at failure. . . .     57.00      %
---------- Calculated values ----------------------
Strain Hardening equation      s  = s0 e**m
Equation constants             s0 = 162738    m  = 0.27208
Yield point                    sy =  23729    ey = 0.00084
Ultimate (Engineering)         Su =  87000    Nu = 0.31269
Ultimate (True)                sut= 114204    eut= 0.27208
Failure  (True)                sft= 167370    eft= 1.10866
```

Similar to section 2.3.1, the power law coefficients for the 304 model used for the general shipping container components were:

K = strength coefficient = 162738 (psi)
m = hardening exponent = 0.27208

The 0.290 lb/in^3 density equates to 7.513 e-4 lb*sec^2/in^4 for the initial mass density.

The drum studs were modeled using the *MAT_PLASTIC_KINEMATIC material model in LS-Dyna using the following 304 material properties. This material model allowed material failure to be used for the studs. With material failure, LS-Dyna removes elements which reach the defined failure strain. The following elastic-plastic model was derived from the above material properties.

Modulus of Elasticity = 2.81e7 psi†
Poisson's Ratio = 0.29
Yield = 34000 psi
Plastic Modulus = 93180 psi
Failure Strain = 0.57 in/in

The modeling of the drum studs with engineering stress/strain data curve is conservative from a design standpoint. This approach has been used and accepted for NNSA-licensed shipping packages that were subject to independent review and verification analysis (i.e., DT-22 and DT-23).

† - Note: the value of 2.9e7 psi (vs 2.81e7 psi) was inadvertently used in the analysis for the modulus of elasticity. This is seen to cause minimal concern due to the minimal energy absorption in the elastic range.

2.3.4 Bronze

The drum lid nuts are made of bronze. A software database obtained from Lawrence Livermore National Lab personnel was used to obtain the material data which is reproduced below.

```
Material . . . .bronze commercial cu.9 zn.1 ½ hard
Material density . . . . . .      0.31800   lb/in**3
Young's Modulus. . . . . .        1.700E+07 psi
Shear Modulus. . . . . .          6.391E+06 psi
Bulk Modulus . . . . . .          1.667E+07 psi
Poisson's ratio. . . . . .        0.3300
Yield stress at offset . . .  45000.0       psi
Engineering ultimate stress.  52000.0       psi
Elongation at failure. . . .     15.00      %
---------- Calculated values ----------------------
Strain Hardening equation      s  = s0 e**m
Equation constants             s0 =  70989    m  = 0.09191
Yield point                    sy =  40775    ey = 0.00240
Ultimate (Engineering)         Su =  52000    Nu = 0.09626
Ultimate (True)                sut=  57006    eut= 0.09191
```

The LS-Dyna power law model was used for the bronze material. The coefficients used were:

K = strength coefficient = 70989(psi)
m = hardening exponent= 0.09191

The density of 0.318 lb/in^3, or 8.2371e-4 lb*sec^2/in^4 was the initial mass density.

2.3.5 Kaolite 1600

Kaolite 1600 properties were used to model the drum and plug kaolite. The LS-DYNA honeycomb material model (*MAT_HONEYCOMB) used for the ES-3100 has been shown to be a good representation of the Kaolite material and approved for NNSA-licensed shipping packages that were subject to independent review and verification analysis (i.e., DPP-2 and ES-2100). There have been several testing programs to determine the structural properties of Kaolite since 1995. Each time new data is obtained, it is compared to the old data to maintain enveloping upper and lower bound stiffness curves. The lower stress/strain portion of the curves presented in this section is shown in Figure 2.3.5.1 below. Each curve shown in Figure 2.3.5.1 is documented in the following sub-sections. The Kaolite test data was obtained from constrained test specimens. For the constrained Kaolite test data, the material data is the same for uniaxial and volumetric strain.

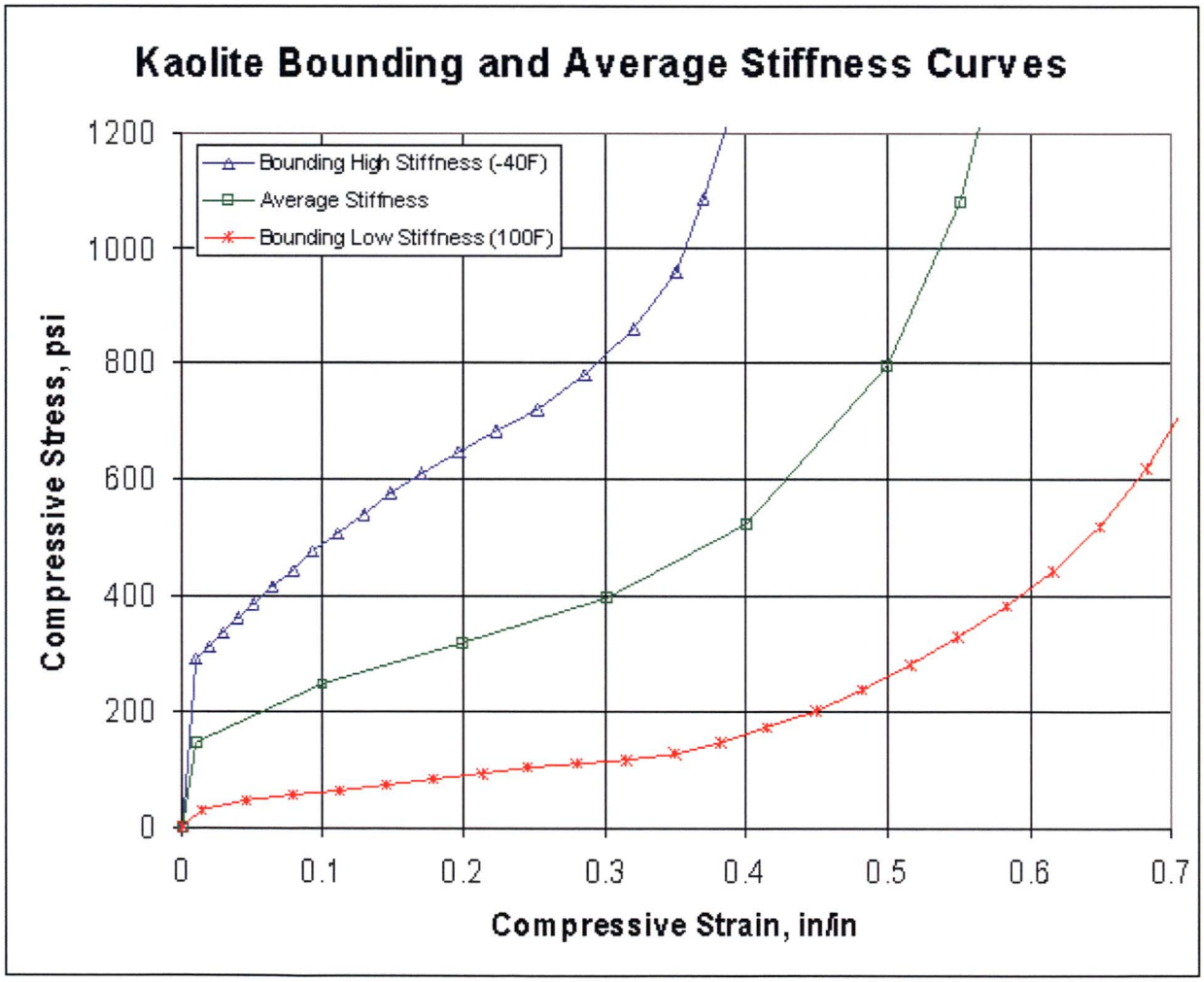

Figure 2.3.5.1 - Bounding Kaolite and Average Stiffness Curves

2.3.5.1 Kaolite 1600 - Averaged Stiffness

A Y12 report gives test data for constrained Kaolite 1600 material at 100°F and -40°F. The maximum peaks from the -40°F high density samples defined an upper bound load deflection curve. The minimum peaks to the 100°F low density samples defined a lower bound load deflection curve. The upper and lower curves were averaged to obtain the average stiffness results. The averaged results up to about 60% strain are then derived from test results for the LS-DYNA material model. The curve is extrapolated above 60% strain, to give a "lock-up" region (collapsing of voids). LS-Dyna does not extrapolate data curves, therefore, the curves must envelope all expected values and assumed values extend the curve well into the lock-up range. Figure 2.3.5.1 shows the lower portion of the averaged stiffness curve. The digital values for the points defined in the LS-DYNA material model are given below in Table 2.3.5.1.1.

Table 2.3.5.1.1 - Digital Load Curve for Kaolite 1600

Strain, in/in	Stress, psi	Strain, in/in	Stress, psi	Strain, in/in	Stress, psi
0.00	0.0	0.40	523.	0.70	5000. †
0.01	148.	0.50	797.	0.75	10000. †
0.10	248.	0.55	1079.	0.775	20000. †
0.20	317.	0.60	1553.	0.79	30000. †
0.30	396.	0.65	2500. †	0.8	40000. †

† - Assumed values to obtain lockup

The Young's Modulus for the compacted kaolite material is taken as the slope of the last two data points.

$$\frac{40000psi - 30000psi}{0.79in/in - 0.80in/in} = 1.0e6psi$$

The initial slope is taken as the uncompressed modulus of elasticity.

$$E_{uncompressed} = \frac{148.11psi - 0.0psi}{0.01 - 0.0} = 14811psi$$

Assuming a low poisson's ratio (0.01), the shear modulus is,

$$G = \frac{E}{2(1+\nu)} = \frac{14811psi}{2(1+0.01)} \approx \frac{14811psi}{2} = 7405\ psi$$

Full compaction is also assumed at a relative volume of 0.20 (this corresponds with the 80% strain assumed data point). The mass density used for the nominal kaolite runs in the analysis is 3.3583e-5 lb*sec^2/in^4, which equates to 22.4lb/ft^3.

2.3.5.2 Kaolite 1600 - Lower Bound Stiffness

The kaolite lower bounding stiffness model shown in Figure 2.3.5.1, originated in the ES2LM shipping container calculation and is associated with 100°F. The digital values for the points which define in the LS-Dyna lower bound stiffness curve are given in Table 2.3.5.2.1.

Table 2.3.5.2.1 - Digital Load Curve for Kaolite 1600, Lower Bound

Strain, in/in	Stress, psi	Origin
0.00	0.0	Test Data and ES2LM Shipping Container Calculation
0.0132	29.	
0.0456	48.	
0.0792	56.	
0.1128	64.	
0.1464	75.	
0.1800	83.	
0.2136	93.	
0.2460	105.	
0.2796	109.	
0.3144	117.	
0.3480	127.	
0.3816	148.	
0.4140	174.	
0.4488	202.	
0.4824	237.	
0.5160	281.	
0.5496	330.	
0.5832	381.	
0.6168	443.	
0.6492	520.	
0.6828	619.	
0.7140	744.	
0.7476	896.	
0.7800	1099.	
0.7944	1205.	
0.8200	3000.	Assumed†
0.8700	10000.	Assumed†
0.9000	40000.	Assumed†

† - Assumed to provide "lock-up"

The Young's Modulus for the compacted kaolite material is taken as the slope of the last two data points.

$$\frac{40000psi - 10000psi}{0.90in/in - 0.87in/in} = 1.0e6psi$$

The initial slope is taken as the uncompressed modulus of elasticity.

$$E_{uncompressed} = \frac{29.psi - 0.0psi}{0.0132 - 0.0} = 2197psi$$

Assuming a low poisson's ratio, the shear modulus is,

$$G \approx \frac{E}{2} = 1099\ psi$$

A low poisson's ratio is assumed, 0.01. Full compaction is also assumed at a relative volume of 0.10. The density used is 27 lb/ft^3, or 4.0479e-5 lb*sec^2/in^4.

2.3.5.3 Kaolite 1600 Upper Bound Stiffness

The upper bound stiffness of the kaolite 1600 material is an enveloping curve obtained from two sets of material test data. Table 2.3.5.3.1 shows the digital values of the curve.

The Young's Modulus for the compacted kaolite material is taken as the slope of the last two data points.

$$\frac{40000psi - 22000psi}{0.88in/in - 0.85in/in} = 6.0e5\ psi$$

The initial slope is taken as the uncompressed modulus of elasticity.

$$E_{uncompressed} = \frac{292.1psi - 0.0psi}{0.01 - 0.0} = 29210psi$$

Assuming a low poisson's ratio, the shear modulus is,

$$G \approx \frac{E}{2} = 14605\ psi$$

A density of 27 lb/ft^3 is used as in the low stiffness run. A low poisson's ratio is assumed, 0.01. Full compaction is also assumed at a relative volume of 0.12.

Table 2.3.5.3.1 - Upper Bounding Kaolite Curve		
Strain, in/in	Stress, psi	Origin
0	292.1	Summer 2004 Material Testing
0.01	292.1	
0.019	313.3	
0.029	336.1	
0.04	360.5	
0.051	386.6	
0.064	414.3	
0.079	443.6	
0.094	474.5	
0.111	506.9	
0.13	540.7	
0.15	575.7	
0.172	611.6	
0.197	647.9	
0.224	684.1	
0.253	719.6	
0.285	780	assumed for smooth transition†
0.32	860	
0.3504	958	DPP2 Shipping Container Calculation
0.3696	1086	
0.3888	1231	
0.45	2000	assumed for lock-up †
0.5	3000	
0.6	6000	
0.7	10000	
0.8	16000	
0.85	22000	
0.88	40000	
† - Assumed values for transition and lock-up		

2.3.6 Borobond 4 Casting Material

The following soil and foam model is used for the borobond 4 casting material. The model is obtained from work done on the Y12, HEU storage pallet and the subsequent physical testing.

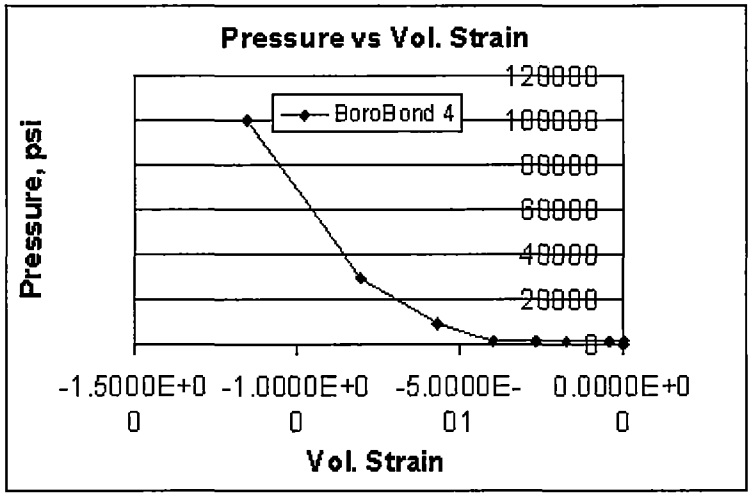

Figure 2.2.3 - Pressure vs Volumetric Strain

The following material data was used for the model of the Borobond 4 casting material.

LS-Dyna Material Model	*MAT_SOIL_AND_FOAM
Density	1.7991e-4 lb-sec^2/in^4 (120 lb/ft^3)
Shear Modulus	1.019e6 psi
Bulk Modulus	2.491e6 psi
A_0	1.008e7 (psi)^2
A_1	0
A_2	0
Tensile Cutoff	309.3 psi

Pressure vs Volumetric Strain Data:

Pressure, psi	Volumetric Strain, in^3/in^3
0	0
1833.3	-7.387e-4
1850	-4.2363e-2
1866	-1.7334e-1
1883	-2.6993e-1
1900	-3.9631e-1
10000	-5.6503e-1
30000	-7.9972e-1
100000	-1.1536

2.3.7 Mild Steel

AISI 1020 carbon steel was used to obtain properties for a typical or nominal low carbon steel. A software database obtained from Lawrence Livermore National Lab personnel was used to obtain the material data for AISI 1020 and is reproduced below.

```
Material . . . .steel carbon AISI 1020 plate bar sheet strip to 18 in.
Young's Modulus. . . . . .      3.000E+07 psi
Shear Modulus. . . . . .        1.163E+07 psi
Bulk Modulus . . . . . .        2.381E+07 psi
Poisson's ratio. . . . . .      0.2900
Yield stress at offset . . .  30000.0       psi
Engineering ultimate stress.  55000.0       psi
Elongation at failure. . . .     25.00      %
```

A modulus of elasticity of 2.9e7 (vs 3.0e7 psi) was inadvertently used in the analysis for this material. This material model was used for the inner CV weights, the crush plate and the punch. This is seen to be of minimal concern due to the fact that the components which use this modulus are not of concern themselves, it is their effect on the package/CV that is of concern.

A density of about 490 lb/ft^3 is also initially assumed, which equates to a mass density of 7.35 lb-sec^2/in^4. This initial mass value was then adjusted based on the expected component weight.

Using the ultimate (55000 psi) and yield (30000 psi); the failure strain of 0.25 and assuming a 2% offset, a simple bi-linear tangent modulus of 1.0e5 is assumed.

$$E_{\tan} = \frac{55000psi - 30000psi}{0.25 - 0.002} \approx 1.0e5psi$$

2.3.8 Rigid Plane

The following properties were assigned to the rigid plane (for contact surface concerns):

Modulus of Elasticity = 28e6 psi
Poisson's Ratio = 0.29

A relatively low value of density was also specified for the rigid plane, 1e-6 lb*sec^2/in^4. Each node of the rigid plane was restrained from rotation and translation in the material definition.

2.3.9 Silicon Rubber

The pads outboard of the CV bottom and top are used to isolate the CV with regards to a transportation vibration concern. The following properties were assumed for the silicon rubber pads:

$E \approx 150000$ psi
Density = 0.0446 lb/in^3 = 1.1554 e-4 lb*sec^2/in^4

A modulus of elasticity for the silicon rubber of about 150 psi can be obtained from Figure 35.13 of reference 5.6 (relative magnitude can be mimicked by various sources on the internet). However, this low E value will not allow a stable solution of LS-Dyna. The value of E = 150000 psi results in a stable solution. The silicon rubber piece at the CV lid/flange and the piece at the base of the CV offer only bearing to the CV. A stiffer silicon material would tend to minimize the bearing footprint on the CV, hence force higher stresses/strains in the CV. Initial runs show this to be the case, up to the point that the softer (E = 150 psi) solution fails. Therefore, the value of E = 150000 psi is used due to the fact that it tends to be conservative with respect to the CV and it allows a stable solution of LS-Dyna.

The density shown above is assumed and was found by averaging several nominal silicon rubber values obtained from the internet.

The shear modulus was calculated as:

$$G = \frac{E}{2(1+\nu)} = \frac{150000 psi}{2(1+0.463)} = 51260 psi$$

The LS-Dyna *MAT_BLATZ-KO_RUBBER was used to model the silicon rubber components. The model defines the poisson's ratio as 0.463.

3.0 Solution Results

In this section, the results of the different analyses are presented. A voluminous amount of data can be obtained for each and every run presented in this DAC. An attempt is made to present the response story of each impact, yet not to overburden the reader, nor the expense of this report with similar images/data. Components of relatively low strain, or whose strain contour patterns are similar to other impacts which have been presented, may be presented digitally in a table (maximum) and not visually in an image. In the bounding kaolite runs, an effort was made to present the same images for comparison purposes.

Results from run1g are presented in detail as are results from the crush impact of run1ga. An effort is made to abbreviate the results of the other runs due to repetition. Only configuration and strain results of note, or uniqueness due to the configuration are included in the other runs. For ease of reading, the plots in sub-sections of Section 3.0 will be shown after the discussion in each section. Time is generally given in seconds, displacements in inches and velocity in inches/seconds.

The kinetic energy and velocity time history plots are nodal averages for the set of nodes that make up the body of concern (e.g., the shipping package for 4-foot impacts or the crush plate for crush impacts). Therefore, the plots are an averaged value to represent the body of concern.

The element mesh is generally not included on package assembly views such as Figure 3.0.1. The element mesh is generally quite small and its inclusion would make it more difficult to observe the components. In close up images, the element mesh is generally included.

The effective plastic strain level contour plots in the shell elements are surface strains (bending/peak strains) unless otherwise noted. Maximum, or in effect, bending strain is the default in LS-Post fringe plotting of shell elements. The maximum value for the plotted elements is given in the title block in the upper left corner of each fringe plot. The maximum fringe value (shown in the upper right hand corner of each fringe plot) may be redefined by the analyst and may or may not reflect the maximum value shown in the left, title block corner. In some fringe plots, the range may be adjusted to show regions in excess of a specific level. Note that shell elements are modeled at the centerline of the thickness. Therefore, in time history plots, one-half the shell thickness needs to be added/subtracted to obtain the desired metal surface for each node.

The nodes on the plane of symmetry and near the rigid plane are termed at "0°". The nodes initially on the Y plane are termed at "90°". And the nodes on the plane of symmetry

and typically nearer the crush plate are termed "180°". This terminology is typically used only in the side and slapdown impacts and denotes the circumferential positions.

The global coordinate system is the default system in LS-Dyna and is the coordinate system of default in this calculation. The global system is centered on the package centerline, at the bottom of the package as shown in Figure 3.0.1 (if the package were sitting on a flat floor, the surface of the floor would define Z = 0.0). The global XZ axes define the plane of symmetry. The global coordinate system triad icon is shown on most images in this section; offset by default in LS-Post for visual purposes. A local coordinate system was defined for the CV assembly due to lid/body flange separation concerns. The local system used is shown in Figure 3.0.2 and moves with the three defining nodes on the CV body and lid. The local X direction is in the direction of CV lid separation at the O-ring location in the flange. The local CV coordinate system is used in the lid separation time history plots in the results sections.

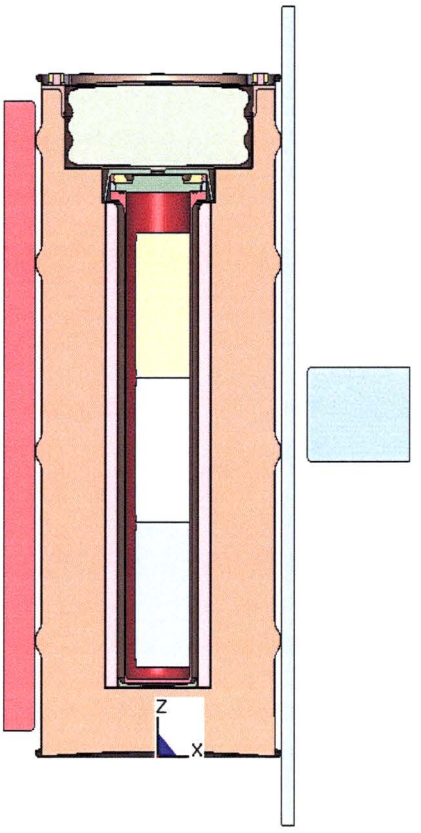

Figure 3.0.1 - Global Coordinate System

Figure 3.02 - CV Local Coordinate System

A study of the slapdown angle was performed using a computer code obtained from Los Alamos National Lab. The code considers a simplified, deformable body whose slapdown angle can be varied through multiple runs. The response of interest was the velocity of the secondary impacting end as it strikes the rigid surface.

To obtain all the input constants needed by the slapdown code, trial runs of the ES-3100 model were made. From the trial run, the load on the rigid surface and the deflection of the ES-3100 package ends were used to obtain the simple spring constants. The overall body dimensions, center of gravity location, mass moment of inertia and container mass were also input to the slapdown code. Figure 2.1.7 shows the results of the slapdown study. The friction factor between the rigid surface and the container was varied between 0.0 and 0.3. An angle of 12° was found to maximize the secondary impact and was chosen for the slapdown angle for the ES-3100.

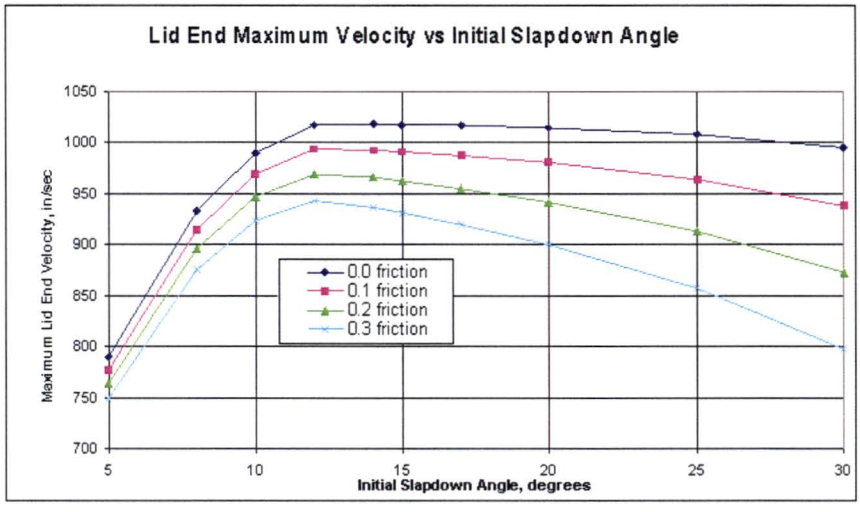

Figure 2.1.7 - Secondary Velocity Maximum from the Slapdown Study

3.1 Run1g - Side

Run1g is a design run with a 30-foot side impact (run time from 0 to about 0.0085 seconds) followed by a 30-foot, centered crush impact (from about 0.0085 to 0.025 seconds). Figure 3.1.1 shows the initial configuration of the model. Note that the punch was in the model, but a punch impact was not included in this run. Figure 3.1.2 shows the configuration of the model after the 30-foot impact. Figure 3.1.3 shows the lid region of the model after the 30-foot impact. Figure 3.1.4 shows the final configuration in the bottom region of the drum nearest the 30-foot impact with the rigid plane.

The effective plastic strain in the CV body at the end of the 30-foot impact is shown in Figure 3.1.5 to be a maximum of 0.0346 in/in. The maximum effective plastic strain occurs near the bottom head as shown in one of the enlarged views in the figure. Figure 3.1.6 shows the maximum effective plastic strain in the CV lid to be 0.0002 in/in for the 30-foot impact. The nut ring remained elastic during the 30-foot impact and is not shown in an image.

The effective plastic strain in the drum angle for the 30-foot impact is shown in Figure 3.1.7. The maximum strain is found to be 0.0682 in/in nearest the rigid plane. Figure 3.1.8 shows the maximum effective plastic strain in the drum to be 0.2218 in/in near the location of the angle and rigid plane. Figure 3.1.9 shows the effective plastic strain in the drum bottom head to be a maximum of 0.2444 in/in. The maximum effective plastic strain in the liner is 0.1189 in/in as given in Figure 3.1.10. The maximum is localized at the junction of the borobond/kaolite liner, near the CV flange, opposite the impact (180°). Figure 3.1.11 shows the maximum effective plastic strain in the drum lid to be 0.3580 in/in and occurs near the stud nearest the impact (0°). The maximum effective plastic strain in the lid stiffener is 0.0060 in/in and is not shown in a Figure. The maximum effective plastic strain in the drum studs is shown in Figure 3.1.12 to be 0.1171 in/in. The maximum effective plastic strain in the drum stud nuts is 0.0005 in/in and in the washers is 0.1628 in/in. The maximum effective plastic strain in the plug liner is 0.08260 in/in. Figures for the nuts, washers and plug liner are not shown.

The time history for the kinetic energy of the package assembly in the 30-foot impact is shown in Figure 3.1.13. Figure 3.1.14 shows the assembly X velocity time history. A constant rebound velocity was obtained at 0.0085 seconds, so the solution was halted at that point. The abrupt response near 0.0085 seconds in both figures is a precipitate of the successive impact restarts (redefining the velocities for the successive impact).

A restart of the LS-Dyna solution is used to create the crush impact. The state of the shipping package at time = 0.0085 seconds was written to a restart file at the end of the 30-foot impact. A second file, the restart input file (user defined) was used to extend the solution to 0.025 seconds, redefine the shipping container nodal velocity to 0.0 in/sec, and

redefine the crush plate nodal velocity to 528 in/sec. With the restart file and the restart input file, the crush impact solution was initiated on the 30-foot damaged container.

The initial configuration of the crush impact was the final configuration of the 30-foot impact as shown in Figure 3.1.2. The final configuration for the crush impact is shown in Figure 3.1.15. Figure 3.1.16 shows a view of the lid region near the rigid plane after the crush impact (0°). Figure 3.1.17 shows the upper lid region (180°). Figure 3.1.18 shows the lower bottom region (0°) and Figure 3.1.19 shows the upper bottom region after the crush impact (180°).

Figure 3.1 20 shows the maximum effective plastic strain in the CV body after the crush impact to be 0.0348 in/in. This is approximately the value after the 30-foot impact. The internal weights bare on the CV side wall forcing the local elevated strain region. Figure 3.1.21 shows the effective plastic strain in the CV lid to be a maximum of 0.0002 in/in. The CV nut ring remains elastic during the crush impact.

Figure 3.1.22 shows the maximum effective plastic strain in the drum angle due to the crush impact to be 0.0945 in/in. The maximum effective plastic strain in the drum is 0.3028 in/in as shown in Figure 3.1.23. Elevated regions of plastic strain occur in localized crimped regions at each end of the crush plate and at the attachment of the angle to the drum near the rigid surface (0°). Figure 3.1.24 shows the effective plastic strain in the drum bottom head. The maximum in the bottom head is 0.2945 in/in. The maximum effective plastic strain in the liner is 0.2063 in/in as shown in Figure 3.1.25. The maximum value occurs at the borobond/kaolite liner junction at 180°, as in the initial 30-foot impact.

The maximum effective plastic strain in the lid due to the crush impact occurs at the base of the hole for the upper stud (180°), near the crush plate. The maximum is 0.6430 in/in as shown in Figure 3.1.26. The membrane strain maximum is 0.4475 in/in and is very localized to the upper stud hole (similar to the bending shown in Figure 3.1.26). If failure were to occur it would be very localized to the lower region of the upper stud hole (near the crush plate - possible surface cracking). There is a lack of a general region of high strain in the lid which would promote an extended tear, or ripping of the lid.

Figure 3.1.27 shows the drum studs with a maximum effective plastic strain of 0.1937 in/in due to the crush impact. Not shown in figures: the maximum effective plastic strain in the lid stiffener is 0.0303 in/in; the maximum effective plastic strain in the drum stud nuts is 0.0005 in/in; the maximum effective plastic strain in the drum stud washers is 0.1628 in/in and the maximum effective plastic strain in the plug liner is 0.1212 in/in.

Figure 3.1.28 shows the kinetic energy time history for the crush plate. Figure 3.1.29

shows the X velocity time history for the plate.

The location of the nodes chosen to investigate the separation of the CV lid and the body flange at the O-rings are shown in Figure 3.1.30. The nodes are at 45° positions around the half model. The nodes are at the inside radius of the inner O-ring groove on the body and are at comparable positions on the opposite, lid surface. Figure 3.1.31 shows the separation time history for the node pairs. A positive value in the plot indicates separation (gap). The plot is quite noisy with ringing (contact chatter) of the node pair separations, but its purpose is to show relative magnitudes of separation in the model. From the figure, it can be seen that a gap spike of almost 0.004 in is obtained in the 30-foot impact just before 0.005 seconds. In the crush impact, spikes of almost 0.005 in in gap separation are seen. When the solution was halted, spikes on the order of 0.004 in are evident (there is no damping in the model other than friction). The ringing maximum is approximately 0.004 in and its minimum is about 0.00 in at the end of the solution (sinusoidal in nature). The ringing would then be about a mid-point value of 0.002 in. An implicit solution, or relaxed state is not obtained. In a relaxed state, if a permanent set were obtained in the flange region, then the average gap would be about 0.002 in, or less would be expected.

Figure 3.1.32 shows the kaolite nodes on the plane of symmetry chosen to obtain the kaolite thickness response to the impacts. Figure 3.1.33 shows the time history thickness at the nodal pairs shown. The thickness is obtained by subtracting one node X-coordinate time history from another nodes. The time in Figure 3.1.33 is in seconds and the X coordinate is the relative value in inches. For example, curve "A" represents the kaolite thickness on the plane of symmetry between the angle and the drum, nearest the crush plate. From Figure 3.1.33 it can be seen that the curve "A" thickness initially is about 1.75 inches and remains at that value for the 30-foot impact. The crush impact is seen to reduce the kaolite thickness to just under 1.0 inches for curve "A". The correlation of nodes, Figure 3.1.33 curve letter and a description of the location is given in Table 3.1.1.

Table 3.1.1 - Location of Kaolite Thickness Measurements			
Model Direction	Description	Figure 3.1.33 Curve	Figure 3.1.32 Nodes
-X	Liner at Base of Angle / Drum	A	191112 / 206004
	Liner at Base of Plug Cavity / Drum	B	188411 / 200529
	Liner at Top of CV Cavity / Drum	C	224181 / 200522
	Liner at Second Drum Roll from the Lid / Drum Roll Extreme	D	222721 / 361713
	Liner at Second Drum Roll from the Bottom / Drum Roll Extreme	E	218049 / 350033
	Liner at First Drum Roll from the Bottom / Drum Roll Extreme	F	213377 / 338353
	Liner at Base of CV Cavity / Drum	G	210749 / 334338
+X	Liner at Base of CV Cavity / Drum	H	333258 / 209669
	Liner at First Drum Roll from the Bottom / Drum Roll Extreme	I	338281 / 213305
	Liner at Second Drum Roll from the Bottom / Drum Roll Extreme	J	349961 / 217977
	Liner at Second Drum Roll from the Lid / Drum Roll Extreme	K	361641 / 222649
	Liner at Top of CV Cavity / Drum	L	199946 / 223677
	Liner at Base of Plug Cavity / Drum	M	199953 / 187835
	Liner at Base of Angle / Drum	N	205932 / 191040

Figure 3.1.34 shows nodes in the drum, drum bottom and drum lid which will be used to define the diameter changes in the outer surfaces of the shipping package. Figure 3.1.35 gives the relative X coordinate values (diameter changes) for the nodes on the plane of symmetry. From the plot it is seen that the minimum diameter reaches approximately 14.5 inches and then rebounds slightly. This minimum is at the lower barrel roll in the drum. From Figure 3.1.35 it is seen that the barrel roll diameters decrease from top to bottom. The greater deflection of the crush plate nearer the bottom of the package is evident in the Figure 3.1.15 final configuration plot. Figure 3.1.36 gives the Y coordinate time history response of the nodes at the Y extreme of the shipping package (see Figure 3.1.34). The values in Figure 3.1.36 are relative to the plane of symmetry and therefore need to be doubled to obtain the diameter changes. The correlation of nodes, curve numbers and a description of the location are given in Table 3.1.2. The ovalization of the package is also evident in comparing Figures 3.1.35 and 3.1.36.

Table 3.1.2 - Nodal Locations for Drum Diameter Time Histories				
Description	Diameter (X Direction)		Radius (Y Direction)	
	Figure 3.1.35 Curve	Figure 3.1.34 Nodes	Figure 3.1.36 Curve	Figure 3.1.34 Nodes
Lid Roll	A	133634 / 133778	A	133706
First Drum Roll Below Lid	B	98158 / 98230	B	98194
Second Drum Roll Below Lid	C	100202 / 100274	C	100238
Second Drum Roll Above Bottom	D	102976 / 103048	D	103012
First Drum Roll Above Bottom	E	105750 / 105822	E	105786
Bottom Attachment Roll to Drum	F	108889 / 108961	F	108925

Figure 3.1.37 shows nodes chosen to obtain liner diameter time histories. Figure 3.1.38 shows the diameter time histories for the node pairs. Table 3.1.3 shows the location of the nodal pairs along the length of the liner.

Table 3.1.3 - Nodal Locations for Liner Diameter Time Histories		
Curve	Node Pairs	Distance Above Base of Liner (in)
A	122522 / 122666	0.0
B	123259 / 129667	5.0
C	123276 / 129684	10.3
D	123292 / 129700	15.3
E	123309 / 129717	20.6
F	123324 / 129732	25.2
G	123340 / 129748	30.2

Part A - Initial Design with Borobond Cylinder

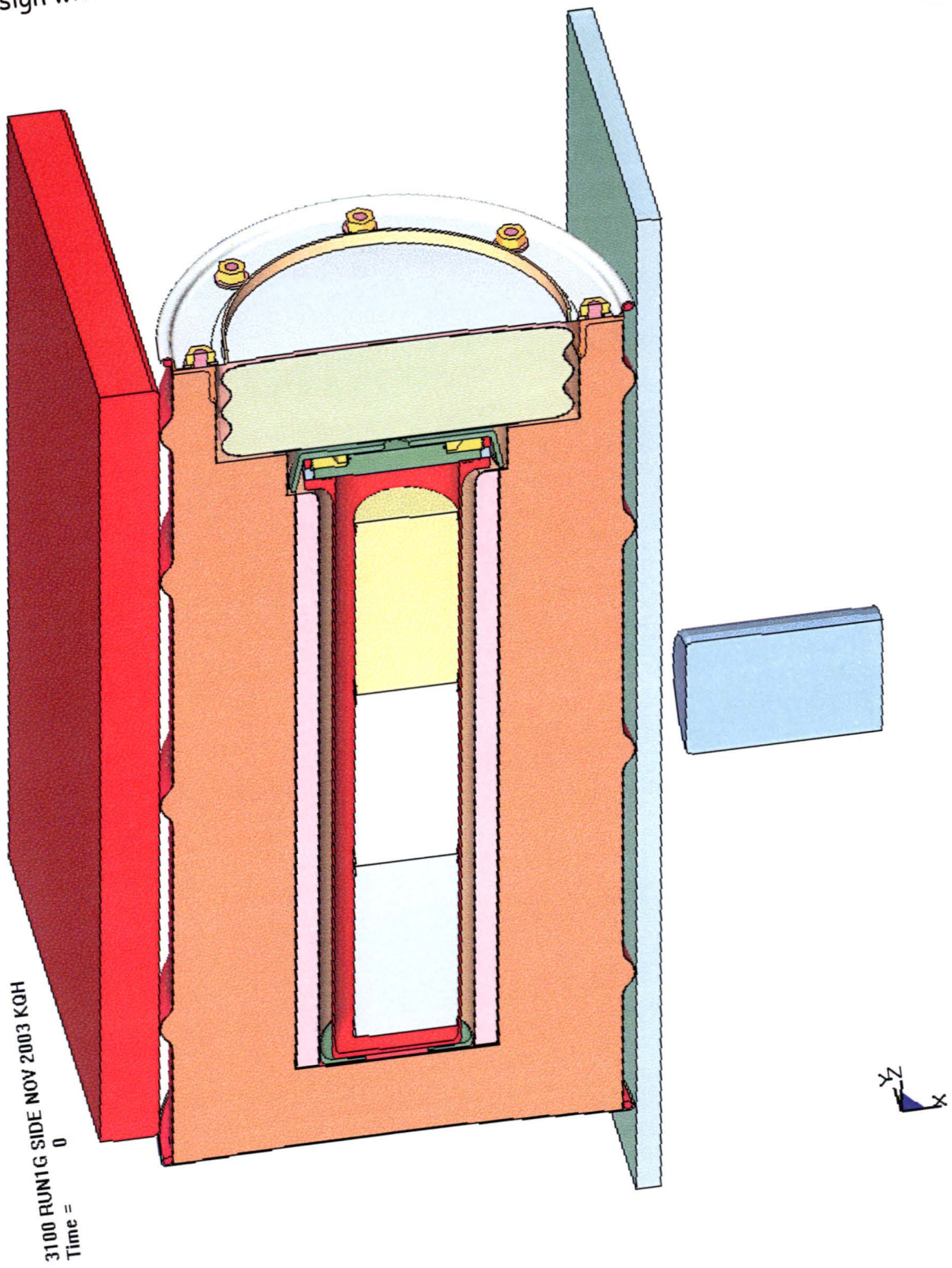

Figure 3.1.1 - Run1g, Initial Configuration

Part A - Initial Design with Borobond Cylinder

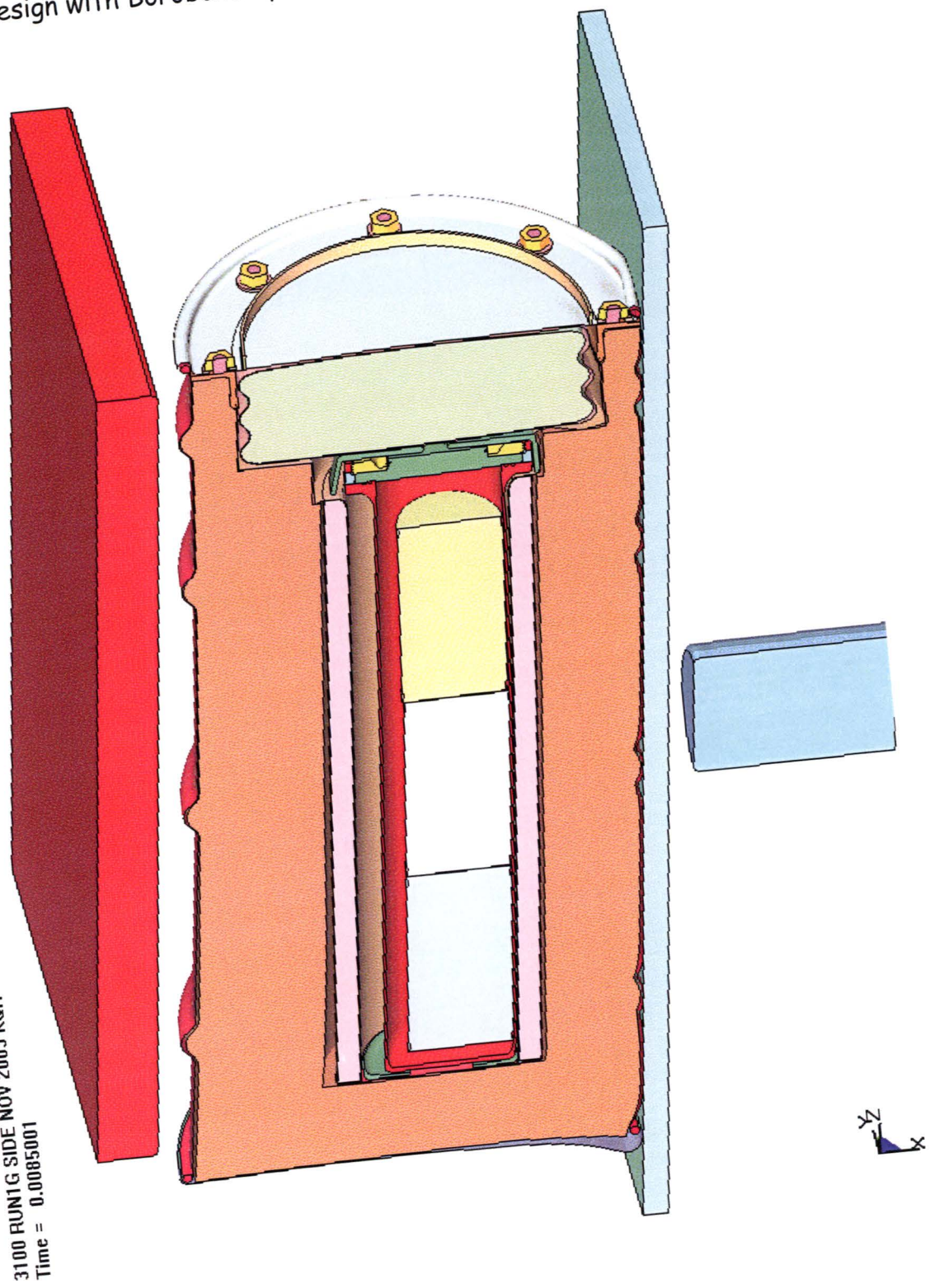

Figure 3.1.2 - Run1g, 30-Foot Impact, Final Configuration

Part A - Initial Design with Borobond Cylinder

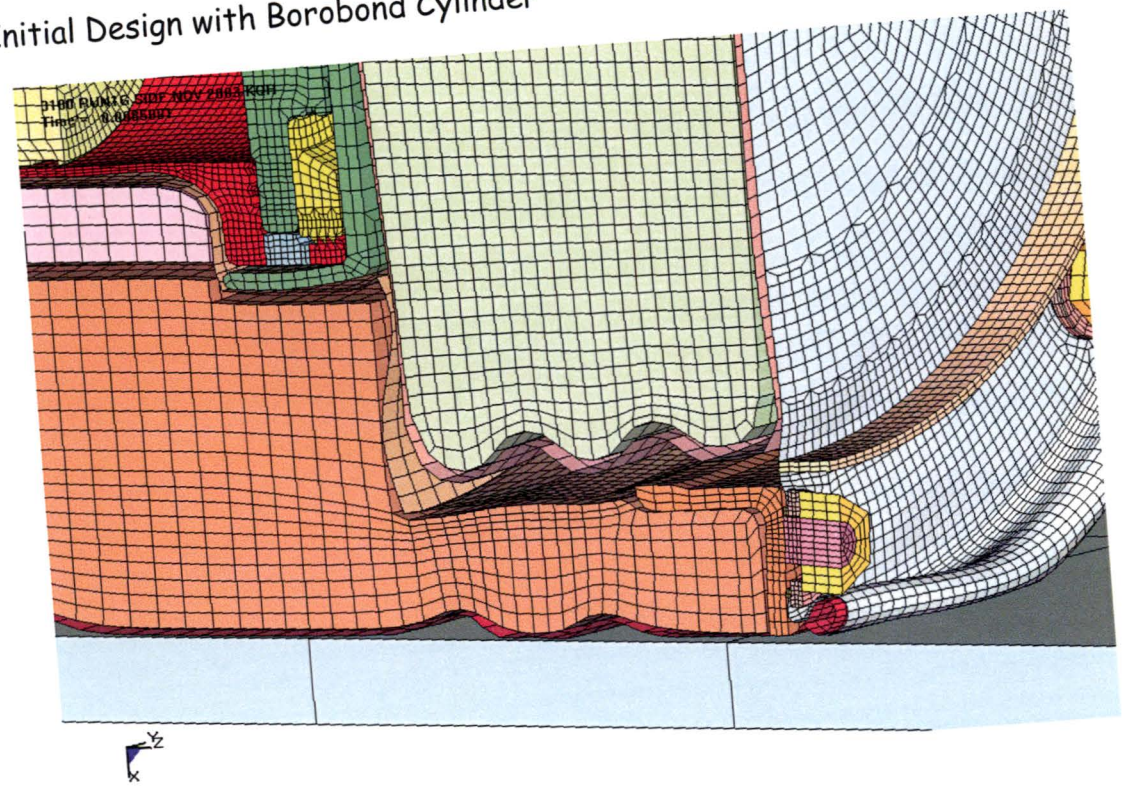

Figure 3.1.3 - Run1g, 30-Foot Impact, Configuration of the Drum Bolted Region

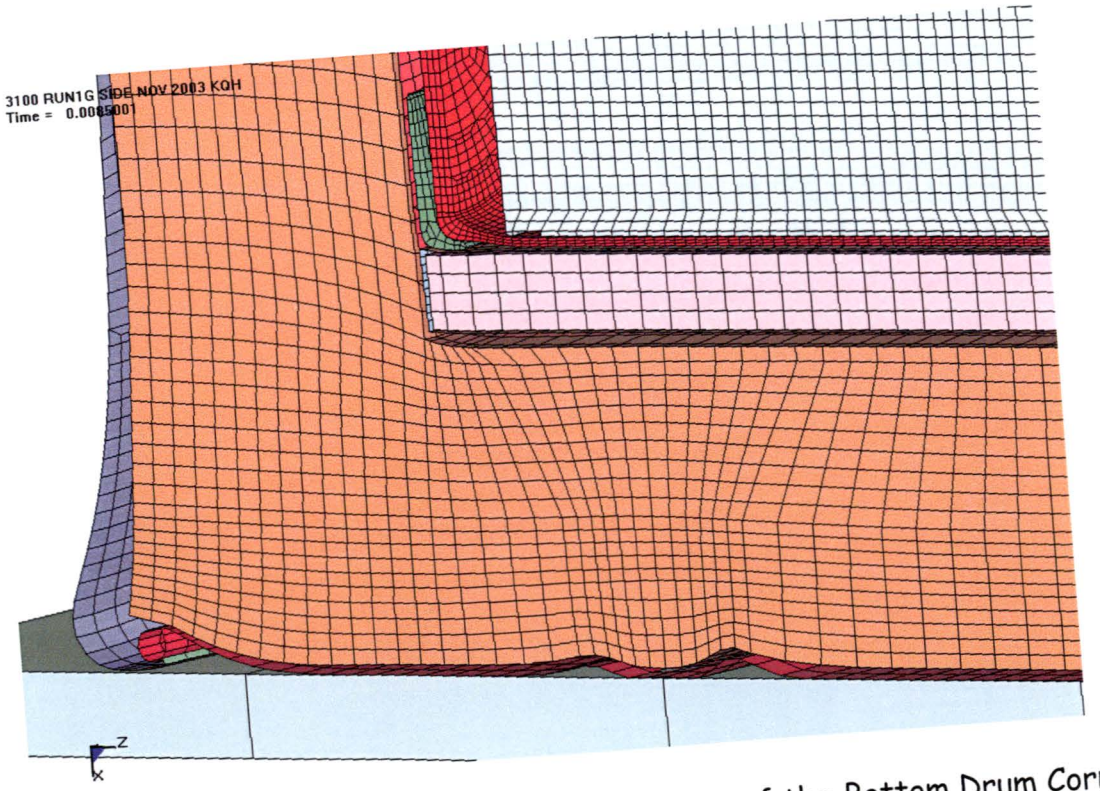

Figure 3.1.4 - Run1g, 30-Foot Impact, Configuration of the Bottom Drum Corner

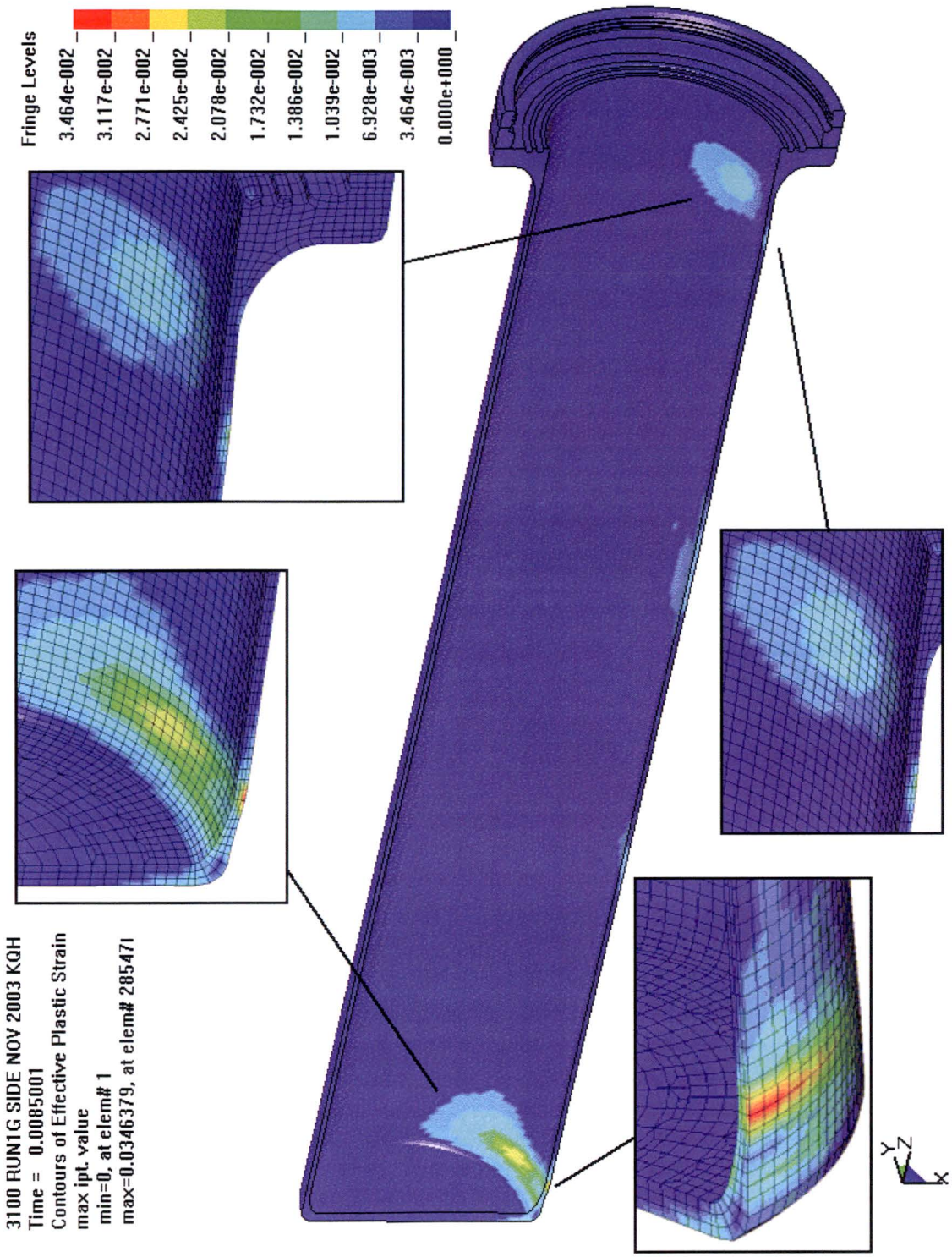

Figure 3.1.5 - Run1g, 30-Foot Impact, Effective Plastic Strain in the CV Body

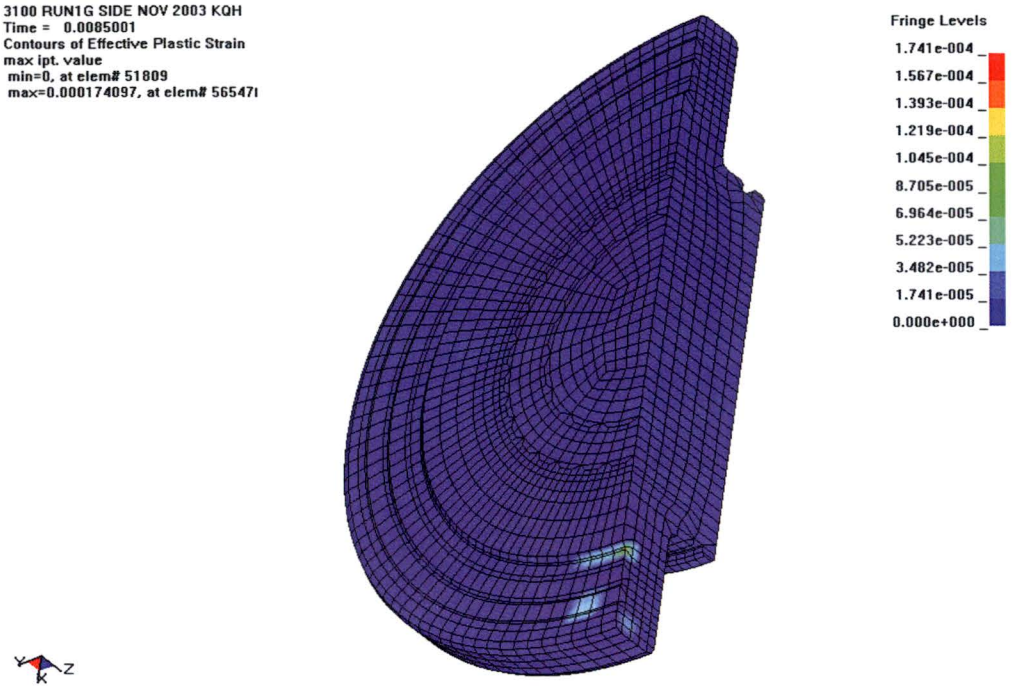

Figure 3.1.6 - Run1g, 30-Foot Impact, Effective Plastic Strain in the CV Lid

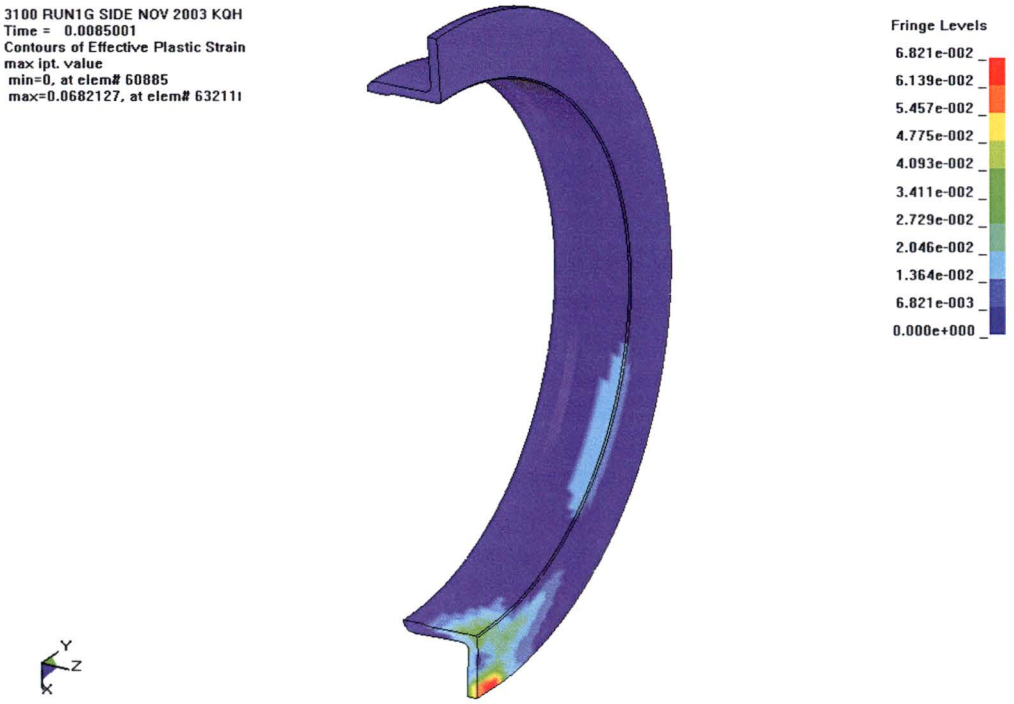

Figure 3.1.7 - Run1g, 30-Foot Impact, Effective Plastic Strain in the Drum Angle

Figure 3.1.8 - Run1g, 30-Foot Impact, Effective Plastic Strain in the Drum Outer Liner

Figure 3.1.9 - Run1g, 30-Foot Impact, Effective Plastic Strain in the Drum Bottom Head

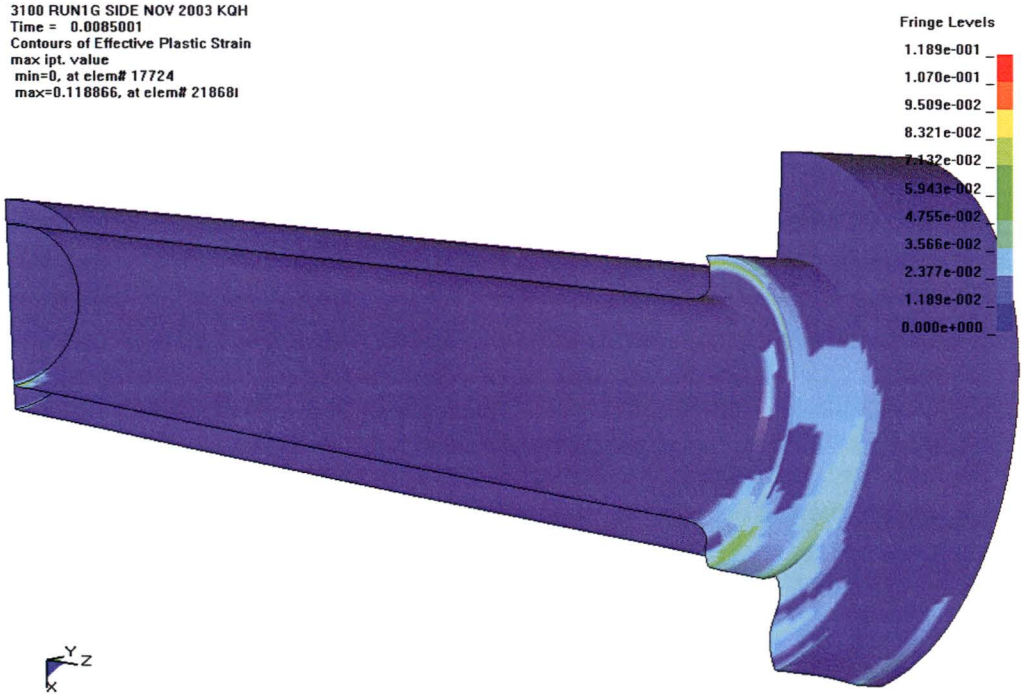

Figure 3.1.10 - Run1g, 30-Foot Impact, Effective Plastic Strain in the Liner

Figure 3.1.11 - Run1g, 30-Foot Impact, Effective Plastic Strain in the Drum Lid

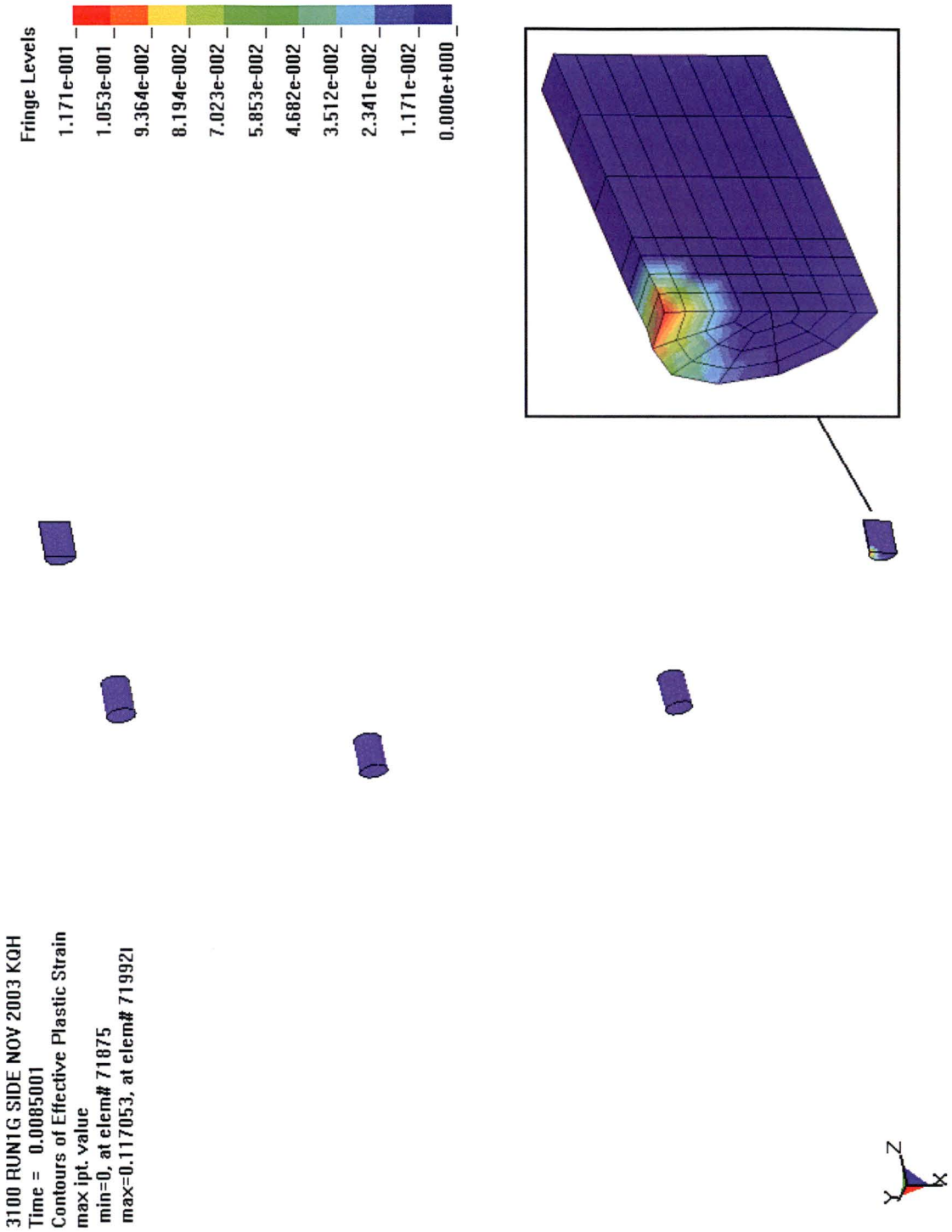

Figure 3.1.12 - Run1g, 30-Foot Impact, Effective Plastic Strain in the Drum Studs

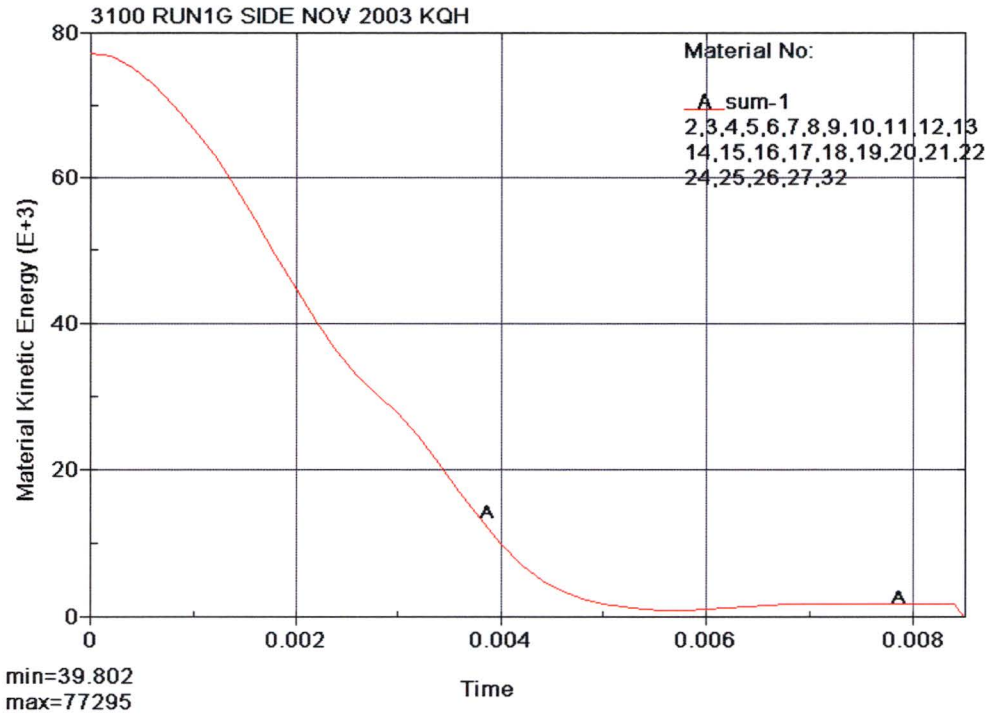

Figure 3.1.13 - Run1g, 30-Foot Impact, Kinetic Energy Time History

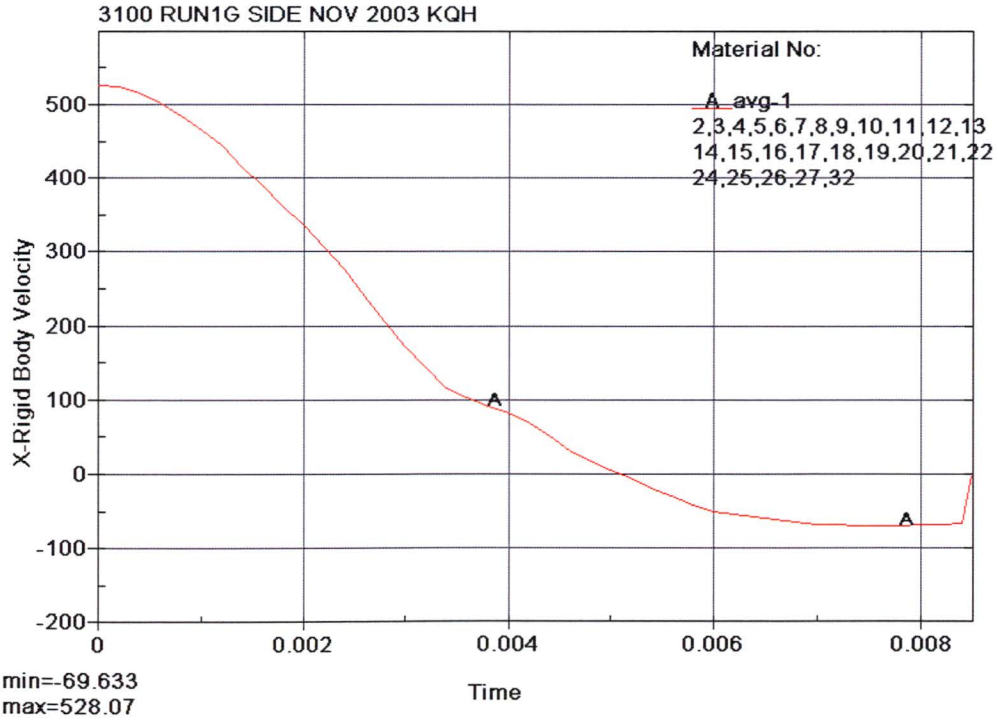

Figure 3.1.14 - Run1g, 30-Foot Impact, X Velocity Time History

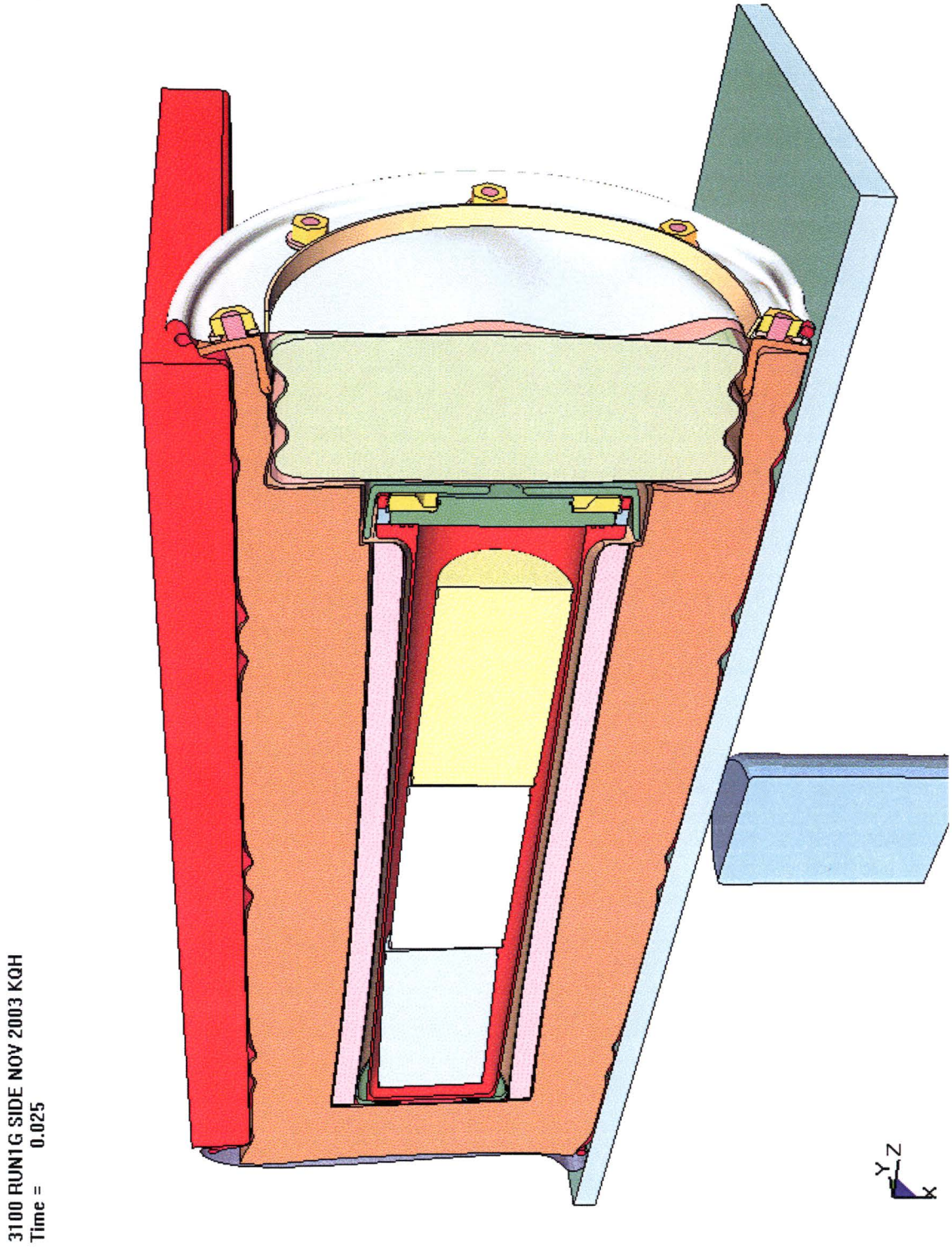

Figure 3.1.15 - Run1g, Crush Impact, Final Configuration

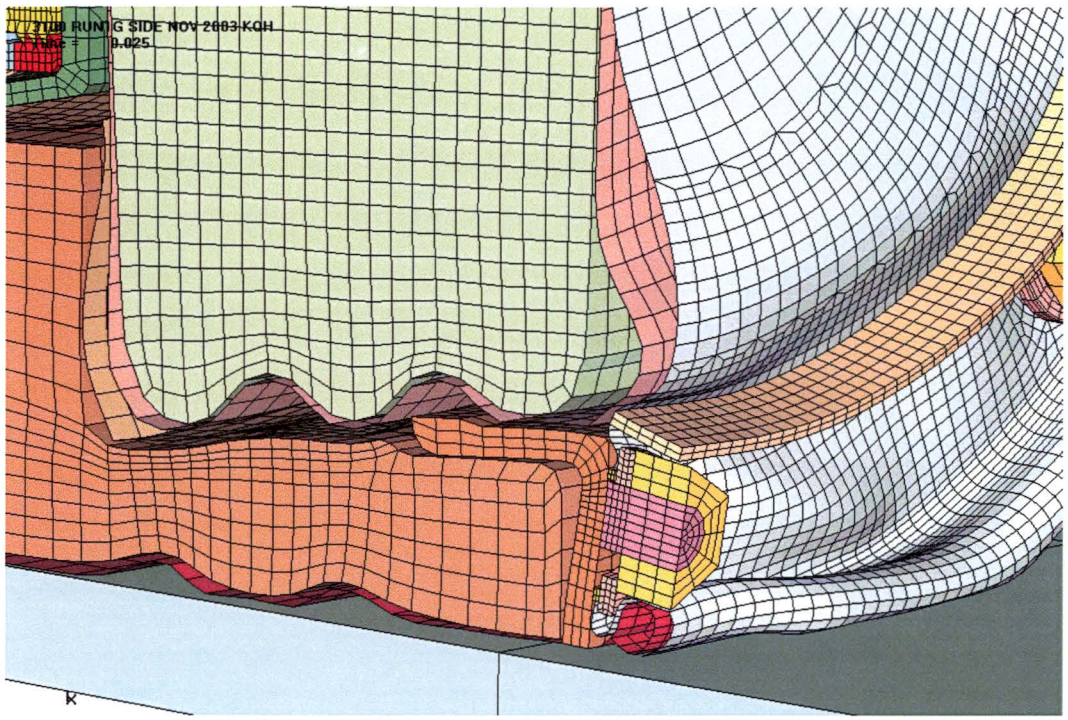

Figure 3.1.16 - Run1g, Crush Impact, Configuration of the Lower Lid Region

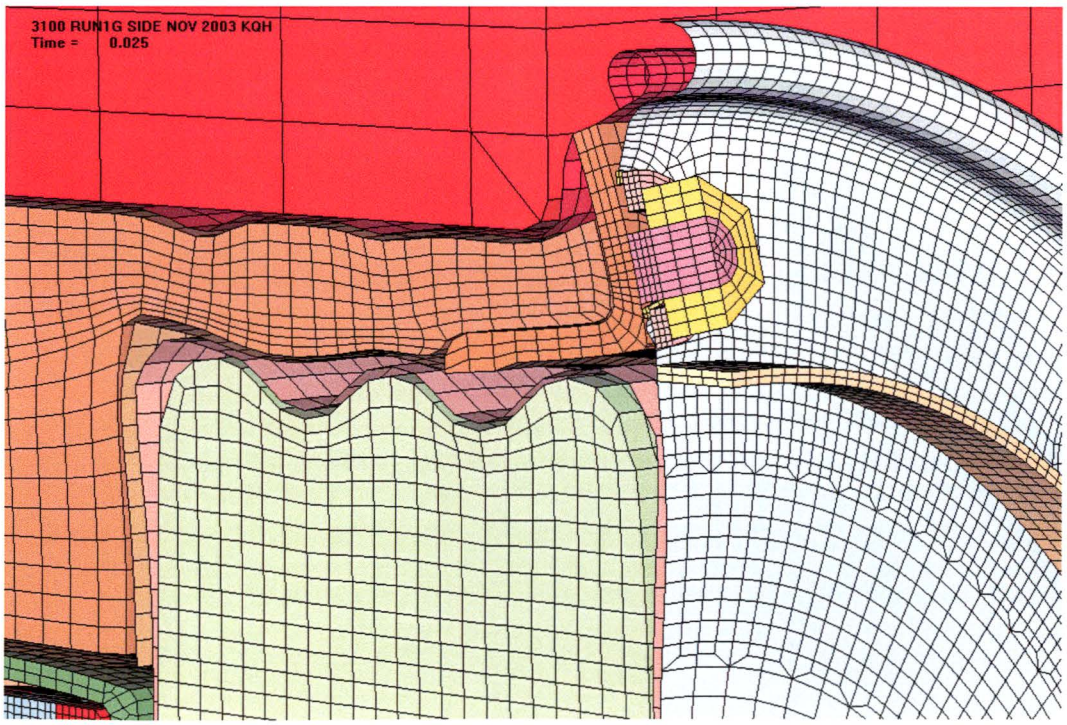

Figure 3.1.17 - Run1g, Crush Impact, Configuration of the Upper Lid Region

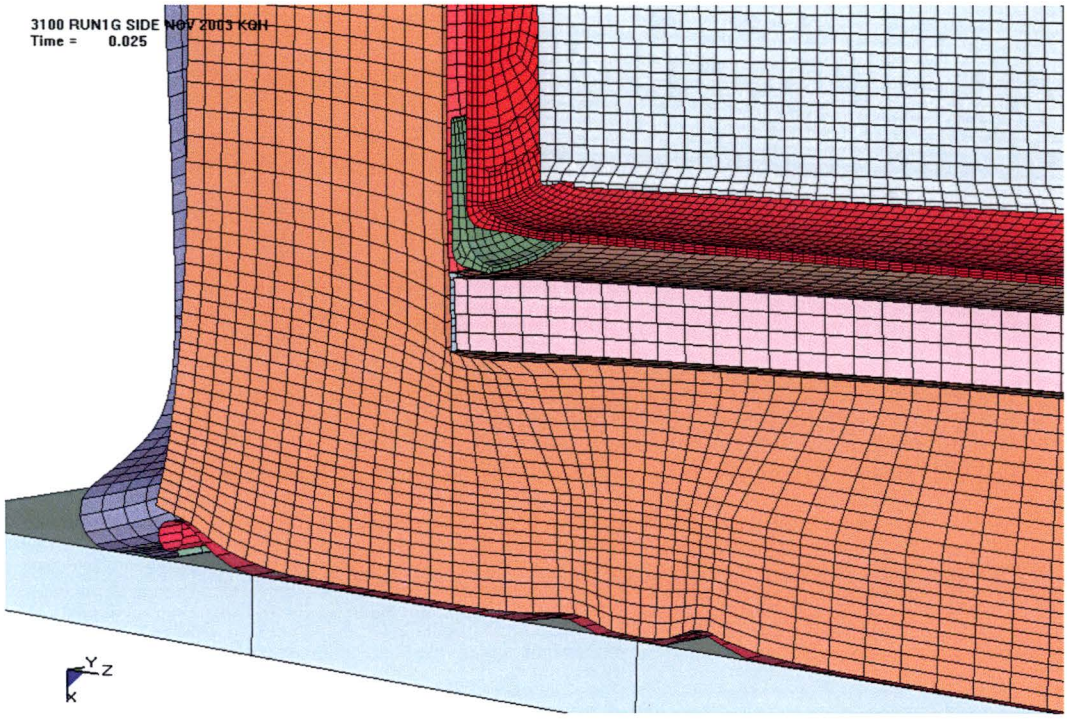

Figure 3.1.18 - Run1g, Crush Impact, Configuration of the Lower Bottom Region

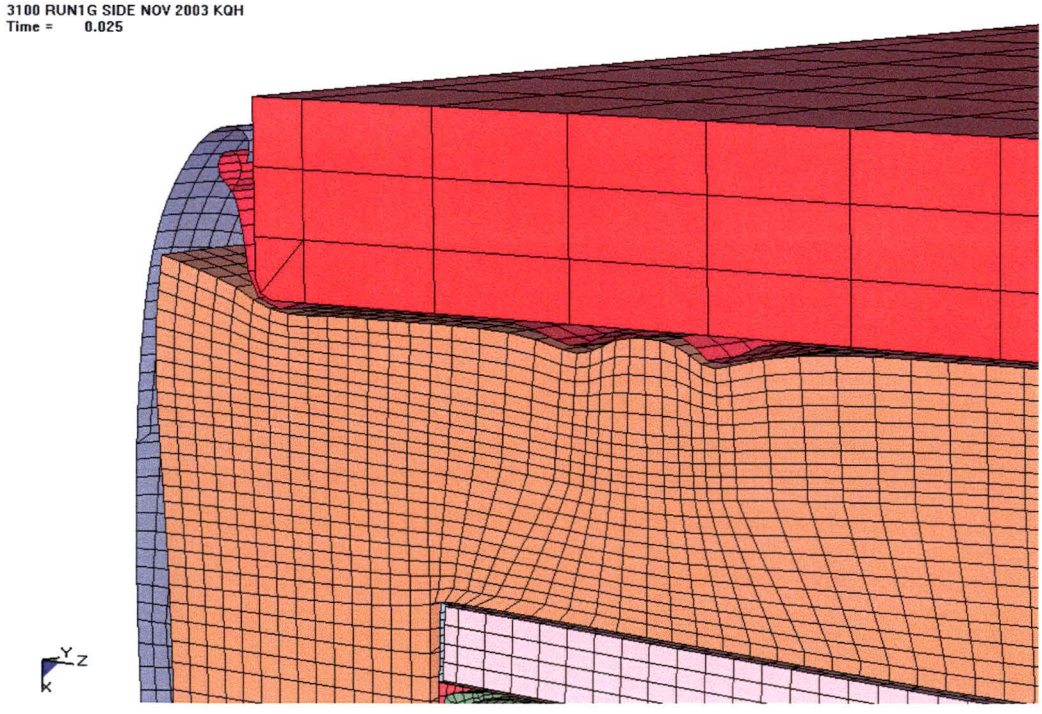

Figure 3.1.19 - Run1g, Crush Impact, Configuration of the Upper Bottom Region

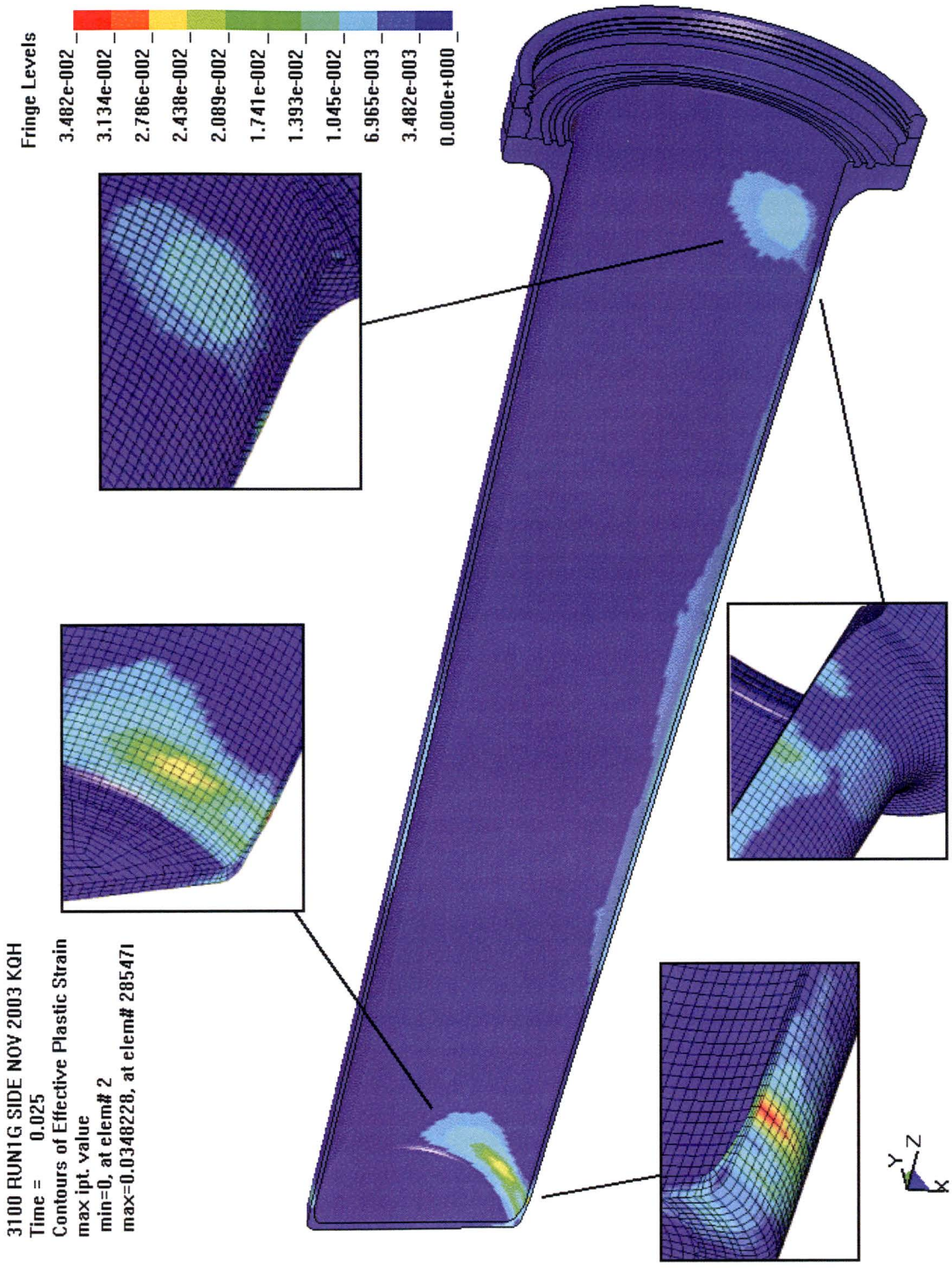

Figure 3.1.20 - Run1g, Crush Impact, Effective Plastic Strain in the CV Body

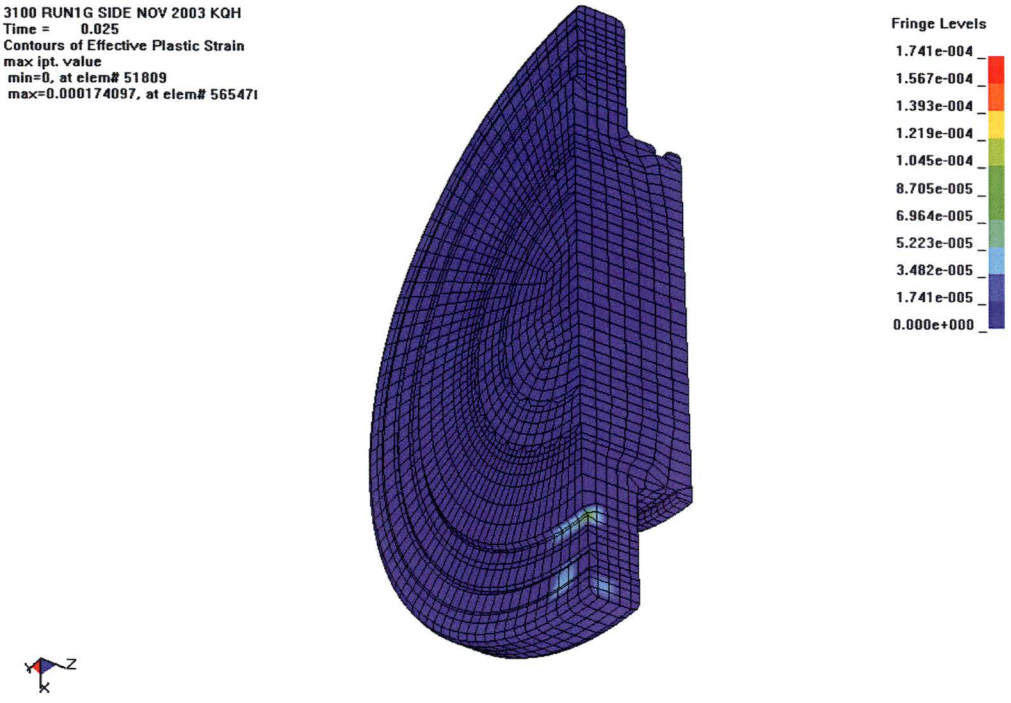

Figure 3.1.21 - Run1g, Crush Impact, Effective Plastic Strain in the CV Lid

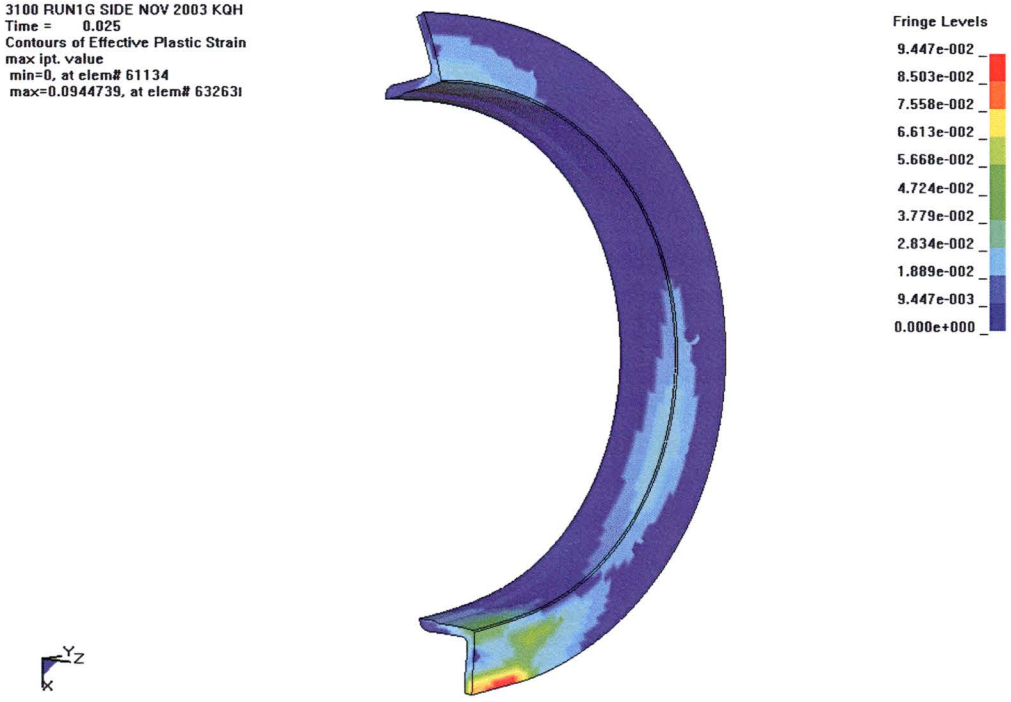

Figure 3.1.22 - Run1g, Crush Impact, Effective Plastic Strain in the Drum Angle

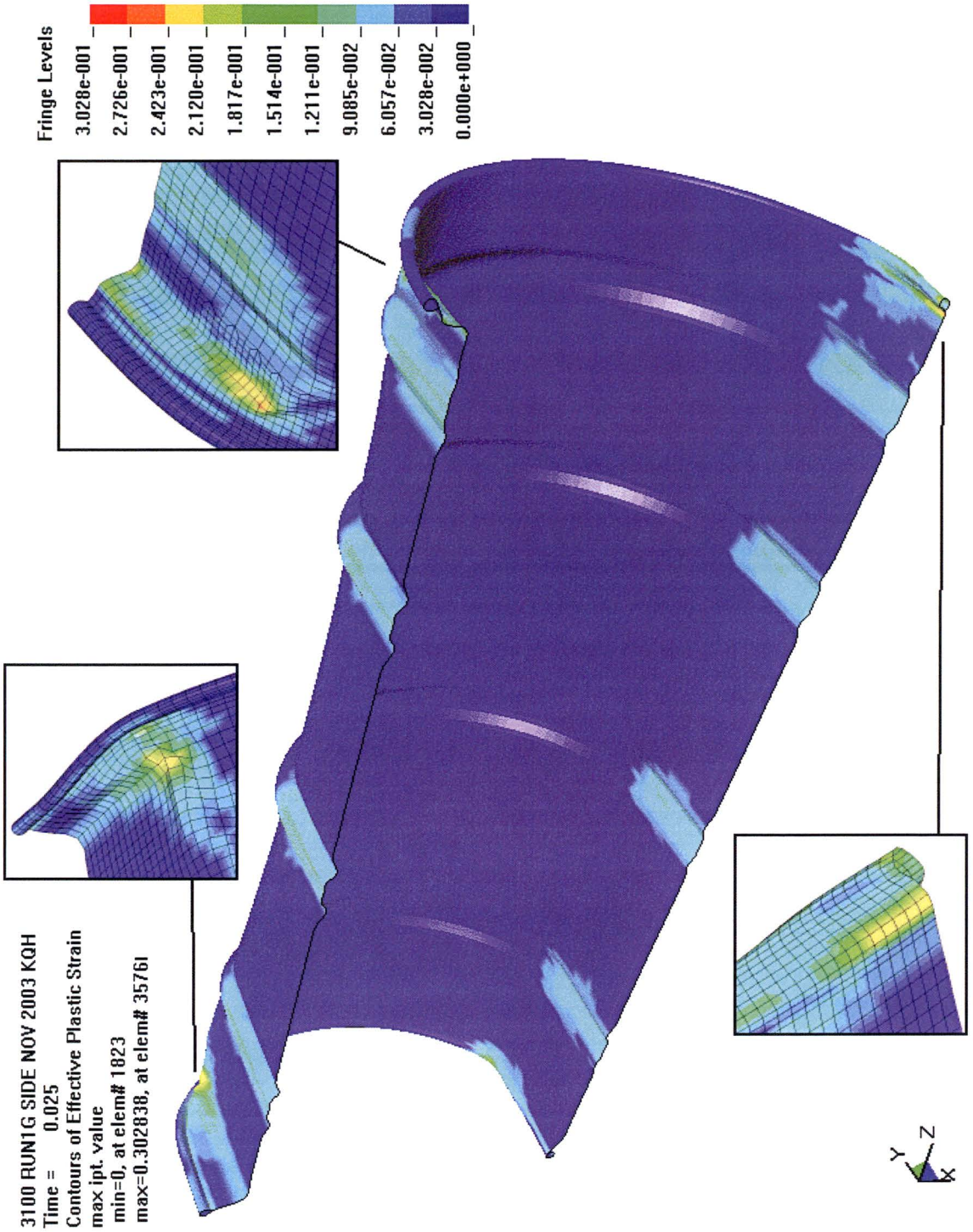

Figure 3.1.23 - Run1g, Crush Impact, Effective Plastic Strain in the Drum

Figure 3.1.24 - Run1g, Crush Impact, Effective Plastic Strain in the Drum Bottom Head

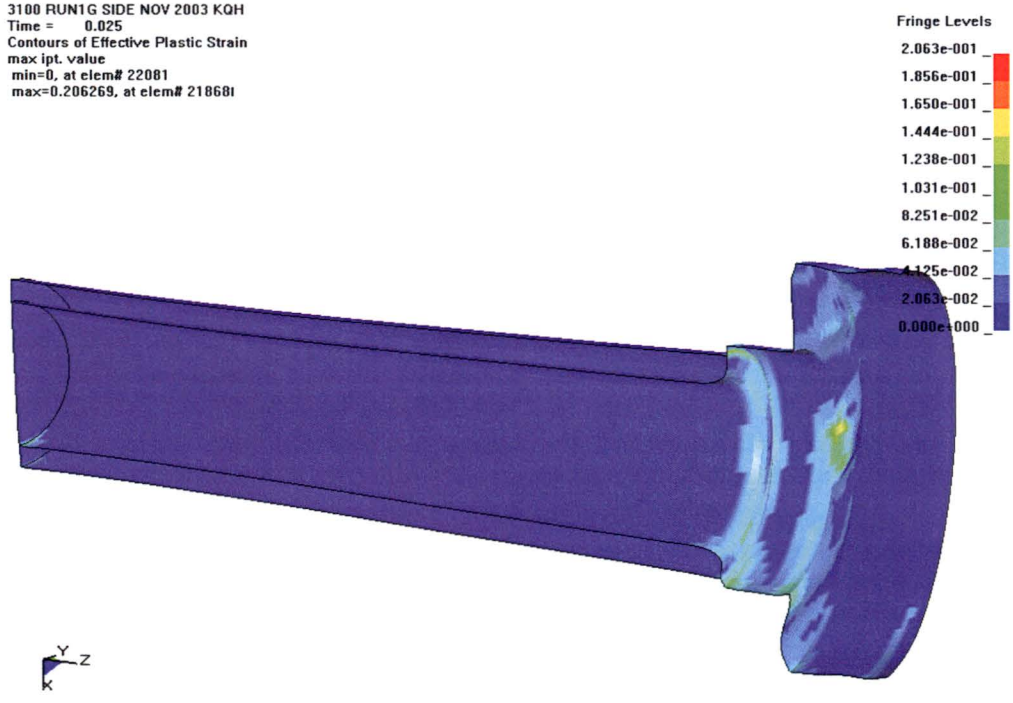

Figure 3.1.25 - Run1g, Crush Impact, Effective Plastic Strain in the Drum Inner Liner

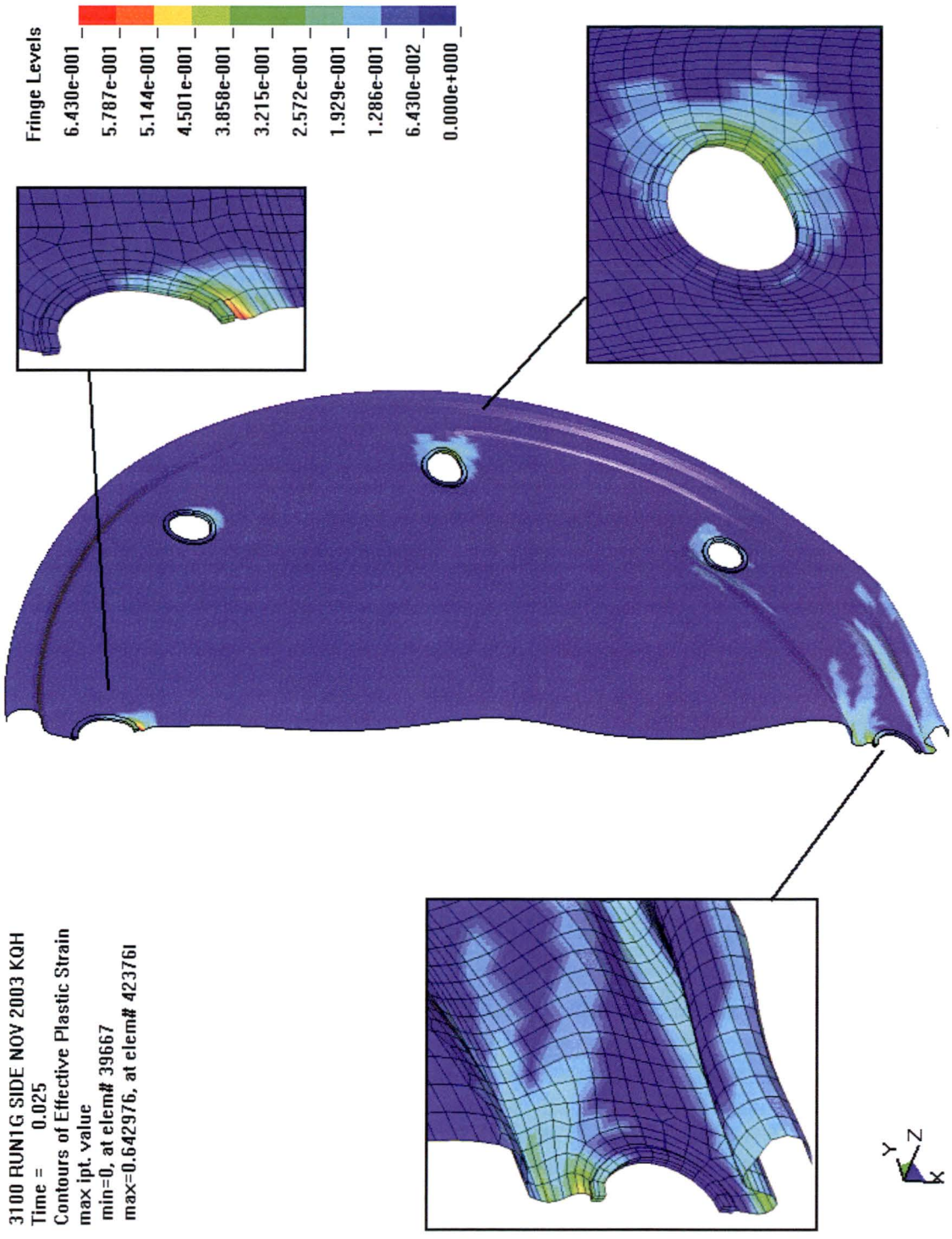

Figure 3.1.26 - Run1g, Crush Impact, Effective Plastic Strain in the Drum Lid

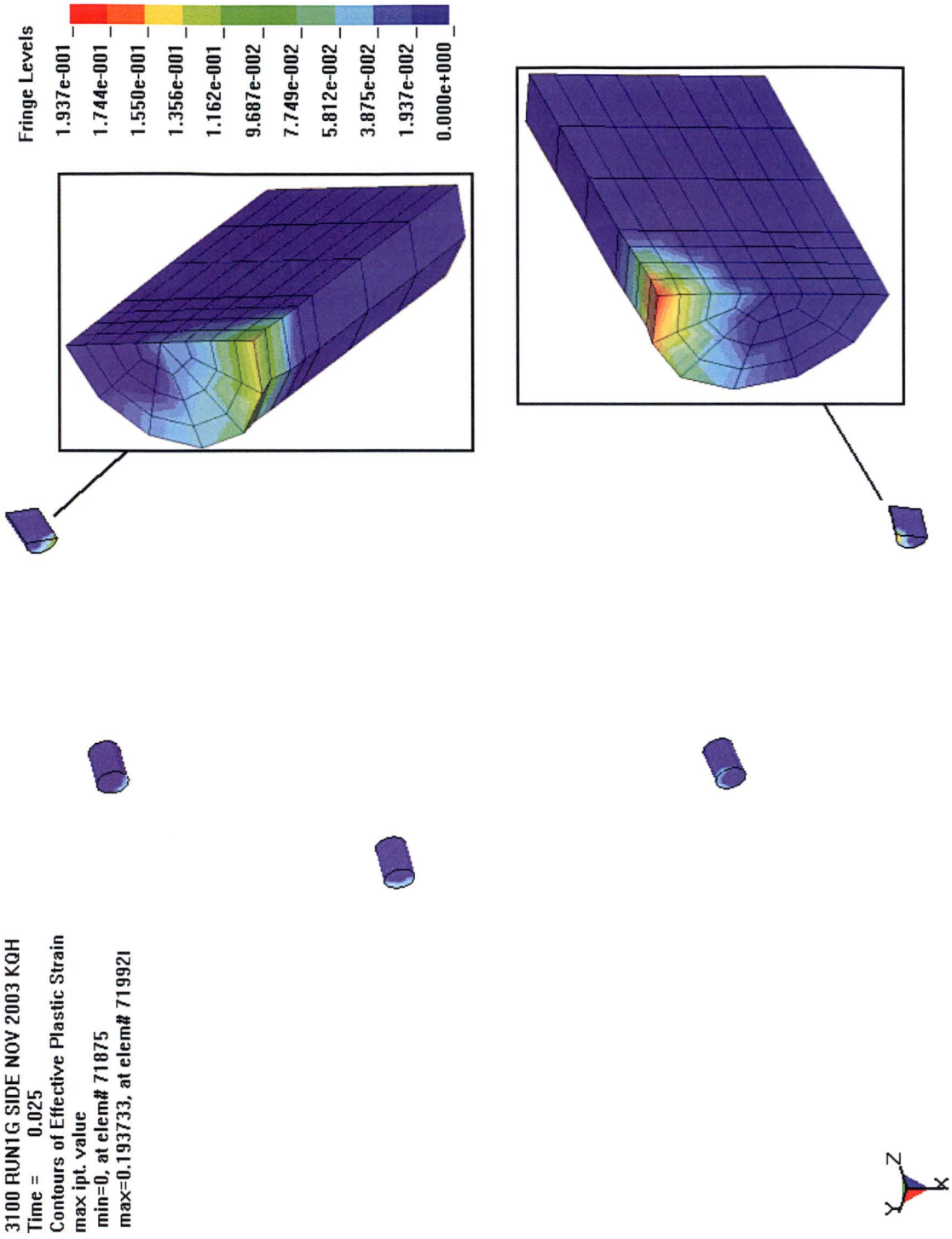

Figure 3.1.27 - Run1g, Crush Impact, Effective Plastic Strain in the Drum Studs

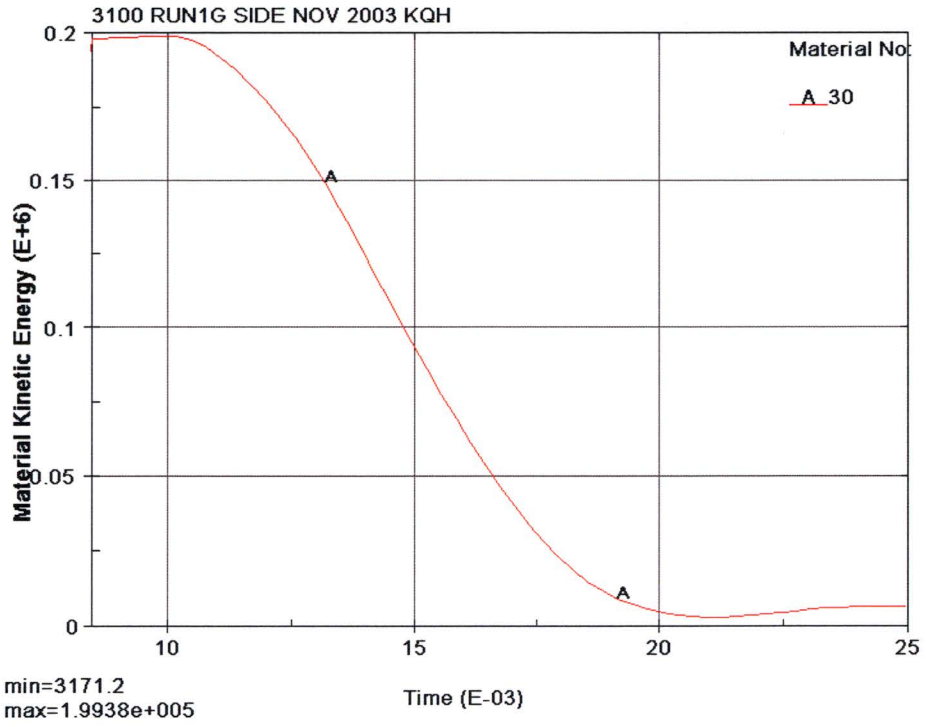

Figure 3.1.28 - Run1g, Crush Impact, Kinetic Energy Time History of the Crush Plate

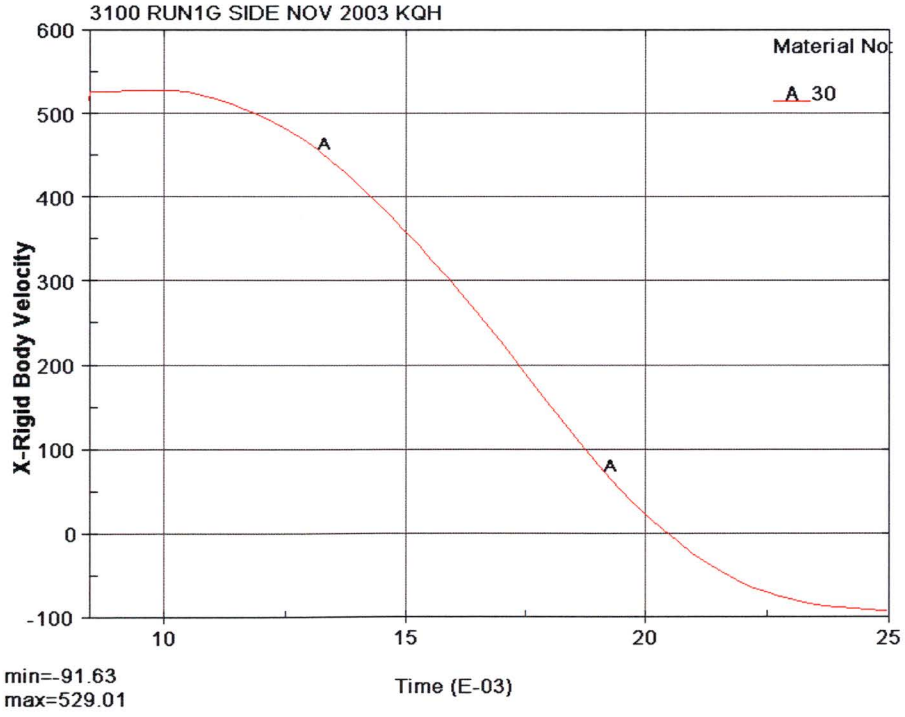

Figure 3.1.29 - Run1g, Crush Impact, X Velocity Time History of the Crush Plate

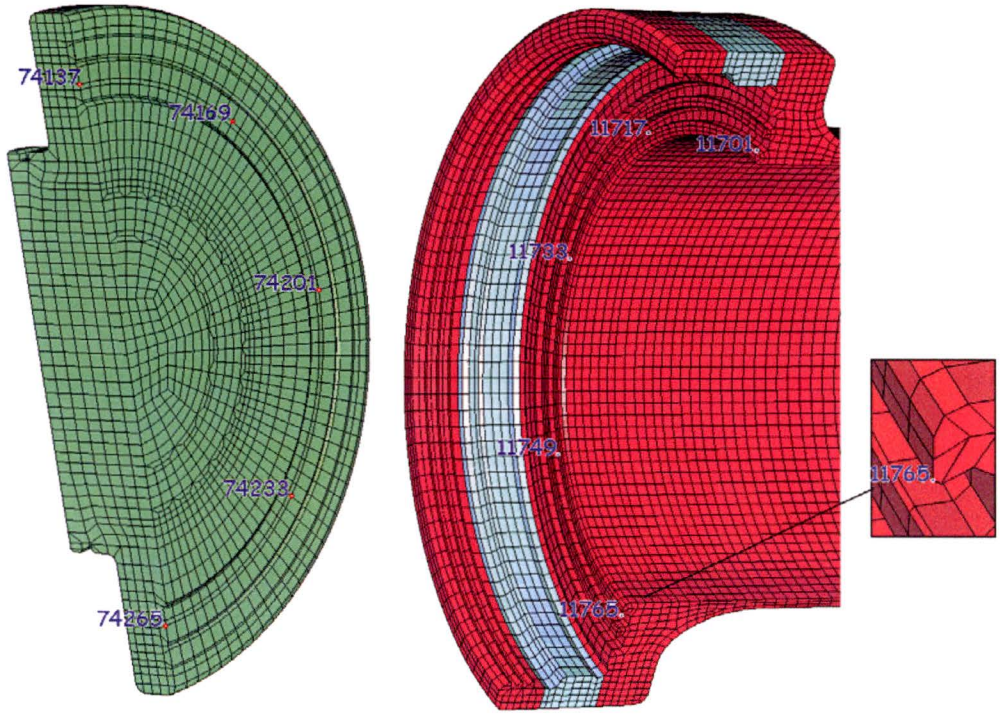

Figure 3.1.30 - Run1g, Nodes on CV Lid and Body Flange for Separation Time History

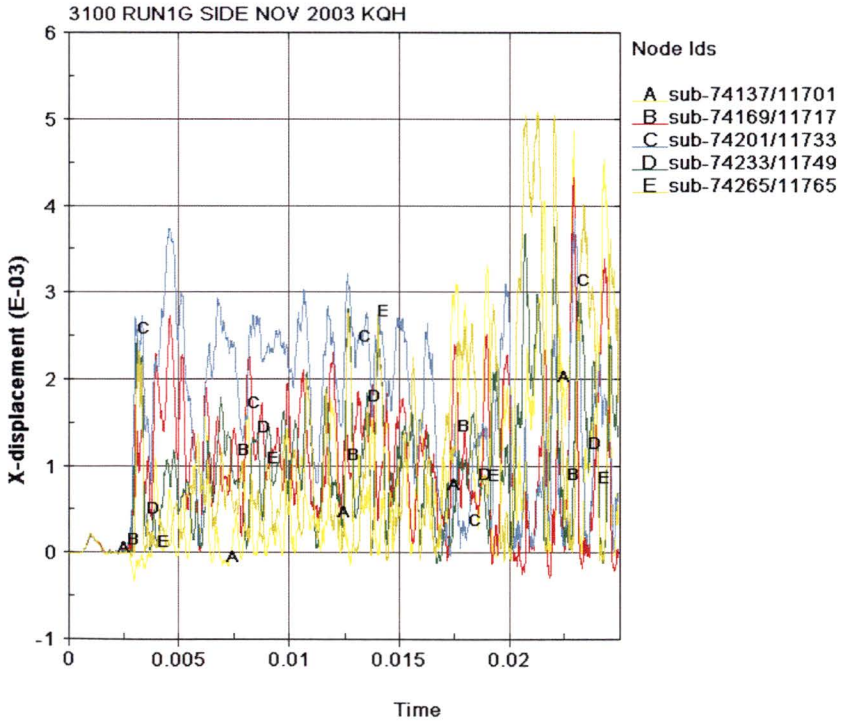

Figure 3.1.31 - Run1g, CV Flange Separation Time History

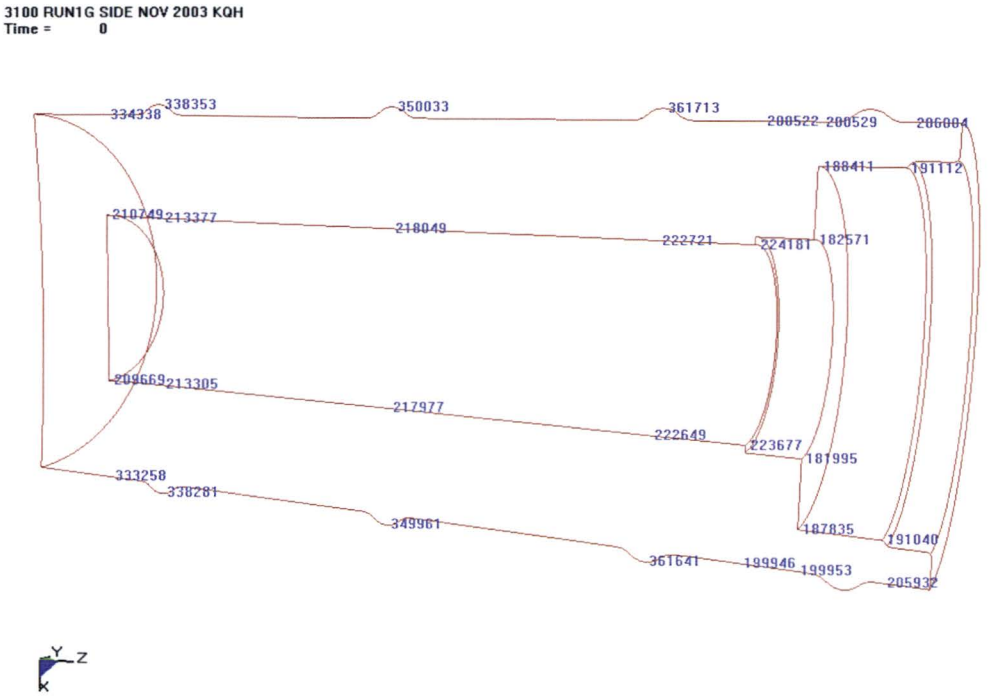

Figure 3.1.32 - Run1g, Drum Kaolite Nodes Used for Thickness Time Histories

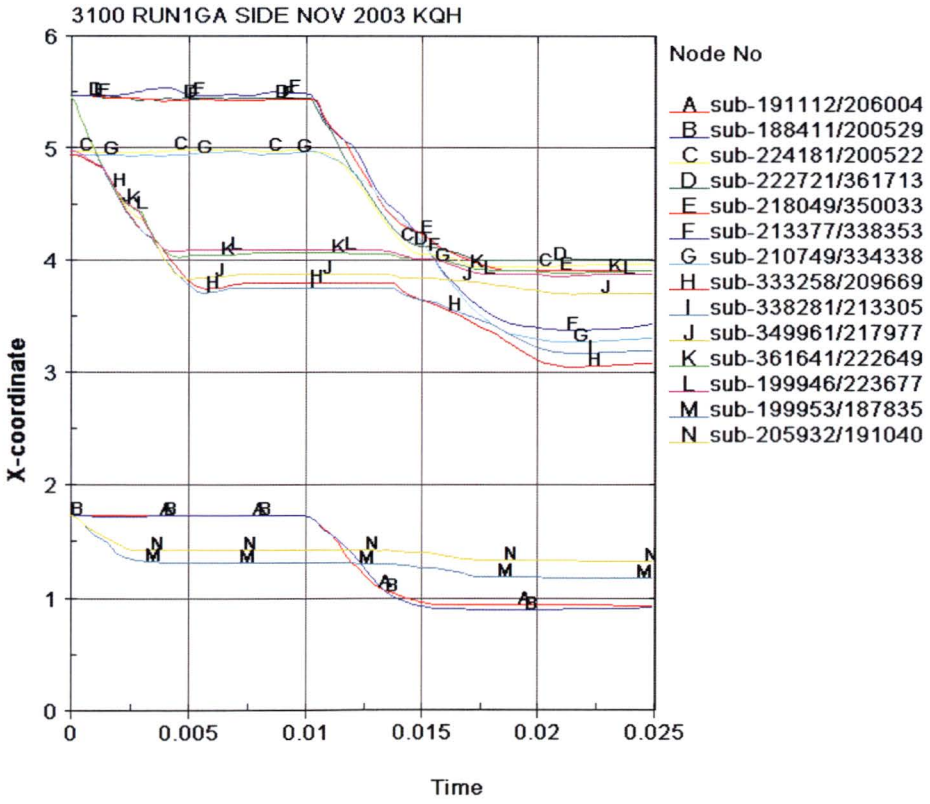

Figure 3.1.33 - Run1g, Drum Kaolite Thickness Time History

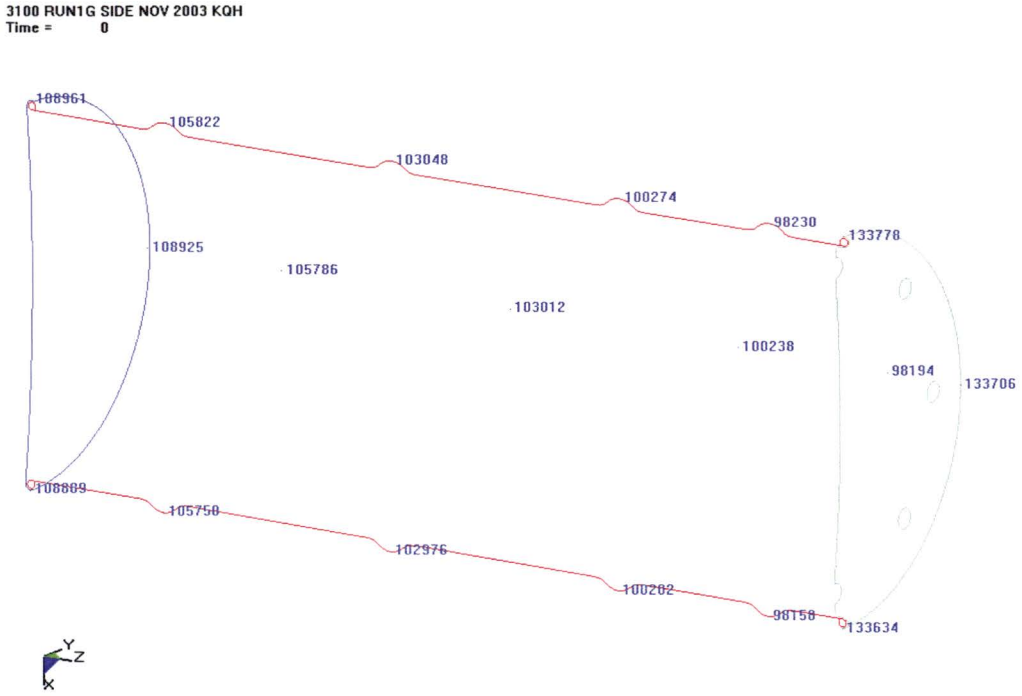

Figure 3.1.34 - Run1g, Drum Nodes Used to Measure Deformation Time Histories

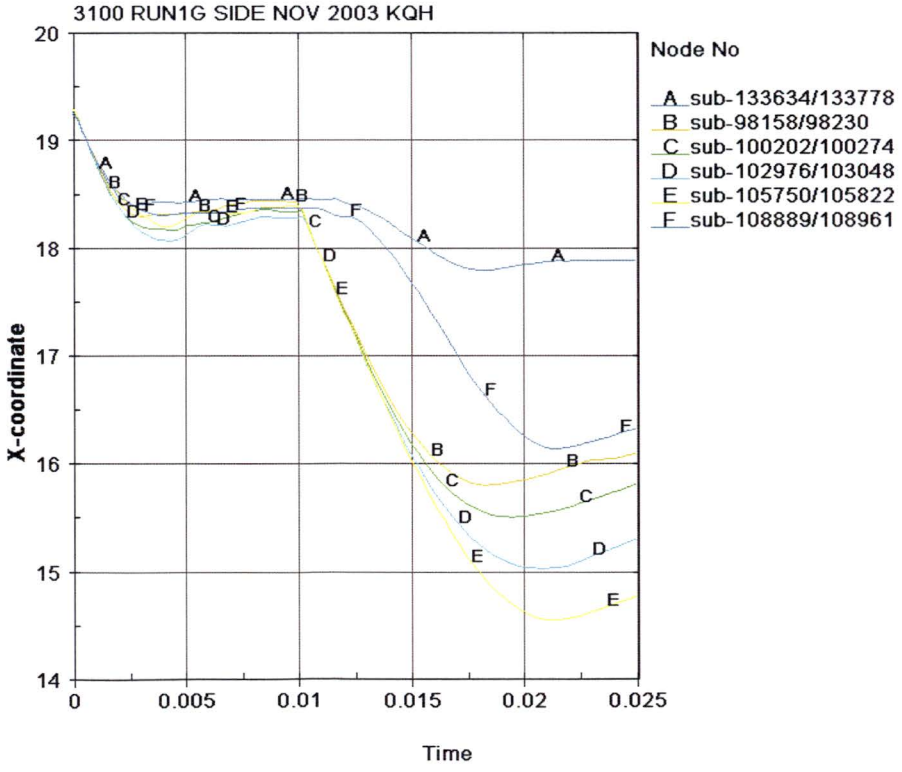

Figure 3.1.35 - Run1g, Drum Measurement Time History in the X-Direction

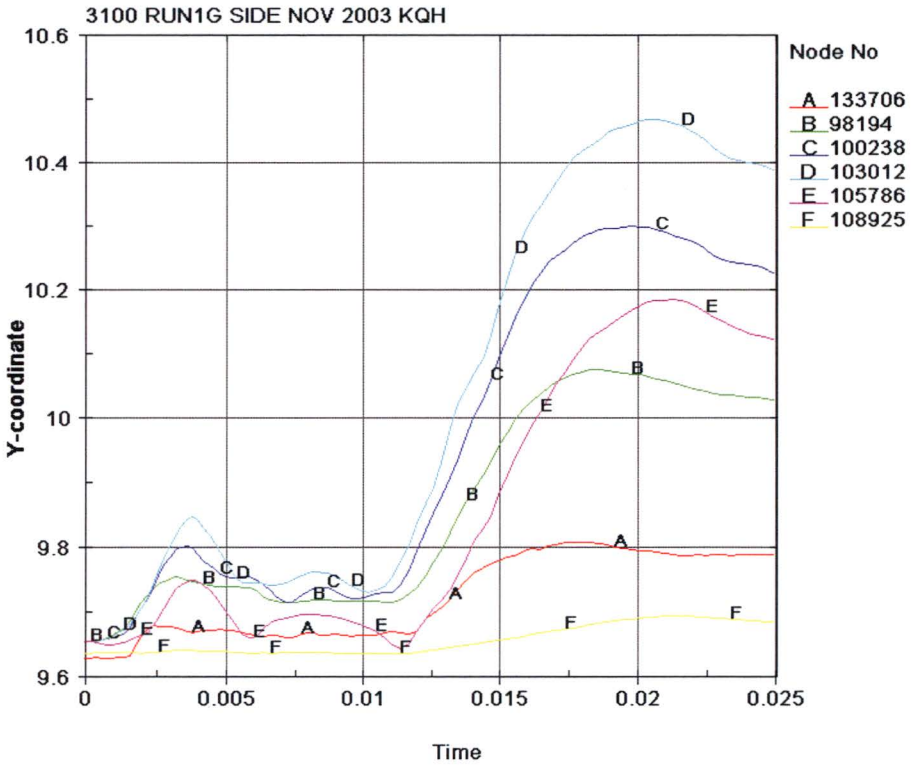

Figure 3.1.36 - Run1g, Drum Measurement Time History in the Y-Direction

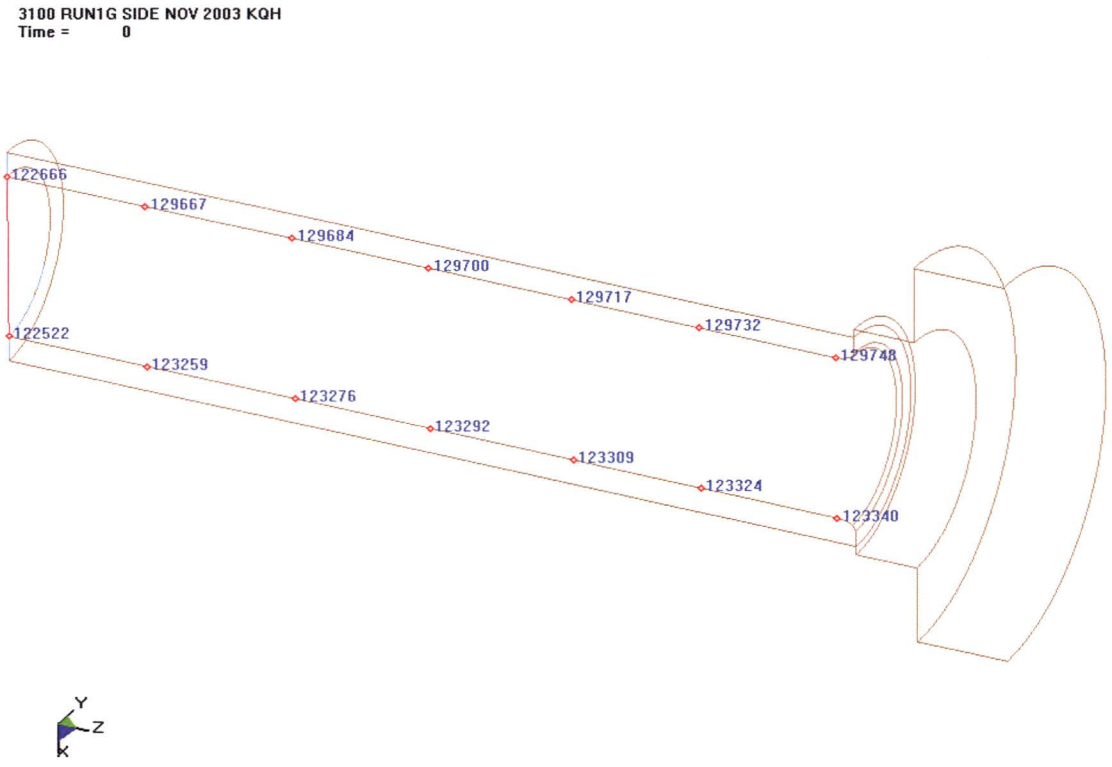

Figure 3.1.37 - Run1g, Position of Inner Liner Nodes Used for Diameter Time History

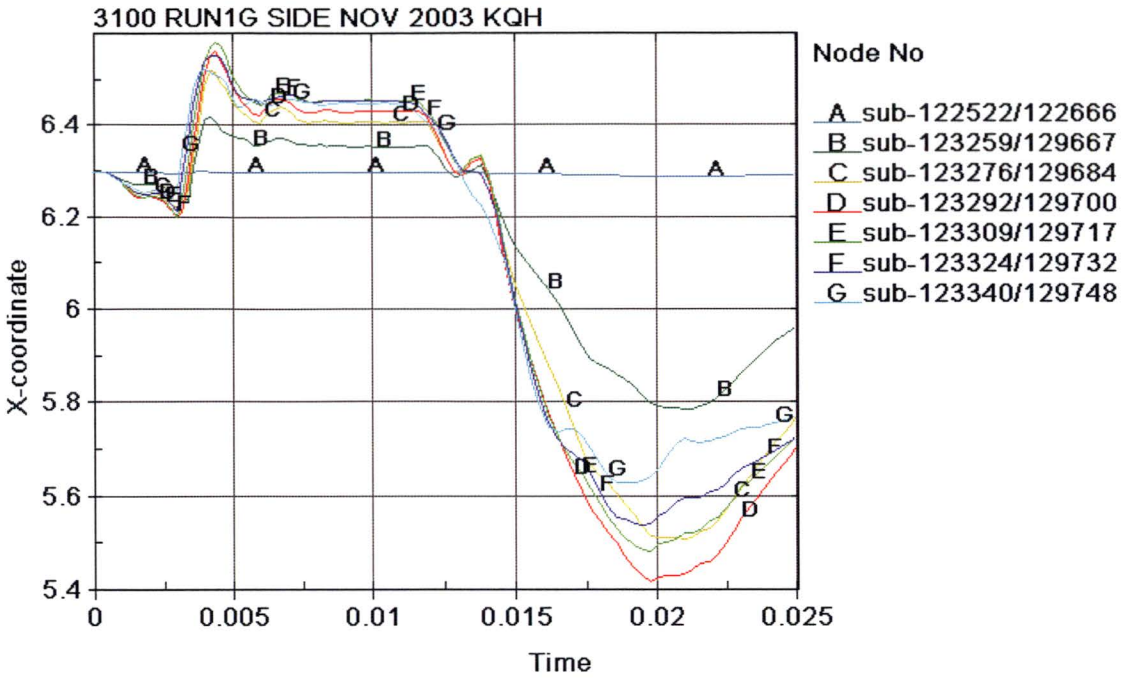

Figure 3.1.38 - Run1g, Inner Liner Diameter Time History